STUDIES ON
MEAN FIELD PROPERTIES AND EQUATION OF STATE OF NUCLEAR MATTER

THESIS SUBMITTED TO

SAMBALPUR  **UNIVERSITY**

IN PARTIAL FULFILMENT OF THE REQUIREMENTS FOR THE DEGREE OF

DOCTOR OF PHILOSOPHY
IN SCIENCE (PHYSICS)
2011

Sunil Kumar Tripathy
Regd. No. : 09/2006/Physics

Prof. T. R. Routray
(Guide)

Prof. B. Behera
(Co Guide)

POST GRADUATE DEPARTMENT OF PHYSICS
SAMBALPUR UNIVERSITY, JYOTIVIHAR, ODISHA

Sunil Kumar Tripathy
Government College of Engineering, Kalahandi
Bhawanipatna,
Kalahandi, Odisha-766002

DECLARATION

I do hereby declare that the work embodied in the thesis entitled "**Studies on Mean field properties and Equation of State of Nuclear Matter**" is the outcome of genuine research work carried out by me under the joint guidance and supervision of Prof. T. R. Routray, and Prof. B. Behera (Retd.), P.G.Deptartment of Physics, Sambalpur University. I also declare that the same has not been submitted by me to any other institution for any other degree.

(Sunil Kumar Tripathy)

Prof. T. R. Routray
Professor of Physics
P.G. Dept. of Physics
Sambalpur University
Jyotivihar, Burla

Prof. B. Behera
Professor of Physics (Retd.)
P. G. Dept. of Physics
Sambalpur University
Jyotivihar, Burla

CERTIFICATE

This is to certify that the thesis entitled "**Studies on Mean field properties and Equation of State of Nuclear Matter**", submitted by **Sri Sunil Kumar Tripathy** for the award of degree of **Doctor of Philosophy (Science)** to **Sambalpur University** is a record of bonafide research work carried out by him under our joint supervision and guidance. This work is original and to the best of our knowledge has not been submitted elsewhere for award of any degree or diploma in any other university or institution. In our opinion the thesis has fulfilled the requirements according to the regulations and has reached the standard necessary for submission. We further certify that to the best of our knowledge Sri Sunil Kumar Tripathy bears a good moral character. The annexure has been incorporated in the present thesis.

(Dr. T. R. Routray) **(Dr. B. Behera)**

ACKNOWLEDGEMENT

I would like to express my deep sense of gratitude and thanks to my supervisors Prof. B. Behera and Prof. T. R. Routray for their guidance, enthusiasm and endless encouragement during this thesis work.

I express my thanks to the H.O.D., P.G. Department of Physics, Sambalpur University for providing me the facilities available in the department to carry out this work. I am also thankful to all the staff members of the department for their help over the past years.

My sincere thanks are also due to Dr. S. K. Patra of Institute of Physics for his encouragement and help during this work. I am also thankful to Dr. K .C. Panda for his encouragement during my early phase of research career.

I am indebted to my family members and friends, who have all through extended their love, support and encouragement. I wish to give special thanks to my wife Dolly for her patience, understanding and encouragement.

The annexure has been incorporated in the present thesis.

(Sunil Kumar Tripathy)

LIST OF PUBLICATIONS

1. T. R. Routray, A. Pradhan, **S. K. Tripathy** and B. Behera, *Temperature dependence of nuclear symmetry energy*, Proc. of DAE-BRNS International Symposium on Nuclear Physics, **50,** (2005).

2. B. Behera, T. R. Routray, A. Pradhan, **S. K. Tripathy**, S. K. Patra and P. K. Sahu, *Density dependence of nuclear symmetry energy*, Proc. of DAE-BRNS Symposium on Nuclear Physics, **51,** 375 (2006).

3. T. R. Routray, **S. K. Tripathy** and B. Behera, *High density behaviour of nuclear symmetry energy,* Proc. of DAE-BRNS Symposium on Nuclear Physics, **53,** 651 (2008).

4. T. R. Routray, **S. K. Tripathy** and B. Behera, *Temperature Dependence of Nuclear Symmetry energy and Equation of State of charge neutral* $n+p+e+\mu$ *mater in beta equilibrium,* Proc. of DAE-BRNS International Symposium on Nuclear Physics, **54,** 624 (2009).

5. B. Behera, T. R. Routray and **S. K. Tripathy**, *Temperature Dependence of Nuclear Symmetry energy and Equation of State of charge neutral* $n+p+e+\mu$ *mater in beta equilibrium,* J.Phys.G: Nucl. Part. Phys, **36,** 125105 (2009).

6. T. R. Routray, **S. K. Tripathy** and B. Behera, Neutron-Proton effective mass splitting and thermal evolution of Nuclear Matter, Proc. of DAE-BRNS Symposium on Nuclear Physics, **55,** 452 (2010).

7. **S. K. Tripathy,** M. Bhuyan, T. R. Routray, and B. Behera, *Composition and EOS of charge neutral* $n+p+e+\mu$ *mater at finite temperature,* Proc. of DAE-BRNS Symposium on Nuclear Physics, **55,** 462 (2010).

8. B. Behera, T. R. Routray and **S. K. Tripathy**, *Neutron-proton effective mass splitting and Thermal evolution in neutron rich matter,* J.Phys.G: Nucl. Part. Phys, **38,** 115104 (2011).

LIST OF FIGURES

LIST OF TABLES

CONTENTS

CHAPTER-I

INTRODUCTION

1.1. Nucleon-nucleon effective interaction and EOS of Nuclear Matter

The most fundamental , challenging and elusive problem in nuclear physics is to understand the nuclear force in terms of the underlying phenomena of nucleonic matter equation of state(EOS), structure of finite nuclei etc. with the help of nucleon-nucleon interaction . Usually, the nucleus being a complex quantum system, the observables of finite nuclei can be obtained by solving many-body Schrödinger equations. However, the amount of difficulties in the computational process has led to the concept of infinite nuclear matter (NM) which is a highly idealized simplified system of infinite number of nucleons where the Coulomb force between the charged protons is switched off. The concept of NM with translational invariance greatly simplifies the calculation and provides first hand information about the underlying intricacies of nuclear structure. Together with the Local Density Approximation (LDA), this approach of NM has been used extensively for finite nuclei structure calculation and for proton-nucleus scattering. Since an exact equation of state for NM is not known, nuclear force is approximated by an effective interaction. There are two different approaches to get the nucleon-nucleon effective interaction. In the first approach, the lowest order interaction is obtained from a realistic two-body force that fits the nucleon-nucleon scattering phase shifts together with the properties of ^{2}He nucleus by applying Brueckner theory in LDA [1, 2]. But the success in this direction is very less as these effective nucleon-nucleon interactions are unable to predict accurately the binding energy or the saturation density [3]. The semi realistic two nucleon interaction models fail to explain the ground state properties of nuclear matter and the D- and F-wave phase shifts they predict are not in good agreement with experimental data. In order to describe the saturation properties of NM, this approach requires higher order correction to the effective nucleon-nucleon interaction. However, Hatree-Fock (HF) calculations with some of the effective interactions with the inclusion of three-body forces and boost corrections provide good results [4]. The so called Brueckener-Hatree-Fock (BHF) approach is based on a linked-cluster perturbation series of the ground state energy of a many body system. Such series was shown to converge when the cluster diagrams are regrouped according to the number of hole lines [1, 5]. Variational method [6-8] with realistic nucleon-nucleon (NN) potential yielded predictions in close agreement with those from Brueckener

theory. The main drawback of BHF approach was its inability to predict the nuclear matter saturation properties. The Dirac-Brueckener-Hatree-Fock (DBHF) approach [9-13] was developed during 1980's which could describe successfully the saturation properties of nuclear matter. The DBHF method uses realistic NN interactions and contains the relativistic features. It describes the nuclear mean field in terms of strong, competing scalar and vector fields. These scalar and vector fields, together, account for the binding of nucleons as well as the large spin-orbit splitting seen in nuclear states. In the second approach, a phenomenological effective interaction with some unknown adjustable parameters is constructed and the interaction parameters are determined by fitting them to reproduce the known ground state saturation properties of NM such as, the binding energy per nucleon , $e_0(\rho_0) = -16 \pm 0.2$ MeV, saturation density $\rho_0 = 0.16 \pm 0.005$ fm^{-3} , pressure at saturation $P = 0$ and the compression modulus or incompressibility $K = 210 \pm 30$ MeV [14]. Although quite less fundamental, the analytical simplicity of the phenomenological effective interactions makes them a useful tool for nuclear structure calculations and in studying the properties of dense matter in neutron stars.

Of late, the incorporation of relativistic effects within the nuclear system has led to the development of another popular approach, the Relativistic Mean Field (RMF) models [15] in the framework of quantum hadrodynamics, where the effective interaction is generated through a Lagrangian constructed for the exchange of mesons. The parameters of the Lagrangian are also fixed up by fitting them to the bulk properties of nuclei [16]. Although the earlier RMF models, having only linear coupling terms, were successful in producing qualitative properties of nuclei they predicted too high NM incompressibility and failed to produce surface properties. In order to overcome this deficiency, Boguta and Bodmer [17] introduced a nonlinear (NL) density dependent term in the σ field. The additional density dependent term helped in reducing nuclear matter incompressibility to reasonable limits. Basing upon the symmetries of Quantum Chromo Dynamics (QCD), Chiral effective theories of nuclear force have been developed recently which can well retain the basic degrees of freedom related to the low-energy nuclear physics. Chiral effective theories provide a well defined scheme to determine the appropriate many-body diagrams to be included at

each order of the perturbation. Since the chiral effective theories are based on a low momentum expansion, interactions derived from them are not suitable for applications in dense nuclear or neutron matter where usually high momenta are involved.

1.2. Skyrme type effective interactions

Right after the fully microscopic non-relativistic self consistent mean-field HF calculations of Vautherin and Brink [18], there have been many attempts to construct Skyrme type phenomenological effective interactions [19, 20]. The analytical simplicity of the Skyrme type effective interactions makes them useful for nuclear structure calculations [21], studying high density behaviour of NM as encountered in neutron stars [22, 23] and in finite temperature calculations such as the thermodynamic properties of nuclear matter and the determination of the critical temperatures in Liquid-Gas-Phase transition of NM[24-26].

Ignoring the spin-orbit contributions, the Skyrme potential that contains the two-body and three-body terms can be written as

$$v(\vec{r}) = t_0(1+x_0P_\sigma)\delta(\vec{r}) + \frac{1}{2}t_1(1+x_1P_\sigma)\left[k'^2\delta(\vec{r}) + \delta(\vec{r})k^2\right] + t_2(1+x_2P_\sigma)\vec{k}'\cdot\delta(\vec{r})\vec{k}$$
$$+ \frac{1}{6}t_3(1+x_3P_\sigma)\left[\rho\left(\vec{R}\right)\right]^\gamma \delta(\vec{r}) \qquad (1.2.1)$$

with $\vec{r} = \vec{r}_1 - \vec{r}_2$ and $\vec{R} = \frac{1}{2}(\vec{r}_1 + \vec{r}_2)$ are the relative wave vectors of two nucleons with positions $\vec{r}_1$ and $\vec{r}_2$. The t's and x's are constants. P_σ is the spin exchange operator. The exponent γ (γ=1 for original Skyrme force) takes care of the density dependence of the potential. The first two terms are the phenomenological representation of an s-wave two-body interaction, with velocity (momentum) dependence in the t_1 term. The 3rd term represents the p-wave two-body interaction and the fourth term is a zero range three-body interaction (with one integration over the coordinates of the third nucleon already performed). In 1972, Vautherin and Brink [18] produced parameter sets SI and SII by fitting the ground state properties, such as binding energies and radii, to experimental data for two spherical nuclei ^{16}O and ^{208}Pb. In 1975, Beiner et al.

generated SIII parameters set [21] that proved to be very successful throughout the mass table. The exponent γ with a value of 1 predicted too high incompressibility for nuclear matter, for example SIII set produced K=356 MeV. The approximate value of K was ascertained from the analysis of the experimental data on the giant monopole resonance (breathing mode) [14]. In order to account for the incompressibility of symmetric nuclear matter, fractional exponent ($\gamma < 1$) of the density dependent term in the Skyrme potential were chosen by many authors. The Ska set of Kohler [27], SkM set of Krivine *et al.* [28], SGII set of Giai and Sagawa [29] used fractional γ (usually γ=1/6) to take into account that the incompressibility of symmetric nuclear matter (SNM) be in the range 210 ± 30 MeV. It was proposed by Zamick [30] that in order to get a reasonable value of the SNM incompressibility the exponent γ should remain in between $\frac{1}{3}$ and $\frac{2}{3}$. So far many sets of Skyrme forces have been constructed to reproduce different aspects of nuclear matter properties, properties of finite nuclei, properties of nuclei at the β –line and nuclei near the proton or neutron drip line. Usual Skyrme forces do not give a reasonable behaviour of the nuclear EOS as a function of neutron-proton asymmetry or the proton fraction $Y_p = \frac{\rho_p}{\rho}$, where ρ_p is the proton density and ρ is NM density. A systematic study [31] of different sets of Skyrme parameterization shows that out of 87 sets only 27 sets are useful for the study of neutron star properties. The nuclear symmetry energy coefficient E_s at normal nuclear matter density is a crucial quantity for the study of neutron star properties. For astrophysical applications, the effective interaction should fit the calculations of pure neutron matter and should reproduce a quite reasonable value of E_s at normal NM density which is believed to be around $30 MeV$ [32-33]. Notable among the parameters sets derived for astrophysical application are that of Siemens and Pandharipande [34], Buchler and Ingber [35], Sjöberg [36], Buchler and Datta [37], Friedman and Pandharipande [6].

It is well known that NM saturation can be achieved with density dependent or momentum dependent interactions or with a combination of both. The short-range or Zero-range Skyrme type interactions are useful for low relative momenta between the

interacting nucleons. When comparatively high relative momenta of the interacting nucleons are involved we have to resort to finite range effective interaction. In 1963, Seyler and Blanchard employed a Yukawa type finite-range effective interaction of the form [38]

$$v(\vec{r},\vec{k}) = -C_{\xi,\nu}\frac{e^{-r/a}}{r/a}\left[1-\frac{k^2}{b^2}\right] \tag{1.2.2}$$

where r is the separation distance between the nucleons, $\vec{k}$ is the relative momentum. $C_{\xi,\nu}$ is the strength of the interaction with the subscripts ξ and ν refer to the spin and isospin degeneracy, a is the range of the Yukawa force, and b is the critical value of the relative momentum at which the force becomes repulsive. The Seyler and Blanchard finite-range effective interaction can be simply expressed as a Skyrme force with $t_3 = 0$ which predicts much higher value of NM incompressibility. Finite-range effective interactions simulated by Gaussian type potentials used in self-consistent calculations are that of Brink-Boeker [39] and Gogny [40]. The Gogny interaction [41] is in the form

$$v(\vec{r}) = \sum_{i=1,2}\left(W_1 + B_1P_\sigma - H_1P_\tau - M_1P_\sigma P_\tau\right)e^{-r^2/\alpha^2_1} + t_0(1+x_0P_\sigma)\left[\rho\left(\frac{\vec{R}}{}\right)\right]^\gamma \delta(\vec{R})$$
$$++iW_0(\sigma_1+\sigma_2)\cdot\left[\vec{k}'\times\delta(\vec{r})\vec{k}\right]. \tag{1.2.3}$$

These interactions upon integration do not lead to analytical simplicity and hence are less or not used in astrophysical applications.

1.3. Nuclear matter incompressibility and Need of a momentum dependent interaction

The NM incompressibility has been traditionally calculated from the breathing mode vibration or the Giant Monopole Resonance [14, 42]. With the availability of nuclear collision data [43] and with the advent of experimental facilities to carry out experiments on Intermediate and high-energy Heavy-Ion (HI) collisions, the studies on the nuclear EOS has gained renewed interest. In these experiments it is possible to create matter of high density and high temperature. From the analysis of the data

available from such experiments it is possible to explore and extract information on the nuclear EOS at extreme situations of density and temperature. These information are also essential for the understanding of certain astrophysical phenomena like neutron star properties, their structure and supernova explosion mechanism. The transport model calculations based on classical Boltzman equation [44, 45] were performed to extract information about the NM EOS. In such calculations the crucial input is the nuclear single-particle potential or the nuclear mean field. With momentum independent effective interactions leading to nuclear mean field in Skyrme parametrization,

$$u(\rho) = A\left(\frac{\rho}{\rho_0}\right) + B\left(\frac{\rho}{\rho_0}\right)^{\sigma} \tag{1.3.1}$$

where A and B are adjustable parameters and $\sigma > 1$, the transport model calculations required a quite high incompressibility (K=380 MeV) to fit the observed data from the pion production and the collective sideward flow [45]. But the explosive shock mechanism of Supernova requires a soft EOS with K in the range of 140 MeV to 220 MeV [46-49]. This contradicting extraction of nuclear EOS leads to the use of momentum dependent effective interactions and momentum dependent nuclear mean fields in transport model calculations [50-52]. Introduction of momentum dependent interaction significantly lowered the value of NM incompressibility. In the density dependent and momentum independent effective interactions the saturation burden is taken by the density dependence of the potential. In a Seyler-Blanchard type effective interaction [38] the entire burden of saturation is shouldered by its momentum dependence. The Skyrme interactions and the Seyler-Blanchard type effective interactions lead to mean fields in NM whose momentum dependent part is repulsive [53] and has a quadratic dependence on momentum. On the other hand, the momentum dependent part of the mean field in NM derived from finite-range effective interactions is attractive and is strong at very low momenta. From the analysis of nucleon-nucleus scattering data at intermediate energy it is observed that with the increase in momentum, the momentum dependence of the mean field weakens and vanishes at a kinetic energy of about 300MeV of incident nucleon and then turns out to be repulsive with the further increase in kinetic energy. This behaviour of the mean field with increase in momentum is an essential feature for a successful interpretation of HI

collision data at intermediate energies [54-60]. Similar behaviour of the NM mean field has also been observed in microscopic Dirac-Brueckener-Hatree-Fock (DBHF) calculations of Li and Machleidt [61, 62]. All of these works strongly suggest that momentum dependence of nuclear mean field is an unavoidable feature for the fundamental understanding of nuclear matter properties and for the successful interpretation of the HI collision data. Hence a correct momentum and density dependence of the nuclear mean field should be employed in the transport model calculations so as to fit the observed energy dependence of the optical potential. The momentum dependent mean field used in earlier calculations [50, 52, 60, 63], is in the form

$$u(\rho) = A\left(\frac{\rho}{\rho_0}\right) + B\left(\frac{\rho}{\rho_0}\right)^{\sigma} + \frac{2C}{\rho_0}\int d^3\vec{k}' \frac{f(\vec{r},\vec{k}')}{1-\left(\frac{\vec{k}-\vec{k}'}{\Lambda}\right)^2} \tag{1.3.2}$$

where the parameters A, B, C, σ and Λ are chosen to reproduce the saturation properties of NM and provide the necessary incompressibility and fit the HI scattering data.

Keeping a view on the above constraints on nuclear EOS, Behera *et al* [64] have constructed some finite-range momentum and density dependent phenomenological effective interactions with minimum number of adjustable parameters. These effective interactions have a zero-range density dependent part similar to Skyrme interactions and a long-range density-independent part of conventional form such as Yukawa, Gaussian or exponential. This effective interaction is very similar to the Skyrme type effective interactions except that the t_1 and t_2 terms have been replaced by a finite-range interaction. The interaction parameters have been calculated by fitting the standard values of NM saturation properties i.e. energy per nucleon $e_0(\rho_0) = -16$ MeV, kinetic energy $T_{F_0} = 37\,\text{MeV}$ corresponding to $\rho_0 = 0.161 fm^{-3}$ and $K(\rho_0) = 210\,\text{MeV}$. This value of NM incompressibility at saturation has also been reported by Blaizot *et al.* [14]. The corresponding nuclear mean field is of the form

$$u(\rho) = A\left(\frac{\rho}{\rho_0}\right) + B\left(\frac{\rho}{\rho_0}\right)^{\sigma} + C\left(\frac{\rho}{\rho_0}\right) I(k,\rho) \qquad (1.3.3)$$

where the third term comes from the finite-range exchange contribution to the effective interaction and takes care of the momentum dependence. In Ref. [65], using the same finite range effective interaction, the authors have shown that the resulting momentum dependence of the mean field in symmetric nuclear matter (SNM) is in very good agreement with the predictions of the microscopic calculations of Wiringa [66], particularly with UV14+UVII. The momentum and density dependence of the nuclear mean field obtained from these interactions are compared well over a wide range of densities and momenta with that of the momentum dependent Yukawa Interaction (MDYI) [63]. These effective interactions of Behera et al.[64] have successfully been applied to study the thermostatic properties of symmetric NM, Phase Transition studies like QGP Phase Transition at finite temperature and the Nuclear Liquid-Gas-Phase Transition [65, 67].

1.4. EOS of Asymmetric Nuclear Matter and neutron-proton effective mass splitting

Analysis of the anisotropies quantified experimentally over a wide range of bombarding energy in the central Au+Au collision has led to fix up a constraint upon the EOS of SNM in the form of a band of Pressure-density relation within a substantially wide range of density i.e. $2\rho_0$ to around $4.6\rho_0$ [68, 69]. This constraint has eliminated some of the much used EOSs in Nuclear Physics.

With the establishment or construction of many radioactive ion beam (RIB) facilities around the world, such as the Cooling Storage Ring (CSR) facility at HIRFL in China [70], RIB factory at RIKEN in Japan [71], the Facility for Antiproton and Ion Research(FAIR)/GSI in Germany [72], SPIRAL2/GANIL in France [73] and the facility for Rare Isotope Beams (FRIB) in USA [74] and the growing experimental facilities using RIBs and that of intermediate energy HI collisions induced with neutron rich nuclei, have provided ample opportunities to explore the EOS of highly dense and hot isospin asymmetric nuclear matter (ANM) with high neutron-proton asymmetry

[75-86]. New detectors such as the Time Projection Chamber (TPC) at NSCL/MSU and the TPC, SAMURAI at RIKEN, Japan are being planned to study the symmetry energy and the nuclear equation of state. In SNM where both the neutron and proton mean fields assume the same form and value, things become simpler to calculate different nuclear matter properties and since there has been so many constraints fixed from different experimental observations, one has a guiding lines to construct the phenomenological mean field equations. The EOS of SNM with equal no of neutrons and protons is somewhat well determined. Particularly, the energy per particle at normal nuclear matter density, is $e(\rho_0) = -16\,MeV$; the incompressibility at saturation density ρ_0, as has been determined from GMR studies , to be $240 \pm 20\,MeV$ [87-94] and the pressure-density band or the EOS in the density region $2\rho_0 < \rho < 5\rho_0$ as has been constrained from the collective flow data [68] , within the limits of experimental errors, are known to some extent. However, in ANM, where the proton mean field is quite different from the neutron mean field, we have a poor knowledge about the momentum and density dependence of nuclear mean field which poses considerable difficulties for the complete understanding of its EOS. The important quantity for the description of EOS of ANM is the isovector part of the nuclear mean field, $u_\tau(\vec{k}, \rho = \rho_n + \rho_p)$ defined as

$$u_\tau(\vec{k},\rho) = \lim_{Y_p \to 1/2} \frac{u^n(\vec{k},\rho,Y_p) - u^p(\vec{k},\rho,Y_p)}{2(1-2Y_p)} \tag{1.4.1}$$

i.e. the difference of the neutron mean field and proton mean field at zero temperature normalized to the neutron-proton asymmetry $(1-2Y_p)$. Various theoretical approaches in the study of EOS of ANM include Dirac-Brueckner-Hartree-Fock (DBHF) calculations using realistic nucleon-nucleon interactions derived from relativistic meson field theory [61-62, 95-98], Brueckner-Hartree-Fock (BHF) calculations with Reid soft core potential [99-102], Brueckner-Bethe-Goldstone (BBG) calculations with the Paris potential [103-104], and variational calculation using different combinations of two and three nucleon interactions [6, 66]. Besides these microscopic approaches, effective theories such as relativistic mean field (RMF) approximations [105-111] and non-

relativistic effective interactions [112-116] have also been used extensively to study the EOS and mean field properties of asymmetric nuclear matter.

The nucleon effective mass is a property that characterizes the propagation of (quasi) nucleons through the nuclear medium. It is a reminder of the non locality and energy dependence of the nucleon self energy originating from the finite range and non locality in the time and space of the nucleon-nucleon interaction. In very exotic systems, the isovector behavior of the neutron and proton effective masses play important role. The momentum dependence of the isovector part of nuclear mean field drives the splitting of neutron and proton effective masses with neutron proton asymmetry. However, there is no experimental data available from finite nuclei to determine the effective mass splitting as a function of neutron richness. So far the theoretical predictions regarding the momentum and density dependence of the isovector part of nuclear mean field $u_\tau(\vec{k},\rho)$ are extremely contradicting. Some BHF calculations with realistic nucleon-nucleon interactions predict that $u_\tau(\vec{k},\rho)$ should decrease with the increase in momentum $\vec{k}$ giving rise to a neutron effective mass going above that of the proton [117-119] where as relativistic Dirac-Brueckener calculation [120] and RMF models using Quantum Hadrodynamics (QHD) [105-107] predict that $u_\tau(\vec{k},\rho)$ should increase with the increase in $\vec{k}$ implying the proton effective mass going above that of neutron However, experimentally extracted results on the energy dependence of $u_\tau(\vec{k},\rho_0)$ show a decreasing trend supporting the fact that the neutron effective mass goes above the proton one although the data are available up to energy 100 MeV and are associated with large uncertainty [121-123]. The decreasing trend of $u_\tau(\vec{k},\rho_0)$ with momentum k is also predicted in BHF calculations [118, 124] and in the calculations of the non-relativistic effective theories till the construction of Sly series of Skyrme parametrization [112,125-126]. The confusion on neutron and proton effective mass splitting became complex with the prediction of DBHF calculation in Ref [120] that the proton effective mass lies above the neutron one. It was clarified in the works of Ref. [127,128] that by considering the energy dependence of self energy

and comparing the non relativistic effective mass with the vector effective mass in the relativistic framework [129], the DBHF calculation also predicts the neutron effective mass above the proton one. This was further confirmed in the DBHF calculation in Ref. [130]. In view of this, now there is an almost a consensual opinion has reached that the neutron effective mass in a neutron rich matter will lie above the proton one. There have been attempts to constrain the effective mass splitting from the study of observables sensitive to the isovector features of the nuclear EOS [81, 84, 131], but the task has not yet been accomplished and magnitude of effective mass splitting still remains as an open problem in nuclear physics.

1.5. Nuclear Symmetry Energy

The behaviour of the mean fields at Fermi momentum is directly related to the density dependence of nuclear symmetry energy $E_s(\rho)$ which may be defined as the difference in energy per nucleon in pure neutron matter (PNM) and that in SNM. Symmetry energy is an important quantity which determines the composition of neutron star and the structure of exotic nuclei. It controls the proton fraction in beta stable matter. Both theoretically and experimentally, significant progress has been made on constraining the behaviour of $E_s(\rho)$ at subnormal density using heavy ion reactions [85, 132-139]. The density dependence of nuclear symmetry energy for subnormal densities is believed to be linear and is mostly model dependent. Experimentally, the symmetry energy is not a directly measurable quantity and has to be extracted indirectly from observables that are related to the symmetry energy. The experimental determination of the symmetry energy is therefore depends on reliability of the model in describing the experimental observables. Usually two different experimental approaches are made to study the nuclear symmetry energy. In the first category, a certain form of the density dependence of the symmetry energy is assumed in the theoretical calculation and experimental observables are reproduced using dynamical models such as Isospin Boltzmann Uehling Uhlenbech (IBUU) [82], the improved quantum molecular dynamics(ImQMD) [140] and the antisymmetrized molecular dynamics (AMD) [141]. In the second category, the symmetry energy is studied by mapping its value at each density by drawing a relationship between the symmetry energy, excitation energy,

density and temperature [133]. These studies make use of the statistical multifragmentation model. The density dependence of nuclear symmetry energy $E_s(\rho)$ and thus the EOS of ANM are largely unknown, except the value of $E_s(\rho)$ at saturation density to be around $E_s(\rho_0) = 30\ MeV$, as determined from the empirical liquid drop mass formula [142, 143]. However at densities away from the normal NM density and at densities relevant to neutron stars, the density dependence of $E_s(\rho)$ has been poorly understood [119, 136], which pushes the understanding of EOS of ANM into bare uncertainties. The principal cause of this uncertainty is the lack of terrestrial data to constrain model predictions. In order to probe the density dependence of nuclear symmetry energy away from saturation density, many efforts have been made through the studies of proton differential elliptic flow and the neutron-proton transverse flow [144, 145], isospin diffusion studies [132], the π^-/π^+ ratio [83], Σ^-/Σ^+ (hyperons) ratio in HI collisions at SIS (Schwer Ionis Synchroton) energies [146] and within the microscopic transport model, ultra relativistic Quantum Molecular Dynamics (QMD) models [147]. Recently, there have been attempts to extract nuclear symmetry energy at suprasaturation densities from the FOPI data on the π^-/π^+ ratio in $^{40}Ca+^{40}Ca$, $^{96}Ru+^{96}Ru$, $^{96}Zr+^{96}Zr$ and $^{197}Au+^{197}Au$ reactions at SIS/GSI [139] and from the structure of finite nuclei such as neutron skin thickness studies [148]. Another observable that has been suggested for probing high density behaviour of the symmetry energy is the relative and differential collective flow between triton and ^3He particles [149].

The prediction of the density dependence of $E_s(\rho)$ at densities away from the normal nuclear matter density, from different theoretical calculations is quite interesting. The density dependence of $E_s(\rho)$ can be roughly classified into two groups. In one category of calculations, $E_s(\rho)$ increases monotonically with the increase in density whereas in another category of calculations it increases initially and after attaining a maximum decreases to have negative values at very high density. Since nuclear symmetry energy controls the neutron star composition and cooling mechanism

through the proton fraction $Y_p = \frac{\rho_p}{\rho}$ and is required for the understanding of certain phenomena beyond the standard nuclear physics, a more accurate knowledge of its high density behaviour becomes an important goal of nuclear physics in the present time. Recently Stone *et al.* [31] have examined 87 Skyrme type interactions on the basis of their prediction on equilibrium proton fraction and EOS of beta stable matter as well as neutron star properties. They have shown that only 27 out of the 87 sets are appropriate for astrophysical applications on the basis that $E_s(\rho)$ should have an increasing behaviour over a wide range of density. Microscopic calculations of Zuo *et al.* [118] based on realistic nucleon-nucleon interactions and RMF calculations [150] also predict such a monotonically increasing behaviour of $E_s(\rho)$. Recently Klahn *et al.* [151] have summarized some of the constraints on the high density behaviour of the nuclear symmetry energy by applying some recently discovered astronomical bounds from compact star cooling phenomenology and neutron star mass measurements together with information about the elliptical flow in HI collisions. They have suggested a scheme, may not be considered in its final shape, to test different models providing successful NM EOS at densities close to the saturation density. Recent measurements on PSR J0751+1807 imply a pulsar mass of $2.1 \pm 0.2(^{+0.4}_{-0.5})M_\odot$ with $1\sigma\,(2\sigma)$ confidence level which constrains maximum neutron star masses to $1.6M_\odot$ in the 2σ confidence level or even $1.9M_\odot$ within the 1σ confidence level. Within the set of EOSs tested by Klahn et al. only DD, D^3C and DBHF survived the test. Mass of pulsar B in the system J0737-3039 is merely $1.249 \pm 0.001M_\odot$, which is the lowest reliably measured mass for any neutron star. Any viable EOS proposed for neutron star matter must predict a baryon number in the range $1.366 \le M_N \le 1.375M_\odot$ for a neutron star whose gravitational mass is in the range $M = 1.249 \pm 0.001M_\odot$. None of the EOSs tested in the work satisfied this constraint. The density dependence of symmetry energy of all the EOSs considered in Ref[151] vary considerably from each other, however, the asymmetric contribution to the energy per particle in neutron star matter shows a marginal dependence on different EOSs forming a narrow band. This universal high density behavior of the asymmetric part of the energy per nucleon in neutron star matter

helps the EOSs to pass the direct URCA constraint. However, in the absence of any experimental or empirical information, the theoretical determination of nuclear symmetry energy at suprasaturation density has loomed as a challenge in nuclear physics.

1.6. Objective and Plan of the thesis

The objective behind the present work is to analyse the momentum and density dependence of the isovector part of the nuclear mean field $u_\tau(k,\rho)$ and to focus on the existing controversies in the high density behaviour of nuclear symmetry energy as well as the two opposite types of splitting of neutron and proton effective masses using a simple parametrization of the energy density in ANM based on density dependent finite range effective interactions within the framework of non relativistic mean field formalism. The simplicity of the energy density we have used, allows us to calculate the isospin part of the nuclear mean field and other properties of ANM at zero temperature analytically. The density dependent finite range effective interaction constructed for the purpose has minimum number of adjustable parameters and yet capable of predicting the properties of nuclear matter. Such a simple effective interaction can provide a physical insight to the underlying phenomena of the behaviour of momentum and density dependence of the nuclear mean field.

In Chapter-II, we have reviewed the current status on the momentum and density dependence of the isospin part of nuclear mean field and on the puzzle of the neutron and proton effective mass splitting. The riddle has been analysed through a most general EOS by considering four interactions, direct and exchange, acting between like and unlike pairs of nucleons. The reason behind the controversy on the issue of the neutron and proton effective mass splitting is explored by using a simple two parameter finite range Yukawa effective interaction. It has been shown in the chapter that the existing controversies of the neutron-proton effective mass splitting can be attributed to the splitting of the exchange strength parameter into like and unlike channels. It is shown that the isovector part of the nuclear mean field becomes a decreasing function of momentum in the case of stronger exchange interaction in the unlike channel than that of the like channel and consequently the neutron effective mass goes above the

proton effective mass in ANM. On the contrary, if the splitting of the exchange interaction into the like channel is stronger compared to that in the unlike channel then the isovector part of the mean field becomes an increasing function of momentum and the proton effective mass lies over that of the neutron. We have extended the formalism to examine the controversies in cases of Skyrme type interactions and Gogny interaction. In order to have a clear picture of the status of the existing controversies of neutron-proton effective mass splitting in neutron rich ANM, some of the important works such as the works of B.A.Li *et al.* in Ref.[81] and Rizzo et al. in Ref.[84] have been discussed.

In Chapter-III, we have constructed a density dependent finite range effective interaction useful for the investigation of the neutron-proton effective mass splitting and the momentum and density dependence of neutron and proton mean fields as well as the high density behaviour of nuclear symmetry energy. The parameters of this effective interaction are fixed from the saturation properties in SNM and the behaviour of symmetry energy at saturation. In order to constrain certain parameters we have used the universal high density behaviour of nuclear symmetry energy which envisages a stiffest asymmetric part of the nucleonic energy density in neutron star matter (NSM). The assumption that neutron effective mass will go above that of the proton restricts the exchange strength parameter in the like channel within certain allowed range. Variation of the parameter within its allowed range does not affect appreciably the density dependence of nuclear symmetry energy. Hence, the zero temperature properties of either ANM or NSM are unable to constrain the parameters of the effective interaction relevant for the settlement of the controversies regarding the neutron and proton effective mass splitting. It is expected that finite temperature calculation may provide some ways to constrain the corresponding parameters particularly the exchange strength parameter between a pair of like or unlike nucleons.

In Chapter-IV, thermal evolution of nuclear symmetry energy and nuclear free symmetry energy along with other properties of ANM are investigated. It has been emphasized in the chapter that, only the knowledge of exchange strength parameter and range of the exchange interaction between a pair of like or unlike nucleons are sufficient to explore the thermal evolution of the properties of ANM. The role of momentum

dependence on the thermal evolution of nuclear symmetry energy and free symmetry energy has been analysed. The results of ideal Fermi gas case have also been calculated for comparison. It is interesting to note that the momentum dependent interaction has a quenching effect on the impact of temperature on the properties of nuclear matter. The quenching effect of the momentum dependent interaction is discussed on the basis of the entropy density in SNM and PNM. The behaviour of entropy density in SNM and PNM for different splitting of the exchange strength parameter has been analysed which may help in sorting out an answer to address the existing neutron-proton effective mass splitting.

In Chapter-V, using the density dependent finite range Yukawa interaction constructed in earlier chapters, we have studied the temperature and density dependence of nuclear symmetry energy, free symmetry energy and other properties of NSM for three different representative splitting of the exchange strength parameter into like and unlike channel within its allowed range as decided in the earlier chapters. Nuclear symmetry energy and free symmetry energy are used to calculate the equilibrium proton fraction and the EOS of charge neutral beta-stable matter in neutron star.

In Chapter-VI, summary, conclusion and outlook of the work have been presented.

CHAPTER-II

EQUATION OF STATE OF NUCLEAR MATTER

2.1. EOS of Nuclear Matter for general effective interaction

In this chapter we shall discuss the general formalism in the framework of non-relativistic mean field theory that can be used to study the momentum and density dependence of nuclear mean fields and equation of state of nuclear matter using any effective interaction that depends on the separation distance between the two interacting nucleons as well as the density of the interacting medium. Some of the works performed in this context using various effective models shall be reviewed and also be elaborated at appropriate places relevant to the work undertaken in this thesis. The neutron and proton mean fields are the quantities of crucial importance in the studies of nuclear matter. Under the formalism developed in this chapter it will be shown that the EOS of nuclear matter is connected to the values of these nucleonic mean fields at the Fermi momentum. It is therefore necessary to consider the momentum dependence aspect of the nuclear mean field to be the primary thing that needs to be taken care of properly at the beginning of the studies of nuclear matter using any model. This important point has been realized at length during the last few decades with the experimental advents of high energy heavy-ion collision experiment facilities using radioactive ion beam. The momentum dependence of nuclear mean field in SNM as well as the density dependence of the EOS in SNM has been understood to a reasonable extent. However, in asymmetric nuclear matter, these two important aspects of momentum and density dependence of nucleonic mean fields and EOS of ANM are still poorly understood. The neutron-proton effective mass splitting in ANM comes from the momentum dependence of nucleonic mean fields in ANM, whereas, the density dependence of nuclear symmetry energy is connected to the EOS of ANM. In the followings we shall formulate the nucleonic mean fields and EOS of ANM in the framework of non-relativistic mean field theory using phenomenological effective interactions staring from the first principle. Some of the works done in these important areas shall also be discussed.

The equation of state (EOS) of isospin-asymmetric nuclear matter is described by the energy per nucleon $e(\rho)$ expressed as a function of total nuclear density $\rho = \rho_n + \rho_p$, proton fraction $Y_p = \frac{\rho_p}{\rho}$ and temperature T which can be derived from

the effective nucleon-nucleon interaction. ρ_n and ρ_p are respectively the neutron and proton densities. The total energy of a nuclear system can be expressed as

$$E=\sum_i\langle i|T_k|i\rangle+\frac{1}{2}\sum_{i\neq j}\left[\langle ij|v_d|ij\rangle+\langle ij|v_{ex}|ji\rangle\right] \tag{2.1.1}$$

where $|i\rangle$ and $|j\rangle$ are single particle states which can be represented by plane waves for infinite nuclear matter with the coulomb force between the charged protons being switched off. v_d and v_{ex} are the direct and exchange part of the effective nucleon-nucleon interaction.

Considering the spin saturated isospin asymmetric matter we have altogether four direct and exchange interactions acting between like (l) nucleons (i.e. nn and pp) and unlike (ul) nucleons (i.e. np). These four interactions, namely, $v_d^l(r)$, $v_{ex}^l(r)$, $v_d^{ul}(r)$ and $v_{ex}^{ul}(r)$, are expressed as,

$$v_{d(ex)}^l(r)=\frac{1}{4}v^{se}(r)\pm\frac{3}{4}v^{to}(r) \tag{2.1.2}$$

$$v_{d(ex)}^{ul}(r)=\frac{1}{8}v^{se}(r)+\frac{3}{8}v^{te}(r)\pm\frac{1}{8}v^{so}(r)\pm\frac{3}{8}v^{to}(r) \tag{2.1.3}$$

where, the superscript indices 's' and 't' imply interaction in singlet and triplet spin states and 'e' and 'o' imply the interaction in even and odd parity states of the two interacting nucleons. $v^{se}(r)$, $v^{te}(r)$, $v^{so}(r)$ and $v^{to}(r)$ are the respective interactions averaged over angles, spins, and isospins of the two interacting nucleons and are functions of separation distance r between the two interacting nucleons and the total density $\rho=\rho_n+\rho_p$ of the medium. The charge symmetry of nuclear interaction implies that $v^{nn}(r)=v^{pp}(r)=v^{l}(r)$ and $v^{np}(r)=v^{ul}(r)$. In the eqs.(2.1.2 and 2.1.3), +ve sign is meant for direct interaction and $-$ve sign is for the exchange interaction.

With the help of the above consideration, the total energy in a nuclear system given in eq.(2.1.1) can be written as,

$$\begin{aligned}E(\rho_n,\rho_p)=&\sum_{\tau}^{n,p}\sum_i\langle i|(C^2\hbar^2k_\tau^2+M^2C^4)^{1/2}|i\rangle+\frac{1}{2}\sum_{l=n,p}\sum_{i\neq j}\langle ij|v_d^l|ij\rangle+\frac{1}{2}\sum_{ul=n,p}\sum_{i\neq j}\langle ij|v_d^{ul}|ij\rangle\\&+\frac{1}{2}\sum_{l=n,p}\sum_{i\neq j}\langle ji|v_{ex}^l|ij\rangle+\frac{1}{2}\sum_{ul=n,p}\sum_{i\neq j}\langle ji|v_{ex}^{ul}|ij\rangle\end{aligned} \tag{2.1.4}$$

where, for kinetic part we have used the relativistic relationship between energy and momentum in order to take into account the possible relativistic effects that may arise at high temperature as well as at high density. For nuclear matter in thermal equilibrium at temperature T, the neutron and proton occupation probabilities of the single particle states are described in terms of their respective Fermi-Dirac distribution functions given by

$$f_T^i(\vec{k}) = \frac{\xi}{(2\pi)^3} \frac{1}{1+\exp[\{\varepsilon_T^i(\vec{k},\rho_n,\rho_p) - \mu_T^i\}/T]} \tag{2.1.5}$$

with $i = n, p$, where, $\xi = 2$ is the spin degeneracy factor, $\varepsilon_T^i(\vec{k},\rho_n,\rho_p)$ is the single particle energy, μ_T^i is the chemical potential of the nucleon and $\vec{k}$ is the momentum of the nucleon. The normalization factor $\frac{\xi}{(2\pi)^3}$ has been taken in the expression of the Fermi-Dirac distribution function in the above eq.(2.1.5) subject to the condition that integration over the momentum space of proton and neutron distribution functions shall result into respective densities ρ_p and ρ_n,

$$\rho_i = \int f_T^{\,i}(\vec{k})\, d^3k\,,\ i = n, p. \tag{2.1.6}$$

The total energy of nuclear system in eq.(2.1.4) can now be expressed in terms of these single particle distribution functions as,

$$\begin{aligned}
E(\rho_n,\rho_p) = {} & \iint f_T^n(\vec{k})(C^2\hbar^2k^2 + M^2C^4)^{1/2} d^3k\, d^3R + \iint f_T^p(\vec{k})(C^2\hbar^2k^2 + M^2C^4)^{1/2} d^3k\, d^3R \\
& + \frac{1}{2}\int\iiint f_T^n(\vec{k}) f_T^n(\vec{k}')\, v_d^{nn}\, d^3r_1\, d^3r_2\, d^3k\, d^3k' + \frac{1}{2}\int\iiint f_T^p(\vec{k}) f_T^p(\vec{k}')\, v_d^{pp}\, d^3r_1 d^3r_2\, d^3k\, d^3k' \\
& + \frac{1}{2}\int\iiint \left[f_T^n(\vec{k}) f_T^p(\vec{k}') + f_T^p(k) f_T^n(\vec{k}')\right] v_d^{np}\, d^3r_1 d^3r_2\, d^3k\, d^3k' \\
& + \frac{1}{2}\int\iiint e^{-i\vec{k}'\cdot\vec{r}_1 - i\vec{k}\cdot\vec{r}_2}\, v_{ex}^{nn}\, e^{i\vec{k}\cdot\vec{r}_1 + i\vec{k}'\cdot\vec{r}_2} f_T^n(\vec{k}) f_T^n(\vec{k}')\, d^3r_1\, d^3r_2\, d^3k\, d^3k' \\
& + \frac{1}{2}\int\iiint e^{-i\vec{k}'\cdot\vec{r}_1 - i\vec{k}\cdot\vec{r}_2}\, v_{ex}^{pp}\, e^{i\vec{k}\cdot\vec{r}_1 + i\vec{k}'\cdot\vec{r}_2} f_T^p(\vec{k}) f_T^p(\vec{k}')\, d^3r_1\, d^3r_2\, d^3k\, d^3k' \\
& + \frac{1}{2}\int\iiint e^{-i\vec{k}'\cdot\vec{r}_1 - i\vec{k}\cdot\vec{r}_2}\, v_{ex}^{np}\, e^{i\vec{k}\cdot\vec{r}_1 + i\vec{k}'\cdot\vec{r}_2} f_T^n(\vec{k}) f_T^p(\vec{k}')\, d^3r_1\, d^3r_2\, d^3k\, d^3k' \\
& + \frac{1}{2}\int\iiint e^{-i\vec{k}'\cdot\vec{r}_1 - i\vec{k}\cdot\vec{r}_2}\, v_{ex}^{pn}\, e^{i\vec{k}\cdot\vec{r}_1 + i\vec{k}'\cdot\vec{r}_2} f_T^p(\vec{k}) f_T^n(\vec{k}')\, d^3r_1\, d^3r_2\, d^3k\, d^3k'
\end{aligned} \tag{2.1.7}$$

where, M is the nucleonic mass and C is the speed of light in vacuum. Under the transformation of coordinates into the relative and centre of mass coordinates,

$\vec{r} = \vec{r}_1 - \vec{r}_2$, $\vec{R} = \frac{\vec{r}_1 + \vec{r}_2}{2}$ and $d^3r_1 d^3r_2 = d^3r\, d^3R$ the total energy of the nuclear system can be obtained as

$$E = \int H\, d^3R, \tag{2.1.8}$$

where, H is the energy density of the nuclear system. We can write the energy density in nuclear matter at thermal equilibrium, $H_T(\rho_n, \rho_p)$, from the above eq.(2.1.7) as,

$$\begin{aligned} H_T(\rho_n,\rho_p) = {} & \int [f_T^n(\vec{k}) + f_T^p(\vec{k})] \left(C^2\hbar^2k^2 + M^2C^4\right)^{1/2} d^3k \\ & + \frac{\rho_n^{\,2}}{2}\int v_d^{nn}(r) d^3r + \frac{\rho_p^{\,2}}{2}\int v_d^{pp}(r) d^3r + \rho_n\rho_p \int v_d^{np}(r)\, d^3r \\ & + \frac{1}{2}\iiint f_T^n(\vec{k}) f_T^n(\vec{k}')\; v_{ex}^{nn}(r)\, e^{i(\vec{k}-\vec{k}')\cdot\vec{r}}\, d^3k\; d^3k'\; d^3r \\ & + \frac{1}{2}\iiint f_T^p(\vec{k}) f_T^p(\vec{k}')\, v_{ex}^{pp}(r)\, e^{i(\vec{k}-\vec{k}')\cdot\vec{r}}\, d^3k\; d^3k'\; d^3r \\ & + \frac{1}{2}\iiint \left[f_T^n(\vec{k}) f_T^p(\vec{k}') + f_T^p(\vec{k}) f_T^n(\vec{k}')\right] v_{ex}^{np}(r)\, e^{i(\vec{k}-\vec{k}')\cdot\vec{r}}\, d^3k\; d^3k' d^3r \end{aligned} \tag{2.1.9}$$

With the use of the notation $v^{nn}(r) = v^{pp}(r) = v^{l}(r)$ and $v^{np}(r) = v^{ul}(r)$, the energy density $H_T(\rho_n, \rho_p)$ becomes,

$$\begin{aligned} H_T(\rho_n,\rho_p) = {} & \int [f_T^n(\vec{k}) + f_T^p(\vec{k})] \left(C^2\hbar^2k^2 + M^2C^4\right)^{1/2} d^3k \\ & + \frac{1}{2}(\rho_n^2 + \rho_p^2)\int v_d^{l}(r)\, d^3r + \rho_n\rho_p \int v_d^{ul}(r)\, d^3r \\ & + \frac{1}{2}\iint [f_T^n(\vec{k})\, f_T^n(\vec{k}') + f_T^p(\vec{k})\, f_T^p(\vec{k}')]\, g_{ex}^{l}(|\,\vec{k} - \vec{k}'\,|)\, d^3k\; d^3k' \\ & + \frac{1}{2}\iint [f_T^n(\vec{k})\, f_T^p(\vec{k}') + f_T^p(\vec{k})\, f_T^n(\vec{k}')]\, g_{ex}^{ul}(|\,\vec{k} - \vec{k}'\,|)\, d^3k\; d^3k', \end{aligned} \tag{2.1.10}$$

where, $g_{ex}^{l,ul}(|\,\vec{k} - \vec{k}'\,|)$ are Fourier transforms of the respective exchange interactions $v_{ex}^{l,ul}(r)$,

$$g_{ex}^{l,ul}(|\,\vec{k} - \vec{k}'\,|) = \int e^{i(\vec{k}-\vec{k}')\cdot\vec{r}}\, v_{ex}^{l,ul}(r)\, d^3r. \tag{2.1.11}$$

The single particle energies $\varepsilon_T^i(\vec{k}, \rho_n, \rho_p)$, $i = n, p$, are the respective functional derivatives of the energy density $H_T(\rho_n, \rho_p)$ and can be denoted as

$$\varepsilon_T^{n,p}(k,\rho,Y_p)=\frac{\partial H_T}{\partial[f_T^{n,p}]}. \tag{2.1.12}$$

The neutron single particle energy is, now, given by

$$\begin{aligned}\varepsilon_T^n(k,\rho,Y_p)&=(C^2\hbar^2k^2+M^2C^4)^{1/2}+\rho_n\int v_d^l(r)\,d^3r+\rho_p\int v_d^{ul}(r)\,d^3r\\&+\iint f_T^n(\vec{k}')e^{i(\vec{k}-\vec{k}')\cdot\vec{r}}\,v_{ex}^l(r)\,d^3r\,d^3k'+\iint f_T^p(\vec{k}')e^{i(\vec{k}-\vec{k}')\cdot\vec{r}}\,v_{ex}^{ul}(r)\,d^3r\,d^3k'\\&+\frac{(\rho_n^2+\rho_p^2)}{2}\int\frac{\partial v_d^l(r)}{\partial\rho_n}\,d^3r+\rho_n\rho_p\int\frac{\partial v_d^{ul}(r)}{\partial\rho_n}d^3r\\&+\frac{1}{2}\iiint[f_T^n(\vec{k})f_T^n(\vec{k}')+f_T^p(\vec{k})f_T^p(\vec{k}')]e^{i(\vec{k}-\vec{k}')\cdot\vec{r}}\,\frac{\partial v_{ex}^l(r)}{\partial\rho_n}d^3r\,d^3k\,d^3k'\\&+\frac{1}{2}\iiint[f_T^n(\vec{k})f_T^n(\vec{k}')+f_T^p(\vec{k})f_T^p(\vec{k}')]e^{i(\vec{k}-\vec{k}')\cdot\vec{r}}\,\frac{\partial v_{ex}^{ul}(r)}{\partial\rho_n}d^3r\,d^3k\,d^3k',\end{aligned} \tag{2.1.13}$$

and the proton single particle energy as

$$\begin{aligned}\varepsilon_T^p(k,\rho,Y_p)&=(C^2\hbar^2k^2+M^2C^4)^{1/2}+\rho_p\int v_d^l(r)\,d^3r+\rho_n\int v_d^{ul}(r)\,d^3r\\&+\iint f_T^p(\vec{k}')e^{i(\vec{k}-\vec{k}')\cdot\vec{r}}\,v_{ex}^l(r)\,d^3r\,d^3k'+\iint f_T^n(\vec{k}')e^{i(\vec{k}-\vec{k}')\cdot\vec{r}}\,v_{ex}^{ul}(r)\,d^3r\,d^3k'\\&+\frac{(\rho_n^2+\rho_p^2)}{2}\int\frac{\partial v_d^l(r)}{\partial\rho_p}\,d^3r+\rho_n\rho_p\int\frac{\partial v_d^{ul}(r)}{\partial\rho_p}d^3r\\&+\frac{1}{2}\iiint[f_T^n(\vec{k})f_T^n(\vec{k}')+f_T^p(\vec{k})f_T^p(\vec{k}')]e^{i(\vec{k}-\vec{k}')\cdot\vec{r}}\,\frac{\partial v_{ex}^l(r)}{\partial\rho_p}d^3r\;d^3k\,d^3k'\\&+\frac{1}{2}\iiint[f_T^n(\vec{k})f_T^n(\vec{k}')+f_T^p(\vec{k})f_T^p(\vec{k}')]e^{i(\vec{k}-\vec{k}')\cdot\vec{r}}\,\frac{\partial v_{ex}^{ul}(r)}{\partial\rho_p}d^3r\;d^3k\,d^3k'.\end{aligned} \tag{2.1.14}$$

In both the expressions of eqs. (2.1.13 and 2.1.14), the last three terms constitute the rearrangement part of the neutron and proton mean fields. Since the interactions $v_d^l(r)$, $v_{ex}^l(r)$, $v_d^{ul}(r)$ and $v_{ex}^{ul}(r)$ depend on $\rho=\rho_n+\rho_p$ and not separately on ρ_n and ρ_p, the neutron and proton rearrangement contributions to the respective mean fields will be the same and can be written as

$$U_T^R(\rho_n,\rho_p)=\frac{(\rho_n^2+\rho_p^2)}{2}\int\frac{\partial v_d^l(r)}{\partial\rho}d^3r+\rho_n\rho_p\int\frac{\partial v_d^{ul}(r)}{\partial\rho}d^3r$$
$$+\frac{1}{2}\iiint[f_T^n(\vec{k})f_T^n(\vec{k}')+f_T^p(\vec{k})f_T^p(\vec{k}')]e^{i(\vec{k}-\vec{k}')\cdot\vec{r}}\frac{\partial v_{ex}^l(r)}{\partial\rho}d^3r\,d^3k\,d^3k'$$
$$+\frac{1}{2}\iiint[f_T^n(\vec{k})f_T^n(\vec{k}')+f_T^p(\vec{k})f_T^p(\vec{k}')]e^{i(\vec{k}-\vec{k}')\cdot\vec{r}}\frac{\partial v_{ex}^{ul}(r)}{\partial\rho}d^3r\,d^3k\,d^3k'. \tag{2.1.15}$$

If we write the neutron and proton single particle energies as

$$\varepsilon_T^i(\mathrm{k},?_{\mathrm{n}},\rho_{\mathrm{p}})=(\mathrm{C}^2\hbar^2\mathrm{k}^2+\mathrm{M}^2\mathrm{C}^4)^{1/2}+\mathrm{u}_{\mathrm{T}}^{\mathrm{i}}(\mathrm{k},?_{\mathrm{n}},\rho_{\mathrm{p}}), \tag{2.1.16}$$

where $i=n,p$ and $\mathrm{u_T}^{\mathrm{i}}(\mathrm{k},?_{\mathrm{n}},\rho_{\mathrm{p}})$ are the single particle potentials or mean fields as felt in the nuclear medium by the respective nucleon, then the neutron mean field $u_T^n(k,\rho_n,\rho_p)$ at temperature T can, therefore, be given as

$$u_T^n(k,\rho_n,\rho_p)=\left[\rho_n\int\mathrm{v_d}^{l}(\mathrm{r})\mathrm{d}^3\mathrm{r}+\rho_p\int\mathrm{v_d}^{ul}(\mathrm{r})\mathrm{d}^3\mathrm{r}\right]$$
$$+\left[\int f_T^n(\vec{k}')g_{ex}^l(|\vec{k}-\vec{k}'|)d^3k'+f_T^p(\vec{k}')g_{ex}^{ul}(|\vec{k}-\vec{k}'|)d^3k'\right]$$
$$+U_T^R(\rho_n,\rho_p) \tag{2.1.17}$$

Similarly the proton mean field $u_T^p(k,\rho_n,\rho_p)$ at temperature T is given as

$$\mathrm{u_T^p}(\mathrm{k},?_{\mathrm{n}},\rho_{\mathrm{p}})=\left[\rho_p\int\mathrm{v_d}^{l}(\mathrm{r})\mathrm{d}^3\mathrm{r}+\rho_n\int\mathrm{v_d}^{ul}(\mathrm{r})\mathrm{d}^3\mathrm{r}\right]$$
$$+\left[\int f_T^p(\vec{k}')g_{ex}^l(|\vec{k}-\vec{k}'|)d^3k'+f_T^n(\vec{k}')g_{ex}^{ul}(|\vec{k}-\vec{k}'|)d^3k'\right]$$
$$+U_T^R(\rho_n,\rho_p) \tag{2.1.18}$$

The nuclear mean fields have three different parts, the first term coming from the direct part of the effective interaction and is explicitly density dependent, the second part comes from the exchange part of the effective interaction and depends upon the momentum k, neutron and proton distribution functions $f_T^{n,p}$ and temperature T. The third part of the nuclear mean field, U_T^R, is the rearrangement term.

In the studies of nuclear mean fields and EOS of ANM, the most important quantity is the difference between neutron and proton mean fields,

$$u_T^{n-p}(k,\rho,Y_p)=u_T^n(k,\rho,Y_p)-u_T^p(k,\rho,Y_p), \tag{2.1.19}$$

expressed as a function of momentum k, total nucleon density ? and proton fraction $Y_p = \frac{\rho_p}{\rho}$. Using the mean fields given in the above eqs. (2.1.18 and 2.1.19), $u_T^{n-p}(k,\rho,Y_P)$ can now be expressed as,

$$u_T^{n-p}(k,\rho,Y_p) = (1-2Y_p)\rho\int[v_d^l(r) - v_d^{ul}(r)]d^3r + \int[f_T^n(\vec{k}') - f_T^p(\vec{k}')][g_{ex}^l(|\vec{k}-\vec{k}'|) - g_{ex}^{ul}(|\vec{k}-\vec{k}'|)]d^3k' \quad (2.1.20)$$

The first term of $u_T^{n-p}(k,\rho,Y_p)$coming from direct parts of the interactions is independent of temperature and momentum and is directly proportional to the neutron–proton asymmetry $(1-2Y_p)$. The proportionality factor depends only on the total nucleon density ρ. On the other hand, the second part of $u_T^{n-p}(k,\rho,Y_p)$ coming from exchange parts of the interactions has a complicated dependence on temperature T, momentum k, total nucleon density ρ and proton fraction Y_p.

In order to examine the momentum dependence of $u_T^{n-p}(k,\rho,Y_p)$ we introduce a dimensionless quantity,

$$\frac{M}{\hbar^2 k}\frac{\partial u_T^{n-p}(k,\rho,Y_p)}{\partial k} = \frac{M}{\hbar^2 k}\frac{\partial}{\partial k}\left[\int[f_T^n(\vec{k}') - f_T^p(\vec{k}')][g_{ex}^l(|\vec{k}-\vec{k}'|) - g_{ex}^{ul}(|\vec{k}-\vec{k}'|)]d^3k'\right] \quad (2.1.21)$$

The dimensionless quantities $\frac{M}{\hbar^2 k}\frac{\partial u_T^{n,p}(\vec{k},\rho,Y_p)}{\partial k}$ in cases of neutron and proton are directly related to the effective masses $\left(\frac{M^*}{M}\right)_{n,p}$ as functions of k,ρ,Y_p and T. The nucleon effective masses arise from the momentum dependence of the mean fields $u_T{}^{n(p)}(k,\rho,Y_p)$ and are defined through the relation

$$\left\{\frac{1}{\mathrm{k}}\frac{\mathrm{d}}{\mathrm{dk}}(\mathrm{C}^2\hbar^2\mathrm{k}^2 + \mathrm{M}^2\mathrm{C}^4)^{1/2}\right\}_{\mathrm{M=M^*}} = \frac{1}{\mathrm{k}}\frac{\partial\varepsilon_T^{n,p}(\mathrm{k},?,\mathrm{Y_p})}{\partial\mathrm{k}}. \quad (2.1.22)$$

Using the expressions for $\varepsilon_T{}^{n(p)}(k,\rho,Y_p)$ given in eqs.(2.1.16 - 2.1.18), the ratio of effective nucleon masses to the actual mass can be obtained as,

$$\left[\frac{M^*(k,\rho,Y_p)}{M}\right]_T^{n(p)} = \left\{\left[\left(1+\frac{\hbar^2 k^2}{M^2C^2}\right)^{-1/2} + \frac{M}{\hbar^2 k}\frac{\partial u_T^{n(p)}(k,?,Y_p)}{\partial k}\right]^{-2} - \frac{\hbar^2 k^2}{M^2C^2}\right\}^{1/2}. \quad (2.1.23)$$

The dimensionless quantity $\frac{M}{\hbar^2 k}\frac{\partial u_T^{n-p}(k,\rho,Y_p)}{\partial k}$ has a complicated dependence on temperature T, momentum k, total nucleon density ρ and proton fraction Y_p for finite range exchange interactions. However, in the limit of very large k, we can approximate $g_{ex}^{l,ul}(|\vec{k}-\vec{k}'|)$ by $g_{ex}^{l,ul}(k)$ and eq.(2.1.21) reduces to

$$\frac{M}{\hbar^2 k}\frac{\partial u_T^{n-p}(k,\rho,Y_p)}{\partial k} \underset{large\ k}{\sim} (1-2Y_p)\rho\frac{M}{\hbar^2 k}\left[\frac{\partial g_{ex}^{l}(k)}{\partial k} - \frac{\partial g_{ex}^{ul}(k)}{\partial k}\right]. \quad (2.1.24)$$

This is a very important result in the sense that the dimensionless quantity in this limit of large k becomes independent of temperature and is directly proportional to the neutron-proton asymmetry parameter $(1-2Y_p)$. Now we can ascertain the asymptotic behaviour of neutron and proton effective masses from this expression in eq.(2.1.24). If the asymptotic behaviour of $\frac{M}{\hbar^2 k}\frac{\partial u_T^{n-p}(k,\rho,Y_p)}{\partial k}$ is positive, it implies that the neutron effective mass is less than the proton effective mass for given values of k,ρ and Y_p. If the asymptotic behaviour of $\frac{M}{\hbar^2 k}\frac{\partial u_T^{n-p}(k,\rho,Y_p)}{\partial k}$ is negative, it implies that the proton effective mass is less than the neutron effective mass for given values of k,ρ and Y_p.

In connection with the splitting of neutron and proton effective masses in asymmetric nuclear matter it may be mentioned here that the results obtained from different theoretical calculations can be roughly classified into two groups: one in which the neutron effective mass goes above that of proton and conversely in the other case, i.e., the proton effective mass goes above that of neutron. The results obtained from Brueckener-Hatree-Fock (BHF) calculations with realistic nucleon-nucleon interactions [117-119] show that the neutron effective mass goes above that of proton, whereas, the

results obtained in some of the earlier calculations in relativistic Dirac-Brueckener Hatree-Fock (DBHF) model [120] and the relativistic mean field (RMF) calculations using quantum hadrodynamics (QHD) [105,107] exhibit an opposite type of splitting of neutron and proton effective masses. Since the asymptotic behaviour of $\frac{M}{\hbar^2 k}\frac{\partial u_T^{n-p}(k,\rho,Y_p)}{\partial k}$ is proportional to the total nucleon density ρ and the neutron-proton asymmetry parameter $(1-2Y_p)$, the splitting of neutron and proton effective masses can be small in finite nuclei where both ρ and $(1-2Y_p)$ are rather small [106]. However, this difference in neutron and proton effective masses may be quite relevant for the difference between neutron and proton transport properties in highly asymmetric and dense nuclear matter. Such situations can be encountered in astrophysical objects, such as, neutron stars and supernovae matter and in the terrestrial laboratory in high energy heavy-ion collision experiments using radioactive ion beams. Neutron stars are cold objects $(T=0)$ whereas in supernovae matter and the matter formed in the HI collision experiments the temperature is high.

Since the momentum dependent term in the neutron and proton mean fields involve in Fermi-Dirac momentum distribution functions, it implies that the neutron and proton single particle energies, chemical potentials and the distribution functions should be calculated in a self-consistent way at each temperature T, proton fraction Y_p and nuclear density $\rho=\rho_n+\rho_p$. For this purpose an iterative procedure similar to that used in Ref. [65] for SNM can be adopted. The basic input in these self-consistent evaluations are the respective single particle energies at zero temperature, $\varepsilon^{n,p}(k,\rho,Y_p)$. The temperature dependence of nuclear matter properties are therefore built upon the zero temperature results of neutron and proton mean fields $u^{n,p}(\vec{k},\rho,Y_p)$ and hence these are quantities of crucial importance. At zero temperature, $T=0$, the neutron, proton distribution functions take the forms of step functions

$$f^{n,p}(\vec{k})=\frac{\xi}{(2\pi)^3}\theta(k_{n(p)}-k), \tag{2.1.25}$$

where, the neutron and proton Fermi momenta $k_{n(p)}$ are related to the respective densities $\rho_n(\rho_p)$ as $k_n^3 = 3\pi^2\rho_n$ $(k_p^3 = 3\pi^2\rho_p)$. With this, further analytical simplifications of the exchange integrals involving the distribution functions in the expressions of $\varepsilon^{n,p}(k,\rho,Y_p)$ given in eqs (2.1.17 and 2.1.18) can be performed by evaluating the k' – integrations,

$$\iint d^3r\, d^3k'\, f_T^n(\vec{k}')e^{i(\vec{k}-\vec{k}').\vec{r}}v_{ex}^l(r) \underline{\underline{T=0}} \frac{2}{(2\pi)^3}\int d^3r\, e^{i\vec{k}.\vec{r}}v_{ex}^l(r)\int\theta(k_n-k')e^{-i\vec{k}'.\vec{r}}\, d^3k'$$

$$= \rho_n \int d^3r\, j_0(kr)\frac{3j_1(k_nr)}{k_nr}v_{ex}^l(r). \qquad (2.1.26)$$

Similarly, the other exchange integrals in eqs (2.1.17 and 2.1.18) can be analytically simplified and the expressions of $u^{n,p}(k,\rho,Y_p)$ at $T=0$ become,

$$u^n(k,\rho,Y_p) = \left[\rho_n \int v_d{}^l(r)d^3r + \rho_p \int v_d{}^{ul}(r)d^3r\right] + \rho_n \int j_0(kr)\frac{3j_1(k_nr)}{k_nr}v_{ex}^l(r)\,d^3r$$

$$+\rho_p \int j_0(kr)\frac{3j_1(k_pr)}{k_pr}v_{ex}^{ul}(r)\,d^3r + U^R(\rho_n,\rho_p) \qquad (2.1.27)$$

and

$$u^p(k,\rho,Y_p) = \left[\rho_p \int v_d{}^l(r)d^3r + \rho_n \int v_d{}^{ul}(r)d^3r\right] + \rho_p \int j_0(kr)\frac{3j_1(k_pr)}{k_pr}v_{ex}^l(r)\,d^3r$$

$$+\rho_n \int j_0(kr)\frac{3j_1(k_nr)}{k_nr}v_{ex}^{ul}(r)\,d^3r + U^R(\rho_n,\rho_p). \qquad (2.1.28)$$

The rearrangement energy $U^R(\rho_n,\rho_p)$ at zero temperature appearing in these equations can be written as,

$$U^R(\rho_n,\rho_p) = \frac{(\rho_n^2+\rho_p^2)}{2}\int v_d^l(r)d^3r + \rho_n\rho_p\int v_d^{ul}(r)\,d^3r$$

$$+\frac{(\rho_n^2+\rho_p^2)}{2}\int\left[\left(\frac{3j_1(k_nr)}{k_nr}\right)^2+\left(\frac{3j_1(k_pr)}{k_pr}\right)^2\right]\frac{\partial v_{ex}^l)r)}{\partial\rho}d^3r$$

$$+\frac{\rho_n\rho_p}{2}\int\frac{3j_1(k_nr)}{k_nr}\,\frac{3j_1(k_pr)}{k_pr}\,\frac{\partial v_{ex}^{ul})r)}{\partial\rho}d^3r. \qquad (2.1.29)$$

The difference in neutron and proton mean fields, $u^{n-p}(k,\rho,Y_p)$, at zero temperature, $T=0$, can now be obtained from eqs (2.1.17 and 2.1.18) as,

$$\begin{aligned} u^{n-p}(k,\rho,Y_p) &= u^{n}(k,\rho,Y_p) - u^{p}(k,\rho,Y_p) \\ &= (1-2Y_p)\rho \int \left[v_d^{l}(r) - v_d^{ul}(r) \right] d^3r \\ &\quad + \int \left[\rho_n \frac{3j_1(k_n r)}{k_n r} - \rho_p \frac{3j_1(k_p r)}{k_p r} \right] \left(v_{ex}^{l}(r) - v_{ex}^{ul}(r) \right) j_0(kr)\, d^3r. \end{aligned} \tag{2.1.30}$$

The direct part of $u^{n-p}(k,\rho,Y_p)$ is proportional to the isospin asymmetry $(1-2Y_p)$. The proportionality factor being a function of total density ρ. The exchange part of $u^{n-p}(k,\rho,Y_p)$ is also approximately proportional to $(1-2Y_p)$ that can be shown by making a Taylor series expansion of the square bracketed term in the second integral about $Y_p=\frac{1}{2}$ (i.e. $(1-2Y_p)$=0),

$$\begin{aligned} \left[\rho_n \frac{3j_1(k_n r)}{k_n r} - \rho_p \frac{3j_1(k_p r)}{k_p r} \right] &= \left[\rho_n \frac{3j_1(k_n r)}{k_n r} - \rho_p \frac{3j_1(k_p r)}{k_p r} \right]_{Y_p=\frac{1}{2}} \\ &\quad + (1-2Y_p) \left(-\frac{1}{2}\frac{\partial}{\partial Y_p} \right) \left[\rho_n \frac{3j_1(k_n r)}{k_n r} - \rho_p \frac{3j_1(k_p r)}{k_p r} \right]_{Y_p=\frac{1}{2}} + \ldots\ldots \end{aligned} \tag{2.1.31}$$

The first term in the right hand side is zero since at $Y_p=\frac{1}{2}$, $\rho_n=\rho_p=\frac{\rho}{2}$ and, $k_n=k_p=k_f$, k_f being the Fermi momentum in SNM. Hence

$$\left[\rho_n \frac{3j_1(k_n r)}{k_n r} - \rho_p \frac{3j_1(k_p r)}{k_p r} \right] = (1-2Y_p)\rho\, j_0(k_f r) + \text{ higher order terms.} \tag{2.1.32}$$

The function $u^{n-p}(k,\rho,Y_p)$ can now be written as

$$\begin{aligned} u^{n-p}(k,\rho,Y_p) &= (1-2Y_p)\rho \int [v_d^{l}(r) - v_{ex}^{ul}(r)]\, d^3r \\ &\quad + (1-2Y_p)\rho \int j_0(kr) j_0(k_f r) (v_{ex}^{l}(r) - v_{ex}^{ul}(r)\, d^3r \\ &\quad + \text{higher order terms in } (1-2Y_p). \end{aligned} \tag{2.1.33}$$

The higher order terms in this expression will involve only odd powers of $(1-2Y_p)$ as the terms having even powers of $(1-2Y_p)$ in the Taylor series expansion will

identically vanish. We now introduce the isovector part of the nuclear mean field defined as,

$$u_\tau(k,\rho) = \underset{Y_p \to 1/2}{Lim} \frac{u^{n-p}(k,\rho,Y_p)}{2(1-2Y_p)}. \tag{2.1.34}$$

Using eq.(2.1.33) this can be written as

$$u_\tau(k,\rho) = \frac{\rho}{2}\left[\int\left(v_d^l(r) - v_d^{ul}(r)\right)d^3r + \int j_0(kr)\, j_0(k_f r)\left(v_{ex}^l(r) - v_{ex}^{ul}(r)\right)d^3r\right]. \tag{2.1.35}$$

The justification of the approximation of the Taylor series expansion of $\left[\rho_n \frac{3j_1(k_n r)}{k_n r} - \rho_p \frac{3j_1(k_p r)}{k_p r}\right]$ by the first term can be examined in the followings:

$$\int\left[\rho_n \frac{3j_1(k_n r)}{k_n r} - \rho_p \frac{3j_1(k_p r)}{k_p r}\right] j_0(kr)\left[v_{ex}^l(r) - v_{ex}^{ul}(r)\right]d^3r \cong (1-2Y_p)\rho \int j_0(kr)\, j_0(k_f r)\left[v_{ex}^l(r) - v_{ex}^{ul}(r)\right]d^3r. \tag{2.1.36}$$

Under the assumption that the finite range parts of the exchange interactions between like and unlike nucleon pairs have same range but different strengths, the above equation becomes

$$\int\left[\rho_n \frac{3j_1(k_n r)}{k_n r} - \rho_p \frac{3j_1(k_p r)}{k_p r}\right] j_0(kr)\, f(r)\, d^3r \cong (1-2Y_p)\rho \int j_0(kr)\, j_0(k_f r)\, f(r)\, d^3r, \tag{2.1.37}$$

where, $f(r)$ is the functional form of the finite range exchange interaction. The Taylor series expansion is valid for low value of the asymmetry $(1-2Y_p)$ and hence the validity of the inequality in eq. (2.1.37) is to be tested at the other extreme, i.e. $Y_p = 0$, which is the pure neutron matter (PNM) limit. In this limit eq.(2.1.37) becomes

$$\rho_n \int \frac{3j_1(k_n r)}{k_n r} j_0(kr)\, f(r)\, d^3r \cong \rho \int j_0(kr)\, j_0(k_f r)\, f(r)\, d^3r. \tag{2.1.38}$$

Further, both the integrals have maximum values in the limit $k \to 0$ and the above equation in this limit becomes

$$\rho_n \int \frac{3j_1(k_n r)}{k_n r} f(r) d^3 r \cong \rho \int j_0(k_f r) f(r) d^3 r \tag{2.1.39}$$

with $\rho_n = \rho$, $k_n = 3\pi^2 \rho$ and $k_f = \frac{3\pi^2 \rho}{2}$.

Comparison of the values of the integrals on both the sides of the above inequality at different densities can give the degree of correctness of the approximation used in obtaining the isovector part of nuclear mean field in eq. (2.1.35). For the sake of enumeration, we shall use a Yukawa functional form $f(r) = \frac{e^{-r/\alpha}}{(r/\alpha)}$, α being the range parameter. The integrals given in the above inequality can be analytically evaluated and the condition in eq.(2.1.39) becomes,

$$3\left(\frac{1}{(k_n\alpha)^2} - \frac{\tan^{-1}(k_n\alpha)}{(k_n\alpha)^3}\right) \cong \frac{1}{1+(k_f\alpha)^2}. \tag{2.1.40}$$

Defining $x = k_n \alpha$, this equation reduces to

$$3\left(\frac{1}{x^2} - \frac{\tan^{-1} x}{x^3}\right) \cong \frac{1}{1+(0.5)^{2/3} x^2} \tag{2.1.41}$$

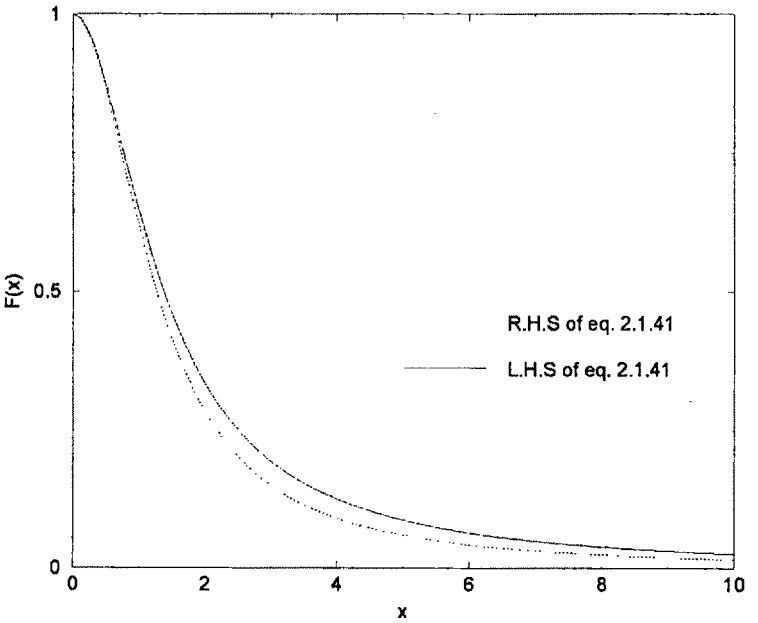

Figure 2.1. Comparison of the left hand side and the right hand side of the eq.(2.1.41) as a function of x.

In Figure 2.1, the left hand side and right hand side of the above eq. (2.1.41) have been compared. The comparison shows that the approximation used to obtain the isovector part of the nuclear mean field $u_\tau(k,\rho)$ given in eq. (2.1.35) is a valid one.

The momentum and density dependence of isovector part of the mean field $u_\tau(k,\rho)$ is crucial in understanding the in-medium nuclear interaction and it is an area in nuclear physics which is poorly understood. The isovector part of the nuclear mean field at Fermi momentum, $u_\tau(k=k_f,\rho)$, is directly connected to the nuclear symmetry energy $E_s(\rho)$, which is shown in the followings. The nuclear symmetry energy is defined as

$$E_s(\rho)=\frac{1}{8\rho}\left(\frac{\partial^2 H(\rho,Y_p)}{\partial {Y_p}^2}\right)\Bigg|_{Y_p=\frac{1}{2}} \tag{2.1.42}$$

where, $H(\rho,Y_p)$ is the energy density of ANM at zero temperature. The expression for $H(\rho,Y_p)$ can be obtained from eqs.(2.1.10 and 2.1.11) by considering the distribution functions to be step functions and the analytical simplification results into the expression for energy density at $T=0$ in ANM as,

$$\begin{aligned}H(\rho,Y_p)=&\frac{3MC^2}{8{x_f}^3}\rho\left[2x_f{u_f}^3-x_fu_f-\ln(x_f+u_f)\right]+\frac{({\rho_n}^2+{\rho_p}^2)}{2}\int v_d^l(r)d^3r\\&+\rho_n\rho_p\int v_d^{ul}(r)d^3r+\frac{{\rho_n}^2}{2}\int\left(\frac{3j_1(k_nr)}{k_nr}\right)^2 v_{ex}^l(r)d^3r+\frac{{\rho_p}^2}{2}\int\left(\frac{3j_1(k_pr)}{k_pr}\right)^2 v_{ex}^l(r)d^3r\\&+\rho_n\rho_p\int\frac{3j_1(k_nr)}{k_nr}\frac{3j_1(k_pr)}{k_pr}v_{ex}^{ul}(r)\,d^3r.\end{aligned} \tag{2.1.43}$$

In the limit of SNM, i.e. $\rho_n=\rho_p=\frac{\rho}{2}$ and $k_n=k_p=k_f$, the energy density becomes

$$\begin{aligned}H_0(\rho)=&\frac{3MC^2}{8{x_f}^3}\rho\left[2x_f{u_f}^3-x_fu_f-\ln(x_f+u_f)\right]+\frac{\rho^2}{4}\int\left[v_d^l(r)+v_d^{ul}(r)\right]d^3r\\&+\frac{\rho^2}{4}\int\left(\frac{3j_1(k_fr)}{k_fr}\right)^2\left[v_{ex}^l(r)+v_{ex}^{ul}(r)\right]d^3r\end{aligned} \tag{2.1.44}$$

where, $x_f=\frac{\hbar k_f}{MC}$ and $u_f=(1+x_f)^{1/2}$.

The symmetry energy defined in eq.(2.1.42) for the energy density in eq.(2.1.43) can be expressed as,

$$E_s(\rho)=\frac{\hbar^2 {k_f}^2}{6M}\left(1+\frac{\hbar^2 {k_f}^2}{M^2C^2}\right)^{-1/2}+\frac{\rho}{4}\int\left(v_d^l(r)-v_d^{ul}(r)\right)d^3r$$
$$+\frac{\rho}{4}\int {j_0}^2(k_f r)\left(v_{ex}^l(r)-v_{ex}^{ul}(r)\right)d^3r\ -\frac{\rho}{4}\int {j_1}^2(k_f r)\left(v_{ex}^l(r)+v_{ex}^{ul}(r)\right)d^3r. \tag{2.1.45}$$

The last term along with the kinetic energy contribution given in the first term in right hand side of this expression is related to the effective mass at Fermi momentum in SNM. The effective mass in SNM is defined as,

$$\left[\frac{\mathrm{M}^*}{\mathrm{M}}(\mathrm{k},\rho)\right]=\left\{\left[\left(1+\frac{\hbar^2\mathrm{k}^2}{\mathrm{M}^2\mathrm{C}^2}\right)^{-1/2}+\frac{\mathrm{M}}{\hbar^2\mathrm{k}}\frac{\partial \mathrm{u(k,?)}}{\partial \mathrm{k}}\right]^{-2}-\frac{\hbar^2\mathrm{k}^2}{\mathrm{M}^2\mathrm{C}^2}\right\}^{1/2} \tag{2.1.46}$$

where, $u(k,\rho)$ is the isoscalar part of the mean field, i.e., the mean field of a nucleon in SNM at zero temperature and is defined as

$$u(k,\rho)=\underset{Y_p\to 1/2}{Lim}\frac{u^n(k,\rho,Y_p)+u^p(k,\rho,Y_p)}{2}. \tag{2.1.47}$$

From the expressions of $u^n(k,\rho,Y_p)$ and $u^p(k,\rho,Y_p)$ in eqs.(2.1.27) and (2.1.28), the isoscalar part of the nuclear mean field is obtained to be

$$u(k,\rho)=(C^2\hbar^2k^2+M^2C^4)^{1/2}$$
$$+\frac{\rho}{2}\int\left[v_d^l(r)+v_d^{ul}(r)\right]d^3r+\frac{\rho}{2}\int j_0(kr)\frac{3j_1(k_f r)}{k_f r}\left[v_{ex}^l(r)+v_{ex}^{ul}(r)\right]d^3r+U^R(\rho) \tag{2.1.48}$$

where,

$$U^R(\rho)=\underset{\substack{\rho_n=\rho_n=\rho/2\\ k_n=k_p=k_f}}{Lim}U^R(\rho_n,\rho_p) \tag{2.1.49}$$

From this expression for $u(k,\rho)$ it follows that,

$$\left(\frac{k}{3}\frac{\partial u(k,\rho)}{\partial k}\right)_{k=k_f}=-\frac{\rho}{2}\int {j_1}^2(k_f r)\left(v_{ex}^l(r)+v_{ex}^{ul}(r)\right)d^3r. \tag{2.1.50}$$

Thus, $E_s(\rho)$ as given in eq.(2.1.45) becomes

$$E_s(\rho)=\frac{\hbar^2 k_f{}^2}{6M}\left(1+\frac{\hbar^2 k_f{}^2}{M^2C^2}\right)^{-1/2}+\left(\frac{k}{6}\frac{\partial u(k,\rho)}{\partial k}\right)_{k=k_f}$$
$$+\frac{\rho}{4}\int\left(v_d^l(r)-v_d^{ul}(r)\right)d^3r \;+\; \frac{\rho}{4}\int j_0{}^2(k_f r)\left(v_{ex}^l(r)-v_{ex}^{ul}(r)\right)d^3r. \tag{2.1.51}$$

Now, the first two terms in this expression can be expressed in terms of the effective mass in SNM at Fermi momentum given in eq.(2.1.46) and the nuclear symmetry energy given in the last equation becomes,

$$E_s(\rho)=\frac{\hbar^2 k_f{}^2}{6M}\left[\left(\frac{M^*}{M}(k,\rho)\right)^2+\frac{\hbar^2 k_f{}^2}{M^2C^2}\right]^{-1/2}_{k=k_f}$$
$$+\frac{\rho}{4}\int\left(v_d^l(r)-v_d^{ul}(r)\right)d^3r \;+\; \frac{\rho}{4}\int j_0{}^2(k_f r)\left(v_{ex}^l(r)-v_{ex}^{ul}(r)\right)d^3r. \tag{2.1.52}$$

With this definitions for nuclear symmetry energy $E_s(\rho)$, the isovector part of the nuclear mean field given in eq.(2.1.35) can be expressed as,

$$u_\tau(k,\rho)=2E_s(\rho)-\frac{\hbar^2 k_f{}^2}{3M}\left[\left(\frac{M^*}{M}(k,\rho)\right)^2+\frac{\hbar^2 k_f{}^2}{M^2C^2}\right]^{-1/2}_{k=k_f}$$
$$+\frac{\rho}{2}\int\left[j_0(kr)-j_0(k_f r)\right]j_0(k_f r)\left(v_{ex}^l(r)-v_{ex}^{ul}(r)\right)d^3r. \tag{2.1.53}$$

This equation has the crucial implication that the density dependence of isovector part of the mean field, $u_\tau(k,\rho)$, has been separated out from its momentum dependence. The momentum dependence of $u_\tau(k,\rho)$ is determined by the last term of the above equation which we shall be denoting by

$$u_\tau^{ex}(k,\rho)=\frac{\rho}{2}\int\left[j_0(kr)-j_0(k_f r)\right]j_0(k_f r)\left(v_{ex}^l(r)-v_{ex}^{ul}(r)\right)d^3r \tag{2.1.54}$$

and is solely dependent on the differences between finite range exchange interactions between pairs of like and unlike nucleons. It may be noted that for contact interactions of $\delta(r)$ – form $u_\tau(k,\rho)$ is determined by evaluating it at Fermi momentum, i.e., $u_\tau(k=k_f,\rho)$. In this limit of $k=k_f$, as may be seen from eq.(2.1.54), the function $u_\tau^{ex}(k,\rho)$ vanishes resulting the expression for $u_\tau^{ex}(k=k_f,\rho)$ to be

$$u_\tau(k=k_f,\rho)=2E_s(\rho)-\frac{\hbar^2 {k_f}^2}{3M}\left[\left(\frac{M^*}{M}(k,\rho)\right)^2+\frac{\hbar^2k^2}{M^2C^2}\right]^{-1/2}_{k=k_f}. \qquad (2.1.55)$$

Thus, the density dependence of the isovector part of the nuclear mean field is completely determined by the density dependence of nuclear symmetry energy $E_s(\rho)$ and the density dependence of effective mass in SNM. The complete knowledge of nuclear properties lies in the understanding of momentum and density dependence of nuclear mean fields both in SNM as well as in ANM. Thus, before making further discussions on the momentum and density dependence of nuclear mean field in ANM it will be of crucial advantage to separate out the density dependence of the isoscalar part of nuclear mean field as given eq.(2.1.48) (i.e. the nuclear mean field in SNM) from its momentum dependence.

The energy per particle in SNM at zero temperature, $e_0(\rho)$is obtained from the energy density, $H_0(\rho)=\rho\, e_0(\rho)$, given in eq.(2.1.43) to be

$$e_0(\rho)=\frac{3MC^2}{8{x_f}^3}\left[2x_f{u_f}^3-x_fu_f\ln(x_f+u_f)\right]+\frac{\rho}{4}\int\left[v_d^l(r)+v_d^{ul}(r)\right]d^3r$$
$$+\frac{\rho}{4}\int\left(\frac{3j_1(k_fr)}{k_fr}\right)^2\left[v_{ex}^l(r)+v_{ex}^{ul}(r)\right]d^3r. \qquad (2.1.56)$$

We can calculate $\rho\dfrac{de_0(\rho)}{d\rho}$ from the above equation to be,

$$\rho\frac{de_0(\rho)}{d\rho}=K.E.\,part+\frac{\rho}{4}\int\left[v_d^l(r)+v_d^{ul}(r)\right]d^3r+\frac{\rho}{4}\int j_0(k_fr)\left(\frac{3j_1(k_fr)}{k_fr}\right)\left[v_{ex}^l(r)+v_{ex}^{ul}(r)\right]d^3r$$
$$+\left\{\frac{\rho^2}{4}\int\left(\frac{\partial v_d^l(r)}{\partial\rho}+\frac{\partial v_d^{ul}(r)}{\partial\rho}\right)d^3r+\frac{\rho^2}{4}\int\left(\frac{\partial v_{ex}^l(r)}{\partial\rho}+\frac{\partial v_{ex}^{ul}(r)}{\partial\rho}\right)\left(\frac{3j_1(k_fr)}{k_fr}\right)d^3r\right\}. \qquad (2.1.57)$$

The single particle energy in SNM $\varepsilon(k,\rho)$ at zero temperature is given by $\varepsilon(k,\rho)=\left(C^2\hbar^2k^2+M^2C^4\right)^{1/2}+u(k,\rho)$. From eqs. (2.1.56), (2.1.57) and (2.1.48), it follows that

$$e_0(\rho)+\rho\frac{de_0(\rho)}{d\rho}=\varepsilon(k=k_f,\rho) \tag{2.1.58}$$

which is the Hugenoltz-VanHoff (HV) theorem, where

$$\varepsilon(k=k_f,\rho)=\left(C^2\hbar^2k_f{}^2+M^2C^4\right)^{1/2}+u(k=k_f,\rho). \tag{2.1.59}$$

By using the HV theorem, the isoscalar part of the nuclear mean field can be written as

$$u(k,\rho)=e_0(\rho)+\rho\frac{de_0(\rho)}{d\rho}-\left(C^2\hbar^2k_f{}^2+M^2C^4\right)^{1/2}+u^{ex}(k,\rho) \tag{2.1.60}$$

where,

$$u^{ex}(k,\rho)=\frac{\rho}{2}\int\left[j_0(kr)-j_0(k_fr)\right]\frac{3j_1(k_fr)}{k_fr}\left(v_{ex}^{l}(r)+v_{ex}^{ul}(r)\right)d^3r. \tag{2.1.61}$$

These last two equations in the case of SNM are analogous to eqs.(2.1.54) and (2.1.55) of ANM respectively. The momentum dependence of nuclear mean field in SNM is solely determined by the functional $u^{ex}(k,\rho)$ given in eq.(2.1.61) and depends on the sum of the finite range exchange interactions between pairs of like and unlike nucleons. $u^{ex}(k,\rho)$ identically vanishes for contact interactions of $\delta(r)$-form. The density dependence of $u(k,\rho)$ is determined at $k=k_f$ and from eqs.(2.1.60 and 2.1.61) , it follows that,

$$\begin{aligned}u(k=k_f,\rho)&=e_0(\rho)+\rho\frac{de_0(\rho)}{d\rho}-\left(C^2\hbar^2k_f{}^2+M^2C^4\right)^{1/2}\\&=e_0(\rho)+\frac{P(\rho)}{\rho}-\left(C^2\hbar^2k_f{}^2+M^2C^4\right)^{1/2}\end{aligned} \tag{2.1.62}$$

where , $P(\rho)=\rho^2\dfrac{de_0(\rho)}{d\rho}$ is the pressure in SNM. Thus, the density dependence of isoscalar mean field is determined by the energy per particle $e_0(\rho)$ in SNM.

It should be remarked here that in eqs.(2.1.53 and 2.1.54) and (2.1.61 and 2.1.62) we have a connection to very old and open problems; momentum and density dependence of the Lane potentials [152] which we see in a much more general framework. It is important to note here that only finite range parts of the exchange interactions between two like and unlike nucleons can contribute to $u^{ex}(k,\rho)$ and $u_\tau^{ex}(k,\rho)$. Moreover, these two functional vanish at the Fermi momentum $k=k_f$. In

the simplest form, momentum and density dependence of the functional $u^{ex}(k,\rho)$ and $u_\tau^{ex}(k,\rho)$ can be simulated by a conventional short range attractive interaction of Yukawa, Gaussian or exponential form having the same range α but different strengths ε_{ex}^{l} and ε_{ex}^{ul} for interactions between two like and unlike nucleons. For these forms of interactions considered in this simplest way, the exchange integrals appearing in eqs.(2.1.61) and (2.1.54) can be calculated analytically[64]. Under this simple consideration, Behera *et al.* have formulated and studied the momentum and density dependence of nuclear mean fields in SNM [64] and ANM [153, 154] which we shall discuss in the followings. In the case of such simple finite range exchange interactions, the exchange integral functions in SNM and ANM can be given as,

$$u^{ex}(k,\rho)=\frac{\left(\varepsilon_{ex}^{l}+\varepsilon_{ex}^{ul}\right)}{2\rho_0\int f(r)d^3r}\rho\int\left[j_0(kr)-j_0(k_f r)\right]\frac{3j_1(k_f r)}{k_f r}f(r)d^3r \tag{2.1.63}$$

and

$$u_\tau^{ex}(k,\rho)=\frac{\left(\varepsilon_{ex}^{l}-\varepsilon_{ex}^{ul}\right)}{2\rho_0\int f(r)d^3r}\rho\int\left[j_0(kr)-j_0(k_f r)\right]j_0(k_f r)f(r)d^3r \tag{2.1.64}$$

where, $f(r)$ is the functional form of the short range interaction of Yukawa, Gaussian or exponential form having the range α. The strength parameters ε_{ex}^{l} and ε_{ex}^{ul} are given by

$$\varepsilon_{ex}^{l}=\rho_0\left(M-\frac{W}{2}+\frac{H}{2}-B\right)\int f(r)d^3r \tag{2.1.65}$$

and

$$\varepsilon_{ex}^{ul}=\rho_0\left(M+\frac{H}{2}\right)\int f(r)d^3r. \tag{2.1.66}$$

Here, M,W,H and B represent the Majorana, Wigner, Heisenberg and Bartlett parts of the short range exchange interactions respectively. The analytical simplifications of these integrals $u^{ex}(k,\rho)$ and $u_\tau^{ex}(k,\rho)$ can be done by using the following prescriptions [64] given by,

$$\frac{1}{\int f(r)d^3r}\int j_0(kr)\frac{3j_1(k_f r)}{k_f r}f(r)d^3r=I(k,\rho) \tag{2.1.67}$$

with

$$I(k,\rho)=\frac{3\Lambda^2(\Lambda^2+k_f{}^2-k^2)}{8kk_f{}^3}\ln\left\{\frac{\Lambda^2+(k+k_f)^2}{\Lambda^2+(k-k_f)^2}\right\} + \frac{3\Lambda^2}{2k_f{}^2}-\frac{3\Lambda^3}{2k_f{}^3}\left\{\tan^{-1}\left(\frac{k+k_f}{\Lambda}\right)-\tan^{-1}\left(\frac{k-k_f}{\Lambda}\right)\right\} \tag{2.1.68}$$

and

$$\frac{1}{\int f(r)d^3r}\int j_0(kr)\,j_0(k_f r)\,f(r)\,d^3r = I_\tau(k,\rho) \tag{2.1.69}$$

with

$$I_\tau(k,\rho)=\frac{\Lambda^2}{4k_f{}^2}\ln\left(1+4\frac{k_f{}^2}{\Lambda^2}\right), \tag{2.1.70}$$

for the Yukawa form of finite range exchange interaction, $f(r)=\frac{e^{-r/\alpha}}{(r/\alpha)}$ and $\Lambda=1/\alpha$. Analogous analytical expressions can be obtained for the other forms of interaction.

There have been consistent attempts to constrain these parameters, ε_{ex}^{l}, ε_{ex}^{ul} and α over last few decades from analysis of nucleon-nucleus scattering of data at intermediate energies as well as from the studies of experimental observables sensitive to the differences between neutron and proton flow data in high energy heavy ion collisions [56, 59-60, 63, 65,67]. Considerable progress has been made in the understanding of the isoscalar part of the nuclear mean field, i.e., in constraining α and the strength parameter combination $(\varepsilon_{ex}^{l}+\varepsilon_{ex}^{ul})$. In the following we have discussed the procedure used by Behera *et al.* [64], in constraining these parameters. They have used the condition that the optical potential, $u(k,\rho=\rho_0)$, should vanish at kinetic energy of the nucleon $\left(C^2\hbar^2k_{300}{}^2+M^2C^4\right)^{1/2}=1239\ MeV$. This important feature follows from the optical model fits to nucleon-nucleus scattering data at intermediate energies that $u(k,\rho_0)$ turns out to be repulsive for momenta around $k>k_{300}$, where, k_{300} corresponds to a kinetic energy of 300 MeV (excluding rest mass energy). Using this constraint for the optical potential $u(k,\rho_0)$, it follows from eqs.(2.1.62 and 2.1.63) that

$$\left[I(k=k_{300},\rho_0)-I(k=k_{f_0},\rho_0)\right]=\frac{\left(C^2\hbar^2k_{f_0}{}^2+M^2C^4\right)^{1/2}-e_0(\rho_0)}{\left(\frac{\varepsilon_{ex}^{l}+\varepsilon_{ex}^{ul}}{2}\right)} \tag{2.1.71}$$

where, $k_{f_0} = \left(3\pi^2 \rho_0 / 2\right)^{1/3}$ is the Fermi momentum corresponding to normal nuclear matter density ρ_0 and $e_0(\rho_0)$ is the energy per particle of nuclear matter at ρ_0. For the Yukawa form, the analytical expressions of the functional $I(k,\rho)$ is given in eq.(2.1.68) which involves only the range parameter α. By adopting a simultaneous minimization procedure, Behera *et al.*[65] have obtained the values of these two parameters, range and strength in SNM, for the Yukawa form of the exchange interaction to be,

$$\varepsilon_{ex} = (\varepsilon_{ex}^{l} + \varepsilon_{ex}^{ul})/2 = -121.8448 \text{ MeV}$$

$$\alpha = 0.4044 \text{ fm.} \qquad (2.1.72)$$

In obtaining these results only the standard values of $MC^2 = 939 MeV$, $e_0(\rho_0) = 923\, MeV$ and $\left(C^2\hbar^2 {k_{f_0}}^2 + M^2C^4\right)^{1/2} = 976\, MeV$ (corresponding to $\rho_0 = 0.1658\, fm^{-3}$) have been used. The result of the minimization method adopted is shown in Figure 2.2. Constraining the finite range exchange strength parameter combination, $(\varepsilon_{ex}^{l} + \varepsilon_{ex}^{ul})$ and range parameter α in this way, the results of the

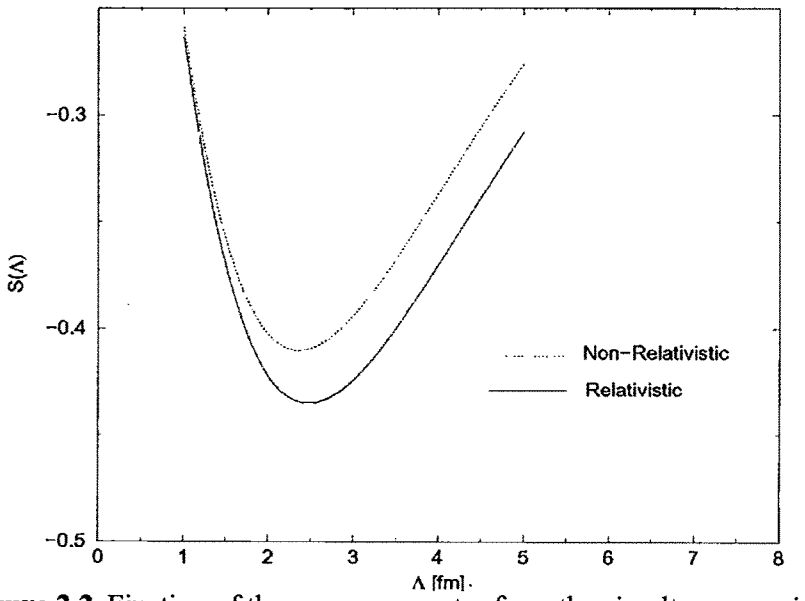

Figure 2.2. Fixation of the range parameter from the simultaneous minimization of α and ε_{ex}. The functional $S(\Lambda) = \left[I(k = k_{300}, \rho_0) - I(k = k_{f_0}, \rho_0)\right]$ is plotted as a function of Λ. The minimum of the curve for $S(\Lambda)$ gives the respective range α of the interaction.

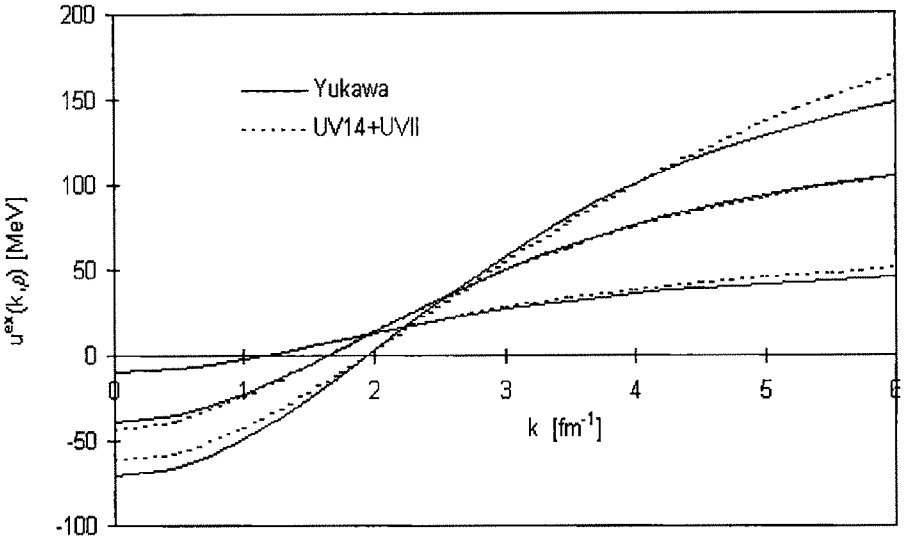

Figure 2.3. The exchange contribution to the isoscalar part of the nuclear mean field $u^{ex}(k,\rho)$ in SNM is plotted as a function of Fermi momentum k for three representative values of density. The lower curves is for $\rho = 0.1\ fm^{-3}$, the middle curve is for $\rho = 0.3\ fm^{-3}$ and the upper curve is for $\rho = 0.5\ fm^{-3}$. The results are compared with the results of the realistic interaction UV14+UVII of Wiringa [66]. The figure has been reproduced from the Ref. [65].

momentum dependence of isoscalar part of the mean field, i.e., $u^{ex}(k,\rho)$, has been found to be in good agreement with the results of the microscopic calculations of Wiringa [66] over a wide range of momentum and density. The same has been given in Figure 2.3. It predicts an effective mass in SNM to be $\frac{M^*}{M}(k_{f_0},\rho_0)=0.67$ which is in good agreement with that found from the study of heavy-ion collision experiment data [59].

Although the exchange strength parameter combination ($\varepsilon_{ex}^{l}+\varepsilon_{ex}^{ul}$) has been constrained to a reasonable extent from the knowledge of isoscalar part of the nuclear mean field obtained from the optical model analysis, the relative strength of the combination ($\varepsilon_{ex}^{l}-\varepsilon_{ex}^{ul}$) associated with the isovector part of the nuclear mean field is still largely unknown [80-84, 109]. In fact, even the sign of the combination ($\varepsilon_{ex}^{l}-\varepsilon_{ex}^{ul}$) which determines the splitting of neutron and proton effective masses is still uncertain. In connection with the splitting of neutron and proton effective masses in asymmetric

nuclear matter, the predictions of different theoretical models are not only diverging but also contradicting. The results obtained in the microscopic relativistic Dirac-Brueckener Hatree Fock (DBHF) calculations performed earlier [120] as well as relativistic mean field (RMF) approximation using quantum hadrodynamics [105-109] exhibit the splitting where proton effective mass goes above the neutron one. On the other hand, the results obtained in non-relativistic microscopic calculations such as Brueckener-Hatree-Fock (BHF) and calculations using realistic nucleon-nucleon interactions [117-118] exhibit a splitting where neutron effective mass goes above the proton one. Most of the Skyrme-type effective interactions successfully used in various domains of nuclear calculations in the non-relativistic mean field approximations predict the splitting similar to the BHF results where neutron effective mass goes above that of proton one. However, Sly [112] and SKI [31] type of parameterization of the Skyrme forces give a splitting of neutron and proton effective masses in opposite direction similar to the early DBHF and RMF calculations where proton effective mass lies above the neutron one. In recent years Li and co workers [80-83] have studied the effects of momentum dependent symmetry potential on heavy ion collisions induced by neutron rich nuclei where they have parameterized the neutron and proton single particle potentials guided by a Hatree-Fock calculation using Gogny effective interaction. This parameterization also gives the splitting where neutron effective mass lies above the proton one. Rizzo et al.[84] have analyzed the influence of the two opposite types of splitting of neutron and proton effective masses on the flow data in heavy-ion collisions using two different simple GBD type parameterization [155] of the energy density.

In the followings we shall be discussing the works of Behera *et al.* [153-154] where the two types of conflicting effective mass splitting have been reproduced by the suitable choice of strength of the exchange interactions acting between pairs of like nucleons and unlike nucleons. We shall also discuss the conditions those can be obtained in the cases of Skyrme type and Gogny-type forces that can predict the two opposite types of neutron and proton effective mass splitting for the interactions.

The nucleonic effective mass $\left[\frac{M^*}{M}(k,\rho,Y_p)\right]_{n,p}$ that is related to the momentum dependence of the in medium interaction is defined through the relations given in

eqs.(2.1.22 and 2.1.23). From these expressions we can write the difference of square of neutron and proton effective masses as,

$$\left[\frac{\mathrm{M}^*}{\mathrm{M}}(\mathrm{k},\rho)\right]_n^2-\left[\frac{\mathrm{M}^*}{\mathrm{M}}(\mathrm{k},\rho)\right]_p^2=-\frac{\frac{M}{\hbar^2 k}\frac{\partial}{dk}u_T^{n-p}(k,\rho,Y_p)}{\left\{\left(1+\frac{\hbar^2k^2}{M^2C^2}\right)^{-1/2}+\frac{M}{\hbar^2 k}\frac{\partial u_T^p}{\partial k}\right\}\left\{\left(1+\frac{\hbar^2k^2}{M^2C^2}\right)^{-1/2}+\frac{M}{\hbar^2 k}\frac{\partial u_T^n}{\partial k}\right\}} \tag{2.1.73}$$

Thus the important quantity for our purpose in the context is the difference in the mean fields between a neutron and a proton having the same kinetic energy

$$u_T^{n-p}(k,\rho,Y_p)=\left[u_T^n(k,\rho,Y_p)-u_T^p(k,\rho,Y_p)\right], \tag{2.1.74}$$

expressed as a function of momentum k, density ρ and proton fraction Y_p at a given temperature T. The terms of $u_T^{n-p}(k,\rho,Y_p)$ which depends on momentum k are only relevant for deciding the neutron, proton effective mass splitting. In the case of our finite range interaction involving two parameters, the range of interaction between a pair of like nucleons and unlike nucleons are same but the interactions differ in strength. For such interaction, the momentum dependent part of $u_T^{n-p}(k,\rho,Y_p)$ given in eq.(2.1.20) becomes

$$\left[u_T^{n-p}(k,\rho,Y_p)\right]_{momentum\ \ dependent\ \ part}=\left(\varepsilon_{ex}^{l}-\varepsilon_{ex}^{ul}\right)G_T(k,\rho,Y_p), \tag{2.1.75}$$

where,

$$G_T(k,\rho,Y_p)=\frac{1}{\rho_0}\int\left[f_T^n(\vec{k}')-f_T^p(\vec{k}')\right]g_{ex}(|\vec{k}-\vec{k}'|)d^3k' \tag{2.1.76}$$

and the strength parameters ε_{ex}^{l} and ε_{ex}^{ul} are given in eqs.(2.1.65 and 66) respectively. f_T^n and f_T^p are the Fermi-Dirac momentum distribution functions for neutron and proton respectively at temperature T. $g_{ex}(|\vec{k}-\vec{k}'|)$ is the normalized Fourier transform of the finite range exchange interaction given by

$$g_{ex}(|\vec{k}-\vec{k}'|)=\frac{\int e^{i(\vec{k}-\vec{k}').\vec{r}}f(r)\,d^3r}{\int f(r)\,d^3r}, \tag{2.1.77}$$

which, for the Yukawa form of the interaction, $f(r)=\dfrac{e^{-r/\alpha}}{(r/\alpha)}$, becomes

$$g_{ex}(|\vec{k}-\vec{k}'|)=\frac{1}{1+\frac{|\vec{k}-\vec{k}'|^2}{\Lambda^2}} \tag{2.1.78}$$

with $\Lambda=\frac{1}{\alpha}$, α being the range of the interaction. The dimensionless function $G_T(k,\rho,Y_p)$ appearing in eq.(2.1.75) has a very complicated dependence on temperature T, momentum k, total nucleon density ρ and proton fraction Y_p. However, in the particular situation of very large k i.e $|\vec{k}|>>|\vec{k}'|$, where $g_{ex}(|\vec{k}-\vec{k}'|)$ appearing inside the integral in eq.(2.1.76) can be approximated by $g_{ex}(k)$ and the functional $G_T(k,\rho,Y_p)$ simplifies to $G_T(k,\rho,Y_p)_{large k}\approx(1-2Y_p)\frac{\rho}{\rho_0}g_{ex}(k)$. We can, now, examine the neutron and proton effective mass splitting without going into detail calculation of $u_T^{n-p}(k,\rho,Y_p)$. In this asymptotic limit of large k, the dimensionless quantity $\frac{M}{\hbar^2 k}\frac{\partial}{dk}u_T^{n-p}(k,\rho,Y_p)$ appearing in the expression of neutron-proton effective mass difference in eq.(2.1.73) can be calculated for the Yukawa form of exchange interaction from eqs.(2.1.75, 2.1.76 and 2.1.78) and is given by

$$\frac{M}{\hbar^2 k}\frac{\partial}{dk}u_T^{n-p}(k,\rho,Y_p)\underset{|\vec{k}|>>|\vec{k}'|}{\longrightarrow}-2(1-2Y_p)\frac{M\rho}{\hbar^2}\frac{\left(\varepsilon_{ex}^{l}-\varepsilon_{ex}^{ul}\right)}{\rho_0}\frac{\alpha^2}{(1+\alpha^2k^2)^2}. \tag{2.1.79}$$

This is the corresponding expression of eq.(2.1.24) for the Yukawa form of the exchange interaction. It is evident from this expression that the asymptotic behaviour of $\frac{M}{\hbar^2 k}\frac{\partial}{dk}u_T^{n-p}(k,\rho,Y_p)$ is positive for negative values of $(\varepsilon_{ex}^{l}-\varepsilon_{ex}^{ul})$. This implies that $\frac{M}{\hbar^2 k}\frac{\partial}{dk}u_T^{n}(k,\rho,Y_p)>\frac{M}{\hbar^2 k}\frac{\partial}{dk}u_T^{p}(k,\rho,Y_p)$ and asymptotically the neutron effective mass $\left[\frac{M^*}{M}(k,\rho,Y_p)\right]_n$ is less than the proton effective mass $\left[\frac{M^*}{M}(k,\rho,Y_p)\right]_p$. On the other hand, the asymptotic behaviour of $\frac{M}{\hbar^2 k}\frac{\partial}{dk}u_T^{n-p}(k,\rho,Y_p)$ is negative for positive values of $(\varepsilon_{ex}^{l}-\varepsilon_{ex}^{ul})$ and asymptotically the proton effective mass will be less than the neutron

effective mass. In order to examine the dependence of neutron-proton effective mass splitting on the splitting of the combined exchange parameter, ($\varepsilon_{ex}^{l}+\varepsilon_{ex}^{ul}$), into like and unlike channels in more detail way we consider the zero-temperature case with the Yukawa form of exchange interaction. In this case the neutron and proton effective masses can be obtained analytically from eq.(2.1.23) with the help of the following relations,

$$\frac{1}{k}\frac{\partial u^{n}(k,\rho,Y_P)}{\partial k}=\varepsilon_{ex}^{l}\frac{\rho_n}{\rho_0}\left[\begin{array}{l}-\dfrac{3\Lambda^2(\Lambda^2+k_n^{\,2}+k^2)}{8k^3k_n^{\,3}}\ln\left\{\dfrac{\Lambda^2+(k+k_n)^2}{\Lambda^2+(k-k_n)^2}\right\}\\ +\dfrac{3\Lambda^2(\Lambda^2+k_n^{\,2}-k^2)}{2k^2k_n^{\,2}}\dfrac{1}{\left[\Lambda^2+(k+k_n)^2\right]\left[\Lambda^2+(k-k_n)^2\right]}+\dfrac{6\Lambda^4}{k_n^{\,2}}\dfrac{1}{\left[\Lambda^2+(k+k_n)^2\right]\left[\Lambda^2+(k-k_n)^2\right]}\end{array}\right]$$

$$+\varepsilon_{ex}^{ul}\frac{\rho_p}{\rho_0}\left[\begin{array}{l}-\dfrac{3\Lambda^2(\Lambda^2+k_p^{\,2}+k^2)}{8k^3k_p^{\,3}}\ln\left\{\dfrac{\Lambda^2+(k+k_p)^2}{\Lambda^2+(k-k_p)^2}\right\}\\ +\dfrac{3\Lambda^2(\Lambda^2+k_p^{\,2}-k^2)}{2k^2k_p^{\,2}}\dfrac{1}{\left[\Lambda^2+(k+k_p)^2\right]\left[\Lambda^2+(k-k_p)^2\right]}+\dfrac{6\Lambda^4}{k_p^{\,2}}\dfrac{1}{\left[\Lambda^2+(k+k_p)^2\right]\left[\Lambda^2+(k-k_p)^2\right]}\end{array}\right] \tag{2.1.80}$$

and

$$\frac{1}{k}\frac{\partial u^{p}(k,\rho,Y_P)}{\partial k}=\varepsilon_{ex}^{l}\frac{\rho_p}{\rho_0}\left[\begin{array}{l}-\dfrac{3\Lambda^2(\Lambda^2+k_p^{\,2}+k^2)}{8k^3k_p^{\,3}}\ln\left\{\dfrac{\Lambda^2+(k+k_p)^2}{\Lambda^2+(k-k_p)^2}\right\}\\ +\dfrac{3\Lambda^2(\Lambda^2+k_p^{\,2}-k^2)}{2k^2k_p^{\,2}}\dfrac{1}{\left[\Lambda^2+(k+k_p)^2\right]\left[\Lambda^2+(k-k_p)^2\right]}+\dfrac{6\Lambda^4}{k_p^{\,2}}\dfrac{1}{\left[\Lambda^2+(k+k_p)^2\right]\left[\Lambda^2+(k-k_p)^2\right]}\end{array}\right]$$

$$+\varepsilon_{ex}^{ul}\frac{\rho_n}{\rho_0}\left[\begin{array}{l}-\dfrac{3\Lambda^2(\Lambda^2+k_n^{\,2}+k^2)}{8k^3k_n^{\,3}}\ln\left\{\dfrac{\Lambda^2+(k+k_n)^2}{\Lambda^2+(k-k_n)^2}\right\}\\ +\dfrac{3\Lambda^2(\Lambda^2+k_n^{\,2}-k^2)}{2k^2k_n^{\,2}}\dfrac{1}{\left[\Lambda^2+(k+k_n)^2\right]\left[\Lambda^2+(k-k_n)^2\right]}+\dfrac{6\Lambda^4}{k_n^{\,2}}\dfrac{1}{\left[\Lambda^2+(k+k_n)^2\right]\left[\Lambda^2+(k-k_n)^2\right]}\end{array}\right] \tag{2.1.81}$$

Now, the two opposite type of neutron-proton effective mass splitting can be reproduced by considering suitable splitting of the exchange strength parameter $\varepsilon_{ex}=\left(\dfrac{\varepsilon_{ex}^{l}+\varepsilon_{ex}^{ul}}{2}\right)$ into like (l) and unlike (ul) channels. In order to examine this two representative values of the splitting of ε_{ex}, namely,

$$\varepsilon_{ex}^{l} = \frac{\varepsilon_{ex}}{3}, \quad \varepsilon_{ex}^{ul} = \frac{5\varepsilon_{ex}}{3} \quad \text{---- (Case A)} \tag{2.1.82}$$

$$\varepsilon_{ex}^{l} = \frac{5\varepsilon_{ex}}{3}, \quad \varepsilon_{ex}^{ul} = \frac{\varepsilon_{ex}}{3} \quad \text{---- (Case B)} \tag{2.1.83}$$

are considered. The neutron and proton effective masses as a function of momentum in asymmetric nuclear matter having density $\rho = \rho_0$ and $Y_p = 0.1$ are shown in the Figures 2.4(a) and 2.4(b) for the two cases A and B. $(\varepsilon_{ex}^{l} - \varepsilon_{ex}^{ul})$ is positive for case A and the neutron effective mass goes above the proton one as expected, whereas, $(\varepsilon_{ex}^{l} - \varepsilon_{ex}^{ul})$ is negative in case B and hence the splitting is in the opposite direction. The asymptotic behaviour of neutron and proton effective mass splitting as obtained from eq.(2.1.79) are also shown in the same figure for comparison. The asymptotic results agree quite well with the exact result for $k >> 3.5\ fm^{-1}$. The density dependence of these two opposite types of splitting of neutron and proton effective masses could also be quite important for the differences between neutron and proton transport properties in highly asymmetric dense nuclear matter. Hence, the neutron and proton effective masses at

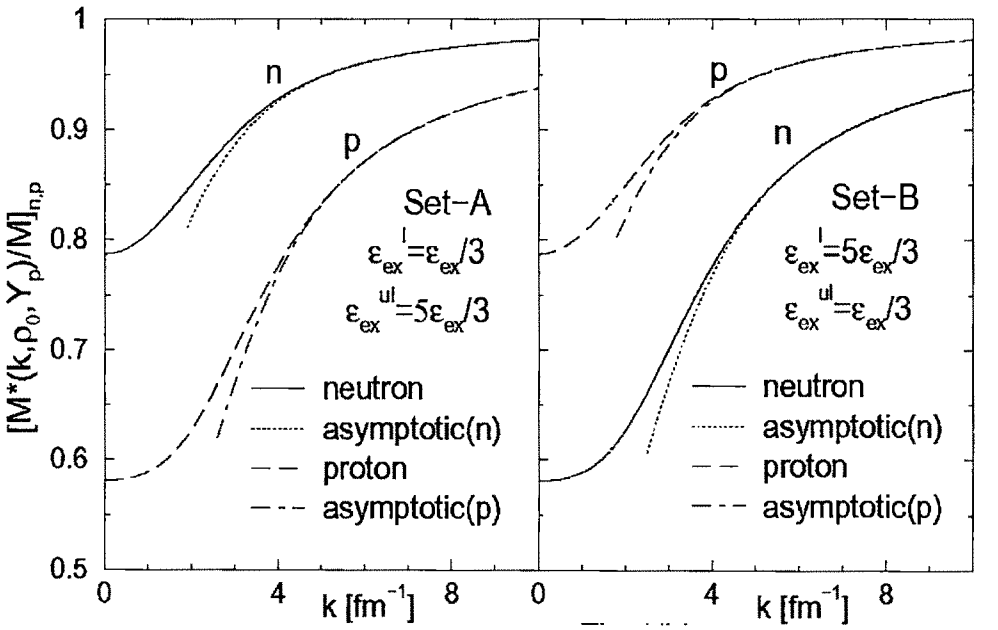

Figure 2.4. (a)Neutron and proton effective mass as function of Fermi momentum for case A. at a fixed density $\rho = \rho_0$ and proton fraction $Y_p = 0.1$(b) Same as (a) for the case B. The asymptotic cases are also shown for comparison.

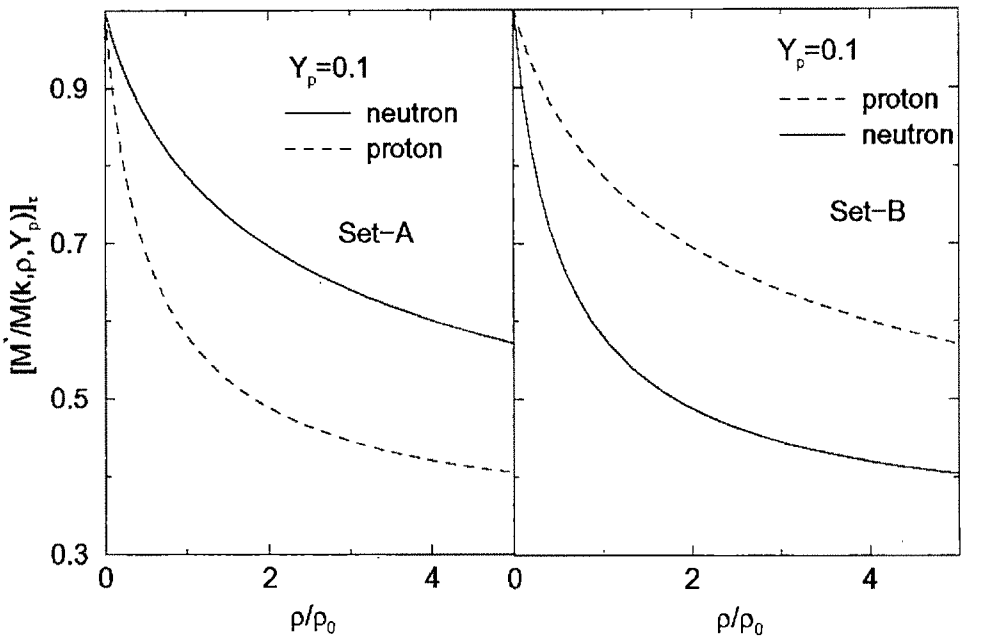

Figure 2.5. (a)Neutron and proton effective mass as function of relative density for case A. at $k = 0$ and at a fixed proton fraction $Y_P = 0.1$. (b) Same as (a) for the case B.

$k = 0$ for these two representative cases as a function of density are shown in Figures 2.5 (a) and (b). As expected, the neutron and proton effective mass splitting has the similar trend in Figures 2.4(a) and 2.5(a) and Figures 2.4(b) and 2.5(b). The density dependence of both neutron and proton effective masses in Figures 2.5(a) and (b) shows that it decreases with increase in density. However, the rate of decrease is considerably slowed down at higher densities. It may be worth noticing here that for the two representative cases A and B, the absolute value of $(\varepsilon_{ex}^{l} - \varepsilon_{ex}^{ul})$ does not change and as a result the curves for the neutron effective mass in Figures 2.4(a) and 2.5(a) are converted to the curves for the proton effective mass in Figures 2.4 (b) and 2.5(b) and conversely.

The two types of neutron and proton effective mass splitting discussed above by considering the two representative sets A and B can be characterized from the behaviour of the momentum dependence of isovector part of nuclear mean field, $u_\tau(k,\rho)$, given in eq.(2.1.53). The expression for the isovector part of the mean field for our Yukawa form of exchange interaction becomes,

$$u_\tau(k,\rho)=2E_s(\rho)-\frac{\hbar^2{k_f}^2}{3M}\left\{\left(\frac{M^*(k,\rho)}{M}\right)+\frac{\hbar^2k^2}{M^2C^2}\right\}^{-1/2}_{k=k_f}+u_\tau^{ex}(k,\rho) \tag{2.1.84}$$

where, the functional $u_\tau^{ex}(k,\rho)$ is now given by

$$u_\tau^{ex}(k,\rho)=\frac{\left(\varepsilon_{ex}^{l}-\varepsilon_{ex}^{ul}\right)}{2\int\frac{e^{-r/\alpha}}{r/\alpha}d^3r}\frac{\rho}{\rho_0}\int\left[j_o(kr)-j_0(k_fr)\right]j_0(k_fr)\frac{e^{-r/\alpha}}{r/\alpha}d^3r. \tag{2.1.85}$$

Now, $\int\frac{e^{-r/\alpha}}{r/\alpha}d^3r=4\pi\alpha^3$ and using the identities,

$$\int j_0(kr)\,j_0(k_fr)\frac{e^{-r/\alpha}}{r/\alpha}d^3r=\frac{\pi\alpha^3}{z_fx_f}\ln\left[\frac{1+(z_f+x_f)^2}{1+(z_f-x_f)^2}\right] \tag{2.1.86a}$$

and

$$\int{j_0}^2(k_fr)\frac{e^{-r/\alpha}}{r/\alpha}d^3r=\frac{\pi\alpha^3}{{x_f}^2}\ln(1+4{x_f}^2), \tag{2.1.86b}$$

the analytical result for $u_\tau^{ex}(k,\rho)$ becomes

$$u_\tau^{ex}(k,\rho)=\frac{\left(\varepsilon_{ex}^{l}-\varepsilon_{ex}^{ul}\right)}{8}\frac{\rho}{\rho_0}\left\{\frac{1}{z_fx_f}\ln\left[\frac{1+(z_f+x_f)^2}{1+(z_f-x_f)^2}\right]-\frac{1}{{x_f}^2}\ln(1+4{x_f}^2)\right\} \tag{2.1.87}$$

where, $z_f=\alpha k$ and $x_f=\alpha k_f$.

The calculation of $u_\tau(k,\rho)$ in eq.(2.1.84) as a function of k requires the knowledge of effective mass in SNM at Fermi momentum, $\frac{M^*}{M}(k=k_f,\rho)$ corresponding to the density ρ and value of nuclear symmetry energy $E_s(\rho)$ at the same density ρ. The effective mass in SNM for our Yukawa form of exchange interaction can be calculated from the momentum dependent part of isoscalar mean field, $u^{ex}(k,\rho)$, given in eq.(2.1.61). The momentum dependence of $\frac{M^*}{M}(k,\rho)$ at different nuclear matter densities have been discussed in Refs [64, 65, 67]. Calculation of nuclear symmetry energy, $E_s(\rho)$, requires the complete knowledge of the interaction. The density dependence of $E_s(\rho)$ still remains as a major area of research in nuclear physics.

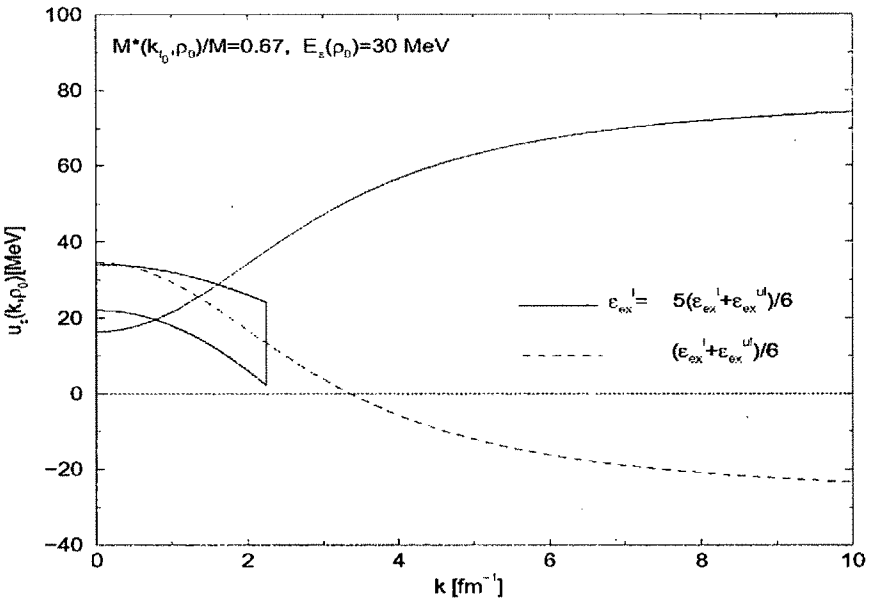

Figure 2.6. $u_\tau(k,\rho_0)$ as a function of k is shown for the two representative splittings of $\varepsilon_{ex} = (\varepsilon_{ex}^{l} + \varepsilon_{ex}^{ul})/2$. The experimentally extracted data are shown by the closed area.

However, its accepted value at normal density ρ_0 lies around 30 MeV. At normal nuclear matter density, the value of effective mass at Fermi momentum is obtained to be $\frac{M^*}{M}(k_{f_0},\rho_0) = 0.67$ for our Yukawa form of interaction. The momentum dependence of $u_\tau(k,\rho_0)$ in normal nuclear matter is calculated for our two representative cases A and B and is given in Figure 2.6. The contradicting behaviour of the isovector part of mean field for the two sets of exchange strength parameters A and B is evident in the Figure 2.6. While $u_\tau(k,\rho_0)$ decreases with increase in momentum for case A, it increases for case B. Thus an increasing behaviour of $u_\tau(k,\rho)$ (i.e. of $u_\tau^{ex}(k,\rho)$) implies that proton effective mass is larger than the neutron effective mass and for decreasing behaviour of $u_\tau^{ex}(k,\rho)$ the opposite is the case. Both the curves of $u_\tau(k,\rho)$ for two types of neutron and proton effective mass splitting intersect each other at the value of k equal to the Fermi momentum k_f corresponding to density ρ. The functional $u_\tau^{ex}(k,\rho)$ vanishes at $k = k_f$ and the value of $u_\tau(k = k_f,\rho)$ is determined from the first two terms in right

hand side of eq.(2.1.84) predicting the same value at Fermi momentum corresponding to a given density for both kinds of neutron-proton effective mass splitting.

The momentum and density dependence of neutron and proton effective masses have still remained as unresolved problems in nuclear physics. From the asymptotic expression of $\frac{M}{\hbar^2 k}\frac{\partial u_\tau^{n-p}(k,\rho,Y_p)}{\partial k}$, as may be seen from eq.(2.1.79) the magnitude of splitting is proportional to the total density and neutron-proton asymmetry parameter $(1-2Y_p)$. The splitting of neutron and proton effective masses may be small around normal nuclear matter density ρ_0 and, therefore, may be small in finite nuclei where the density ρ and asymmetry $(1-2Y_p)$ are rather small in order to give rise to any noticeable effect. However, these two opposite types of splitting of neutron and proton effective masses may be quite relevant in situations where both density and asymmetry are high. Such conditions of highly asymmetric hot and dense matter can be formed in the laboratory in heavy-ion collisions experiments involving radioactive ion beams. Analysis of the transport properties in such dense asymmetric matter produced in the heavy-ion collision experiments have been performed by several workers [80, 81, 83] but little success has been achieved in resolving the puzzle. The formation and cooling mechanism of neutron stars can be considered as another area of interest for studying the effect of neutron-proton effective mass splitting. This we shall be studying in the subsequent chapters. By now it is clear that neutron-proton effective mass splitting arises due to the difference in momentum dependence of the mean fields experienced by a neutron and a proton having same kinetic energy in an asymmetric nuclear matter medium. It will be of interest to examine this aspect of neutron-proton effective mass splitting in case of the existing Gogny type and Skyrme type interactions.

2.2. Neutron-Proton effective mass splitting in Gogny type interactions

The Gogny effective interaction is given by

$$v_{eff}^{Gogny}(\vec{r}) = \sum_{i=1,2}(W_i + B_i P_\sigma - H_i P_\tau - M_i P_\sigma P_\tau) e^{-(r/\mu_i)^2} + t_3(1+x_3 P_\sigma)\rho^\gamma(\vec{R})\delta(\vec{r}) \tag{2.2.1}$$

where, the first two terms represent the short and long range parts of the interaction having ranges μ_1 and μ_2, respectively, and the last term is the zero-range density dependent term.

With the help of the analytical expression of $u^{n-p}(k,\rho,Y_p)$ given in eq.(2.1.33) and the definition of $u_\tau(k,\rho)$ in eq.(2.1.53), the dimensionless quantity $\frac{M}{\hbar^2 k}\frac{\partial u^{n-p}(k,\rho,Y_p)}{\partial k}$ can be expressed as,

$$\frac{M}{\hbar^2 k}\frac{\partial u^{n-p}(k,\rho,Y_p)}{\partial k} = 2(1-2Y_p)\frac{M}{\hbar^2 k}\frac{\partial u_\tau^{ex}(k,\rho)}{\partial k}, \tag{2.2.2}$$

where, $u_\tau^{ex}(k,\rho)$ is given in eq.(2.1.54) . The functional $u_\tau^{ex}(k,\rho)$ for the Gogny effective interaction in eq.(2.2.1) can be

$$u_\tau^{ex}(k,\rho) = \frac{\rho}{2}\sum_{i=1,2}\left[\frac{1}{4}\left(v_i^{se}-3v_i^{to}\right)-\frac{1}{8}\left(v_i^{se}+3v_i^{te}-3v_i^{to}-v_i^{so}\right)\right] \times\left\{\int j_0(kr)j_0(k_f r)e^{-(r/\mu_i)^2}d^3r-\int {j_0}^2(k_f r)e^{-(r/\mu_i)^2}d^3r\right\} \tag{2.2.3}$$

where, $v_i^{se}, v_i^{te}, v_i^{to}, v_i^{so}$ with $i=1,2$ are the finite short and long range strength parameters in singlet-even, triplet-even, triplet-odd and singlet-odd states. Now evaluating the strength factor in the square bracketed term and using the identities,

$$\int j_0(kr)j_0(k_f r)e^{-r^2/\mu^2}d^3r = \frac{\pi^{3/2}\mu^3}{zx}\left[\exp\left\{-\left(\frac{z-x}{2}\right)^2\right\}-\exp\left\{-\left(\frac{z+x}{2}\right)^2\right\}\right] \tag{2.2.4a}$$

and

$$\int {j_0}^2(k_f r)e^{-r^2/\mu^2}d^3r = \frac{\pi^{3/2}\mu^3}{x^2}(1-e^{-x^2}) \tag{2.2.4b}$$

where, $z=\mu k$ and $x=\mu k_f$, the expression for $u_\tau^{ex}(k,\rho)$ in case of Gogny effective interaction can be analytically expressed as,

$$u_\tau^{ex}(k,\rho) = -\frac{2k_f}{3\sqrt{\pi}\Lambda_i}\sum_{i=1,2}\left(\frac{W_i}{2}+B_i\right)\left[\frac{k_f}{k}\left\{e^{-\left(\frac{k+k_f}{\Lambda}\right)^2}\right\}-\left(1-e^{-4k_f^2/\Lambda_i^2}\right)\right]. \tag{2.2.5}$$

Here in this expression Λ_i is related to the range parameter μ_i as $\Lambda_i = \frac{2}{\mu_i}$. Now the dimensionless quantity $\frac{M}{\hbar^2 k}\frac{\partial u^{n-p}(k,\rho,Y_p)}{\partial k}$ becomes,

$$\frac{M}{\hbar^2 k}\frac{\partial u^{n-p}(k,\rho,Y_p)}{\partial k} = 2(1-2Y_p)\frac{M}{\hbar^2 k} \times \sum_{i=1,2}\frac{2k_f}{3\sqrt{\pi}\Lambda_i}\left(\frac{W_i}{2}+B_i\right)\left[\frac{k_f}{k^2}\left\{e^{-\left(\frac{k-k_f}{\Lambda_i}\right)^2} - e^{-\left(\frac{k+k_f}{\Lambda_i}\right)^2}\right\} + \frac{2k_f}{\Lambda_i k}\left\{\left(\frac{k-k_f}{\Lambda_i}\right)e^{-\left(\frac{k-k_f}{\Lambda_i}\right)^2} - \left(\frac{k+k_f}{\Lambda_i}\right)e^{-\left(\frac{k+k_f}{\Lambda_i}\right)^2}\right\}\right] \quad (2.2.6)$$

In Gogny effective interaction the values of the two range parameters μ_1 and μ_2 are $0.7\,fm$ and $1.2\,fm$ respectively. It is evident from the above expression in eq.(2.2.6) that in the asymptotic region of large momentum, the behaviour of the neutron-proton effective mass splitting for the case of Gogny interactions will be determined from the short range part ($\mu_1 = 0.7\,fm$) as the contribution coming from the long range part ($\mu_2 = 1.2\,fm$) can be safely ignored. Thus, the sign of $\left(\frac{W_1}{2}+B_1\right)$ for the short range

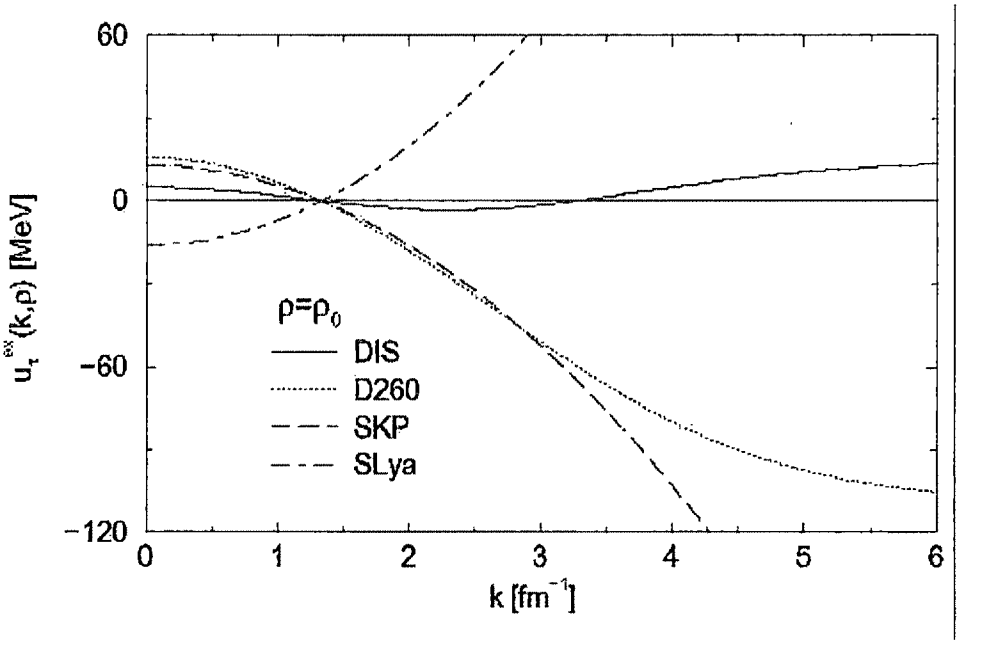

Figure 2.7. $u_\tau^{ex}(k,\rho_0)$ is plotted as a function of Fermi momentum k at a fixed nuclear matter density $\rho = \rho_0$ for different Gogny interactions. The results of the some Skyrme interactions are also shown for comparison.

part of the Gogny effective interaction will determine whether asymptotically for large k the neutron effective mass is above the proton effective mass or the other way around. Amongst the different sets of Gogny effective interactions used by Blaizot et al. [42], this parameter combination is positive for D1S and D250 and therefore asymptotically for large k the proton effective mass goes above the neutron effective mass. On the other hand, asymptotically for large k, $\left(\frac{W_1}{2}+B_1\right)$ is negative for D1, D260, D280 and D300 and as a result the neutron effective mass goes above the proton effective mass. This can be seen from the Figure 2.7 where we have shown the variation of $u_\tau^{ex}(k,\rho_0)$ at normal density ρ_0 over a wide range of momentum $k=0$ to 6 fm^{-1}.

2.3. Neutron-Proton effective mass splitting in Skyrme type interactions

The energy density $H_T(\rho_n,\rho_p)$ in ANM at temperature T for Skyrme type interactions is given by

$$\begin{aligned} H_T(\rho_n,\rho_p) = {} & \frac{\hbar^2}{2M}\tau+\frac{1}{4}t_0[(2+x_0)\rho^2-(2x_0+1)({\rho_n}^2+{\rho_p}^2)] \\ & +\frac{t_3}{24}\rho^\gamma[(2+x_3)\rho^2-(2x_3+1)({\rho_n}^2+{\rho_p}^2)] \\ & +\frac{1}{8}[t_1(2+x_1)+t_2(2+x_2)]\tau\rho \\ & +\frac{1}{8}[(t_2(2x_2+1)-t_1(2x_1+1))(\tau_n\rho_n+\tau_p\rho_p)] \end{aligned} \tag{2.3.1}$$

where, the total density $\rho=\rho_n+\rho_p$, total kinetic energy density $\tau=\tau_n+\tau_p$ with the definition $\tau_{n,p}=\int f_T^{n,p}(\vec{k})k^2dk$, and $t_o,x_0,t_3,x_3,\gamma,t_1,x_1,t_2$ and x_2 are the parameters of Skyrme interaction . At zero temperature, $T=0$, the momentum distribution function $f_{T=0}^{n,p}(\vec{k})$ takes the form of step function $\theta(k_{n,p}-k)$, where $k_{n,p}=\left(3\pi^2\rho_{n,p}\right)^{1/3}$ and the kinetic energy density becomes $\tau=\tau_n+\tau_p=\frac{3}{5}({k_n}^2\rho_n+{k_p}^2\rho_p)$. The energy density $H(\rho_n,\rho_p)$ in ANM at zero temperature for Skyrme type interaction now becomes

$$H(\rho_n,\rho_p)=\frac{\hbar^2}{2M}\frac{3}{5}(k_n{}^2\rho_n+k_p{}^2\rho_p)+\frac{1}{4}t_0[(2+x_0)\rho^2-(2x_0+1)(\rho_n{}^2+\rho_p{}^2)]$$
$$+\frac{t_3}{24}\rho^\gamma[(2+x_3)\rho^2-(2x_3+1)(\rho_n{}^2+\rho_p{}^2)]+\frac{1}{8}[t_1(2+x_1)+t_2(2+x_2)]\tau\rho$$
$$+\frac{1}{8}[t_2(2x_2+1)-t_1(2x_1+1)](\tau_n\rho_n+\tau_p\rho_p)] \tag{2.3.2}$$

Here we have used the non-relativistic expression for kinetic energy density for sake of simplicity. The neutron and proton single particle energies are obtained as the respective functional derivatives of the energy density,

$$\varepsilon_n(k,\rho_n,\rho_p)=\frac{\partial H(\rho_n,\rho_p)}{\partial[f_n]} \tag{2.3.3}$$

and

$$\varepsilon_p(k,\rho_n,\rho_p)=\frac{\partial H(\rho_n,\rho_p)}{\partial[f_p]}. \tag{2.3.4}$$

The neutron single particle energy for the Skyrme energy density given in eq.(2.3.2) becomes

$$\varepsilon_n(k,\rho_n,\rho_p)=\frac{\hbar^2k^2}{2M}+u_n(k,\rho_n,\rho_p), \tag{2.3.5}$$

where, $u_n(k,\rho_n,\rho_p)$ is the neutron single particle potential obtained as

$$u_n(k,\rho_n,\rho_p)=\frac{t_0}{2}[(2+x_0)\rho-(2x_0+1)\rho_n]+\gamma\frac{t_3}{24}\rho^{\gamma-1}[(2+x_3)\rho^2-(2x_3+1)(\rho_n{}^2+\rho_p{}^2)]$$
$$+\frac{t_3}{12}\rho^\gamma[(2+x_3)\rho-(2x_3+1)\rho_n]+\frac{1}{8}[t_1(2+x_1)+t_2(2+x_2)](\tau+\rho k^2)$$
$$+\frac{1}{8}[t_2(2x_2+1)-t_1(2x_1+1)](\tau_n+\rho_n k^2)] \tag{2.3.6}$$

The proton single particle energy for the Skyrme energy density in eq (2.3.2) becomes

$$\varepsilon_p(k,\rho_n,\rho_p)=\frac{\hbar^2k^2}{2M}+u_p(k,\rho_n,\rho_p) \tag{2.3.7}$$

where $u_p(k,\rho_n,\rho_p)$ is the proton single particle potential obtained as

$$u_p(k,\rho_n,\rho_p)=\frac{t_0}{2}[(2+x_0)\rho-(2x_0+1)\rho_p]+\gamma\frac{t_3}{24}\rho^{\gamma-1}[(2+x_3)\rho^2-(2x_3+1)(\rho_n^{\,2}+\rho_p^{\,2})]$$
$$+\frac{t_3}{12}\rho^{\gamma}[(2+x_3)\rho-(2x_3+1)\rho_p]+\frac{1}{8}[t_1(2+x_1)+t_2(2+x_2)](\tau+\rho k^2)$$
$$+\frac{1}{8}[t_2(2x_2+1)-t_1(2x_1+1)](\tau_p+\rho_p k^2)] \qquad (2.3.8)$$

In case of Skyrme type interactions the neutron and proton single particle potentials have k^2-type momentum dependence. This is also the case in case of Seyler-Blanchard interaction [38]. One can derive the equivalent expression for $u_\tau(k,\rho)$ for Skyrme type interaction, in terms of symmetry energy $E_S(\rho)$, effective mass in SNM $\frac{M^*}{M}(k_f,\rho)$ and the functional $u_\tau^{ex}(k,\rho)$ as given in eq.(2.1.53).

The neutron and proton single particle potentials in eqs.(2.3.6) and (2.3.8) can be expanded in powers of asymmetric parameter $\beta=\frac{\rho_n-\rho_p}{\rho_n+\rho_p}$. The neutron and proton densities in terms of β are $\rho_n=\frac{\rho}{2}(1+\beta)$ and $\rho_p=\frac{\rho}{2}(1-\beta)$, respectively. Expanding the neutron and proton single particle potentials in powers of β and retaining terms upto the 1st power in β, one gets,

$$u_n(k,\rho,\beta)\cong u(k,\rho)+\beta\left\{-\frac{t_0}{2}\left(x_0+\frac{1}{2}\right)\rho-\frac{t_3}{12}\left(x_3+\frac{1}{2}\right)\rho^{\gamma+1}+\frac{1}{8}[t_1(2+x_1)+t_2(2+x_2)](k_f^{\,2}+k^2)\frac{\rho}{2}\right\} \qquad (2.3.9)$$

$$u_p(k,\rho,\beta)\cong u(k,\rho)+\beta\left\{\frac{t_0}{2}\left(x_0+\frac{1}{2}\right)\rho+\frac{t_3}{12}\left(x_3+\frac{1}{2}\right)\rho^{\gamma+1}-\frac{1}{8}[t_1(2+x_1)+t_2(2+x_2)](k_f^{\,2}+k^2)\frac{\rho}{2}\right\} \qquad (2.3.10)$$

where, $k_f=\left(\frac{3\pi^2\rho}{2}\right)^{1/3}$. $u(k,\rho)$ is the single particle pctential in SNM for the Skyrme type interaction and is given by

$$u(k,\rho)=\frac{3t_0}{4}\rho+\frac{t_3}{16}(\gamma+2)\rho^{\gamma+1}+\frac{1}{16}[3t_1+(5+4x_2)t_2](\tau+\rho k^2) \qquad (2.3.11)$$

with $\tau = \frac{3}{5}k_f{}^2\rho$. Now the isovector part of the neutron-proton single particle potential, $u_\tau(k,\rho) \cong \frac{u_n(k,\rho,\beta) - u_p(k,\rho,\beta)}{2\beta}$, for the Skyrme energy density functional becomes,

$$u_\tau(k,\rho) \cong -\frac{t_0}{2}\left(x_0 + \frac{1}{2}\right)\rho - \frac{t_3}{12}\left(x_3 + \frac{1}{2}\right)\rho^{\gamma+1} + \frac{Q}{2}(k^2 + k_f{}^2)\rho, \qquad (2.3.12)$$

where, Q is defined as

$$Q = \frac{1}{8}[t_2(2x_2 + 1) - t_1(2x_1 + 1)]. \qquad (2.3.13)$$

2.3.1. Symmetry energy $E_s(\rho)$ for Skyrme energy density

Using the definition of nuclear symmetry energy, $E_S(\rho) = \frac{1}{2\beta}\frac{\partial^2 H(\rho,\beta)}{\partial\beta^2}\Big|_{\beta=0}$, the expression $E_S(\rho)$ for the Skyrme energy density is obtained as,

$$E_s(\rho) = \frac{\hbar^2 k_f{}^2}{6M} - \frac{t_0}{4}\left(x_0 + \frac{1}{2}\right)\rho - \frac{t_3}{24}\left(x_3 + \frac{1}{2}\right)\rho^{\gamma+1} + (P + 2Q)\frac{k_f{}^2\rho}{3}, \qquad (2.3.14)$$

where, the quantity P is defined as

$$P = \frac{1}{8}[(2 + x_1)t_1 + (2 + x_2)t_2] \qquad (2.3.15)$$

and Q is defined in eq.(2.3.13). In obtaining this we have used the non-relativistic expression for kinetic energy term.

2.3.2. Effective mass $\frac{M^*}{M}(k,\rho)$ in SNM for Skyrme type interactions

The expression for effective mass $\frac{M^*}{M}(k,\rho)$ in SNM for the non-relativistic approximation of kinetic energy density is given by $\frac{M^*}{M}(k,\rho) = \left[1 + \frac{M}{\hbar^2 k}\frac{\partial u(k,\rho)}{\partial k}\right]^{-1}$, where, $u(k,\rho)$ is the single particle potential in SNM. For the Skyrme single particle potential in SNM, given in eq.(2.3.11), the effective mass for Skyrme-type interaction becomes,

$$\frac{M^*}{M}(\rho)=\left[1+\frac{2M}{\hbar^2}\left\{\frac{3t_1+(5+4x_2)t_2}{16}\right\}\rho\right]^{-1}. \tag{2.3.16}$$

It may be noted that for Skyrme type interactions or any other effective interactions, such as, Seyler-Blanchard interaction, which results into quadratic momentum dependence of the single particle potential, the effective mass does not have momentum dependence.

The nuclear symmetry energy $E_S(\rho)$ in eq.(2.3.14) can now be expressed in terms of the isovector part of the $n-p$ single particle potential in eq.(2.3.12) as,

$$E_s(\rho)=\frac{1}{2}u_\tau(k,\rho)+\left[\frac{\hbar^2k^2}{6M}+\left(P+\frac{Q}{2}\right)\frac{{k_f}^2\rho}{3}\right]-\frac{Q}{4}(k^2-{k_f}^2). \tag{2.3.17}$$

Thus, the isovector part of the nuclear mean field in ANM given in eq.(2.2.12) in case of Skyrme interactions can now be expressed as,

$$u_\tau(k,\rho)=2E_s(\rho)-\left[\frac{\hbar^2k^2}{3M}\left\{1+(Q+2P)\frac{M}{\hbar^2}\rho\right\}\right]_{k=k_f}+\frac{Q}{2}(k^2-{k_f}^2)\rho, \tag{2.3.18}$$

where, $Q+2P=\frac{1}{8}[3t_1+t_2(5+4x_2)]$and the term inside the curly bracket can be identified as the inverse of the effective mass in SNM given in eq.(2.3.16). So, finally $u_\tau(k,\rho)$ for the Skyrme type interactions can be expressed as,

$$u_\tau(k,\rho)=2E_s(\rho)-\frac{\hbar^2{k_f}^2}{3M}\left(\frac{M^*}{M}(\rho)\right)^{-1}+\frac{Q}{2}(k^2-{k_f}^2)\rho. \tag{2.3.19}$$

This may be compared with the expression for $u_\tau(k,\rho)$ derived for general effective interaction earlier in eq.(2.1.53), but with the consideration of non-relativistic approximation for kinetic energy part in place of relativistic one. It follows from the comparison that the expression for $u_\tau^{ex}(k,\rho)$ for Skyrme type interaction is given by the simple expression,

$$u_\tau^{ex}(k,\rho)=\frac{Q}{2}(k^2-k_f^2)\rho=\frac{1}{16}[t_2(2x_2+1)-t_1(2x_1+1)](k^2-k_f^2)\rho \tag{2.3.20}$$

Now, the dimensionless quantity $\frac{M}{\hbar^2k}\frac{\partial u_\tau^{ex}(k,\rho)}{\partial k}$ for the Skyrme case results into a very simple structure,

$$\frac{M}{\hbar^2 k}\frac{\partial u_\tau^{ex}(k,\rho)}{\partial k}=\frac{M}{8\hbar^2}[t_2(2x_2+1)-t_1(2x_1+1)]\rho, \qquad (2.3.21)$$

which is independent of momentum k. This implies that in case of Skyrme interactions, as well as, in the cases of effective interactions which have k^2-momentum dependence in the single particle potentials, there will be no temperature dependence in the neutron and proton effective mass. The neutron-proton effective mass splitting at a given density ρ will only depend on the neutron-proton asymmetry, i.e., $(1-2Y_p)$ and will be same at all finite temperatures to its zero-temperature value. The sign of the parameter $Q=\frac{1}{8}[t_2(2x_2+1)-t_1(2x_1+1)$ will determine whether the neutron effective mass is above that of the proton or the other way around. The Skyrme parameterizations such as SGII, RATP, SKP, SKX, SKXm, SKSC, LNS, BSk17, BSk17st [29, 131, 156] have also negative values of parameter Q. In all these cases $u_\tau^{ex}(k,\rho)$ in eq.(2.3.20) will be a decreasing function of k and hence the neutron effective mass is above the proton effective mass irrespective of temperature, momentum and density. On the other hand, all the SLY type and SKI-SKI6 give positive value of the parameter Q and in these cases the proton effective mass is above the neutron one. For Skyrme parameterizations such as SKSC4 and T6 for which $x_1=x_2=-0.5$, the parameter Q vanishes and the neutron and proton effective masses are identical. The values of the parameter Q for different Skyrme sets are listed in Table-1.

From the general expressions of isoscalar and isovector parts of the nuclear mean fields given in eqs.(2.1.60 and 2.1.61) and (2.1.53 and 54) it is evident that momentum dependence of nuclear mean field and density dependence of nuclear EOS are two distinct features. The study on one of these two aspects of nuclear matter using an effective theoretical model requires the other aspect to remain unchanged in the process of calculation. This was not possible with the Skyrme effective forces having a single conventional density dependent term, proportional to ρ^γ, where the exponent γ is strongly correlated to the incompressibility $K(\rho)$ as well as the effective mass

Table-1. Values of the parameter Q for different Skyrme sets.

Skyrme sets	x_1	x_2	t_1	t_2	$Q/2$
GS	0	0	336.2	-85.7	-26.37
RS	0	0	336.0	-84.8	-26.3
SGI	-0.50	-1.73	515.9	84.5	-12.99
SLY0	-0.50	-0.93	485.2	-440.5	23.68
SLY1	-0.31	-1.0	488.3	-568.9	23.96
SLY10	-0.67	-1.0	431.0	-305.0	28.22
SLY2	-0.73	-0.78	482.2	-290.0	24.01
SLY230a	-0.84	-1.0	489.5	-566.6	56.22
SLY3	-0.34	-1.0	481.0	-540.8	24.18
SLY4	-0.34	-1.0	486.8	-546.4	24.41
SLY5	-0.32	-1.0	484.2	-556.7	23.90
SLY6	-0.47	-1.0	462.2	-448.6	26.30
SLY7	-0.49	-1.0	461.3	-433.9	26.54
SLY8	-0.34	-1.0	480.8	-538.3	24.03
SLY9	-0.62	-1.0	510.6	-429.8	34.52
SV	0	0	970.6	107.2	-53.96
SKI1	-5.78	-1.29	439.8	2697.6	23.88
SKI2	-1.74	-1.53	438.4	305.4	28.63
SKI3	-1.17	-1.09	561.6	-227.1	63.78
SKI4	-2.89	-1.33	473.8	1006.9	37.08
SKI5	-1.31	-1.05	550.8	-126.7	64.48
SKI6	-2.14	-1.38	483.9	528.4	41.08
SKMP	-0.40	-2.96	503.6	57.3	-23.91
SKO	-2.81	-1.46	303.4	791.7	-7.39
SKO'	-1.33	-2.32	301.5	154.8	-3.94
SkT4	-0.50	-0.50	303.4	-303.4	0
SkT5	-0.50	-0.50	328.8	-328.8	0
GSkI	-1.7586	-1.8068	397.23	264.63	19.27
GSkII	-0.7203	-1.8369	393.08	266.08	-33.64
SSk	-0.4519	-0.9214	435.0	-382.04	17.51
LNS	0.65845	-0.95382	266.735	-337.135	-19.5
BSk17	-0.832102	49.4875	389.102	-3.1742	-3.68
BSk17st	-0.834832	29.0669	388.916	-5.3076	-3.34

$\frac{M^*}{M}(\rho)$ in nuclear matter. We shall show it in the followings. The energy per particle in SNM,

$e_0(\rho)=\frac{H_0(\rho)}{\rho}$, for the Skyrme forces as follows from eq.(2.3.2) with $\rho_n=\rho_p=\rho/2$ is,

$$e_0(\rho)=\frac{3\hbar^2}{10M}\left(\frac{3\pi^2}{2}\right)^{2/3}\rho^{2/3}+\frac{3}{8}t_0\rho+\frac{t_3}{16}\rho^{\gamma+1}+\frac{3}{5}\frac{[3t_1+t_2(5+4x_2)]}{16}\left(\frac{3\pi^2}{2}\right)^{2/3}\rho^{5/3} \quad . \quad (2.3.22)$$

The pressure in nuclear matter, $P(\rho)=\rho^2\frac{\partial e_0(\rho)}{\partial\rho}$, can be

$$P(\rho)=\frac{\hbar^2}{5M}\left(\frac{3\pi^2}{2}\right)^{2/3}\rho^{5/3}+\frac{3}{8}t_0\rho^2+\frac{t_3}{16}(\gamma+1)\rho^{\gamma+2}+\frac{[3t_1+t_2(5+4x_2)]}{16}\left(\frac{3\pi^2}{2}\right)^{2/3}\rho^{8/3}, \quad (2.3.23)$$

and nuclear matter incompressibility, $K(\rho)=9\frac{\partial P(\rho)}{\partial\rho}=18\frac{P(\rho)}{\rho}+9\rho^2\frac{\partial^2 e_0(\rho)}{\partial\rho^2}$, becomes

$$K(\rho)=-\frac{3\hbar^2}{5M}\left(\frac{3\pi^2}{2}\right)^{2/3}\rho^{5/3}+\frac{9t_3}{16}\gamma(\gamma+1)\rho^{\gamma+1}+\frac{3}{8}[3t_1+t_2(5+4x_2)]\left(\frac{3\pi^2}{2}\right)^{2/3}\rho^{5/3}$$
$$+\frac{18}{\rho}\left[\frac{\hbar^2}{5M}\left(\frac{3\pi^2}{2}\right)^{2/3}\rho^{5/3}+\frac{3}{8}t_0\rho^2+\frac{t_3}{16}(\gamma+1)\rho^{\gamma+2}+\frac{[3t_1+t_2(5+4x_2)]}{16}\left(\frac{3\pi^2}{2}\right)^{2/3}\rho^{8/3}\right] \quad (2.3.24)$$

These three quantities at saturation density, $\rho=\rho_0$, becomes

$$e_0(\rho_0)=\frac{3\hbar^2}{10M}\left(\frac{3\pi^2}{2}\right)^{2/3}\rho_0^{2/3}+\frac{3}{8}t_0\rho_0+\frac{t_3}{16}\rho_0^{\gamma+1}+\frac{3[3t_1+t_2(5+4x_2)]}{80}\left(\frac{3\pi^2}{2}\right)^{2/3}\rho_0^{5/3} \quad (2.3.25)$$

$$P(\rho_0)=0=\frac{\hbar^2}{5M}\left(\frac{3\pi^2}{2}\right)^{2/3}\rho_0^{5/3}+\frac{3}{8}t_0\rho_0^2+\frac{t_3}{16}(\gamma+1)\rho_0^{\gamma+2}+\frac{[3t_1+t_2(5+4x_2)]}{16}\left(\frac{3\pi^2}{2}\right)^{2/3}\rho_0^{8/3} \quad (2.3.26)$$

$$K(\rho_0)=-\frac{3\hbar^2}{5M}\left(\frac{3\pi^2}{2}\right)^{2/3}\rho_0{}^{5/3}+\frac{9t_3}{16}\gamma(\gamma+1)\rho_0{}^{\gamma+1}+\frac{3}{8}[3t_1+t_2(5+4x_2)]\left(\frac{3\pi^2}{2}\right)^{2/3}\rho_0{}^{5/3} \tag{2.3.27}$$

For a given set of values for ρ_0, $e_0(\rho_0)$ and $K(\rho_0)$, these three equations (2.3.25 - 27) can be solved to obtain the values of three unknown parameters t_0, t_3 and θ_s, where,

$$\theta_s=[3t_1+t_2(5+4x_2)]. \tag{2.3.28}$$

This parameter θ_s thus obtained, uniquely determines the effective mass $\frac{M^*}{M}(\rho)$ in SNM given in eq.(2.3.16). This conclusion is, however, not correct in a special case corresponding to the value of the exponent $\gamma=\frac{2}{3}$. For this special case, the above three eqs. (2.3.25 -27) are given by,

$$\frac{3\hbar^2}{10M}\left(\frac{3\pi^2}{2}\right)^{2/3}\rho_0{}^{5/3}+\frac{3}{8}t_0\rho_0+\frac{3}{5}F(\theta_s,t_3)\rho_0{}^{5/3}=e(\rho_0) \tag{2.3.29}$$

$$\frac{\hbar^2}{5M}\left(\frac{3\pi^2}{2}\right)^{2/3}\rho_0{}^{2/3}+\frac{3}{8}t_0\rho_0+F(\theta_s,t_3)\rho_0{}^{5/3}=0 \tag{2.3.30}$$

and

$$-\frac{3\hbar^2}{5M}\left(\frac{3\pi^2}{2}\right)^{2/3}\rho_0{}^{2/3}+6F(\theta_s,t_3)\rho_0{}^{5/3}=K(\rho_0), \tag{2.3.31}$$

where, the new parameter $F(\theta_s,t_3)$ is given by,

$$F(\theta_s,t_3)=\frac{1}{16}\left[\theta_s\left(\frac{3\pi^2}{2}\right)^{2/3}+\frac{5}{3}t_3\right]. \tag{2.3.32}$$

Thus, in this particular case of $\gamma=\frac{2}{3}$, there are two unknowns t_0 and $F(\theta_s,t_3)$ in eqs. (2.3.29- 31). The first two equations can be used to determine these two parameters, t_0 and $F(\theta_s,t_3)$, and then the corresponding value of $K(\rho_0)$can be calculated. The definition of $F(\theta_s,t_3)$ in eq.(2.3.32) above allows to choose θ_s freely. Thus, for the

given value of nuclear matter incompressibility $K(\rho_0)$ corresponding to $\gamma=\frac{2}{3}$, the effective mass can be freely chosen. This important feature is illustrated well in the work of Cochet *et al.* [157]. This work of Cochet *et al.* is a major breakthrough in disentangling the strong correlation between the effective mass and incompressibility in cases of Skyrme forces with single density dependent term. Inclusion of a second density dependent term enabled to chose the incompressibility and effective mass independently. The theoretical justification of the two independent density dependent terms, as discussed by Cochet *et al.*[157], originates from Brueckener correlations in the context of mixed non orthogonal vacua [158] and renormalization of three body forces through a density-dependent two body interaction[8, 131, 158-160]. With the development of this improved version of Skyrme interaction that is able to disentangle the strong correlation between incompressibility and effective mass, Leisinki *et al.* [131] in their work studied the effect of the variation of neutron-proton effective mass splitting on properties sensitive to the isovector features of nuclear EOS. The Skyrme effective force containing two density dependent terms used by Leisinki et al. in their study, is given by,

$$V(\vec{R},\vec{r})=\sum_{i=0}^{2}t_{0i}(1+x_{0i}P_\sigma)\delta(\vec{r})[\rho(\vec{R})]^{i/3}+\frac{1}{2}t_1(1+x_1P_\sigma)[\delta(\vec{r})k^2+k'^2\,\delta(\vec{r})]$$
$$+t_2(1+x_2P_\sigma)\vec{k}'\cdot\delta(\vec{r})\vec{k}+iW_0(\vec{\sigma}_1+\vec{\sigma}_2)\vec{k}'\times\delta(\vec{r})\vec{k} \qquad (2.3.33)$$

where, the symbols have their usual meaning. The neutron and proton effective masses have been obtained from the energy density resulting from this Skyrme interaction in eq.(2.3.33) in ANM by using the relation

$$\frac{\hbar^2}{2M_q^*}=\frac{\partial H}{\partial\tau_q}=\frac{\hbar^2}{2M}+\frac{[3t_1+t_2(5+4x_2)]}{16}\rho+q\beta\frac{[t_2(1+2x_2)-t_1(1+2x_1)]}{16}\rho \qquad (2.3.34)$$

where, $q=+1,-1$ respectively for neutrons and protons. Thus, the neutron, proton effective masses can now be given as

$$\frac{M}{M_q^*}=\frac{M}{M_s^*}+q\beta\left(\frac{M}{M_s^*}-\frac{M}{M_v^*}\right), \qquad (2.3.35)$$

where, $\frac{M_s^*}{M}$ and $\frac{M_v^*}{M}$ are defined as the isoscalar and isovector effective masses given as

$$\frac{M}{M_s^*} = 1 + \frac{2M}{\hbar^2}\frac{[3t_1 + t_2(5+4x_2)}{16}\rho = 1 + \kappa_s \tag{2.3.36}$$

$$\frac{M}{M_v^*} = 1 + \frac{2M}{\hbar^2}\left[\frac{[3t_1 + t_2(5+4x_2)}{16} - \frac{[-t_1(1+2x_1) + t_2(1+2x_2)}{16}\right]\rho = 1 + \kappa_v \tag{2.3.37}$$

with, $\kappa_s = \frac{M}{8\hbar^2}[3t_1 + t_2(5+4x_2)]$ and $\kappa_v = \frac{M}{4\hbar^2}[t_1(2+x_1) + t_2(2+x_2)]$ is defined as the isovector enhancement factors. The quantities M_v^* and κ_v are not isovector quantities in the sense of isovector couplings of the functional. It follows through the terminology used for κ_v of the Thomas-Reiche-Kahn sum rule in Ref. [161]. The splitting of effective masses is quantified by

$$\begin{aligned}\frac{\Delta M^*}{M} &= \frac{M_n^*}{M} - \frac{M_p^*}{M} \\ &= \frac{2(\kappa_v - \kappa_s)}{(1+\kappa_s)^2 - (\kappa_v - \kappa_s)^2}\end{aligned} \tag{2.3.38}$$

such that $\Delta M^* > 0$, for $\kappa_v > \kappa_s$, or equivalently $M_v^* < M_s^*$ or $[-t_1(1+2x_1) + t_2(1+2x_2)] < 0$. It may be noted here that the expression of the quantity $\left(\frac{M}{M_s^*} - \frac{M}{M_v^*}\right)$ in the work of Leisinki *et al.* as obtained from eqs.(2.3.36) and (2.3.37) is exactly same with the result of dimensionless functional $\frac{M}{\hbar^2 k}\frac{\partial u_\tau^{ex}(k,\rho)}{\partial k}$ obtained in our formalism for Skyrme interaction given in eq (2.3.21).

The advantage of using a second density dependent term lies in the fact that it provides additional freedom to adjust the high-density part of pure neutron matter (PNM) allowing a free choice of neutron and proton effective masses with a good fit to EOS of PNM. This can be better understood if we write the expressions for energy per particle in SNM, $e_0(\rho)$, and PNM $e_n(\rho)$ for the Skyrme interaction given in eq.(2.3.33),

$$e_0(\rho) = \frac{3\hbar^2}{10M}\left(\frac{3\pi^2}{2}\right)^{2/3}\rho^{2/3} + C_0^{\rho}\rho + \frac{3}{5}C_0^{\tau}\left(\frac{3\pi^2}{2}\right)^{2/3}\rho^{5/3} \tag{2.3.39}$$

and

$$e_n(\rho) = \frac{3\hbar^2}{10M}(3\pi^2)^{2/3}\rho^{2/3} + (C_0^{\rho} + C_1^{\rho})\rho + \frac{3}{5}(C_0^{\tau} + C_1^{\tau})(3\pi^2)^{2/3}\rho^{5/3} \tag{2.3.40}$$

where,

$$C_0^{\rho} = \sum_{i=0}^{2}\frac{3}{8}t_{0i}\rho^{i/3} = \frac{3}{8}t_{00} + \frac{3}{8}t_{01}\rho^{1/3} + \frac{3}{8}t_{02}\rho^{2/3} \tag{2.3.41a}$$

$$C_0^{\tau} = \frac{3t_1 + (5+4x_2)t_2}{16}$$

$$C_1^{\rho} = \sum_{i=0}^{2} -\frac{1}{8}t_{0i}(1+2x_{0i})\rho^{i/3} \tag{2.3.41b}$$

(2.3.41c)

$$C_1^{\tau} = \frac{-(1+2x_1)t_1 + (1+2x_2)t_2}{16}. \tag{2.3.41d}$$

It may be noted that if we set $t_{02} = 0$, $t_{00} = t_0$ and $t_{01} = \frac{t_3}{6}$ then we get the conventional expression for energy per particle $e_0(\rho)$ of Skyrme interaction with single density dependent term with $\gamma = \frac{1}{3}$ as given in eq.(2.3.22). Alorg with this, if we take $x_{02} = 0$, $x_{00} = x_0$ and $x_{01} = x_3$ then we get corresponding conventional expression for $e_n(\rho)$ in PNM.

Now if C_1^{ρ} coefficients will contain one low power of the density ($\propto \rho^{1/6}$) as in case of Sly-type interaction [112], this will influence more on the low density behaviour of the EOS of PNM. The effective mass term then determines the high-density part of the EOS. Thus, in case of PNM, the EOS above the saturation density is then mostly fixed by the terms proportional to $(C_0^{\tau} + C_1^{\tau})$ of eq.(2.3.40) and any attempt to use the density dependence to counteract its effects results in a very strong constraint on the incompressibility of SNM. This in turn degrades the behaviour of the functional at and below saturation density. It may be recalled that for $\Delta M^* > 0$, corresponds to $C_1^{\tau} < 0$, i.e. $[-(1+2x_1)t_1 + (1+2x_2)t_2] < 0$, which drives the high-density behaviour of EOS in PNM down and explains why the usual Skyrme functionals predict either a collapse of the

PNM if $\Delta M^* > 0$, or like the Sly functionals fitted to EOS in PNM that results into $\Delta M^* < 0$, i.e., proton effective mass is greater than neutron one.

In case of the present form of Skyrme interaction containing two density dependent terms ($\propto \rho^{1/3}, \rho^{2/3}$) the above discussion does not apply and allows a free choice of neutron, proton effective masses along with a good fit to EOS of PNM and satisfactory nuclear matter properties. With the help of this advantage of the additional second density dependent term Leisinki *et al.* [131] have constructed three new Skyrme parameter sets those corresponding to $M_n^* < M_p^*$ (set named f_), $M_n^* = M_p^*$ (set named f_0), $M_n^* > M_p^*$ (set named f_+), in their work in Ref.[131] and have used them in calculating the observables of infinite nuclear matter and finite nuclei, paying particular attention to controlling the agreement with Brueckner-Hatree-Fock calculations of spin-isospin content of the finite nuclear equation of state. In this attempt of resolving the existing uncertainty in neutron-proton effective mass splitting using Skyrme force, Leisinski *et al.* have concluded that the various constraints arising in their study cannot be fulfilled simultaneously, calling at least for an extension of its P-wave part of the Skyrme forces. Similar attempts in other areas have also been made in recent years to resolve the neutron-proton effective mass splitting problem as well as the high density behaviour of nuclear symmetry energy. In this context the works of Li *et al.*[81] and Rizzo *et al.* [84] can be discussed. In their works they have made attempts to constrain the momentum and density dependence of the isovector part of the nuclear mean field from the analysis of observables sensitive to neutron and proton flow data resulting from medium and high energy heavy-ion collision experiments using radioactive ion beams. During that period the development in the area of radioactive ion beam experiment facilities had inspired a good deal of hope in resolving these two important and long standing issues in the field of nuclear research.

2.4. Work of B. A. Li *et al.*

In the work of Li *et al.* [81], they have basically made an attempt to constrain the density dependence of nuclear symmetry energy. The effective energy density in ANM used in the work for transport model analysis of HI collision flow data is given by,

$$H_T(\rho_n,\rho_p)=\frac{\hbar^2}{2M}\sum_{\tau=-1/2}^{\tau=1/2}\int f_\tau(k)\,k^2dk+V(\rho,T,\beta),$$

where, the interaction part is given by

$$\begin{aligned}V(\rho,T,\beta)=&\frac{A_u\rho_n\rho_p}{\rho_0}+\frac{A_l}{2}(\rho_n{}^2+\rho_p{}^2)+\frac{B}{\sigma+1}\frac{\rho^{\sigma+1}}{\rho_0{}^{\sigma}}(1-x\beta^2)\\&+\frac{1}{\rho_0}\sum_{\tau,\tau'}C_{\tau,\tau'}\iint d^3p\,d^3p'\frac{f_\tau(\vec{r},p)f_{\tau'}(\vec{r},\vec{p}')}{1+\frac{(\vec{p}-\vec{p}')^2}{\Lambda^2}}.\end{aligned}\tag{2.3.42}$$

In this expression $A_u, A_l, B, C_{\tau,\tau'}, \Lambda, x, \sigma$ are the parameters involved. $\tau,\tau'=\frac{1}{2}$ for neutron and $-\frac{1}{2}$ for proton and $\tau\neq\tau'$, $\sigma=\frac{4}{3}$ and $f_\tau(\vec{r},\vec{p})$ is the momentum distribution function. The nucleonic mean fields in ANM under thermal equilibrium follow from the above eq.(2.3.42) by taking the functional derivative and is given as,

$$\begin{aligned}U(\rho,T,\beta,\vec{p},\tau)=&A_u(x)\frac{\rho_{\tau'}}{\rho_0}+A_l(x)\frac{\rho_\tau}{\rho_0}+B\left(\frac{\rho}{\rho_0}\right)^{\sigma}(1-x\beta^2)-8\tau x\frac{B}{\sigma+1}\frac{\rho^{\sigma-1}}{\rho_0{}^{\sigma}}\beta\rho_\tau\\&+\frac{2C_{\tau,\tau}}{\rho_0}\int d^3p'\frac{f_\tau(\vec{r},\vec{p})}{1+(\vec{p}-\vec{p}')^2/\Lambda^2}+\frac{2C_{\tau,\tau'}}{\rho_0}\int d^3p'\frac{f_\tau(\vec{r},\vec{p})}{1+(\vec{p}-\vec{p}')^2/\Lambda^2}\end{aligned}\tag{2.3.43}$$

The parameters $A_u(x), A_l(x), B, C_{\tau,\tau}, C_{\tau,\tau'}$ and Λ are considered to be temperature independent and have been obtained by fitting the momentum dependence of $U(\rho,T=0,\beta,\vec{p},\tau)$ to that predicted by the Gogny Hatree-Fock and/or the Brueckener-Hatree-Fock calculations, along with the constraints, such as, saturation properties of symmetric nuclear matter and the symmetry energy $E_s(\rho_0)=30\,MeV$ at normal nuclear matter density $\rho_0=0.16\,fm^{-3}$. The parameter $B=106.35\,MeV$ along with the value of $\sigma=\frac{4}{3}$ is adjusted to give the value of the nuclear matter incompressibility $K(\rho_0)=211\,MeV$. The momentum dependence of neutron and proton mean fields is adjusted from the fitting to the Gogny Hatree-Fock and/or BHF calculations that results the values of the strength parameters for the momentum dependent parts $C_{\tau,\tau}=-103.4\,MeV$ and $C_{\tau,\tau'}=-11.7\,MeV$ for the value of the parameter $\Lambda=p_F^0$, i.e.,

Fermi momentum in normal SNM. The parameter x is considered as a free parameter in terms of which the rest two parameters, $A_{\mu}(x)$ and $A_l(x)$, are expressed as

$$A_{\mu}(x) = -95.98 - x\frac{2B}{\sigma+1} \quad \text{and} \quad A_l(x) = -120.57 + x\frac{2B}{\sigma+1}. \tag{2.3.44}$$

In this work of Li *et al.* the free parameter x is varied to reproduce different density dependence of nuclear symmetry energy for a given effective mass splitting. The value of the parameter x is put by hand and two values, namely, $x=1$ and 0 are considered in this work. In subsequent works [85] other values of $x=-1,-2$ are also considered. The density dependence of symmetry energy $E_s(\rho)$ for the case $x=1$ is the same as the default Gogny interaction, i.e., it has decreasing trend beyond normal density ρ_0. The density dependence of $E_s(\rho)$ for the case $x=0$ has a stiffer behaviour and do not show a decreasing behaviour at higher values of density, in agreement with the predictions of RMF calculations. The contribution of the kinetic energy part of $E_s(\rho)$ and the different potential part contributions for the cases $x=1$ and 0 given in the Figure 2 of Ref. [81] is shown below in Figure 2.8 for reference. The widely different behaviour of the potential parts, as can be seen from the figure, for the cases $x=0$ and 1 results into

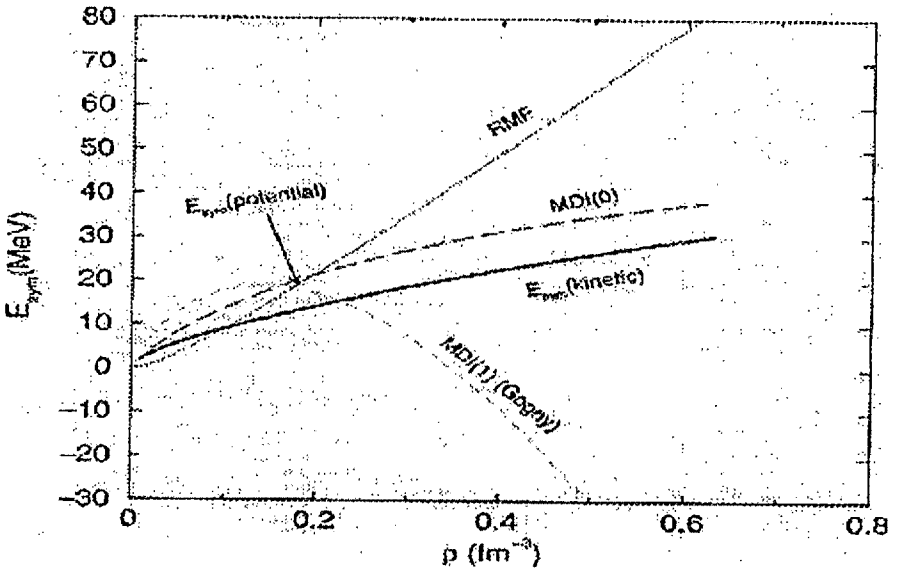

Figure 2.8. Contributions of the potential and kinetic parts of the nuclear symmetry energy calculated for the MDI interaction of B. A.Li et al.[81]. In the figure RMF result and calculations for Gogny interaction are also shown for comparison. The figure has been reproduced from Ref.[81].

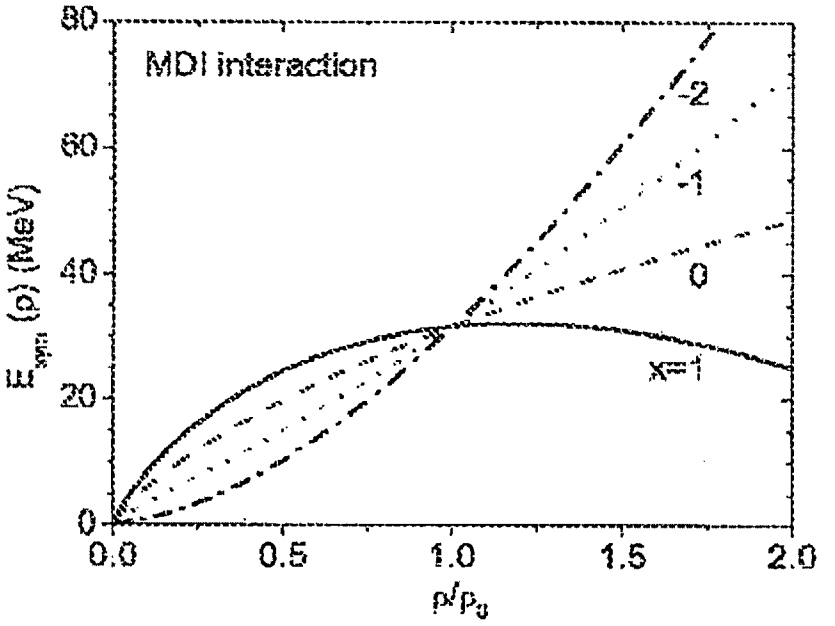

Figure 2.9. The density dependence of nuclear matter symmetry energy is shown for different values of the parameter x in the MDI interaction of Chen *et al.* [85]. The present figure is reproduced from Ref. [85].

the different behaviour of $E_s(\rho)$ for the two cases. The density dependence of the symmetry energy $E_s(\rho)$ is still stiffer for the values of $x=-1$ and -2. The plot of $E_s(\rho)$ as a function of $\frac{\rho}{\rho_0}$ as given in Figure 1 of Ref. [85] for these four different cases $x=1,0,-1$ and -2 are given here in Figure 2.9 for reference. The purpose of Li *et al.* in this work was to obtain EOSs predicting widely varying symmetry energy $E_s(\rho)$ at supranormal densities for same neutron-proton effective mass splitting. This is accomplished by the use of the parameter x in the density dependent term. As it is well known that the momentum dependence of isovector part of the neutron-proton mean fields, $\frac{u_n - u_p}{2\beta}$, determines the effective mass splitting, both the symmetry energy corresponding to $x=1$ and 0 will have the same effective mass splitting as momentum dependent part of single particle potential in eq.(2.3.43) is independent of x. For each case of symmetry energy, Li *et al.* have examined the role of momentum dependence in the isovector potential by comparing the results for the present case with the results for the cases with nucleon potential $U_{noms}(\rho,\beta,\vec{p},\tau)=U_0(\rho,\vec{p})+U_{sym}(\rho,\beta,\tau)$ that has

the same momentum dependence for the isoscalar part and a momentum independent symmetry potential $U_{sym}(\rho,\beta,\tau)$ that gives the same $E_s(\rho)$ as that of the case in eq.(2.3.43). The momentum dependent and the corresponding momentum independent symmetry potentials for the different cases of symmetry energy density, $x=1,0$, have been used by Li *et al.* in their transport model analysis of data of several experimental observables in heavy-ion collision reactions induced by neutron-rich nuclei at rare isotope accelerator(RIA). In this attempt Li *et al.* have found significantly different predictions for the two cases of symmetry potentials with and without momentum dependence. But they have not been able to extract the accurate behaviour of the density dependence of symmetry energy $E_s(\rho)$ and have concluded that momentum- and density- dependence of symmetry potential (i.e. the isovector part of the neutron-proton mean fields, $\frac{u_n-u_p}{2\beta}$) have to be determined simultaneously for the purpose of extracting actual behaviour of $E_s(\rho)$. The reason of this unsuccessful attempt may be attributed to the limited scope of the formalism to vary simultaneously the momentum- and density-dependence of isovector part of the mean field, $u_\tau(k,\rho)$. In their formalism Li *et al.* could obtained different density-dependence of $u_\tau(k,\rho)$, i.e., different behaviour of $E_s(\rho)$, by changing the value of the parameter x. However, for each case of $E_s(\rho)$ thus obtained there was no scope to vary the momentum dependence of $u_\tau(k,\rho)$, as the strength and range of the momentum dependent parts, i.e., $C_{\tau,\tau}, C_{\tau,\tau'}$ and Λ are fixed. During the same period Rizzo *et al.* [84] had made an attempt to study the effect of momentum dependence of the isovector part of the mean field on the flow dynamics. Let us now compare the momentum dependence of isovector potential of the works in Refs. [81, 85] with the results obtained with our two parameter finite range Yukawa interaction as discussed in section 2.1. The momentum dependent parts of the nucleonic mean field in ANM used by Li *et al.* given in eq (2.3.43) are similar to the exchange part of the neutron/proton mean field obtained for the Yukawa form of finite range part of the interaction used by us. The strength parameters $2C_{\tau,\tau}$ and $2C_{\tau,\tau'}$ of the momentum dependent parts of the work of Li *et al.* can be identified with those of ε_{ex}^{l} and ε_{ex}^{ul} used in our work given in eqs.(2.1.65) and

(2.1.66), respectively. The parameter Λ that specifies the range of the interaction has been taken to be $\Lambda = 1.0\, p_F^0$ by Li *et al.* The parameter Λ used in our work is related to that of Li *et al.* by a factor of $\hbar$, i.e., Λ of Li *et al.* is equivalent to $\hbar\Lambda$ of our work. We have expressed our Λ in the units of wave number in normal nuclear matter , k_{f_0}, i.e. $\Lambda = \lambda k_{f_0}$, λ being the multiplying constant factor. Thus the value of λ corresponding to $\Lambda = 1.0\, p_F^0$ of Li *et al.* is 1. However, for our case with finite range Yukawa interaction Λ and the exchange strength parameter $\varepsilon_{ex} = \frac{\varepsilon_{ex}^{l} + \varepsilon_{ex}^{ul}}{2}$ of the isoscalar part of the mean field are obtained by adopting a simultaneous minimization procedure subject to the available constraint on energy dependence of optical potential, as has been discussed in the section 2.1. The value of λ thus obtained in our case of Yukawa interaction is 1.833. The strength of the exchange parameter, $\varepsilon_{ex} = \frac{\varepsilon_{ex}^{l} + \varepsilon_{ex}^{ul}}{2}$, of the isoscalar part of the mean field obtained in our work is -121.84 MeV, whereas, the corresponding value of strength parameter of Li *et al.* is $\frac{1}{2}(2C_{\tau\tau} + 2C_{\tau\tau'}) = -115.1 MeV$. It may be seen that the strength of exchange interaction of isoscalar part of the mean field of Li *et al.* and our case of Yukawa interaction are in good agreement, whereas, they differ largely in the range of the interaction. Now we shall compare the results of $u_\tau(k, \rho_0)$ for this case of Li *et al.* with our results obtained for different splittings of exchange parameter ε_{ex} in SNM into two like and unlike channels ε_{ex}^{l} and ε_{ex}^{ul}. The results are calculated from the expression of $u_\tau(k, \rho_0)$ given in eq.(2.1.53). It requires values of symmetry energy and effective mass in SNM at normal density ρ_0 apart from the momentum dependent term defined through the functional, $u_\tau^{ex}(k, \rho_0)$. The value of the symmetry energy at normal nuclear matter density used by Li *et al.* is, $E_S(\rho_0) = 30\ MeV$. The momentum dependent part of the isoscalar potential of Li *et al.* can be analytically expressed as,

$$(C_{\tau\tau} + C_{\tau\tau'})\left[\frac{3\Lambda^2(\Lambda^2 + {k_f}^2 - k^2)}{8k{k_f}^3}\ln\left(\frac{\Lambda^2 + (k+k_f)^2}{\Lambda^2 + (k-k_f)^2}\right)\right] + \frac{3\Lambda^2}{2{k_f}^2} - \frac{3\Lambda^3}{2{k_f}^3}\left\{\tan^{-1}\left(\frac{k+k_f}{\Lambda}\right) - \tan^{-1}\left(\frac{k-k_f}{\Lambda}\right)\right\} \tag{2.3.45}$$

The value of effective mass in SNM at normal density $\frac{M^*}{M}(k_{f_0},\rho_0)=\left[1+\frac{M}{\hbar k}\frac{\partial U(k,\rho_0)}{\partial k}\right]^{-1}_{k=k_{f_0}}$ for the case is calculated to be 0.6684. Here in the above expression we have used our notation except the exchange strength parameter, $C_{\tau,\tau}$ and $C_{\tau,\tau'}$. The expression of $u_\tau(k,\rho)$ can now be written as

$$u_\tau(k,\rho_0)=2E_s(\rho_0)-\frac{\hbar^2 {k_{f_0}}^2}{2M^*}-(C_{ex}^{l}-C_{ex}^{ul})\left[\frac{1}{8zx_0}\ln\left\{\frac{1+(z+x_0)^2}{1+(z-x_0)^2}\right\}-\frac{1}{8{x_0}^2}\ln\left\{1+4{x_0}^2\right\}\right] \tag{2.3.46}$$

where, $x_0=\alpha k_{f_0}$ and $z=\alpha k$. The plot of $u_\tau(k,\rho_0)$ as a function of energy $E=\frac{\hbar^2k^2}{2M}$ is given in the Figure 2.10. The result of our Yukawa form of the finite range interaction for different representative splittings of ε_{ex} into ε_{ex}^{l} and ε_{ex}^{ul} are also given for comparison. It may be seen that the result of Li et. al. and our result for $\varepsilon_{ex}^{l}-\varepsilon_{ex}^{ul}=1.1\varepsilon_{ex}$ are close to each other. In our calculation we have used the same value of $E_S(\rho_0)=30\ MeV$ and value of $\frac{M^*}{M}(k_{f_0},\rho_0)=0.67$ obtained for our case.

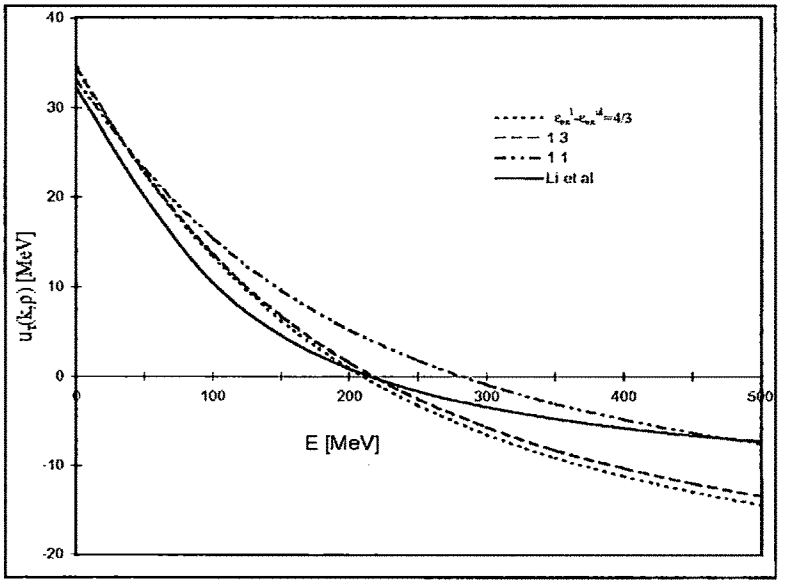

Figure 2.10. Isovector part of nuclear mean field $u_\tau(k,\rho_0)$ plotted as a function of energy for different values $(\varepsilon_{ex}^{l}-\varepsilon_{ex}^{ul})/\varepsilon_{ex}$. The work of B.A.Li *et al.*[81] has been compared with the present calculation.

The slope of the curve of $u_\tau(k,\rho_0)$ is another relevant quantity that has been extracted from optical model analysis of nucleon-nucleus scattering data, as discussed by *Li et al.* in their work [81], should be within 0.1-0.2. We shall obtain here analytical expression for the slope of the curve $u_\tau(k,\rho)$. In order to obtain this one needs to evaluate $\frac{\partial u_\tau(k,\rho)}{\partial E}$. We shall evaluate it for the general case of $u_\tau(k,\rho)$ obtained from eq.(2.1.53) for our two parameter exchange interaction as given by,

$$u_\tau(k,\rho) = 2E_s(\rho) - \frac{\hbar^2 k_{f_0}{}^2}{3M}\left[\left(\frac{M^*}{M}(k_f,\rho)\right)^2 - \left(\frac{\hbar k_f}{MC}\right)^2\right]^{\frac{1}{2}} + \frac{\left(\varepsilon_{ex}^{l} - \varepsilon_{ex}^{ul}\right)\rho}{2\rho_0 \int f(r) d^3r} \int\left[j_0(kr) - j_0(k_f r)\right] j_0(k_f r) f(r) d^3r. \tag{2.3.47}$$

Differentiation with respect to energy gives

$$\frac{\partial u_\tau(k,\rho)}{\partial E} = \frac{\partial u_\tau(k,\rho)}{\partial k}\frac{\partial k}{\partial E} \quad . \tag{2.3.48}$$

(i) For the case of small values of E:

For the case $pC << MC^2$, $\frac{\partial E}{\partial k} = \frac{\hbar^2 k}{M}$ and $\frac{\partial u_\tau(k,\rho)}{\partial E} = \frac{M}{\hbar^2 k}\frac{\partial u_\tau(k,\rho)}{\partial k}$.
From the expression of $u_\tau(k,\rho)$ given above, we get

$$\frac{\partial u_\tau(k,\rho)}{\partial E} = \frac{M}{\hbar^2 k}\frac{\left(\varepsilon_{ex}^{l} - \varepsilon_{ex}^{ul}\right)\rho}{2\rho_0 \int f(r) d^3r}\frac{\partial}{\partial k}\int j_0(kr)\, j_0(k_f r)\, f(r)\, d^3r \tag{2.3.49}$$

Now, in case of $E \to 0$, i.e. $k \to 0$, we can use approximation $j_o(kr) = 1 - \frac{(kr)^2}{6} + \cdots$ and in this limit the expression for slope of the curve for $u_\tau(k,\rho)$ becomes

$$\lim_{E\to 0}\frac{\partial u_\tau(k,\rho)}{\partial E}=\frac{M}{\hbar^2 k}\frac{\left(\varepsilon_{ex}^{l}-\varepsilon_{ex}^{ul}\right)\rho}{2\rho_0\int f(r)d^3r}\frac{\partial}{\partial k}\int[1-\frac{(kr)^2}{6}+\cdots]\ j_0(k_f r)f(r)d^3r$$

$$=-\frac{M}{6\hbar^2}\frac{\left(\varepsilon_{ex}^{l}-\varepsilon_{ex}^{ul}\right)\rho}{\rho_0\int f(r)d^3r}\int r^2 j_0(k_f r)f(r)d^3r \qquad (2.3.50)$$

For the case of our Yukawa form of finite range interaction the integral in the above expression becomes

$$\int r^2 j_0(k_f r)f(r)d^3r=4\pi\int_0^\infty\frac{\sin(k_f r)}{k_f r}\frac{e^{-r/\alpha}}{r/\alpha}r^4 dr \qquad (2.3.51)$$

Using the identity

$$\int_0^\infty \sin bx\, e^{-\beta x}x^n dx=(-1)^n\frac{\partial^n}{\partial\beta^n}\left(\frac{b}{b^2+\beta^2}\right),\quad \text{Re}\,\beta>0 \text{ and } b>0, \qquad (2.3.52)$$

we evaluate the last integral in eq (2.3.51) as

$$\begin{aligned}\int r^2 j_0(k_f r)f(r)d^3r&=\frac{4\pi\alpha}{k_f}(-1)^2\frac{\partial^2}{\partial\Lambda^2}\left(\frac{k_f}{k_f^{\,2}+\Lambda^2}\right)\\&=-8\pi\alpha^5\frac{(x_f^{\,2}-3)}{(x_f^{\,2}+1)^3}\end{aligned} \qquad (2.3.53)$$

with $\Lambda=\frac{1}{\alpha}$ and $x_f=\frac{k_f}{\Lambda}$.

Thus, the slope parameter of the curve of $u_\tau(k,\rho)$ in the limit $k\to 0$ can be calculated from the expression

$$\frac{\partial u_\tau(k,\rho)}{\partial k}=-\frac{M}{3\hbar^2}\frac{\left(\varepsilon_{ex}^{l}-\varepsilon_{ex}^{ul}\right)\rho}{\rho_0}\alpha^2\frac{(x_f^{\,2}-3)}{(x_f^{\,2}+1)^3} \qquad (2.3.54)$$

(ii) For any value of E:

We can have

$$\frac{\partial E}{\partial k}=\frac{\partial}{\partial k}(C^2\hbar^2k^2+M^2C^4)^{1/2}=C\hbar\left(1-\frac{M^2C^4}{E^2}\right)^{1/2}$$

and

$$\frac{\partial u_\tau(k,\rho)}{\partial E} = \frac{1}{C\hbar}\left(1-\frac{M^2C^4}{E^2}\right)^{-\frac{1}{2}} \frac{\partial}{\partial k}\left\{\frac{\left(\varepsilon_{ex}^{l}-\varepsilon_{ex}^{ul}\right)\rho}{2\rho_0\int f(r)d^3r}\int\left[j_0(kr)-j_0(k_f r)\right]j_0(k_f r)\,f(r)\,d^3r\right\}$$

$$= -\frac{1}{C\hbar}\left(1-\frac{M^2C^4}{E^2}\right)^{-\frac{1}{2}} \frac{\left(\varepsilon_{ex}^{l}-\varepsilon_{ex}^{ul}\right)\rho}{2\rho_0\int f(r)d^3r}\int r\,j_1(kr)\,j_0(k_f r)\,f(r)\,d^3r \tag{2.3.55}$$

For Yukawa form of $f(r)$, the integral in the above expression becomes

$$\int r\,j_1(kr)\,j_0(k_f r)\,f(r)\,d^3r = \frac{\pi\alpha}{kk_f}\left[\frac{1}{k}\ln\left\{\frac{\Lambda^2+(k+k_f)^2}{\Lambda^2+(k-k_f)^2}\right\} - 2\left\{\frac{k+k_f}{\Lambda^2+(k+k_f)^2} - \frac{k-k_f}{\Lambda^2+(k-k_f)^2}\right\}\right] \tag{2.3.56}$$

2.5. Work of Rizzo *et al.*

The emphasis of the work of Rizzo *et al.* [84] in their work was to search for observational effects of the two opposite types of neutron-proton effective mass splittings in the interpretation of collective flow data through collision simulations. In the work, the simulation has been performed for the two opposite types of effective mass splittings by using an effective energy density that has been widely used for symmetric nuclear matter case. They have obtained the two opposite types of effective mass splittings by suitably adding a parameter, z_1, to the momentum dependent part of the energy density, to be more specific, to the isovector part. The variation of this parameter results in the variation of neutron and proton effective masses keeping the symmetry energy and its density dependence unchanged. The compelling force behind this work of Rizzo *et al.* was the predictions of newly constructed Skyrme-Lyon interaction sets (SLy-force) [112] those predict the proton effective mass value higher than the neutron one, in contradiction to the predictions of earlier Skyrme sets. This predictions of SLy forces gained profound support at that time by the same finding of Hoffmann *et al.* [120] from the microscopic relativistic-Dirac-Brueckner (DBHF) calculations, although non-relativistic BHF calculations are leading to opposite conclusion [118, 162]. The effective energy density in asymmetric matter used by Rizzo *et al.* is given by

$$H(\rho_n,\rho_p)=\frac{2}{(2\pi)^3}\int\frac{\hbar^2k^2}{2M}\left[f_n(k)+f_p(k)\right]d^3k+\frac{A}{2}\frac{\rho^2}{\rho_0}\left[1-\frac{2}{3}\left(\frac{1}{2}+x_0\right)\beta^2\right]$$
$$+\frac{B}{\sigma+1}\frac{\rho^{\sigma+1}}{\rho_0{}^{\sigma}}\left[1-\frac{2}{3}\left(\frac{1}{2}+x_3\right)\beta^2\right]+C\frac{\rho}{\rho_0}\left(\tau_n+\tau_p\right)+\frac{C-8z_1}{5}\frac{\rho}{\rho_0}\left(\tau_n-\tau_p\right)\beta \tag{2.3.57}$$

where,

$$\tau_i=\frac{2}{(2\pi)^3}\int d^3k\, f_i(k)\,g(k,\Lambda) \tag{2.3.57a}$$

with $i=n,p$ and the functional $g(k,\Lambda)$ is given by

$$g(k,\Lambda)=\left[1+\left(\frac{k-<k>}{\Lambda}\right)^2\right]^{-1}. \tag{2.3.57b}$$

In this eq.(2.3.57) for energy density, the first term is the kinetic energy term where $f_i(k)$, $i=n,p$ are the respective Fermi-Dirac distribution functions and the last term is the momentum dependent term. This energy density is referred to as BGBD parameterization which reduces to the GBD parameterization version, for $\beta=0$, proposed earlier by Gale, Bertsch and Das Gupta [50] in connection to the study of EOS in symmetric nuclear matter. The parameters A,B,C,σ and Λ are taken to be same as in the GBD parameterization version, namely, $A=-144\,MeV$, $B=203.3\,MeV$, $C=-75\,MeV$, $\sigma=\frac{7}{6}$ and $\Lambda=1.5p_f^{(0)}$, $p_f^{(0)}$ being the Fermi momentum at normal density, $\rho_0=0.16\,fm^{-3}$. The energy density predicts an incompressibility in normal nuclear matter $K(\rho_0)=210\,MeV$. The value of the parameter z_1 decides the strength of the momentum dependence in the isospin channel. In terms our notation, a given z_1 decides the splitting of the exchange strength parameter, $\varepsilon_{ex}=\frac{\varepsilon_{ex}^{l}+\varepsilon_{ex}^{ul}}{2}$, into two different channels of interaction between the like nucleons and unlike nucleons. The rest two parameters x_0 and x_3 of the BGBD parameterization are adjusted to give the same value of symmetry energy at normal density, $E_s(\rho_0)=33MeV$, for the different cases of effective mass splitting considered in their work. The neutron and proton mean fields are now obtained by the functional derivatives of the BGBD energy density in eq.(2.3.57) as,

$$U_i(k,\rho,\beta)=A\left(\frac{\rho}{\rho_0}\right)+B\left(\frac{\rho}{\rho_0}\right)^{\sigma}-\frac{2}{3}(\sigma-1)\frac{B}{\sigma+1}\left(\frac{1}{2}+x_3\right)\left(\frac{\rho}{\rho_0}\right)^{\sigma}\beta^2-\frac{1}{3}A\left(\frac{\rho}{\rho_0}\right)\left(\frac{1}{2}+x_0\right)\beta^2$$
$$\pm\left[-\frac{2}{3}A\left(\frac{\rho}{\rho_0}\right)\left(\frac{1}{2}+x_0\right)-\frac{4}{3}\frac{B}{\sigma+1}\left(\frac{1}{2}+x_3\right)\left(\frac{\rho}{\rho_0}\right)^{\sigma}\right]\beta+\frac{4}{5\rho_0}\left\{\frac{1}{2}(3C-4z_1)\tau_i+(C+2z_1)\tau_{i'}\right\}$$
$$+\left(C\pm\frac{C-8z_1}{5}\beta\right)\left(\frac{\rho}{\rho_0}\right)g(k) \tag{2.3.58}$$

with $i\neq i'=n,p$ and the upper sign refers to neutrons and lower sign refers to protons. The last term, besides the GBD momentum dependence, contains an isospin dependent part which results into different effective masses for protons and neutrons. From the definitions of effective mass, $\left[\frac{M^*(k,\rho)}{M}\right]_{i=n,p}=\left[1+\frac{M}{\hbar k}\frac{\partial U_i}{\partial k}\right]^{-1}_{i=n,p}$, the nucleon effective mass in the present case of BGBD parameterization becomes,

$$\frac{M^*(k,\rho)}{M}=\left[1+\frac{M}{\hbar^2 k}\frac{d}{dk}\left\{C\pm\frac{C-8z_1}{5}\beta\right\}\left(\frac{\rho}{\rho_0}\right)g(k)\right]^{-1}$$
$$=\left[1+\frac{M}{\hbar^2}\left(C\pm\frac{C-8z_1}{5}\beta\right)\frac{1}{k}\frac{dg(k)}{dk}\right]^{-1}. \tag{2.3.59}$$

The factor $\frac{1}{k}\frac{dg(k)}{dk}$ inside the square bracket for the GBD version of $g(k)$ given in eq.(2.3.57b) becomes

$$\frac{1}{k}\frac{dg(k)}{dk}=-\frac{\frac{2(k-<k>)}{\Lambda^2 k}}{\left[1+\left(\frac{k-<k>}{\Lambda}\right)^2\right]^2} \tag{2.3.60}$$

Under the GBD parameterization the average momentum in all directions is considered to be zero, i.e. $<k>=0$.

Hence, $\left(\frac{k-<k>}{\Lambda}\right)^2\Big|_{k=k_i}\overset{GBD}{=}\left(\frac{k_i}{\Lambda}\right)^2$ with $i=n,p$, which becomes

$$\left(\frac{k-<k>}{\Lambda}\right)^2\Big|_{k=k_i}=\left(\frac{k_{f_0}}{\Lambda}\right)^2\left\{(1\pm\beta)\frac{\rho}{\rho_0}\right\}^{2/3},$$

where, the upper sign is for neutron and lower one is for proton and $k_{f_0} = 1.5\pi^2\rho$ is the Fermi momentum in normal nuclear matter. The neutron and proton effective masses at their respective Fermi momenta for the present case is given by

$$\left[\frac{M^*(k,\rho_0)}{M}\right]_{k=k_{n,p}} = \left[1+\frac{-\frac{2M}{\hbar^2\Lambda^2}\frac{d}{dk}\left\{C \pm \frac{C-8z_1}{5}\beta\right\}\left(\frac{\rho}{\rho_0}\right)}{\left[1+\left(\frac{k_{f_0}}{\Lambda}\right)^2\left\{(1\pm\beta)\frac{\rho}{\rho_0}\right\}^{2/3}\right]^2}\right]^{-1} \tag{2.3.61}$$

where, upper sign is for neutron and lower one is for proton. Rizzo *et al.* have produced both types of effective mass splittings in ANM, the proton effective mass going above that of the neutron and vice versa, by adjusting the parameter z_1 appearing in the expression for effective mass in eq.(2.3.61). Two sets of values for z_1, x_0 and x_3 are chosen, those give opposite neutron and proton effective mass splittings but provide almost similar behaviour of the symmetry energy $E_s(\rho)$, having the same value at saturation $E_s(\rho_0) = 33\,MeV$. In particular, they have chosen $z_1 = +50, x_0 = 1.589$ and $x_3 = -0.195$ that give proton effective mass above the neutron one and $z_1 = -36.75, x_0 = -1.477$ and $x_3 = -1.101$ that give neutron effective mass above that of the proton. The potential part of the symmetry energy along with the separate contributions from momentum independent part and momentum dependent parts are shown in the Figure 2.11 for the two cases and the corresponding results of neutron-proton effective mass splitting are shown in the inside blocks of the respective figures.

Rizzo *et al.* have studied the flow observables, in particular the transverse and elliptical flow differences in Au+Au collision at 250 MeV, using the mean fields for these two cases and found them to be selective probes of momentum dependence of the isovector part of the nuclear EOS. In order to examine the effect of stiffness of nuclear symmetry energy on these flow observables, Rizzo *et al.* have produced relatively soft symmetry energy by adjusting the values of the parameters x_0 and x_3 while keeping the values of z_1 for the two cases to be the same. This way they could produce relatively soft density dependence of nuclear symmetry energy for the same neutron-proton

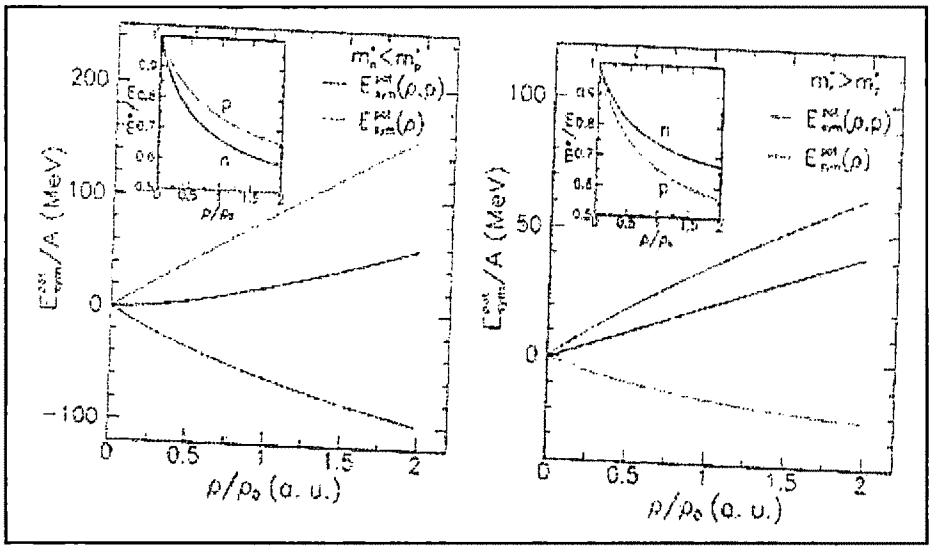

Figure 2.11. Potential part of the nuclear symmetry energy plotted as a function of the relative density ρ / ρ_0. Separate contribution of the momentum dependent part and momentum independent part are also shown in the figure. The left panel is for $M_n^* < M_p^*$ and the right panel is meant for $M_n^* > M_p^*$. The figure is reproduced from the work of Rizzo *et al* [84].

effective mass splitting and have examined the effect on the flow observables. They have found that the observed effects are not changed by largely changing the density dependence of symmetry energy while keeping the momentum dependence of the isovector part of the mean field unchanged.

In another contemporary work[163], B.A. Li has studied the energy dependence of the isovector part of the mean field for the two cases considered by Rizzo *et al.* and have compared the results with the experimentally extracted results of Lane potential [152]. Li has also compared the isoscalar parts of the potentials for these two cases as a function of density for four values of momentum $k = 1, 2, 3$ and $4\, fm^{-1}$, with the results of realistic interaction UV14+UVII of Wiringa [66]. The figures depicting the results of Li as obtained in the work of Ref. [163] are given in Figure 2.12. It may be seen that the results for isoscalar potentials for the two cases are same and compares reasonably well with the realistic calculation up to $k = 3\, fm^{-1}$. However, the isovector

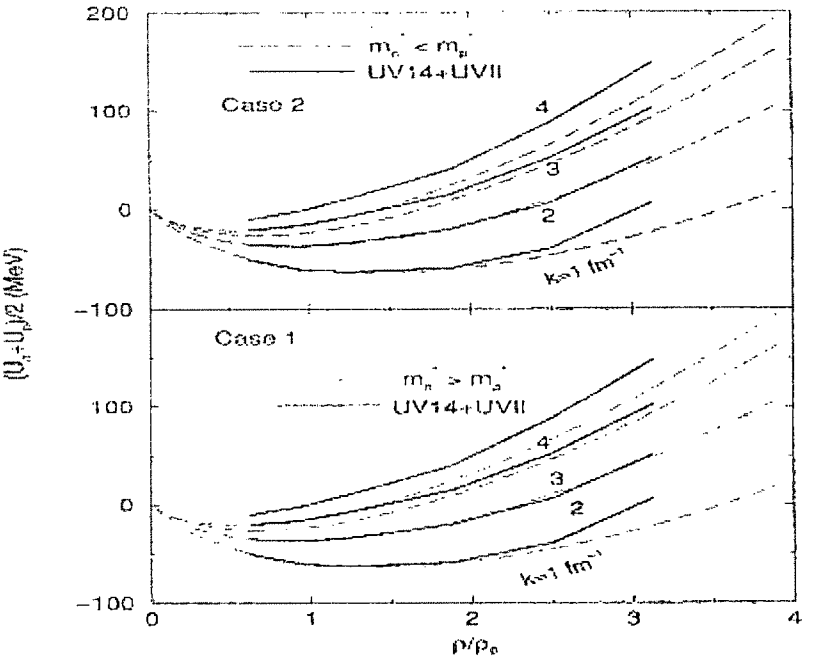

Figure 2.12. Isoscalar potentials as functions of relative density. The results are compared with the results of realistic interaction UV14+UVII.. The figure has been reproduced from the Ref. [163].

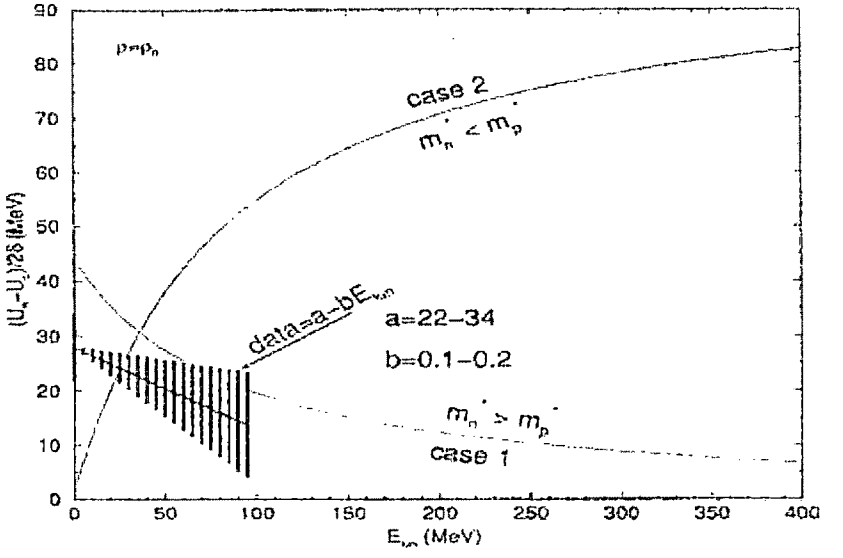

Figure 2.13. Isovector part of the nuclear mean at normal nuclear matter density, i.e, the Lane potential is plotted as a function of the energy. The experimentally extracted data is shown as the shaded region in the graph. The Figure is reproduced from the Ref. [163].

part of the mean field at normal density, i.e., Lane potential, as function of energy is found to have completely different and opposite behaviour for the two cases as may be seen from Figure 2.13. Comparing with the results as depicted in the same figure, extracted on the Lane potential from the nucleon-nucleus reaction studies up to $E=100\,MeV$, Li has given his opinion in favour of the neutron effective mass greater than the proton effective mass, $M_n^* > M_p^*$, in neutron-rich dense matter.

Effective energy densities resulting into similar momentum dependent terms in their resulting neutron and proton mean fields, as in case of BGBD, have been used widely in the studies of EOS of ANM, in recent years by Moustakidis [164, 165] and Moustakidis and Panos [166]. In their works the authors have mainly emphasized on examining the contribution of the momentum dependent part of the neutron-proton mean fields at finite temperature, $T \neq 0$, to the various relevant properties of ANM. The energy density used in these works for ANM is given by

$$H(\rho_n,\rho_p,T)=\frac{2}{(2\pi)^3}\int\frac{\hbar^2k^2}{2M}\left[f_n(\rho_n,k,T\right]+\left[f_p(\rho_p,k,T\right]d^3k$$
$$+\frac{1}{3}\frac{A}{\rho_0}\left[\frac{3}{2}-\left(\frac{1}{2}+x_0\right)\beta^2\right]\rho^2+\frac{\frac{2}{3}B\rho_0\left[\frac{3}{2}-\left(\frac{1}{2}+x_3\right)\beta^2\right]\left(\frac{\rho}{\rho_0}\right)^{\sigma+1}}{1+\frac{2}{3}B'\left[\frac{3}{2}-\left(\frac{1}{2}+x_3\right)\beta^2\right]\left(\frac{\rho}{\rho_0}\right)^{\sigma-1}}$$
$$+\frac{\rho}{\rho_0}\sum_{i=1,2}\left[C_i\left(\tau_n+\tau_p\right)+\frac{(C_i-8z_i)}{5}\beta\left(\tau_n-\tau_p\right)\right] \qquad (2.3.62)$$

where, the first term is the kinetic energy density defined through the Fermi-Dirac distribution functions, f_τ with $\tau=n,p$, for neutron and proton defined in eq. (2.3.57a) and the rest part is the interaction part with the functions τ_τ defined as

$$\tau_\tau(\rho,\beta,T)=\frac{2}{(2\pi)^3}\int d^3k\;\; g(k,\Lambda_i)\,f_\tau(\rho_\tau,k,T). \qquad (2.3.63)$$

It may be noted that the above energy density is similar to the energy density used in the work of Rizzo *et al.* given in eq.(2.3.57), except that here Moustakidis has taken two momentum dependent terms having two different range parameters $\Lambda_1=1.5k_{f_0}$ and $\Lambda_2=3k_{f_0}$. The parameters A,B,σ,C_1,C_2 and B' have been obtained from the

description of SNM and the additional parameters x_0, x_3, z_1 and z_2 are constrained by empirical knowledge of ANM. Using this energy density given in eq.(2.3.62) and the nucleonic mean field resulting from it, Moustakidis have studied the effect of temperature on the symmetry energy and neutron and proton mean fields [164]. In this work, Moustakidis have approximated the energy density of ANM in eq.(2.3.62) by a quadratic approximation

$$H(\rho,T,Y_p) = H(\rho,T,Y_p = 1/2) + H_{asy}(\rho,T,Y_p) \tag{2.3.64}$$

where,

$$H_{asy}(\rho,T,Y_p) = (1-2Y_p)^2 \rho E_s(\rho). \tag{2.3.64a}$$

He has also calculated the equilibrium proton fraction Y_p of the $n+p+e$ matter under beta-equilibrium. In a subsequent work [165], Moustakidis has studied the effect of parameterization of interaction part of the symmetry energy, i.e., $E_s^{\text{int}}(\rho)$, as well as, the momentum dependence generator function $g(k,\Lambda_i)$ on the isovector part of the mean field and neutron-proton effective mass splitting by considering different functional forms for these two quantities. In this investigation, Moustakidis has considered three forms of parameterized version of $E_s^{\text{int}}(\rho)$, namely,

$$E_s^{\text{int}}(\rho) \propto \sqrt{\frac{\rho}{\rho_0}}, \qquad E_s^{\text{int}}(\rho) \propto \frac{\rho}{\rho_0} \text{ and } \quad E_s^{\text{int}}(\rho) \propto \frac{2(\rho/\rho_0)^2}{1+(\rho/\rho_0)}$$

and two different forms of $g(k,\Lambda_i)$, namely,

$$g(k,\Lambda_i) = \left[1+\left(\frac{k}{\Lambda_i}\right)^2\right]^{-1} \text{ and } \qquad g(k,\Lambda_i) = \left[1-\left(\frac{k}{\Lambda_i}\right)^2\right].$$

Parameterization of the interaction part of the symmetry energy, $E_s^{\text{int}}(\rho)$, into the above three forms have been done by adjusting the parameters x_0, x_3, z_1 and z_3. In another work [166], Moustakidis and Panos have studied the equation of state of beta-stable $n+p+e+\mu$ matter at finite temperature by using the same model. It may be mentioned here that the momentum and temperature dependence of nuclear mean fields resulting from the energy density used by Moustakidis and co-workers arise solely from the last term in eq.(2.3.62). The discussion can be more transparently seen by

considering the case of SNM by setting $\beta = 0$ and $f_n = f_p = f$, for which the energy density of Moustakidis becomes

$$H(\rho,T) = \frac{4}{(2\pi)^3}\int \frac{\hbar^2 k^2}{2M} f(k,T)\, d^3k + \frac{1}{2}A\frac{\rho^2}{\rho_0} + \frac{B\rho_0\left(\frac{\rho}{\rho_0}\right)^{\sigma+1}}{1+B_0'\left(\frac{\rho}{\rho_0}\right)^{\sigma-1}} + \frac{4}{(2\pi)^3}\frac{\rho}{\rho_0}\sum_{i=1,2} C_i \int d^3k\; g(k,\Lambda_i) f(k,T) \tag{2.3.65}$$

The single particle energy and nuclear mean field can be obtained by taking the functional derivative of the energy density, i.e., $\varepsilon(\rho,k,T) = \frac{\partial H}{\partial [f]}$, and we get,

$$\varepsilon(\rho,k,T) = \frac{\hbar^2 k^2}{2M} + A\frac{\rho}{\rho_0} + B\left(\frac{\rho}{\rho_0}\right)^{\sigma}\frac{\left(\sigma+1+2B'(\rho/\rho_0)^{\sigma-1}\right)}{\left(1+B'(\rho/\rho_0)^{\sigma-1}\right)^2} + \frac{4}{(2\pi)^3\rho_0}\sum_{i=1,2} C_i \int d^3k\; g(k,\Lambda_i) f(k,T) + \frac{\rho}{\rho_0}\sum_{i=1,2} C_i\, g(k,\Lambda_i) \tag{2.3.66}$$

In this expression, the first term in the right hand side is the kinetic energy term which has quadratic momentum dependence and the rest terms give the mean field. The 1st and 2nd terms of the mean field are functions of density ρ only (independent of momentum k and temperature T); the third term of the mean field is dependent on density ρ and temperature T (independent of momentum k) which is responsible for accounting for the temperature effect of the interaction part and the last term of the mean field depends on density ρ and momentum k (independent of temperature T), which along with the kinetic energy term constitute the effective mass term. This type of density ρ, momentum k and temperature T dependences in the single particle energy expression is characteristic of the GBD approximated energy densities used by Moustakidis and co-workers as well as Rizzo *et al.*[84].

The GBD type momentum dependence in the mean field used in the above works of Moustakidis and Rizzo *et al.* can be obtained as an approximation of the general expression of the momentum dependent part of the mean field resulting from

the two parameter Yukawa form of exchange interaction used in section 2.1 in the study of momentum dependence of isovector part of the mean field and neutron-proton effective mass splitting. The contribution of the finite range part of the exchange interaction to the energy density in SNM at a given density ρ and temperature T is given by

$$\begin{aligned} H(\rho,T) &\rightarrow \iiint f_T(k) f_T(k') e^{i(\vec{k}-\vec{k}')\cdot\vec{r}} f(r) d^3k d^3k' d^3r \\ &\sim \iint f_T(k) f_T(k') \; g(|\vec{k}-\vec{k}'|) \; d^3k d^3k' \end{aligned} \tag{2.3.67}$$

where, $g(|\vec{k}-\vec{k}'|)$ is normalized Fourier transform of the finite range interaction $f(r)$, which for the Yukawa form becomes,

$$g_{ex}(|\vec{k}-\vec{k}'|) = \frac{1}{1+\frac{|\vec{k}-\vec{k}'|^2}{\Lambda^2}},$$

given in eq (2.1.78). Thus, the contribution to the energy density from the finite range Yukawa interaction part becomes

$$\iint f_T(\vec{k}) f_T(\vec{k}') \; \frac{1}{1+\frac{|\vec{k}-\vec{k}'|^2}{\Lambda^2}} \; d^3k d^3k'. \tag{2.3.68}$$

In this expression $\vec{k}$ and $\vec{k}'$ are the momenta of the two interacting nucleons. Under GBD approximation, momentum $\vec{k}$ is measured with respect to the average of the momenta $\vec{k}'$ for the particles in the neighborhood of $\vec{k}$. Thus the above contribution under GBD approximation becomes,

$$\iint f_T(\vec{k}) f_T(\vec{k}') \; \frac{1}{1+\frac{|\vec{k}-<\vec{k}'>|^2}{\Lambda^2}} \; d^3k d^3k'. \tag{2.3.69}$$

Now, under the normalization, $\int f_T(\vec{k}) \; d^3k = \rho$, the above expression further simplifies to

$$\rho \int f_T(\vec{k}) \; \frac{1}{1+\frac{|\vec{k}-<\vec{k}'>|^2}{\Lambda^2}} \; d^3k. \tag{2.3.70}$$

Now we compare the contribution of the exact expression in eq.(2.3.68) and GBD approximated expression in eq.(2.3.70) to the mean field in SNM. The contribution of the exact case is

$$\rho \int f_T(\vec{k}) \frac{1}{1+\frac{|\vec{k}-\vec{k}'|^2}{\Lambda^2}} d^3k, \tag{2.3.71}$$

where as, that of the GBD approximation is

$$\int f_T(\vec{k}) \frac{d^3k}{1+\frac{|\vec{k}-\vec{k}'|^2}{\Lambda^2}} + \frac{\rho}{1+\frac{|\vec{k}-\vec{k}'|^2}{\Lambda^2}}. \tag{2.3.72}$$

The contribution of the exact case as given above in eq.(2.3.71), has all the three functional dependence of momentum k, density ρ and temperature T. This coupled contributions of k, ρ and T warrants self-consistent evaluation at finite temperature. On the other hand, the contribution of the GBD approximated case, given eq (2.3.72), comprises of two terms, the first term is a function of temperature and density and the second term is a function of density and momentum. This is the type of ρ, k and T dependence of the nuclear mean field obtained in the works of Moustakidis as well as Rizzo *et al.* For such GBD approximated case where the temperature and momentum dependence of the mean field have been decoupled, no self-consistent calculation is required in finite temperature calculations.

The objective of all the studies of nuclear mean fields and EOSs discussed in our forgoing discussions mainly lies in its application to analyze the flow data produced in heavy ion collision experiments and/or to predict neutron star properties and its formation mechanism. In these works the thrust have been on the use of suitable effective energy density as well as the neutron and proton mean fields resulting from these energy densities which are capable of producing neutron-proton effective mass splittings of different magnitudes. In this context it is mentioned here that the neutron-proton effective mass splittings of different magnitudes can be achieved from the variation of exchange strength parameters of the finite range exchange interaction acting between a pair of like nucleons and a pair of unlike nucleons. This has been

shown in Figures 2.4(a) and (b) by considering a single Yukawa form of the finite range part of the interaction. We shall be mainly using this Yukawa form for the finite range part of the interaction in our subsequent studies. The effective interaction in complete form that will be used in our subsequent investigations is obtained by adding a zero-range density dependent part to the finite range part and is given by

$$v(\vec{r}) = t_0(1+x_0P_\sigma)\delta(\vec{r}) + \frac{1}{6}t_3(1+x_3P_\sigma)\left[\frac{\rho(\vec{R})}{1+b\rho(\vec{R})}\right]^\gamma \delta(\vec{r}) + (W + BP_\sigma - HP_\tau - MP_\sigma P_\tau)\frac{e^{-r/\alpha}}{r/\alpha} \tag{2.3.73}$$

In this expression $\vec{r} = \vec{r}_1 - \vec{r}_2$, $\vec{R} = \frac{1}{2}(\vec{r}_1 + \vec{r}_2)$ are relative and centre of mass coordinates of the two interacting nucleons; W, B, H and M are the strengths of the Wigner, Bartlet, Heisenberg and Majorana components; $P_\sigma = \frac{1+\vec{\sigma}_1\cdot\vec{\sigma}_2}{2}$, $P_\tau = \frac{1+\vec{\tau}_1\cdot\vec{\tau}_2}{2}$ are spin and isospin exchange operators respectively and α is the range of the finite range Yukawa interaction. This interaction in eq (2.3.73) is similar to the Skyrme type interaction except that the t_1- and t_2- terms are replaced by the finite range term and the density dependent t_3-term has been modified. The replacement of t_1- and t_2- terms by the finite range term is essential so as to account for the correct momentum dependence of the nuclear mean field as extracted from the optical model fits in heavy-ion collision studies at intermediate energies [52-59, 67]. The density dependence taken in the t_3-term of the Skyrme- type interactions have the form $\rho^\gamma(\vec{R})$, whereas we have considered it in the modified form having the denominator $\left[1+b\rho(\vec{R})\right]^\gamma$ with an additional parameter b from the consideration of avoiding supraluminous behaviour of the nuclear EOS at high density which is a common feature observed with the typical Skyrme- type interactions constructed prior to the Sly type interactions. It may be noted here that Skyrme parameterizations have been very successful in predicting results at and around normal nuclear matter density, low isospin asymmetry and momentum upto Fermi momentum corresponding to normal density. However, they fail in their

prediction of experimental/ empirical results when extrapolated to high density, high asymmetry and high momentum region. The finite range effective interaction in eq.(2.3.73) to be used in our present analysis of EOS of nuclear matter with particular emphasis to dense and highly isospin asymmetric case and at high momentum region contains altogether 11 parameters, namely, $t_0, x_0, t_3, x_3, b, \gamma, W, B, H, M$ and α. This interaction in its simple form in eq.(2.3.73) was developed by Behera *et al.*[64] and has been used in the study of momentum and density dependence of the isoscalar part of nuclear mean field at zero as well as at finite temperature [64, 65, 67]. This interaction has also been used in the analysis of the momentum and density dependence of isovector part of nuclear mean field at zero temperature [153]. The motivation of the thesis is to search for constraints on the momentum and density dependence of isovector part of the nuclear mean field, which has not been possible on the zero temperature studies as will be discussed in chapter-III. We shall study ANM at finite temperature using this interaction. For this purpose we shall discuss the fixation of the parameters of this interaction from the studies of symmetric matter and asymmetric matter under beta equilibrium in chapter-III. We shall also compare the zero temperature results of this interaction with the results obtained from different microscopic model

2.6. Conclusion

In chapter-II, we have reviewed the momentum and density dependence of nuclear mean field using the formalism developed by Behera *et al.* [64, 65, 67, 153, 154]. Under this formalism, it has been shown that the nuclear mean field as function of momentum and nucleonic density is the fundamental importance for the study. At Fermi momentum, the nuclear mean field describes the density dependence of nuclear EOS. Detailed derivation has been made in order to establish the fact. In this formalism, the exchange part of the finite range effective interaction accounts for the momentum dependence of nuclear mean field and thereby the neutron-proton effective masses in the medium. Using a two parameter Yukawa interaction, not only diverging but contracting behaviour of neutron-proton effective masses in neutron rich matter, as obtained by Behera *et al.* [153], has been worked out. Several parametrized sets for a given interaction are found in literature. While parametrizing the interaction for certain

purpose, the momentum dependence aspect of the mean field is not being properly taken care of. This has been explicitly demonstrated in the cases of different Gogny and Skyrme sets. With the gain of importance for the study of momentum dependence of nuclear mean field, it was required to vary the momentum dependence keeping the density dependence of the EOS unchanged. In case of Skyrme sets it was not possible till the work of Cochet *et al.*[157]. Cochet *et al.* have shown that this could be possible in case of Skyrme sets by considering more than one density dependent term in the interaction. Subsequently, Leisinski *et al.*[131] have attempted to constrain the momentum dependent aspect of nuclear mean field using Skyrme interactions with the prescription of Cochet *et al.*[157]. The works of Cochet *et al.* and Leisinski *et al.* have been reviewed in this chapter. The analysis of flow data from heavy ion collision experiments through transport model has motivated Li *et al.*[81] and Rizzo *et al.*[84] in attempting to constrain these two important aspects of nuclear mean field. With the advent of producing the different density dependent nuclear EOS having same momentum dependence of nuclear mean field and the other way around, they have constructed phenomenological energy densities. The works of the Li *et al.* [81] and Rizzo *et al.* [84] have been reviewed in good detail. The momentum dependence of the isovector part of the nuclear mean field resulting from the work of Li *et al.*[81] has been compared with that of Behera *et al.* The analytical expression for the slope of $u_\tau(k, \rho_0)$ has been derived. The contribution of the finite range part of the interaction to the energy density under GBD approximation has been derived and used in reviewing the works of Moustakidis and co-workers [164, 165, 166].

CHAPTER-III

EQUATION OF STATE OF ASYMMETRIC NUCLEAR MATTER WITH FINITE RANGE YUKAWA INTERACTION

3.1. Finite Range Yukawa Interaction and EOS of ANM

In this chapter we shall obtain the equation of state of asymmetric nuclear matter using the finite range interaction having Yukawa form given in eq.(2.3.73) in the last chapter. The EOS of ANM involves altogether nine adjustable parameters expressed as combinations of the eleven parameters of the effective interaction. The energy density, $H(\rho,Y_p,T)$, at density ρ, asymmetry $(1-2Y_p)$ and temperature T for effective interaction in general form is given in eq.(2.1.9) in the previous chapter. The expression of the energy density resulting from the density dependent finite range Yukawa interaction in eq.(2.3.73) is given by

$$
\begin{aligned}
H(\rho,Y_p,T) &= \int[f_T^n(\vec{k})+f_T^p(\vec{k})](C^2\hbar^2k^2+M^2C^4)^{1/2}\,d^3k \\
&+\frac{1}{2}\left[\frac{\varepsilon_0^l}{\rho_0}+\frac{\varepsilon_\gamma^l}{\rho_0^{\gamma+1}}\left(\frac{\rho}{1+b\rho}\right)^\gamma\right](\rho_n^2+\rho_p^2)+\left[\frac{\varepsilon_0^{ul}}{\rho_0}+\frac{\varepsilon_\gamma^{ul}}{\rho_0^{\gamma+1}}\left(\frac{\rho}{1+b\rho}\right)^\gamma\right]\rho_n\rho_p \\
&+\frac{\varepsilon_{ex}^l}{2\rho_0}\iint[f_T^n(\vec{k})f_T^n(\vec{k}')+f_T^p(\vec{k})f_T^p(\vec{k}')\,g_{ex}(|\vec{k}-\vec{k}'|)\,d^3k\;d^3k' \\
&+\frac{\varepsilon_{ex}^{ul}}{2\rho_0}\iint[f_T^n(\vec{k})f_T^p(\vec{k}')+f_T^p(\vec{k})f_T^n(\vec{k}')\,g_{ex}(|\vec{k}-\vec{k}'|)\,d^3k\;d^3k'
\end{aligned}
\tag{3.1.1}
$$

where, $f_T^\tau(\vec{k})$, $\tau=n,p$, are the respective Fermi-Dirac distribution functions and $g_{ex}(|\vec{k}-\vec{k}'|)$ is the normalized Fourier transform of the finite range interaction given in eq.(2.3.73), which for the Yukawa form becomes $g_{ex}(|\vec{k}-\vec{k}'|)=\dfrac{1}{1+\dfrac{|\vec{k}-\vec{k}'|^2}{\Lambda^2}}$.

$b,\gamma,\varepsilon_0^l,\varepsilon_0^{ul},\varepsilon_\gamma^l,\varepsilon_\gamma^{ul},\varepsilon_{ex}^l,\varepsilon_{ex}^{ul}$ and α are the nine adjustable parameters required for complete description of ANM. The new parameters $\varepsilon_0^l,\varepsilon_0^{ul},\varepsilon_\gamma^l,\varepsilon_\gamma^{ul},\varepsilon_{ex}^l$ and ε_{ex}^{ul} in terms of the interaction parameters $t_0,x_0,t_3,x_3,b,\gamma,W,B,H,M$ and α are expressed by

$$
\varepsilon_0^l=\rho_0\left[\frac{t_0}{2}(1-x_0)+4\pi\alpha^3\left(W+\frac{B}{2}-H-\frac{M}{2}\right)\right], \tag{3.1.2a}
$$

$$
\varepsilon_0^{ul}=\rho_0\left[\frac{t_0}{2}(2+x_0)+4\pi\alpha^3\left(W+\frac{B}{2}\right)\right], \tag{3.1.2b}
$$

$$\varepsilon_{\gamma}^{l} = \rho_0^{\gamma+1}\left[\frac{t_3}{12}(1-x_3)\right], \tag{3.1.2c}$$

$$\varepsilon_{\gamma}^{ul} = \rho_0^{\gamma+1}\left[\frac{t_3}{12}(2+x_3)\right], \tag{3.1.2d}$$

$$\varepsilon_{ex}^{l} = 4\pi\alpha^3\rho_0\left(M - \frac{W}{2} + \frac{H}{2} - B\right), \tag{3.1.2e}$$

$$\varepsilon_{ex}^{ul} = 4\pi\alpha^3\rho_0\left(M + \frac{H}{2}\right). \tag{3.1.2f}$$

The neutron-proton single particle energy resulting from this energy density in eq.(3.1.1) can be given by

$$\begin{aligned}\varepsilon^{n(p)}(\rho, Y_p, k, T) = (C^2\hbar^2k^2 + M^2C^4)^{1/2} &+ \left[\frac{\varepsilon_0^{l}}{\rho_0} + \frac{\varepsilon_{\gamma}^{l}}{\rho_0^{\gamma+1}}\left(\frac{\rho}{1+b\rho}\right)^{\gamma}\right]\rho_{n(p)} \\ &+ \left[\frac{\varepsilon_0^{ul}}{\rho_0} + \frac{\varepsilon_{\gamma}^{ul}}{\rho_0^{\gamma+1}}\left(\frac{\rho}{1+b\rho}\right)^{\gamma}\right]\rho_{p(n)} + \frac{\varepsilon_{ex}^{l}}{2\rho_0}\int f_T^{n(p)}(\vec{k}')\, g_{ex}(|\vec{k}-\vec{k}'|)\, d^3k' \\ &+ \frac{\varepsilon_{ex}^{ul}}{2\rho_0}\int f_T^{p(n)}(\vec{k}')\, g_{ex}(|\vec{k}-\vec{k}'|)\, d^3k' + u_R(\rho)\end{aligned} \tag{3.1.3}$$

where, $u_R(\rho)$ is the rearrangement energy that arises from the explicit density dependence of the interaction and for our interaction in eq.(2.3.73), it is given by

$$u_R(\rho) = \left[\frac{\varepsilon_{\gamma}^{l}}{\rho_0^{\gamma+1}}\frac{(\rho_n^2+\rho_p^2)}{2} + \frac{\varepsilon_{\gamma}^{ul}}{\rho_0^{\gamma+1}}\rho_n\rho_p\right]\frac{\gamma\rho^{\gamma-1}}{(1+b\rho)^{\gamma+1}}. \tag{3.1.4}$$

At zero temperature, $T=0$, the neutron and proton Fermi-Dirac distribution functions reduces to step functions,

$$f_{T=0}^{\tau}(k) = \frac{\xi}{(2\pi)^3}\theta(k_{\tau}-k), \quad \tau = n, p$$

where, $\xi = 2$ is the spin degeneracy factor, $k_n = (3\pi^2\rho_n)^{1/3}$ and $k_p = (3\pi^2\rho_p)^{1/3}$ are respectively the Fermi momenta corresponding to the neutron and proton densities ρ_n and ρ_p.

The expression for energy density in ANM, at zero temperature (T=0), for the finite range Yukawa interaction (2.3.73) becomes,

$$H(\rho,Y_p)=\frac{3MC^2\rho}{8}\sum_{\tau=n,p}\left[\frac{1}{x_\tau^3}\left\{2x_\tau u_\tau^3-x_\tau u_\tau-\ln(x_\tau+u_\tau)\right\}\right]$$
$$+\frac{1}{2}\left[\frac{\varepsilon_0^l}{\rho_0}+\frac{\varepsilon_\gamma^l}{\rho_0^{\gamma+1}}\left(\frac{\rho}{1+b\rho}\right)^\gamma\right](\rho_n^2+\rho_p^2)+\left[\frac{\varepsilon_0^{ul}}{\rho_0}+\frac{\varepsilon_\gamma^{ul}}{\rho_0^{\gamma+1}}\left(\frac{\rho}{1+b\rho}\right)^\gamma\right]\rho_n\rho_p$$
$$+\frac{\varepsilon_{ex}^l}{2\rho_0}\left\{\rho_n^2\int\left(\frac{3j_1(k_nr)}{k_nr}\right)^2\frac{e^{-r/\alpha}}{r/\alpha}d^3r+\rho_p^2\int\left(\frac{3j_1(k_pr)}{k_pr}\right)^2\frac{e^{-r/\alpha}}{r/\alpha}d^3r\right\}$$
$$+\frac{\varepsilon_{ex}^{ul}}{\rho_0}\rho_n\rho_p\int\frac{3j_1(k_nr)}{k_nr}\frac{3j_1(k_pr)}{k_pr}\frac{e^{-r/\alpha}}{r/\alpha}d^3r$$

(3.1.5)

with $x_\tau=\frac{\hbar k_\tau}{MC}$, $u_\tau=(1+x_\tau)^{1/2}$, $j_1(k_\tau r)$ with $\tau=n,p$ are first order Spherical Bessel functions.

The neutron single particle energy, for the finite range interaction having Yukawa form, considered in the present work, becomes

$$\varepsilon^n(k,\rho,Y_p)=(C^2\hbar^2k^2+M^2C^4)^{1/2}+\left[\frac{\varepsilon_0^l}{\rho_0}+\frac{\varepsilon_\gamma^l}{\rho_0^{\gamma+1}}\left(\frac{\rho}{1+b\rho}\right)^\gamma\right]\rho_n+\left[\frac{\varepsilon_0^{ul}}{\rho_0}+\frac{\varepsilon_\gamma^{ul}}{\rho_0^{\gamma+1}}\left(\frac{\rho}{1+b\rho}\right)^\gamma\right]\rho_p$$
$$+\frac{\varepsilon_{ex}^l}{\rho_0}\rho_n\int j_o(k_nr)\left(\frac{3j_1(k_nr)}{k_nr}\right)^2\frac{e^{-r/\alpha}}{r/\alpha}d^3r+\frac{\varepsilon_{ex}^{ul}}{\rho_0}\rho_p\int j_o(k_pr)\left(\frac{3j_1(k_pr)}{k_pr}\right)^2\frac{e^{-r/\alpha}}{r/\alpha}d^3r$$
$$+u_R(\rho).$$

(3.1.6)

The proton single particle energy $\varepsilon^p(k,\rho,Y_p)$ can be written from the above expression for neutron single particle energy by interchanging n and p i.e. $n\leftrightarrow p$ in the right hand side of the equation. These expressions of neutron and proton single particle energies can be written in terms of the mean fields as

$$\varepsilon^{n(p)}(k,\rho,Y_p)=(C^2\hbar^2k^2+M^2C^4)^{1/2}+u^{n(p)}(k,\rho,Y_p) \qquad (3.1.7)$$

where the first term is the kinetic energy of neutron(proton) under consideration and the rest part can be identified as the respective mean fields, $u^{n(p)}(k,\rho,Y_p)$. In the expressions for energy density and mean fields the exchange integrals (integrals associated with the terms containing ε_{ex}^l and ε_{ex}^{ul}) can be evaluated analytically. The

complete description of ANM now requires the knowledge of the nine parameters $b, \gamma, \varepsilon_0^l, \varepsilon_0^{ul}, \varepsilon_\gamma^l, \varepsilon_\gamma^{ul}, \varepsilon_{ex}^l, \varepsilon_{ex}^{ul}$ and α as discussed earlier. We shall now consider the case of symmetric nuclear matter in order to constrain the possible number of parameters from the empirical and experimental data available.

3.2. Symmetric Nuclear Matter

The energy density $H(\rho,T)$ and the single particle energy $\varepsilon(k,\rho,T)$ in SNM at finite temperature can be obtained from eqs.(3.1.1) and (3.1.7) by substituting $f_T^n(k) = f_T^n(k) = \frac{1}{2} f_T(k)$ and $\rho_n = \rho_p = \frac{\rho}{2}$ in these equations and are given by

$$H(\rho,T) = \int f_T(\vec{k})(C^2\hbar^2k^2 + M^2C^4)^{1/2}\, d^3k + \frac{(\varepsilon_0^l + \varepsilon_0^{ul})}{4}\frac{\rho^2}{\rho_0} + \frac{(\varepsilon_\gamma^l + \varepsilon_\gamma^{ul})}{4\rho_0^{\gamma+1}}\frac{\rho^{\gamma+2}}{(1+b\rho)^\gamma} + \frac{(\varepsilon_{ex}^l + \varepsilon_{ex}^{ul})}{4\rho_0}\iint [f_T(\vec{k}) f_T(\vec{k}') g_{ex}(|\vec{k} - \vec{k}'|) d^3k\, d^3k' \tag{3.2.1}$$

and

$$\varepsilon(\rho,k,T) = (C^2\hbar^2k^2 + M^2C^4)^{1/2} + u(k,\rho,T) \tag{3.2.2}$$

with $u(k,\rho,T)$ being the mean field in SNM at finite temperature and is given as

$$u(k,\rho,T) = \frac{(\varepsilon_0^l + \varepsilon_0^{ul})}{2\rho_0}\rho + \frac{(\varepsilon_\gamma^l + \varepsilon_\gamma^{ul})}{2\rho_0^{\gamma+1}}\left(\frac{\rho}{1+b\rho}\right)^{\gamma+1}(1 + b\rho + \frac{\gamma}{2}) + \frac{(\varepsilon_{ex}^l + \varepsilon_{ex}^{ul})}{2\rho_0}\int f_T(\vec{k}')\, g_{ex}(|\vec{k} - \vec{k}'|)\, d^3k. \tag{3.2.3}$$

We shall hence forth identify the strength parameter combinations as

$$\varepsilon_0 = \frac{(\varepsilon_0^l + \varepsilon_0^{ul})}{2}, \quad \varepsilon_\gamma = \frac{(\varepsilon_\gamma^l + \varepsilon_\gamma^{ul})}{2}, \quad \varepsilon_{ex} = \frac{(\varepsilon_{ex}^l + \varepsilon_{ex}^{ul})}{2} \quad . \tag{3.2.4}$$

At zero temperature, $T = 0$, the energy density $H_0(\rho)$ and mean field $u(k,\rho)$ in SNM become,

$$H_0(\rho)=\frac{3MC^2\rho}{8x_f}\left\{2x_f u_f^3 - x_f u_f - \ln(x_f+u_f)\right\} + \frac{\varepsilon_0}{2}\frac{\rho^2}{\rho_0} + \frac{\varepsilon_\gamma}{2\rho_0^{\gamma+1}}\left(\frac{\rho}{1+b\rho}\right)^\gamma \rho^2 + \frac{\varepsilon_{ex}}{2\rho_0}\rho^2 J(\rho) \tag{3.2.5}$$

and

$$u(k,\rho)=\varepsilon_0\frac{\rho}{\rho_0}+\frac{\varepsilon_\gamma}{\rho_0^{\gamma+1}}\left(\frac{\rho}{1+b\rho}\right)^{\gamma+1}(1+b\rho+\frac{\gamma}{2})+\varepsilon_{ex}\frac{\rho}{\rho_0}I(k,\rho) \tag{3.2.6}$$

where the functional $J(\rho)$ and $I(\rho)$ are

$$J(\rho)=\frac{\int\left(\frac{3j_1(k_f r)}{k_f r}\right)^2\frac{e^{-r/\alpha}}{r/\alpha}\,d^3r}{\int\frac{e^{-r/\alpha}}{r/\alpha}d^3r} = \left[\left(\frac{3\Lambda^6}{32k_f^6}+\frac{9\Lambda^4}{8k_f^4}\right)\ln\left(1+\frac{4k_f^2}{\Lambda^2}\right)-\frac{3\Lambda^4}{8k_f^4}+\frac{9\Lambda^2}{4k_f^2}-\frac{3\Lambda^3}{k_f^3}\tan^{-1}\left(\frac{2k_f}{\Lambda}\right)\right] \tag{3.2.7}$$

and

$$I(k,\rho)=\frac{\int j_o(k_p r)\left(\frac{3j_1(k_f r)}{k_f r}\right)^2\frac{e^{-r/\alpha}}{r/\alpha}d^3r}{\int\frac{e^{-r/\alpha}}{r/\alpha}d^3r} = \frac{3\Lambda^2(\Lambda^2+k_f^2-k^2)}{8kk_f^3}\ln\left\{\frac{\Lambda^2+(k+k_f)^2}{\Lambda^2+(k-k_f)^2}\right\}+\frac{3\Lambda^2}{2k_f^2}-\frac{3\Lambda^3}{2k_f^3}\left\{\tan^{-1}\left(\frac{k+k_f}{\Lambda}\right)-\tan^{-1}\left(\frac{k-k_f}{\Lambda}\right)\right\} \tag{3.2.8}$$

with $x_f=\frac{\hbar k_f}{MC}$, $u_f=(1+x_f)^{1/2}$ and $k_f=(1.5\,\pi^2\rho)^{1/3}$ being the Fermi momentum in SNM and $\Lambda=\frac{1}{\alpha}$, α being the range of the finite range interaction.

The energy per particle in SNM at $T=0$, for our interaction given in eq.(2.3.73), can now be expressed as

$$e_0(\rho)=\frac{3MC^2}{8x_f}\left\{2x_f u_f^3 - x_f u_f - \ln(x_f+u_f)\right\}+\frac{\varepsilon_0}{2}\frac{\rho}{\rho_0}+\frac{\varepsilon_\gamma\rho}{2\rho_0^{\gamma+1}}\left(\frac{\rho}{1+b\rho}\right)^\gamma+\frac{\varepsilon_{ex}}{2\rho_0}\rho J(\rho) \tag{3.2.9}$$

From these equations it is evident that complete description of EOS of SNM requires the knowledge of six parameters $b, \gamma, \varepsilon_0, \varepsilon_\gamma, \varepsilon_{ex}$ and α which can be adjusted from the saturation condition of normal nuclear matter and from the available empirical and experimental data.

3.2.1. Parameter fixation in SNM

Out of the six number of parameters, the two parameters ε_{ex} and α which are involved in the momentum dependent part of the nuclear mean field in SNM are constrained by adopting a simultaneous minimization procedure, as discussed in the last chapter, so as to give a correct behaviour of momentum dependence as extracted from optical model fits to nucleon-nucleus scattering data at intermediate energies [52-59, 67]. The mean field thus obtained reproduces the results of the realistic interaction quite accurately over a wide range of momentum and density, as has been shown in Figure 2.3 in the last chapter. The effective nucleon mass, $\frac{M^*(k=k_f,\rho_0)}{M}$ in SNM at normal density, is predicted to be 0.67.

The parameter b appearing in the denominator of the density dependent term of the interaction is constrained so as to avoid supraluminous behaviour of the SNM at high density. As discussed in Ref [65], the constraint on the parameter b results into the expression,

$$b\rho_0 \geq \left[\left(\frac{MC^2}{S_{f_0} - e(\rho_0)}\right)^{\frac{1}{\gamma+1}} - 1\right]^{-1}, \qquad (3.2.10a)$$

where, $$S_{f_0} = \left\{\frac{MC^2}{4x_f^3}\left[3x_f u_f + 2x_f^3 u_f - 3\ln(x_f + u_f)\right]\right\}_{\rho=\rho_0}, \qquad (3.2.10b)$$

MC^2 is the rest mass energy of the nucleon, $e_0(\rho_0)$ is the energy per particle at normal density ρ_0. The remaining two strength parameters ε_0 and ε_γ can be obtained from the saturation conditions of SNM. In the present work, we have taken standard values of $MC^2 = 939\,MeV$, energy per nucleon in SNM $e_0(\rho_0) = 923\,MeV$ and

$(C^2\hbar^2k_{f_0}^2 + M^2C^4)^{1/2} = 976\,MeV$ (corresponding to ρ_0=0.1658 fm^{-3}). The exponent γ determines the stiffness of the EOS of SNM at high densities and can be constrained by using the pressure~density relationship extracted from analysis of flow data in high energy heavy-ion collisions [68] and depicted in Figure 3.1 by the bounded region in the density range 0.32 fm^{-3} $\leq \rho \leq$0.736 fm^{-3} (i.e., $2.0 \leq \rho/\rho_0 \leq 4.6$, with $\rho_0 = 0.16$ fm^{-3}). In the same figure pressure~density curves calculated with the Yukawa form of interaction for different values of exponent γ are also shown for comparison. It can be seen from the figure that the experimentally allowed region approximately constrains the value of γ in the range $1/12 \leq \gamma \leq 1$. While all EOSs of SNM in this range of γ give similar results at saturation and sub-saturation densities they differ considerably from each other when extrapolated to high densities. It may be noted here that the two parameters ε_0 and ε_γ diverge rapidly when γ decreases below 1/12 and approaches the catastrophic region of the EOS as $\gamma \to 0$. Transport model calculations have also

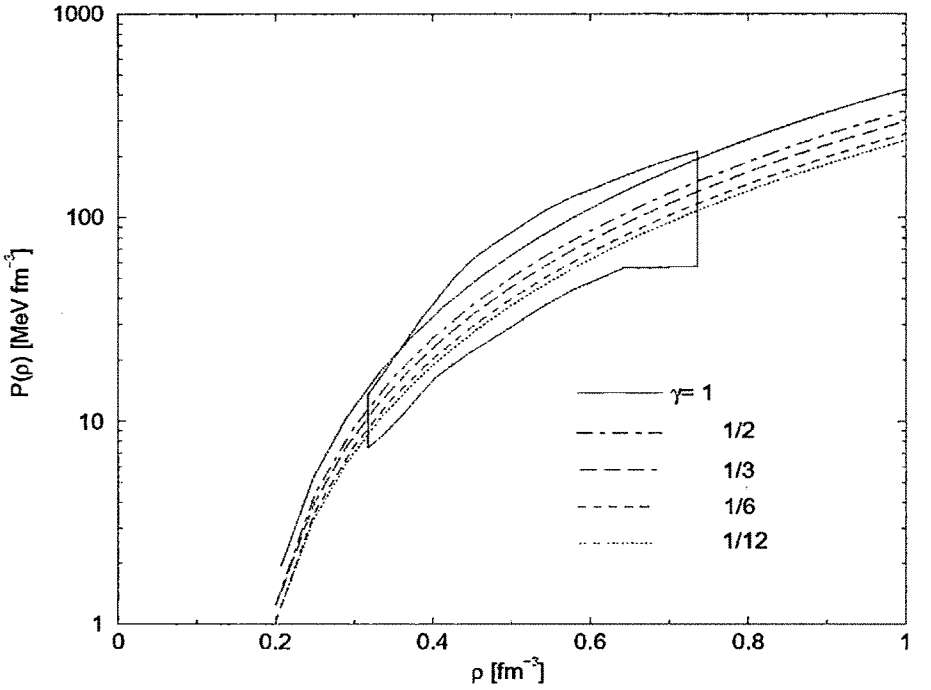

Figure 3.1. Pressure-density relations for five different EOSs of SNM with γ =1/12, 1/6, 1/3, 1/2 and 1 compared with the EOS of Danielewicz *et al.* [68] extracted from flow data in heavy-ion collisions and depicted by the bounded region.

demonstrated that subthreshold K^+production in high energy heavy-ion collisions can provide a suitable tool to constrain the EOS of SNM at densities $\rho \leq 3\rho_0$[167-169]. Theoretical analysis of the subthreshold K^+ production data implies behaviour of the EOS in the considered density range is consistent with the flow data constraint shown in Figure 3.1.

The behaviour of EOSs of SNM around normal density ρ_0 is determined by energy per particle $e_0(\rho_0)$ and incompressibility $K(\rho_0)$. While different theoretical models predict similar values for $e_0(\rho_0)$, they differ widely in the values of $K(\rho_0)$. The value of $K(\rho_0)$ for the allowed range of γ in Figure 3.1 varies from 190 MeV to 287 MeV. It may be noted here that the centroid energies for giant monopole resonances in finite nuclei depend mainly on the value of $K(\rho_0)$ [42, 87, 170-171]. Studies on monopole vibrations in heavy nuclei using Gogny-type effective interactions [42] as well as Skyrme-type interactions [14, 172-174] have approximately constrained the value of nuclear matter incompressibility $K(\rho_0)$ in the range 200 MeV to 240 MeV. This range of $K(\rho_0)$ constrains the value of γ in the range 1/6 to 1/2 for the interaction in eq.(2.3.73). In a recent work [175], employing the Lagrangian models such as non linear-σ model (NLσ), the scalar-vector interaction model (SVI) and the $\sigma-\omega$ coupling model(SIGO) to analyze the breathing mode giant monopole resonance for the nuclei ^{208}Pb, ^{120}Sn, ^{90}Zr, ^{48}Ca and ^{40}Ca(which cover a broad range of nuclear mass), Sharma has predicted that the nuclear matter incompressibility at saturation should be around 272 MeV. This value of nuclear incompressibility corresponds to a value of γ somewhat close to 1 for our interaction. However, in order to study the effect of momentum dependence on the nuclear EOS and nuclear mean field we shall use $\gamma=\frac{1}{2}$ which corresponds to nuclear matter incompressibility $K(\rho_0)=240\ MeV$ and the $P\sim\rho$ curve for this value of γ passes almost through the middle of the $P\sim\rho$ region experimentally extracted from the analysis of heavy-ion collision flow data.

The supraluminous behaviour is a serious defect of the nuclear effective interactions. At least within the density region of the nuclear matter where the

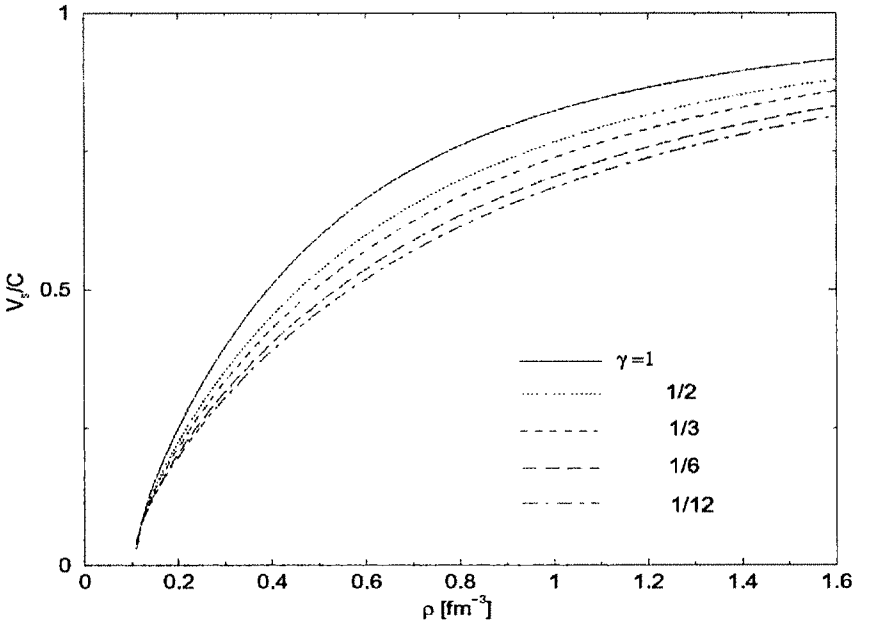

Figure 3.2. The velocity of sound in SNM as a function of density ρ for five different values of the exponent γ =1/12, 1/6, 1/3, 1/2 and 1.

Table 2. Values of interaction parameters in SNM.

Parameters in SNM	γ	b [fm^3]	α [fm]	ε_{ex} [MeV]	ε_γ [MeV]	ε_0 [MeV]
	1/2	0.5668	0.4044	-121.84	76.91	-57.86

interaction is used for studies of nuclear matter properties, should be free from this supraluminous defect, i.e., the velocity of sound within that density region should not cross the value of the velocity of light in vacuum. In our case, for all the five values of γ , the interactions do not show any supraluminous behaviour and the values of velocity of sound for all values of γ, remain well below the value of velocity of light in vacuum up to quite a high range of density, as shown in the Figure 3.2. This is due to the fact that this important aspect has been taken care up by suitably modifying the density dependent term of the interaction. The values of the six parameters $b, \gamma, \varepsilon_0, \varepsilon_\gamma, \varepsilon_{ex}$ and α thus determined for the study of EOS in SNM are given in table 2. Considering the range of the interaction between a pair of like nucleons (p-p, n-n) to

be the same as that of a pair of unlike nucleons (n-p), we need to know how the strength parameters $\varepsilon_{ex} = (\varepsilon^{l}_{ex} + \varepsilon^{ul}_{ex})/2$, $\varepsilon_{\gamma} = (\varepsilon^{l}_{\gamma} + \varepsilon^{ul}_{\gamma})/2$ and $\varepsilon_0 = (\varepsilon^{l}_0 + \varepsilon^{ul}_0)/2$ split as we go from symmetric matter to isospin asymmetric nuclear matter.

3.3. Parameter fixation in Asymmetric Nuclear Matter

Once the parameters b, γ, α, $\varepsilon_{ex} = (\varepsilon^{l}_{ex} + \varepsilon^{ul}_{ex})/2$, $\varepsilon_{\gamma} = (\varepsilon^{l}_{\gamma} + \varepsilon^{ul}_{\gamma})/2$ and $\varepsilon_0 = (\varepsilon^{l}_0 + \varepsilon^{ul}_0)/2$ are fixed by the mean field properties and EOS of SNM, the complete calculation of neutron and proton mean field properties and EOS of ANM would require the correct splittings of the three parameters $(\varepsilon^{l}_{ex} + \varepsilon^{ul}_{ex})$, $(\varepsilon^{l}_0 + \varepsilon^{ul}_0)$ and $(\varepsilon^{l}_{\gamma} + \varepsilon^{ul}_{\gamma})$ into two specific channels for interactions between like (l) and unlike (ul) nucleons. However, there are no experimental/ empirical constraints on the splittings of these three combined parameters except for the value of nuclear symmetry energy $E_s(\rho_0)$ at normal density. Different choices of these splittings can therefore lead to extremely divergent and even contradicting results on the momentum and density dependence of isovector part of nuclear mean field, $u_{\tau}(k,\rho)$. For example, the sign of the combination $(\varepsilon^{l}_{ex} - \varepsilon^{ul}_{ex})$ determines the nature of splitting of neutron and proton effective masses [154]. In this context we note that momentum dependence of the Lane potential [152], $v_1 = 4u_{\tau}(k,\rho_0)$ at normal density ρ_0, has been extracted from nucleon-nucleus scattering data upto 100 MeV [121, 122] and has been used to constrain the isospin splitting of nuclear mean field [124, 163]. This is shown in Figure 3.3 by the bounded region which indicates that $u_{\tau}(k,\rho_0)$ has a value of about 28±6 MeV at $k = 0$ and decreases as a function of k. It may be noted that the experimentally extracted results on the energy dependence of $u_{\tau}(k,\rho_0)$ show a decreasing trend supporting the fact that neutron effective mass goes above the proton one although the data is available upto energy 100 MeV and is associated with large uncertainty [121-123]. This decreasing trend of $u_{\tau}(k,\rho_0)$ with momentum k is also the theoretical predictions of Brueckner-Hartree-Fock (BHF) calculations [118, 124] and of the non relativistic effective theories till the construction of Sly series [112, 125, 126] of Skyrme

parameterizations. The confusion on neutron and proton effective mass splitting became complex with the prediction of DBHF calculation in Ref. [120] that proton effective mass lies above the neutron one. It was clarified in the works of Refs. [127, 128] that by considering the energy dependence of self-energy and comparing the non relativistic effective mass with the vector effective mass in the relativistic framework [129], the DBHF calculation also predicts the neutron effective mass above the proton one. This was further confirmed in the DBHF calculation in Ref. [130]. In view of this it is almost the consensus opinion that the neutron effective mass in a neutron rich asymmetric matter will lie above the proton one. There have been attempts to constrain the effective mass splitting from the study of observables sensitive to the isovector features of the nuclear EOS [81, 84, 131], but the task has not been accomplished yet and the magnitude of effective mass splitting still remains as an open problem.

3.3.1. Constraining the splitting of the parameter $\left(\varepsilon_{ex}^{l}+\varepsilon_{ex}^{ul}\right)$

For the above mentioned purpose, the functional, $u_\tau(k,\rho_0)$, is calculated as a function of momentum k from the relations given in eq.(2.3.47) for the present interaction in eq.(2.3.73) with different splittings of $\left(\varepsilon_{ex}^{i}+\varepsilon_{ex}^{ul}\right)$ into ε_{ex}^{l} and ε_{ex}^{ul}, where we have used the standard value of symmetry energy at normal density, $E_s(\rho_0)$=30MeV, the value of effective mass, $\frac{M^*(k_f,\rho_0)}{M}$=0.67, in SNM of the interaction and the results are given in the Figure 3.3. The results of DBHF [130] and BHF with three body rearrangement force [124] is also given in the same figure for comparison. The curve for $\varepsilon_{ex}^{l}=\left(\varepsilon_{ex}^{l}+\varepsilon_{ex}^{ul}\right)/6$ in our case is in close agreement with the DBHF result, whereas, in case of BHF results, there is a reasonable agreement with our case of $\varepsilon_{ex}^{l}=\left(\varepsilon_{ex}^{l}+\varepsilon_{ex}^{ul}\right)/3$ within the experimentally extracted region. Since, in the case of the splitting, $\varepsilon_{ex}^{l}=\left(\varepsilon_{ex}^{l}+\varepsilon_{ex}^{ul}\right)/6$, the curve of $u_\tau(k,\rho_0)$ in the low momentum region lies close to the upper boundary of the experimental results we have considered it as one case for our study. For values of ε_{ex}^{l} less in magnitude than this value the curves will lie well outside in the experimentally extracted data at low momentum region. The other extreme case considered here is $\varepsilon_{ex}^{l}=\varepsilon_{ex}^{ul}$ for which the neutron and proton effective

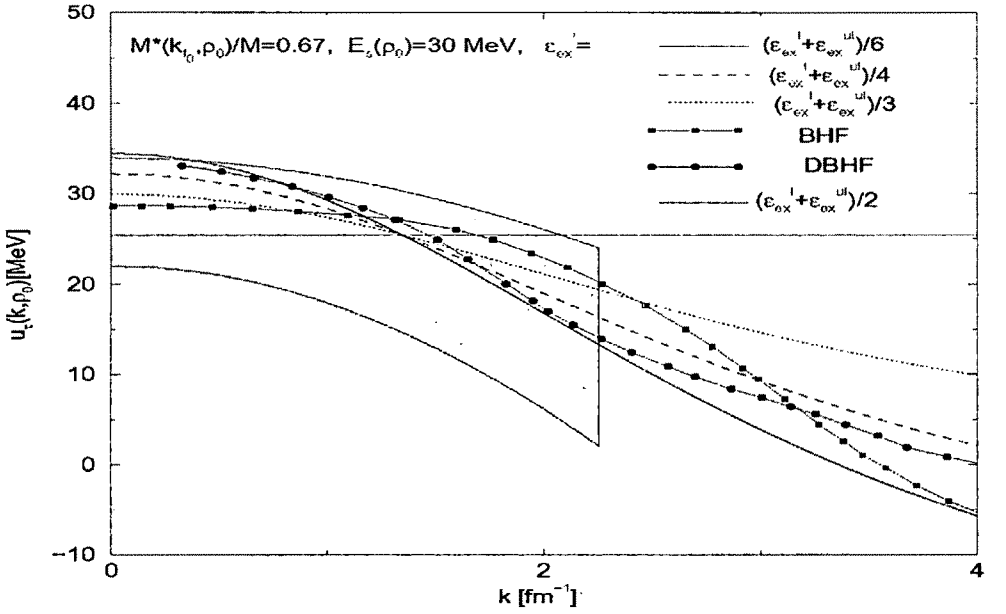

Figure 3.3. $u_\tau(k,\rho_0)$ as a function of k is shown for different splittings of $\left(\varepsilon_{ex}^{l}+\varepsilon_{ex}^{ul}\right)$ within the range $\varepsilon_{ex}^{l}=\left(\varepsilon_{ex}^{l}+\varepsilon_{ex}^{ul}\right)/6$ and $\left(\varepsilon_{ex}^{l}+\varepsilon_{ex}^{ul}\right)/2$ considered in the work. The experimentally extracted data is shown by the closed area. The results of DBHF [130], BHF [124] are also shown.

masses calculated as a function of momentum k at given temperature T, total nucleon density ρ and proton fraction Y_p in ANM will be the same. Beyond this limiting value, $\varepsilon_{ex}^{l}=\varepsilon_{ex}^{ul}$, the exchange interaction between a pair of like nucleons become stronger compared to that between a pair of unlike nucleons resulting into the proton effective mass above the neutron one which contradicts to the predictions of various microscopic models on neutron and proton effective mass splitting.

3.3.2. Constraining the splitting of the parameter $\left(\varepsilon_0^{l}+\varepsilon_0^{ul}\right)$ and $\left(\varepsilon_\gamma^{l}+\varepsilon_\gamma^{ul}\right)$

3.3.2.(a) Role of Symmetry Energy in β-stable matter and EOS of NSM

For a given splitting of $(\varepsilon_{ex}^{l}+\varepsilon_{ex}^{ul})$ into ε_{ex}^{l} and ε_{ex}^{ul}, the complete study of ANM requires the splittings of the other two combinations $(\varepsilon_0^{l}+\varepsilon_0^{ul})$ and $(\varepsilon_\gamma^{l}+\varepsilon_\gamma^{ul})$ into two different channels for interaction between two like and unlike nucleons. While different theoretical models predict similar values of $E_s(\rho_0)$ they widely differ in the

values of $E_s^{'}(\rho_0) = \left[\rho \frac{dE_s(\rho)}{d\rho}\right]_{\rho=\rho_0}$ which is directly related to the slope of the symmetry energy at normal density ρ_0. We have used these two nuclear matter properties in deciding the splitting of the parameter combinations $(\varepsilon_0^l + \varepsilon_0^{tl})$ and $(\varepsilon_\gamma^l + \varepsilon_\gamma^{tl})$. In this context, we assume a given splitting of $(\varepsilon_{ex}^{l} + \varepsilon_{ex}^{tl})$ into ε_{ex}^{l} and ε_{ex}^{tl}, take a standard value of $E_s(\rho_0)$ that decide the splitting of one of the two parameter combinations and then assign arbitrary values to $E_s^{'}(\rho_0)$ that decides the splitting of the rest one parameter combination. The EOSs of ANM corresponding to the different values of $E_s^{'}(\rho_0)$ thus obtained will give different high density behaviour of nuclear symmetry energy $E_s(\rho)$. In order to constrain the EOS of ANM out of these infinitely large numbers of possible EOSs, we have calculated, in each case of these EOSs, the equilibrium proton fraction in charge neutral $n+p+e+\mu$ matter under beta equilibrium, i.e., neutron star matter (NSM) that is the major composition of the interior of normal neutron stars. As will be shown in the followings the asymmetric part of the nuclear EOS, more specifically the nuclear symmetry energy, is crucial in determining the equilibrium proton fraction in NSM, and hence plays the crucial part in the composition and cooling mechanism of the neutron stars.

The conditions for beta equilibrium is

$$\mu_n - \mu_p = \mu_e = \mu_\mu, \tag{3.3.1}$$

and charge neutrality condition is

$$Y_p = Y_e + Y_\mu \tag{3.3.2}$$

where, μ_i, $i = n, p, e, \mu$, are the corresponding chemical potentials and $Y_i = \frac{\rho_i}{\rho}$, $i = p, e, \mu$, are the respective particle fractions. In the followings we shall show that these conditions completely depend on the asymmetric part of the nucleonic energy density.

The isospin symmetry of nuclear forces allows to expand the energy density of asymmetric nuclear matter, $H(\rho, Y_p)$, in even powers of asymmetry $(1-2Y_p)$,

$$H(\rho,Y_p) = H(\rho) + H_s(\rho)(1-2Y_p)^2 + \text{ terms involving higher even powers of } (1-2Y_p). \tag{3.3.3}$$

It is a well known fact that the contributions of the higher order terms, $(1-2Y_p)^n$ with $n > 2$, is very small and the quadratic approximation of the infinite series in the right hand side of eq. (3.3.3) is a very good and quite accurate approximation [117, 164, 166, 176, 177].

Under this quadratic approximation, we have

$$H(\rho,Y_p) \cong H_0(\rho) + H_s(\rho)(1-2Y_p)^2 \tag{3.3.4}$$

Now as the symmetric nuclear matter and pure neutron matter constitute the two extremes of the asymmetric nuclear matter, corresponding to the limiting values of $Y_p = \frac{1}{2}$ and 0 respectively, we can identify $H_0(\rho)$ as the energy density in SNM and $H_s(\rho)$ to be the difference of energy densities in PNM and SNM,

$$H_s(\rho) = H_n(\rho) - H_0(\rho) \tag{3.3.5}$$

Using the fact that $H_n(\rho) = \rho e_n(\rho)$ and $H_0(\rho) = \rho e_0(\rho)$, where , $e_n(\rho)$ and $e_0(\rho)$ are the energy per particle in PNM and SNM, respectively, we can write $H_s(\rho)$ as

$$H_s(\rho) = \rho[e_n(\rho) - e_0(\rho)]. \tag{3.3.6}$$

The energy density in ANM given in eq.(3.3.4) now becomes

$$H(\rho,Y_p) \cong \rho e_0(\rho) + (1-2Y_p)^2 \rho[e_n(\rho) - e_0(\rho)] \tag{3.3.7}$$

and comparing it with the conventional expression for $H(\rho,Y_p) \cong \rho e_0(\rho) + (1-2Y_p)^2 \rho E_s(\rho)$,

we can identify the nuclear symmetry energy $E_s(\rho)$ by,

$$E_s(\rho) = e_n(\rho) - e_0(\rho). \tag{3.3.8}$$

The validity of the quadratic approximation at zero-temperature, $T = 0$, can be examined by calculating energy per particle in ANM at given density as a function of asymmetry $(1-2Y_p)^2$. This is shown in the Figure 3.4 for different densities.

The neutron and proton chemical potentials, μ_n and μ_p are defined as

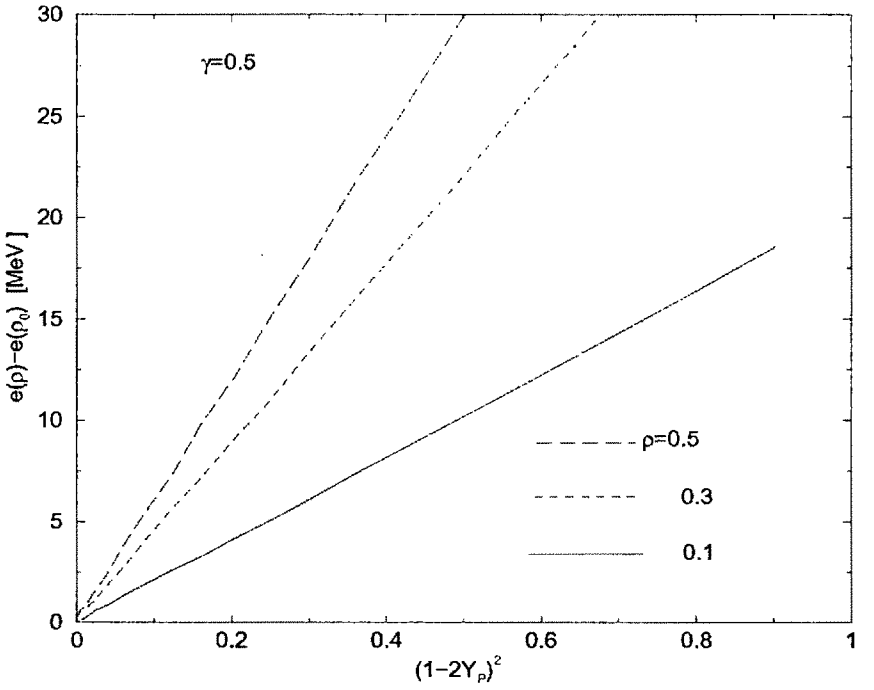

Figure 3.4. The energy per particle in ANM relative to the energy per particle in SNM is plotted as a function of the square of the asymmetry parameter for different nuclear matter densities. The linear curves show the quadratic dependence of the energy per particle on the asymmetry parameter.

$$\mu_n = \frac{\partial H(\rho, Y_p)}{\partial \rho_n} \tag{3.3. 9a}$$

and

$$\mu_p = \frac{\partial H(\rho, Y_p)}{\partial \rho_p} \tag{3.3. 9b}$$

The difference of the neutron and proton chemical potential can be expressed as

$$\mu_n - \mu_p = -\frac{1}{\rho}\frac{\partial H(\rho, Y_p)}{\partial Y_p}, \tag{3.3.10}$$

which for the energy density $H(\rho, Y_p)$ in eq.(3.3.7) becomes

$$\mu_n - \mu_p = 4(1-2Y_p)E_s(\rho). \tag{3.3.11}$$

The electrons and muons present inside the neutron star core can be treated as non interacting relativistic Fermi gas and the electron and muon chemical potentials are given by

$$\mu_i = \left(C^2\hbar^2 k_i^2 + M_i^2 C^4\right)^{1/2}, \qquad i = e, \mu \tag{3.3.12}$$

k_i being the Fermi momentum of the respective leptonic system and is given in terms of the leptonic density as $k_i = \left(3\pi^2 \rho_i\right)^{1/3}$. The conditions of the charge neutral beta stable matter are now given as

$$4(1-2Y_p)E_s(\rho) = \left[C^2\hbar^2\left(3\pi^2\rho Y_e\right)^{2/3} + M_e^2C^4\right]^{/2} = \left[C^2\hbar^2\left(3\pi^2\rho Y_\mu\right)^{2/3} + M_\mu^2C^4\right]^{/2} \tag{3.3.13a}$$

and

$$Y_p = Y_e + Y_\mu . \tag{3.3.13b}$$

From the above two equations it is evident that at a given density ρ, if the value of nuclear symmetry energy $E_s(\rho)$ is known, then both the equations can be solved simultaneously to get Y_p, Y_e and Y_μ at that density. Hence it is the asymmetry part of the nucleonic energy density of the neutron star matter that solely determines the composition of the normal neutron stars. With the knowledge of nucleonic (protons and neutrons) and leptonic (electrons and muons) fractions, the energy density and pressure of the nucleonic part can be calculated for the EOS of ANM given in eq.(3.3.4) and the leptonic counterparts are obtained from the non-interacting relativistic Fermi gas model. The total energy density and pressure of NSM can be given as,

$$H^{NSM} = H^N(\rho, Y_p) + H^e(\rho, Y_e) + H^\mu(\rho, Y_\mu) \tag{3.3.14}$$

$$P^{NSM} = P^N(\rho, Y_p) + P^e(\rho, Y_e) + P^\mu(\rho, Y_\mu) . \tag{3.3.15}$$

These quantities H^{NSM} and P^{NSM} are the inputs to the hydrodynamic equilibrium equations of neutron star, known as Tolmann-Oppenheimer-Volkov (TOV) equations,

$$\frac{dP}{dr} = -G\left(\varepsilon + \frac{P}{C^2}\right)\frac{m + 4\pi r^3 \frac{P}{C^2}}{r\left(r - 2Gm/C^2\right)} \tag{3.3.16}$$

$$M = \int 4\pi r^2 \varepsilon \, dr \tag{3.3.17}$$

which are solved to obtain the mass and radius of neutron stars. In these equations ε is the energy density, $m(r)$ is the gravitational mass inside the radius of sphere r, M is the gravitational mass of the star and G is the universal gravitational constant. These equations are solved from the interior of the star to its exterior where $P(R) = 0$ and $m(R) = M$, where R is the radius of the star. The TOV equations are integrated for a

given value of the central density ε_c and can be solved when the relation $P(r) = P(\varepsilon(r))$ between the pressure and the energy density is known at each point. That means the structure of the star depends upon the EOS of NSM. Thus it is the density dependence of nuclear symmetry energy $E_s(\rho)$ that is crucial in determining the structure and composition of the normal neutron stars. However, the high density behaviour of nuclear symmetry energy is still a standing question to be answered and as mentioned earlier the predictions of different models are not only divergent but also contradicting. In a recent work, Klahn et al. [151] have examined the abilities of several relativistic EOSs, very much successful in predicting the results at normal nuclear matter density, in reproducing the constraints resulting from recent observations on neutron star phenomenology and constraint resulting from the heavy ion collision (HIC) experiments. They have found that none of the EOSs could reproduce more than 50% of the tests. However, they have observed that the EOSs which remain at the top of the test, their asymmetric contributions of the nucleonic part in NSM form a close group although their density dependence of symmetry energies differ considerably in a wider range. In the following we shall show that in case of our EOS of ANM given eq.(3.1.5) we can obtain widely varying high density behaviour of nuclear symmetry energy by considering different splittings of the strength parameters $\varepsilon_0 = \frac{\varepsilon_0^l + \varepsilon_0^{ul}}{2}$ and $\varepsilon_\gamma = \frac{\varepsilon_\gamma^l + \varepsilon_\gamma^{ul}}{2}$ into like (l) and unlike (ul) channels where all of these EOSs have the same value of nuclear symmetry energy at normal nuclear matter density, $E_s(\rho_0)$. Out of these large number of EOSs obtained from arbitrary splittings of the parameters ε_0 and ε_γ, we find a group of EOSs giving almost the same asymmetric contribution in NSM.

3.3.2.(b) Universal High density behaviour of the asymmetric contribution of nucleonic part in NSM

Earlier it has been shown that different splittings of the exchange strength parameter $\varepsilon_{ex} = \frac{\varepsilon_{ex}^l + \varepsilon_{ex}^{ul}}{2}$ into like and unlike channels solely account for the different

neutron-proton effective mass splittings in ANM and we shall consider two representative values of this splitting. We shall examine the high density behaviour of nuclear symmetry energy for these two representative cases of effective mass splitting which may give us an insight into the measure of influence of momentum dependence, if any, on the density dependence of nuclear EOS. In obtaining the different splittings of the strength parameters ε_0 and ε_γ into the like and unlike channels, we have assumed a standard value for $E_s(\rho_0)$ that decides the splitting of one of the two parameter combinations and then assign arbitrary values to $E_s'(\rho_0)=\rho_0\left.\frac{dE_s(\rho)}{d\rho}\right|_{\rho_0}$ that decides the splitting of the rest parameter combination. In the present work, the symmetry energy $E_s(\rho)$ has been calculated as the difference between the energy per particle in PNM and SNM, where the expression for the energy per particle of SNM is given in eq.(3.2.9) for our interaction given in eq.(2.3.73). The expression for the energy density in PNM at $T=0$, for our interaction , is given by

$$H_n(\rho)=\frac{3MC^2\rho}{8x_n^3}\left\{2x_nu_n^3-x_nu_n-\ln(x_n+u_n)\right\}+\frac{\varepsilon_0^l}{2}\frac{\rho^2}{\rho_0}+\frac{\varepsilon_\gamma^l}{2}\frac{\rho^2}{\rho_0^{\gamma+1}}\left(\frac{\rho}{1+b\rho}\right)^\gamma+\frac{\varepsilon_{ex}^l}{2}\frac{\rho^2}{\rho_0}J^N(\rho)\,, \tag{3.3.18}$$

so that the energy per particle in PNM is

$$e_n(\rho)=\frac{3MC^2}{8x_n^3}\left\{2x_nu_n^3-x_nu_n-\ln(x_n+u_n)\right\}+\frac{\varepsilon_0^l}{2}\frac{\rho}{\rho_0}+\frac{\varepsilon_\gamma^l}{2}\frac{\rho}{\rho_0^{\gamma+1}}\left(\frac{\rho}{1+b\rho}\right)^\gamma+\frac{\varepsilon_{ex}^l}{2}\frac{\rho}{\rho_0}J^N(\rho)\,, \tag{3.3.19}$$

where,

$$J^N(\rho)=\left[\left(\frac{3\Lambda^6}{32k_n^6}+\frac{9\Lambda^4}{8k_n^4}\right)\ln\left(1+\frac{4k_n^2}{\Lambda^2}\right)-\frac{3\Lambda^4}{8k_n^4}+\frac{9\Lambda^2}{4k_n^2}-\frac{3\Lambda^3}{k_n^3}\tan^{-1}\left(\frac{2k_n}{\Lambda}\right)\right], \tag{3.3.20}$$

with $k_n=\left(3\pi^2\rho\right)^{1/3}$ is the Fermi momentum in PNM at density ρ, $x_n=\frac{\hbar k_n}{MC}$ and $u_n=(1+x_n^{\,2})^{1/2}$. Here we have taken the standard value of $E_s(\rho_0)=30\ MeV$ that determines splitting of one of the two parameters ε_0 and ε_γ into like and unlike

channel and the splitting of the other parameter is constrained from the assigned value of $E_s'(\rho_0)$. The different density dependence of $E_s(\rho)$ thus obtained for different representative values of $E_s'(\rho_0)$ for the two cases of effective mass splitting, $\varepsilon_{ex}^{l} = \frac{\varepsilon_{ex}^{l} + \varepsilon_{ex}^{ul}}{6}$ and $\varepsilon_{ex}^{l} = \frac{\varepsilon_{ex}^{l} + \varepsilon_{ex}^{ul}}{3}$ discussed earlier in this section, are shown in Figures 3.5(a) and 3.5(b) respectively. For each EOS in both cases of effective mass splitting, the beta equilibrium proton fraction Y_p have been calculated by solving the eqs. (3.3.13a) and (3.3.13b) simultaneously by adopting an iterative procedure. The equilibrium proton fractions Y_p thus obtained as a function of density ρ for the two cases of ε_{ex}^{l} have been shown in Figures 3.6(a) and 3.6(b). With the knowledge of proton fraction Y_p, we can calculate the nucleonic part of the energy density, $H^N(\rho, Y_p)$, in charge neutral beta stable $n+p+e+\mu$ matter, i.e., neutron star matter, by the help of the equation for ANM given in eq. (3.3.4). Now the asymmetric contribution of the nucleonic part in neutron star matter can be calculated by subtracting

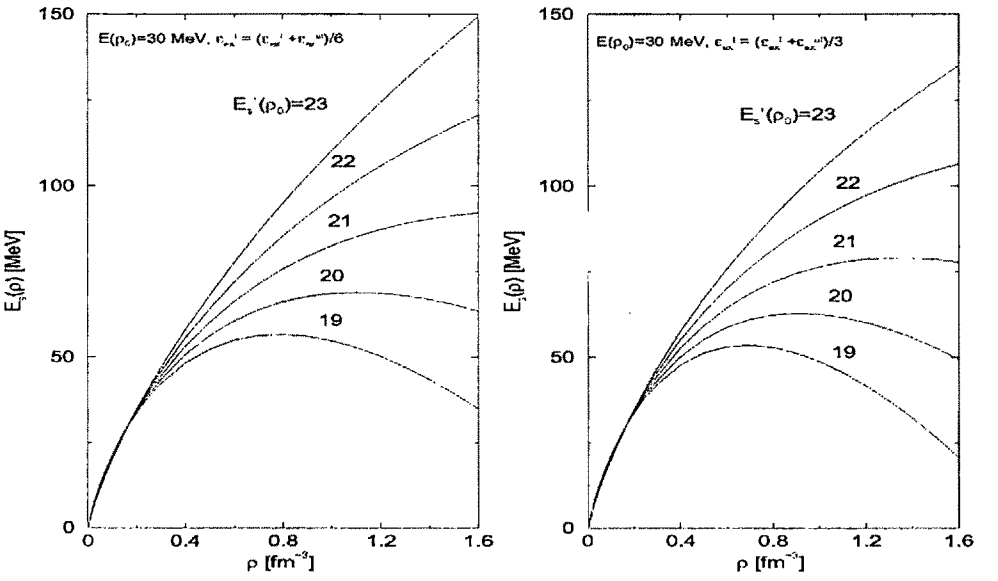

Figure 3.5. (a) High density behaviour of nuclear symmetry energy $E_s(\rho)$ for $\varepsilon_{ex}^{l} = (\varepsilon_{ex}^{l} + \varepsilon_{ex}^{ul})/6$ at different slope parameters of the nuclear symmetry energy. (b) The same as (a) for $\varepsilon_{ex}^{l} = (\varepsilon_{ex}^{l} + \varepsilon_{ex}^{ul})/3$. The value of the slope parameter $E_s'(\rho_0)$ is given in the unit of MeV.

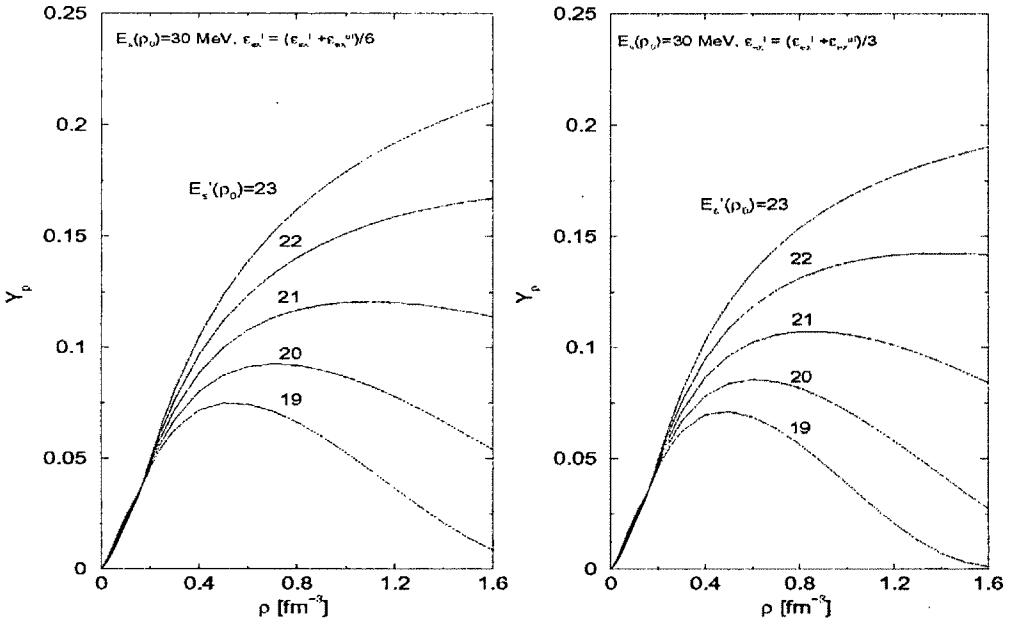

Figure 3.6. (a) Equilibrium proton fraction Y_p in Neutron Star Matter for $\varepsilon_{ex}^{l}=(\varepsilon_{ex}^{l}+\varepsilon_{ex}^{ul})/6$ at different slope parameters of the nuclear symmetry energy. (b) The same as (a) for $\varepsilon_{ex}^{l}=(\varepsilon_{ex}^{l}+\varepsilon_{ex}^{ul})/3$.

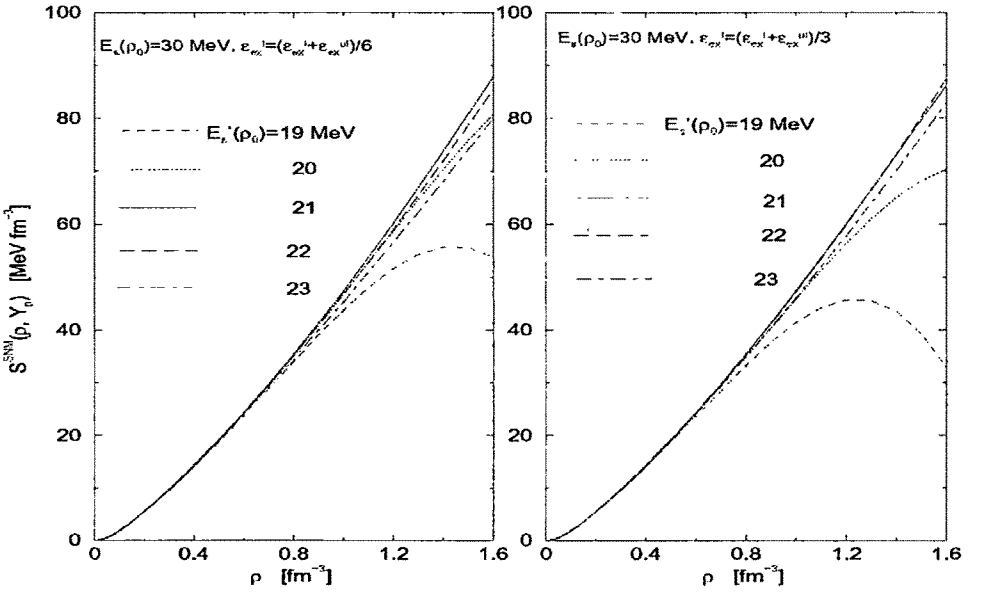

Figure 3.7. (a) Asymmetric contribution to the nucleonic part of energy density in Neutron Star Matter for $\varepsilon_{ex}^{l}=(\varepsilon_{ex}^{l}+\varepsilon_{ex}^{ul})/6$ at different slope parameters of the nuclear symmetry energy. (b) The same as (a) for $\varepsilon_{ex}^{l}=(\varepsilon_{ex}^{l}+\varepsilon_{ex}^{ul})/3$.

the energy density in SNM from $H^N(\rho,Y_p)$ and we get,

$$S^{NSM}(\rho,Y_p)=\left[H^N(\rho,Y_p)-H(\rho,Y_p=1/2)\right]. \qquad (3.3.21)$$

$S^{NSM}(\rho,Y_p)$ as a function of density ρ is calculated for the different EOSs of ANM and is shown in Figures 3.7(a) and 3.7(b) for each of the two cases of ε_{ex}^{l}. It is seen that in eachcase of splitting of ε_{ex}, there is a critical value of $E_s'(\rho_0)$ for which the density dependence of $S^{NSM}(\rho,Y_p)$ is a maximum over the range of density considered and also it remains almost stationary within a narrow range around this critical value of $E_s'(\rho_0)$. This is shown in Figure 3.8(a) for the case $\varepsilon_{ex}^{l}=2(\varepsilon_{ex}^{l}+\varepsilon_{ex}^{ul})/6$, where we have shown the density dependence of $S^{NSM}(\rho,Y_p)$ for the range of $E_s'(\rho_0)$ for which $S^{NSM}(\rho,Y_p)$remains almost the same. In the adjacent two figures we have shown the curves for density dependences of symmetry energy $E_s(\rho)$ and proton fraction $Y_p(\rho)$ for the EOSs corresponding to the same cases of $E_s'(\rho_0)$ considered in the first figure.

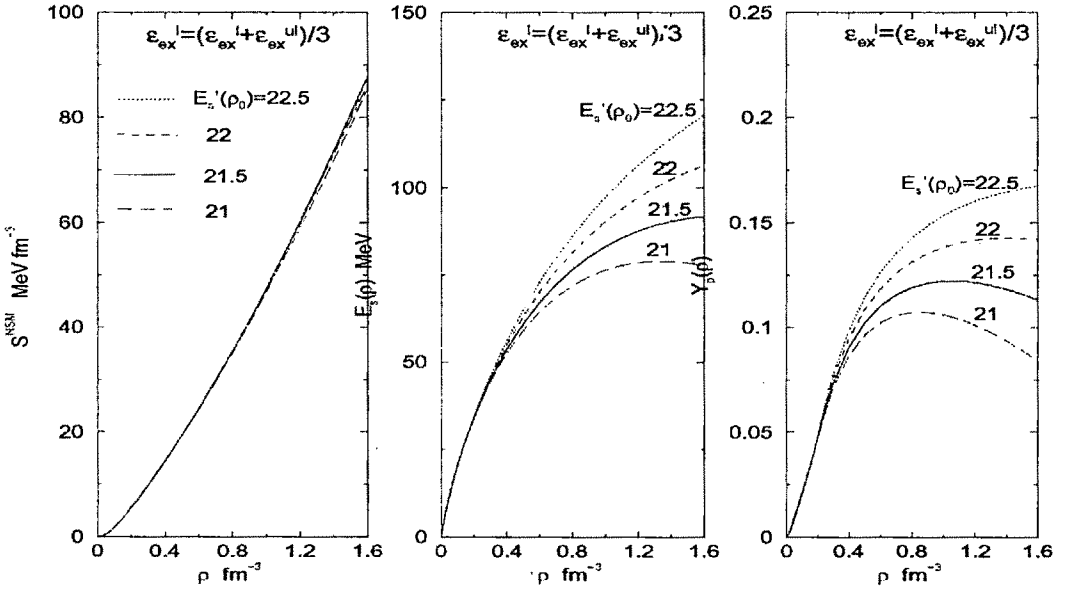

Figure 3.8. (a) Asymmetric contribution to the nucleonic part of energy density in Neutron Star Matter for $\varepsilon_{ex}^{l}=2(\varepsilon_{ex}^{l}+\varepsilon_{ex}^{ul})/6$ at different slope parameters of the nuclear symmetry energy (b) The nuclear symmetry energy as function of density for the same case of ε_{ex}^{l} and (c) the corresponding equilibrium proton fraction $Y_p(\rho)$ as functions of density ρ.

Table 3. Critical values of $E_S'(\rho_0, T=0)$ for the three different cases of effective mass splitting as obtained from the stiffest high-density behaviour of $S^{NSM}(\rho, Y_p, T=0)$ in NSM and the interaction parameters in ANM.

Parameters in ANM	$\varepsilon_{ex}^{l}=(\varepsilon_{ex}^{l}+\varepsilon_{ex}^{ul})/6$	$\varepsilon_{ex}^{l}=2(\varepsilon_{ex}^{l}+\varepsilon_{ex}^{ul})/6$	$\varepsilon_{ex}^{l}=(\varepsilon_{ex}^{l}+\varepsilon_{ex}^{ul})/2$
$E_S'(\rho_0, T=0)$(MeV)	21.02	21.49	21.97
ε_{ex}^{l} (MeV)	-40.61	-81.23	-121.84
ε_{γ}^{l} (MeV)	75.81	65.73	55.69
ε_{0}^{l} (MeV)	-87.46	-50.49	-13.57

The symmetry energy and proton fraction curves for the EOSs show considerable difference from each other, whereas, for all of these EOSs the asymmetric contributions of nucleonic part in NSM are almost same. This stationary behaviour of $S^{NSM}(\rho, Y_p)$ over a narrow range around the critical value of $E_s'(\rho_0)$ is referred to as the universal high density behaviour of $S^{NSM}(\rho, Y_p)$. This universal high density behaviour of $S^{NSM}(\rho, Y_p)$ has been calculated for the other cases of effective mass splitting and found to be almost same as that given in Figure 3.8(a) for their respective critical values of $E_s'(\rho_0)$. Since the principle of extremity is a law of nature, we have finally considered the value of $E_s'(\rho_0)$ (out of the infinitely large number of possible values) for which the functional $S^{NSM}(\rho, Y_p)$ is maximum over the range of density 0 to $10\,\rho_0$ in each case of the different effective mass splittings. The values of $E_s'(\rho_0)$ thus obtained for the different cases of $\varepsilon_{ex}^{l}=(\varepsilon_{ex}^{l}+\varepsilon_{ex}^{ul})/6$, $2(\varepsilon_{ex}^{l}+\varepsilon_{ex}^{ul})/6$ and $(\varepsilon_{ex}^{l}+\varepsilon_{ex}^{ul})/2$ are 21.02 MeV, 21.49 MeV and 21.97 MeV respectively. The interaction parameters in ANM thus obtained for the different cases of neutron-proton effective mass splitting corresponding to different values of ε_{ex}^{l} are given in table 3. The case of splitting $\varepsilon_{ex}^{l}=(\varepsilon_{ex}^{l}+\varepsilon_{ex}^{ul})/2$ is a boundary case beyond which the neutron-proton effective mass splitting reverses its sign.

3.4. Comparison of the predictions with the results of microscopic calculation

It may be noted here that $E_s'(\rho_0)$ is related to the slope parameter L as $L = 3E_S'(\rho_0)$. Thus the values of slope parameter obtained for the two cases are 63 MeV and 64.5 MeV. The value of L has been constrained within range $L = 86 \pm 25 MeV$ from the analysis of isospin diffusion studies [83, 85, 132, 134, 138] in heavy-ion collisions using the isospin-dependent Boltzmann-Uehling-Uhlenbeck (IBUU) transport model with the momentum dependent MDI interaction. From the analysis of neutron skin thickness of Shetty et al.have predicted the value within the range $30 < L < 80 MeV$ [134]. The value of L has been constrained within range $60 \leq L \leq 107$ MeV from the analysis of neutron skin thickness studies as well as isospin diffusion studies [83]. The value of L parameter predicted from our analysis of beta stable matter conforms well to this range and remains towards the lower side.

The nine parameters required for the calculations of mean field properties and EOS of nuclear matter are thus constrained as discussed above. The predictability of the nuclear matter results with our interaction in eq.(2.3.73) can now be examined by comparing with the results of the realistic as well as other calculations that reproduce the results of microscopic calculations. The density dependence of energy per particle, $e_n(\rho) = H_n(\rho)/\rho$, in PNM at zero-temperature for our interaction for each of the two representative cases $\varepsilon_{ex}^{l} = (\varepsilon_{ex}^{l} + \varepsilon_{ex}^{nl})/6$ (Case A) and $\varepsilon_{ex}^{l} = (\varepsilon_{ex}^{l} + \varepsilon_{ex}^{nl})/2$ (Case B) of neutron-proton effective mass splitting are shown in Figure 3.9. The curves of $e_n(\rho)$ for both the cases are almost same over the entire range of density ρ shown in the figure. The energy per particle, $e_0(\rho) = H_0(\rho)/\rho$, in SNM at zero-temperature which is same for both the cases is also shown in Figure 3.9 as a function of density ρ. The density dependence of $e_n(\rho)$ and $e_0(\rho)$ obtained by Akmal et. al. [4] for the realistic interaction A18+dv+UIX* are shown in Figure 3.9 for comparison. The results of $e_n(\rho)$ and $e_0(\rho)$ calculated for the LNS interaction set [178] are also given in the same figure. The LNS interaction is the Skyme parameterization of the EOS calculated in the framework of BHF model. The LNS interaction parameters are constrained to reproduce

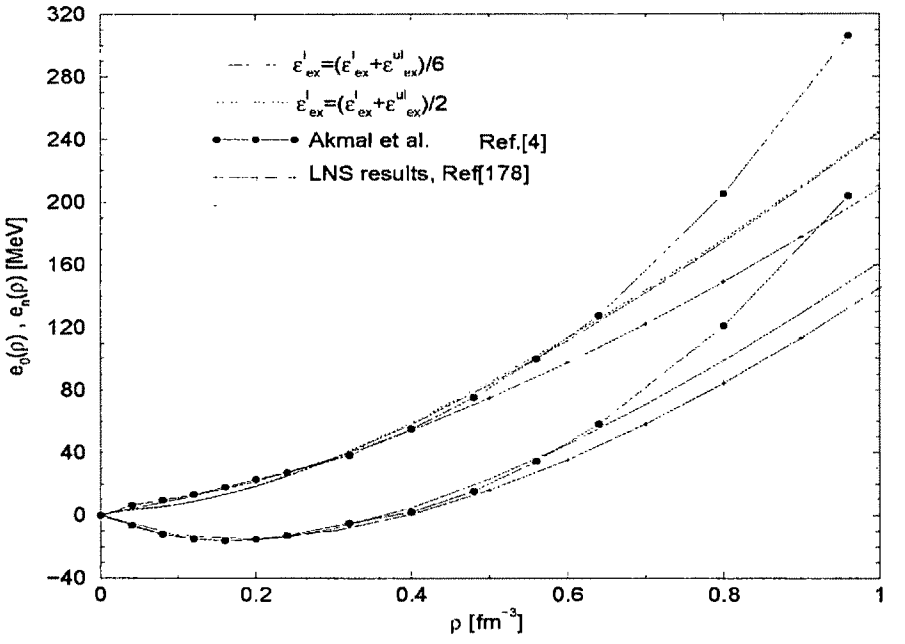

Figure 3.9. Energy per particle in SNM and PNM, $e_0(\rho_0)$ and $e_n(\rho_0)$, as functions of ρ for the two cases A and B are compared with the results of A18+dv+UIX* [4] and LNS interaction [178].

the BHF results of neutron and proton effective masses in ANM [178]. The results of $e_n(\rho)$ and $e_0(\rho)$ for the two cases A and B are in good agreement with those of Akmal et. al. upto a density $\rho=0.65\,fm^{-3}$. However, beyond this density the curves of $e_n(\rho)$ and $e_0(\rho)$ obtained by Akmal et. al. become more and more stiff compared to our results. The agreement of our results with the LNS case for both $e_n(\rho)$ and $e_0(\rho)$ are good upto a density $\rho=0.4\,fm^{-3}$ beyond which the LNS curves in both cases become soft compared to our curves.

The density dependence of nuclear symmetry energy $E_S(\rho,T=0)$ at zero-temperature with our interactions for the two cases A and B are shown in Figure 3.10. The two curves of $E_S(\rho,T=0)$ differ little from each other in the entire range of density shown. It can also be seen that the stiffest high density behaviour of the functional $S^{NSM}(\rho,Y_p,T=0)$ constrains the density dependence of $E_S(\rho,T=0)$ in both the cases which are neither very stiff nor soft at high densities. This is a very

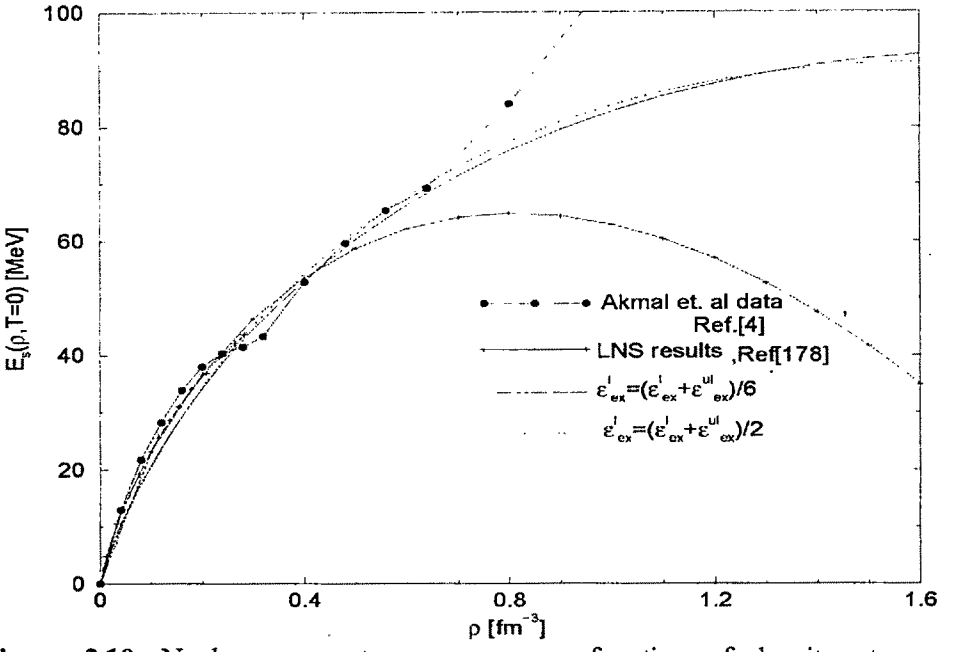

Figure 3.10. Nuclear symmetry energy as a function of density at zero temperature (T=0) for the two cases A and B and compared with the results of A18+dv+UIX* [4] and LNS [178] interactions.

important conclusion on this elusive high density behaviour of nuclear symmetry energy predicted from the extrapolation of the experimental multifragmentation studies [133]. However the degree of stiffness and/or softness is still remained unanswered. The density dependence of $E_S(\rho, T=0)$ for both cases of A18+dv+UIX* [4] and LNS interaction [178] are also shown in Figure 3.10 for comparison. The curves of $E_S(\rho, T=0)$ obtained in the present work compares well with the results of A18+dv+UIX* upto a density $\rho = 0.65\, fm^{-3}$. However, beyond this density the curve of $E_S(\rho, T=0)$ in case of A18+dv+UIX* interaction becomes more and more stiff compared to our results. On the other hand the comparison of our results with that of LNS interaction case is good upto density $\rho = 0.4\, fm^{-3}$. Beyond this density the LNS results become softer and softer and start decreasing after attaining a peak about density, $\rho = 0.8\, fm^{-3}$.

3.5. Conclusion

The parameter fixation in SNM and PNM using various available constraints is discussed in detail in the frame work of Behera et al.[64]. It has been shown that, it is possible to construct EOSs differing widely in their momentum dependence while giving the same density dependence of isovector part of the nuclear mean field. The results of such EOSs have been compared with the results from microscopic calculations. The two cases, Case A and Case B considered above are the examples of the EOSs those give same density dependence but widely varying in their momentum dependence. In other words, both the EOSs give the same density dependence of energy per particle in SNM and nuclear symmetry energy but different neutron-proton effective mass splitting in ANM. Such EOSs having same density dependence (momentum dependence) but differing in momentum dependence (density dependence) are of crucial relevance in the transport model analysis of heavy-ion collision data in the attempt to ascertain the momentum and density dependence of isovector part of the nuclear mean field. At present although there is by and large consensus among the various microscopic and effective theories on the nature of the neutron-proton effective mass splitting that neutron effective mass in neutron rich asymmetric matter will lie above the proton one, the magnitude of the neutron-proton effective mass splitting still remains as an open problem. From the above attempts to constrain the splitting of the parameter $\varepsilon_{ex}^{l}+\varepsilon_{ex}^{ul}$ into like and unlike channels by restricting to the region of experimentally extracted results as shown in Figure 3.3 and the fact that the neutron effective mass should go above the proton one, it is certain that the permitted range for this parameter ε_{ex}^{l} is $\frac{\varepsilon_{ex}^{l}+\varepsilon_{ex}^{ul}}{6} \le \varepsilon_{ex}^{l} \le \frac{\varepsilon_{ex}^{l}+\varepsilon_{ex}^{ul}}{2}$. The zero temperature properties of

asymmetric nuclear matter like the nuclear symmetry energy or the equilibrium proton fraction behave in the same way for both the extreme cases as can be ascertained from Figure 3.10. In other words the zero temperature calculations of asymmetric nuclear matter may not be able to constrain further the splitting of the parameter ε_{ex}^{l}. In view of this and in the absence of any precise experimental or empirical information, finite temperature calculation may be useful to constrain further the parameter ε_{ex}^{l}. It is important to note here that the interaction has no explicit temperature dependence but the thermal evolution of the properties of nuclear matter is simulated through the Fermi-Dirac distribution functions appearing in the exchange part of the energy density and mean fields. Thus the exchange strength parameter is crucial in deciding the nature and extent of thermal evolution in nuclear matter. Hence it is expected that finite temperature calculations of ANM can be useful in further constraining the splitting of ε_{ex} into ε_{ex}^{l} and ε_{ex}^{ul}. In this attempt we shall calculate the thermal evolution of various properties of SNM , PNM and ANM in the next chapter with the different effective mass splittings as obtained in this chapter for the finite range effective interaction in eq.(2.3.73).

CHAPTER-1V

THERMAL EVOLUTION IN NEUTRON RICH MATTER

4.1. Thermal evolution of Nuclear Matter Properties

The energy density and single particle energy in ANM at temperature T for our interaction in eq.(2.3.73) with Yukawa form for the finite range part are given in eqs.(3.1.1)-(3.1.3). The exact calculations of these properties in ANM requires the knowledge of neutron and proton momentum distribution functions, $f_T^n(\vec{k})$ and $f_T^p(\vec{k})$, at given temperature T, density ρ and asymmetry $(1-2Y_p)$. The distribution functions at temperature T are given by

$$f_T^i(\vec{k}) = \frac{\xi}{(2\pi)^3} \frac{1}{\exp\{\in^i(k,\rho,T) - \mu^i(\rho,T)]/T\}+1}, \tag{4.1.1}$$

where, $i = n, p$ and the distribution functions are subjected to the constraint

$$\int f_T^{n(p)}(\vec{k}) d^3k = \rho_{n(p)}. \tag{4.1.2}$$

Here, the spin degeneracy factor ξ takes values $\xi = 2$ and $\in^i$ and μ^i, with $i = n, p$ are the respective single particle energies and chemical potentials. In the evaluation of the neutron and proton distribution functions we require the knowledge of respective single particle energies which in turn involve the distribution functions warranting a self-consistent calculation. Further, in the evaluation of the distribution function for one type of nucleon we require the knowledge of respective single particle energies which in turn involves the distribution functions of both kinds of particles making the self-consistent calculation a difficult one. Instead of entering into such a complicated self-consistent calculation, we have adopted the quadratic approximation as discussed in chapter-III for the case of zero-temperature, $T = 0$, generalized to the case of finite temperature T. The energy density and pressure in ANM under this generalized quadratic approximation at temperature T can now be given as,

$$H(\rho, Y_p, T) = H_0(\rho, T) + (1-2Y_p)^2 H_s(\rho, T) \tag{4.1.3}$$

$$P(\rho, Y_p, T) = P_0(\rho, T) + (1-2Y_p)^2 P_s(\rho, T), \tag{4.1.4}$$

These expressions have the crucial advantage that the Y_p dependence of $H(\rho, Y_p, T)$ and $P(\rho, Y_p, T)$ are separated out from their dependence on ρ and T. The quadratic

approximation is a very good and quite accurate approximation at zero temperature [117, 164, 166] as well at finite temperature [176, 177,179]. In order that eqs. (4.1.3) and (4.1.4) be valid in the complete do main of ANM, i.e. from PNM to SNM, we can identify $H_s(\rho,T)$ and $P_s(\rho,T)$ to be the symmetry energy density and symmetry energy pressure respectively at temperature T and define them in terms of the differences between the energy densities as well as pressure in PNM and SNM,

$$H_s(\rho,T)=\rho E_S(\rho,T)=H_n(\rho,T)-H_0(\rho,T), \tag{4.1.5}$$

$$P_s(\rho,T)=P_n(\rho,T)-P_0(\rho,T). \tag{4.1.6}$$

where, $E_s(\rho,T)$ is the nuclear symmetry energy as a function of ρ and T. It is evident from eqs. (4.1.3)-(4.1.6) that a complete description of EOS of ANM at finite temperature amounts to separate descriptions of EOSs of PNM and SNM at same temperature T and same total nucleon density ρ.

The energy density and single particle energy in SNM at temperature T for our interaction in eq.(2.3.73) with Yukawa form for the finite range part are given in eqs.(3.2.1)-(3.2.3). These properties in case of PNM at temperature T with our interaction having Yukawa form are also given by similar expressions as,

$$H_n(\rho,T)=\int f_T^{PNM}(\vec{k})\left(C^2\hbar^2k^2+M^2C^4\right)^{1/2}d^3k+\frac{\varepsilon_0^l}{2}\frac{\rho^2}{\rho_0}+\frac{\varepsilon_\gamma^l}{2\rho_0^{\gamma+1}}\left(\frac{\rho}{1+b\rho}\right)^\gamma\rho^2$$
$$+\frac{\varepsilon_{ex}^l}{2\rho_0}\iint f_T^{PNM}(\vec{k})f_T^{PNM}(\vec{k'})g_{ex}(|\vec{k}-\vec{k'}|)d^3k\,d^3k' \tag{4.1.7}$$

The parameters ε_0^l, ε_γ^l and ε_{ex}^l appearing in this equation are defined in eqs.(3.2.1a-3.2.1f). The functional $g_{ex}(\vec{k}-\vec{k'}|)$ is the normalized Fourier transformation of the Yukawa interaction. The Fermi-Dirac momentum distribution functions in SNM and PNM, i.e., $f_T^{SNM}(\vec{k})$ and $f_T^{PNM}(\vec{k})$, are given by,

$$f_T^i(\vec{k})=\frac{\xi}{(2\pi)^3}n_T^i(k), \tag{4.1.8a}$$

with the occupation probability defined as

$$n_T^i(k) = \frac{1}{\exp\{[\epsilon^i(k,\rho,T) - \mu^i(\rho,T)]/T\} + 1} \tag{4.1.8b}$$

with $i = 0(n)$ for SNM(PNM) and subject to the constraint $\int f_T^{SNM(PNM)}(\vec{k})d^3k = \rho$. Here, the spin-isospin degeneracy factor ξ takes values $\xi = 4(2)$ in SNM (PNM) and ϵ^i and μ^i, with $i = 0(n)$, are the respective single particle energies and chemical potentials.

The single particle energies in SNM and PNM can be obtained as the functional derivatives of respective energy densities and are given by,

$$\epsilon^0(k,\rho,T) = \left(C^2\hbar^2k^2 + M^2C^4\right)^{1/2} + \frac{(\varepsilon_0^l + \varepsilon_0^{ul})}{2}\frac{\rho}{\rho_0} + \frac{(\varepsilon_\gamma^l + \varepsilon_\gamma^{ul})}{2\rho_0^{\gamma+1}}\left(\frac{\rho}{1+b\rho}\right)^{\gamma+1}\left(1 + b\gamma + \frac{\gamma}{2}\right)$$
$$+ \frac{(\varepsilon_{ex}^l + \varepsilon_{ex}^{ul})}{2\rho_0}\int f_T^{SNM}(\vec{k})g_{ex}(|\vec{k} - \vec{k}'|)d^3k' \tag{4.1.9}$$

and

$$\epsilon^n(k,\rho,T) = \left(C^2\hbar^2k^2 + M^2C^4\right)^{1/2} + \varepsilon_0^l\frac{\rho}{\rho_0} + \frac{\varepsilon_\gamma^l}{\rho_0^{\gamma+1}}\left(\frac{\rho}{1+b\rho}\right)^{\gamma+1}\left(1 + b\gamma + \frac{\gamma}{2}\right)$$
$$+ \frac{\varepsilon_{ex}^l}{\rho_0}\int f_T^{PNM}(\vec{k})g_{ex}(|\vec{k} - \vec{k}'|)d^3k'. \tag{4.1.10}$$

It is evident from the expressions of energy density and single particle energy in both SNM and PNM that the temperature dependence of the mean fields and the interaction parts of energy densities are simulated through the respective Fermi-Dirac momentum distribution functions while the interaction itself has no explicit temperature dependence. The momentum dependent parts of the mean fields involve the respective distribution functions and therefore imply self-consistent calculations. The momentum distribution functions as well as mean fields both in SNM and PNM can be evaluated self-consistently at each density ρ and temperature T by adopting an iterative procedure [62]. Here the basic input is the respective single particle energies at zero temperature. At $T = 0$ the Fermi-Dirac distribution functions take the form of step functions and the respective single particle energies as well as the complete EOSs of

SNM and PNM can be calculated analytically. The single particle energy in SNM at $T=0$ is given in eq.(3.2.2). The single particle energy in PNM at $T=0$ for our interaction with Yukawa type finite range part is given by

$$\in^{n}(k,\rho,T=0)=\left(C^2\hbar^2k^2+M^2C^4\right)^{1/2}+\varepsilon_0^l\frac{\rho}{\rho_0}+\frac{\varepsilon_\gamma^l}{\rho_0^{\gamma+1}}\left(\frac{\rho}{1+b\rho}\right)^{\gamma+1}\left(1+b\gamma+\frac{\gamma}{2}\right)$$

$$+\varepsilon_{ex}^l\frac{\rho}{\rho_0}\left[\begin{array}{l}\dfrac{3\Lambda^2\left(\Lambda^2+k_n^2-k^2\right)}{8kk_n^3}\ln\left\{\dfrac{\Lambda^2+(k+k_n)^2}{\Lambda^2+(k-k_n)^2}\right\}+\dfrac{3\Lambda^2}{2k_n^2}\\ -\dfrac{3\Lambda^3}{2k_n^3}\left\{\tan^{-1}\left(\dfrac{k+k_n}{\Lambda}\right)-\tan^{-1}\left(\dfrac{k-k_n}{\Lambda}\right)\right\}\end{array}\right] \qquad (4.1.11)$$

where, the Fermi momentum k_n is related to the density ρ as $k_n^3=3\pi^2\rho$. The temperature dependence of single particle energies as well as chemical potentials are obtained in the process of self-consistent evaluation of distribution functions in SNM and PNM at given density ρ and temperature T. Once the distribution functions, single particle energies and chemical potentials are obtained, the pressure in SNM as well as in PNM can be calculated by adopting standard procedure.

4.1.1. Effective Single particle energy and Fermi-Dirac distribution function at finite temperature

As has been discussed earlier, the temperature dependence of the mean fields and the interaction parts of energy densities are simulated through the respective Fermi-Dirac momentum distribution functions. In view of this, thermal evolution of EOSs of SNM and PNM, i.e. properties of SNM and PNM relative to their zero-temperature results, can be calculated only in terms of the exchange parameters $\varepsilon_{ex}^l, \varepsilon_{ex}^{ul}$ and the range α without having to require the knowledge of other parameters ε_0^l, ε_0^{ul}, ε_γ^l, ε_γ^{ul} and the exponent γ. The momentum distribution functions both in SNM and PNM can be obtained self-consistently at each nucleon density ρ and temperature T by introducing effective single particle energies in SNM and PNM which contain only the momentum dependent parts and can be written as,

$$\in^{0}_{eff}(k,\rho,T)=\left[(C^2\hbar^2k^2+M^2C^4)^{1/2}+\frac{(\varepsilon^{l}_{ex}+\varepsilon^{ul}_{ex})}{2\rho_0}\int f^{SNM}_{T}(\vec{k'})g_{ex}(|\vec{k}-\vec{k'}|)\,d^3k'\right], \tag{4.1.12}$$

And

$$\in^{n}_{eff}(k,\rho,T)=\left[(C^2\hbar^2k^2+M^2C^4)^{1/2}+\frac{\varepsilon^{l}_{ex}}{\rho_0}\int f^{PNM}_{T}(\vec{k'})g_{ex}(|\vec{k}-\vec{k'}|)d^3k'\right]. \tag{4.1.13}$$

These effective single particle energies would correspond to the respective effective chemical potentials $\mu^{0}_{eff}(\rho,T)$ and $\mu^{n}_{eff}(\rho,T)$ such that $\left[\in^{i}(k,\rho,T)-\mu^{i}(\rho,T)\right]=\left[\in^{i}_{eff}(k,\rho,T)-\mu^{i}_{eff}(\rho,T)\right]$ with $i=0,\ n$.

In order to obtain the thermal evolution of properties of PNM we require the splitting of the combination $(\varepsilon^{l}_{ex}+\varepsilon^{ul}_{ex})$ into ε^{l}_{ex} and ε^{ul}_{ex} for interactions between pairs of like and unlike nucleons. Different splittings of the combined parameter $(\varepsilon^{l}_{ex}+\varepsilon^{ul}_{ex})$ into like and unlike channels will, therefore, predict different thermal evolution of properties of PNM. As mentioned earlier, the controversy on the nature of $n-p$ effective mass splitting is more or less resolved and now there is a consensus opinion that neutron effective mass goes over that of proton in neutron rich ANM. This implies that ε^{l}_{ex} should lie within 0 and ε_{ex} [153]. However, there is no consensus among different theoretical models on the actual value of ε^{l}_{ex}. Under the circumstances, we therefore vary the parameter ε^{l}_{ex} in the range 0 to ε_{ex} and examine its influence on the thermal evolution of different properties of PNM. The results in SNM and PNM thus obtained are also compared with the respective predictions of ideal Fermi gas model where the mean fields are momentum independent. The momentum distribution functions in the ideal Fermi gas model are evaluated by considering only the kinetic energy terms in the expressions of the effective single particle energies in eqs. (4.1.12) and (4.1.13) and the thermal evolutions of properties of SNM and PNM are calculated. Comparison of the results for our interaction with the predictions of ideal Fermi gas model will bring out the effect of momentum dependence of the nuclear mean fields on the thermal evolutions of the properties.

The basic ingredients in the finite temperature calculation of properties of SNM and PNM are the respective occupation probabilities, $n_T^i(k)$, $i=0,n$ calculated self-consistently using the effective single particle energies given in eqs.(4.1.12) and (4.1.13). The effective single particle energies $\epsilon_{eff}^i(k,\rho,T)$ and the respective chemical potentials $\mu_{eff}^i(\rho,T)$ are obtained in the process of self-consistent evaluation of $n_T^i(k)$. The occupation probabilities, $n_T^i(k)$, $i=0,n$ as a function of momentum k for both momentum dependent and momentum independent mean field cases in SNM and PNM are shown in Figures 4.1(a) and (b), respectively, at three different temperatures $T=0$, 20, 40 MeV for density $\rho=0.1$ fm^{-3}. In case of PNM in Figure 4.1(b) we have

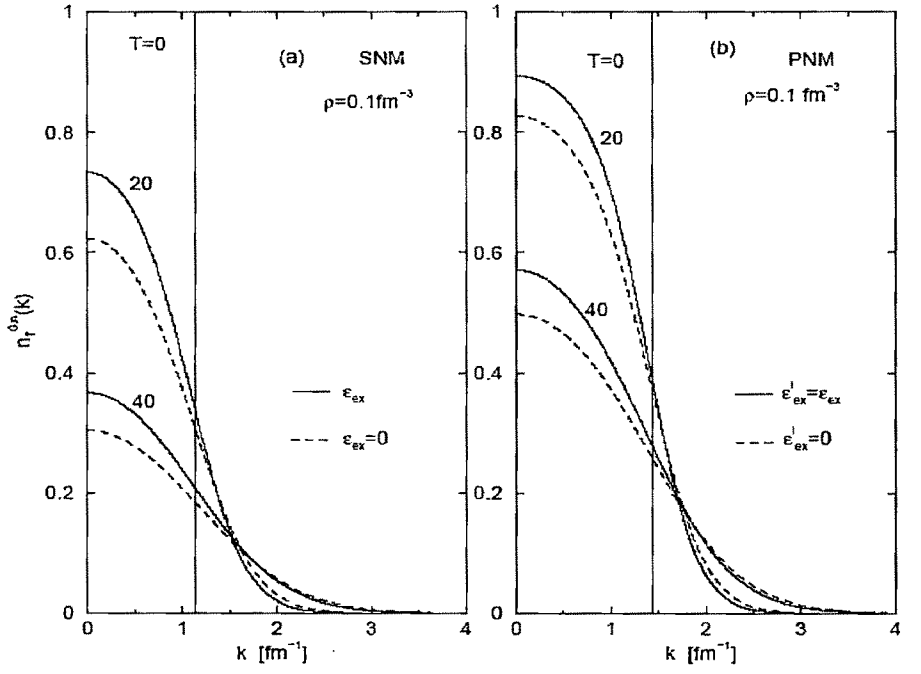

Figure 4.1. (a) Fermi-Dirac occupation probability, $n_T^0(k)$, in SNM for momentum dependent and momentum independent mean fields shown as a function of momentum k at temperatures, T=0, 20 and 40 MeV for nuclear matter density, $\rho=0.1\ fm^{-3}$. The momentum independent cases ($\varepsilon_{ex}=0$) correspond to ideal Fermi-gas model results (b) Fermi-Dirac occupation probability, $n_T^n(k)$, in PNM for the same cases as in (a). Curves for $\varepsilon_{ex}^l=0$ corresponds to ideal Fermi-gas model results in PNM.

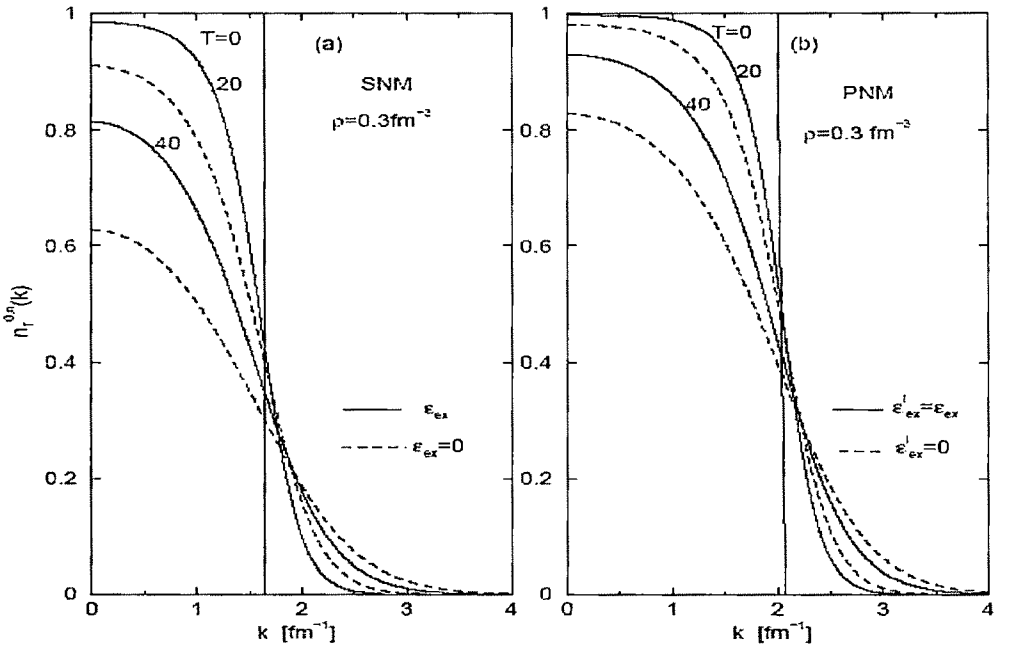

Figure 4.2. (a) Fermi-Dirac occupation probability in SNM for momentum dependent and momentum independent mean fields shown as a function of momentum k at temperatures, T=0, 20 and 40 MeV for nuclear matter density, $\rho = 0.3\ fm^{-3}$. The momentum independent cases ($\varepsilon_{ex} = 0$) correspond to ideal Fermi-gas model results. (b) Fermi-Dirac occupation probability, $n_T^n(k)$, in PNM for the same cases as in (a). Curves for $\varepsilon_{ex}^l = 0$ corresponds to ideal Fermi-gas model results in PNM

considered the two extreme values of ε_{ex}^l in its allowed range, namely, $\varepsilon_{ex}^l = 0$ and ε_{ex}. The occupation probabilities in PNM for different ε_{ex}^l, within its allowed range, lie in between the results of these two extreme cases. The Fermi gas model results in SNM and

PNM are also given in the Figures 4.1(a) and (b) for comparison with the respective momentum dependent mean field cases. In Figures 4.2(a) and (b) the results of occupation probabilities for the same cases as in Figures 4.1(a) and (b) are shown at a higher density, $\rho = 0.3\,\text{fm}^{-3}$. From Figures 4.1 and 4.2 it can be seen that the occupation probabilities, $n_T^i(k)$, of the states $k \le k_i$, $i = f, n$, decrease with increase in temperature extending the tail to higher k values in both SNM and PNM. The results of SNM and PNM in each of the Figures 4.1 and 4.2 show that the effect of temperature

is relatively larger in SNM as compared to PNM. It is also evident from both the figures that temperature has a larger effect in case of momentum independent mean fields (Fermi gas model results) than that of momentum dependent mean fields in both SNM and PNM. This effect is larger at higher temperature. Thus a momentum dependent attractive nuclear mean field that increases with a rise in momentum has the important role in lowering the effect of temperature on the occupation probability in SNM as well as in PNM. We shall now examine the effect of these features of occupation probabilities in SNM and PNM on the thermal evolution of various nuclear matter properties. The momentum dependence of nuclear mean field in SNM is constrained with the fixed values of ε_{ex} and α thereby fixing the evolution of occupation probability at given temperature and density in SNM. However, the actual momentum dependence of the mean field in PNM is yet to be decided and the possible range of ε_{ex}^{l} is 0 to ε_{ex}. Different ε_{ex}^{l} in this range will give different occupation probabilities in PNM. In our study of thermal evolution of nuclear matter properties we have, therefore, considered four representative cases of ε_{ex}^{l}, namely, $\varepsilon_{ex}^{l} = 0, \varepsilon_{ex}/3, 2\varepsilon_{ex}/3, \varepsilon_{ex}$ that covers the whole range of allowed momentum dependence of PNM mean field.

4.1.2. Entropy density

The entropy densities, $S_i(\rho,T)$, $i = 0,n$ in SNM and PNM can be calculated from the relation,

$$S_{0,n}(\rho,T) = -\frac{\xi}{(2\pi)^3}\int\left[n_T^{0,n}(k)\ln n_T^{0,n}(k) + \left(1-n_T^{0,n}(k)\right)\ln\left(1-n_T^{0,n}(k)\right)\right]d^3k, \tag{4.1.14}$$

where, ξ= 4(2) for SNM (PNM) and $n_T^{0,n}(k)$ are the respective occupation probabilities at temperature T. The results of entropy densities in SNM and the four different cases of PNM, namely, $\varepsilon_{ex}^{l} = 0, \varepsilon_{ex}/3, 2\varepsilon_{ex}/3$ and ε_{ex}, as a function of density ρ are shown at two different temperatures, T= 40 and 60 MeV, in figures 4.3(a) and (b) respectively. Comparing our results with those obtained from ideal Fermi gas model in both SNM and PNM, it is seen that momentum dependence of the mean fields plays

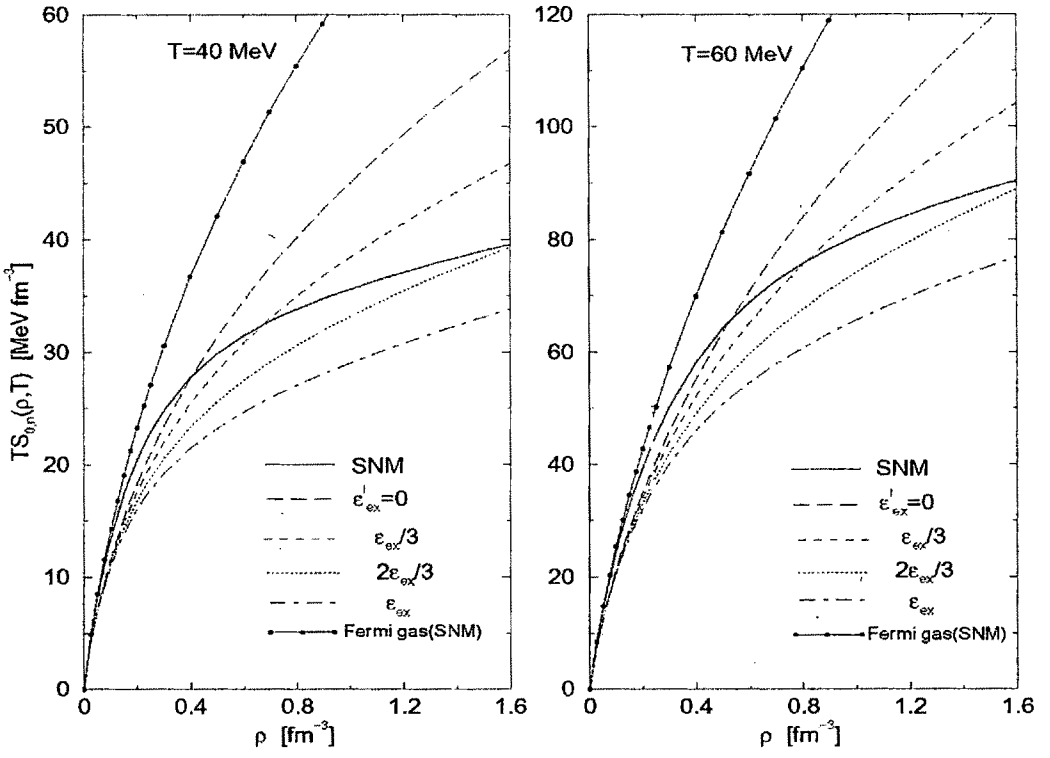

Figure 4.3. (a) Entropy density, $TS_{0,n}(\rho,T)$, in SNM and four cases of PNM corresponding to $\varepsilon^{l}_{ex}=0$, $\varepsilon_{ex}/3$, $2\varepsilon_{ex}/3$ and ε_{ex} shown as a function of density ρ at temperature T= 40 MeV. Fermi-gas model results in SNM and PNM correspond to $\varepsilon_{ex}=0$ and $\varepsilon'_{ex}=0$, respectively. (b) Same as (a) but at temperature, T=60 MeV.

important roles to reduce the effect of temperature. It is also seen from the figures that the entropy density obtained in the ideal Fermi gas model in SNM goes above that of PNM and the difference increases with density. On the other hand our results of entropy density in PNM exceeds that of SNM at a higher density if the parameter ε^{l}_{ex} lies in between 0 to $2\varepsilon_{ex}/3$, which is contrary to the results obtained with ideal Fermi gas model. The density at which the entropy density in PNM exceeds that of SNM gradually increases with increase in the magnitude of the parameter ε^{l}_{ex} from 0 to $2\varepsilon_{ex}/3$. With increase in temperature the crossing over point shifts to higher density. For the specific choice of $\varepsilon^{l}_{ex}=2\varepsilon_{ex}/3$ the entropy density in PNM approaches that of SNM asymptotically at large density. With increase in the magnitude of ε^{l}_{ex} from

$2\varepsilon_{ex}/3$ towards ε_{ex} the curves of entropy are pushed more and more below that of SNM. In case of $\varepsilon_{ex}^{l}=\varepsilon_{ex}$, the entropy density in PNM is always less than that of SNM. This kind of behaviour is similar to results obtained in the ideal Fermi gas model over the whole range of density. With increase in temperature the curve of PNM lies more and more below that of SNM one and the difference $T[S_n(\rho,T)-S_0(\rho,T)]$ assumes larger and larger negative values in the high density region. Thus it is found that the whole range of ε_{ex}^{l} is now divided into two parts based on the consideration that whether the quantity $T[S_n(\rho,T)-S_0(\rho,T)]$ can change sign at any value of density or not.

The question, now, automatically arises whether the entropy density in PNM being a system of one kind of particles can exceed that of SNM which is a two component system or not!! A plausible answer to this pertinent question may be searched in the areas of study of heavy-ion collision dynamics involving highly neutron rich radioactive nuclei. If an answer to this basic question can be obtained then it can help constrain the magnitude of neutron and proton effective mass splitting in ANM. In the absence of a satisfactory answer to this fundamental question we can still divide the whole possible range of splitting, $0\le\varepsilon_{ex}^{l}\le\varepsilon_{ex}$, of our combined exchange strength parameter $(\varepsilon_{ex}^{l}+\varepsilon_{ex}^{ul})$ into like and unlike channels in two parts, (a) $0\le\varepsilon_{ex}^{l}<2\varepsilon_{ex}/3$ and (b) $2\varepsilon_{ex}/3<\varepsilon_{ex}^{l}\le\varepsilon_{ex}$. In case the answer to the question raised above is 'yes' then the possible range of ε_{ex}^{l} is confined to the range as given in (a) $0\le\varepsilon_{ex}^{l}<2\varepsilon_{ex}/3$ and if 'no' then the possible range of ε_{ex}^{l} is (b) $2\varepsilon_{ex}/3<\varepsilon_{ex}^{l}\le\varepsilon_{ex}$ and accordingly the magnitude of neutron and proton effective mass splitting in ANM can be further constrained.

4.2. Thermal evolution of Bulk properties in SNM and PNM

The allowed range of ε_{ex}^{l} is now divided into two groups, namely, (a) 0 to $2\varepsilon_{ex}/3$ and (b) $2\varepsilon_{ex}/3$ to ε_{ex}, on the basis of the two contrasting behaviours found in the results of entropy density in PNM relative to the SNM one for different momentum

dependence of PNM mean field in this range. We now examine the thermal evolution in other properties of SNM and PNM, such as, internal energy density, free energy density and pressure for different choices of ε_{ex}^{l} within its allowed range $0 \le \varepsilon_{ex}^{l} < \varepsilon_{ex}$. The thermal evolutions of these quantities in SNM and PNM are defined as their values at temperature T relative to the zero-temperature values,

$$H_i^{th}(\rho,T) = H_i(\rho,T) - H_i(\rho,T=0), \tag{4.1.15}$$

$$F_i^{th}(\rho,T) = F_i(\rho,T) - F_i(\rho,T=0), \tag{4.1.16}$$

$$P_i^{th}(\rho,T) = P_i(\rho,T) - P_i(\rho,T=0), \tag{4.1.17}$$

with i=0,n for SNM and PNM respectively.

4.2.1. Thermal evolution of internal energy density

The thermal evolution of internal energy density in SNM (PNM), $H_{0(n)}^{th}(\rho,T)$, can be given by,

$$H_{0(n)}^{th}(\rho,T) = \frac{\xi}{(2\pi)^3}\left[\int\left(C^2\hbar^2k^2 + M^2C^4\right)^{1/2} n_T^{0(n)}(\vec{k})\, d^3k - \int_{k_{f(n)}}\left(C^2\hbar^2k^2 + M^2C^4\right)^{1/2} d^3k\right]$$
$$+\frac{A}{2}\left(\frac{\xi}{(2\pi)^3}\right)^2\left[\iint n_T^{0(n)}(\vec{k})\, n_T^{0(n)}(\vec{k}')\, g_{ex}(|\vec{k}-\vec{k}'|) d^3k\, d^3k' - \iint_{k_{f(n)}} g_{ex}(|\vec{k}-\vec{k}'|) d^3k\, d^3k'\right] \tag{4.1.18}$$

where, $A = \frac{(\varepsilon_{ex}^{l} + \varepsilon_{ex}^{ul})}{2\rho_0}\left(\frac{\varepsilon_{ex}^{l}}{\rho_0}\right)$ and $\xi = 4(2)$. The integral $\int_{k_{f(n)}}$ implies integration over the Fermi sphere of radius $k_{f(n)}$ in SNM (PNM). As has been mentioned earlier, it is evident from eq.(4.1.18) that only the kinetic energy terms and finite range exchange terms contribute to the thermal evolution in SNM (PNM). The results of thermal evolution of internal energy density in SNM and the four cases of PNM, namely, $\varepsilon_{ex}^{l} = 0,\ \varepsilon_{ex}/3,\ 2\varepsilon_{ex}/3$ and ε_{ex} are given in Figure 4.4 as a function of density at temperature, T= 40 MeV. The ideal Fermi gas model results in SNM is also given in the same figure.

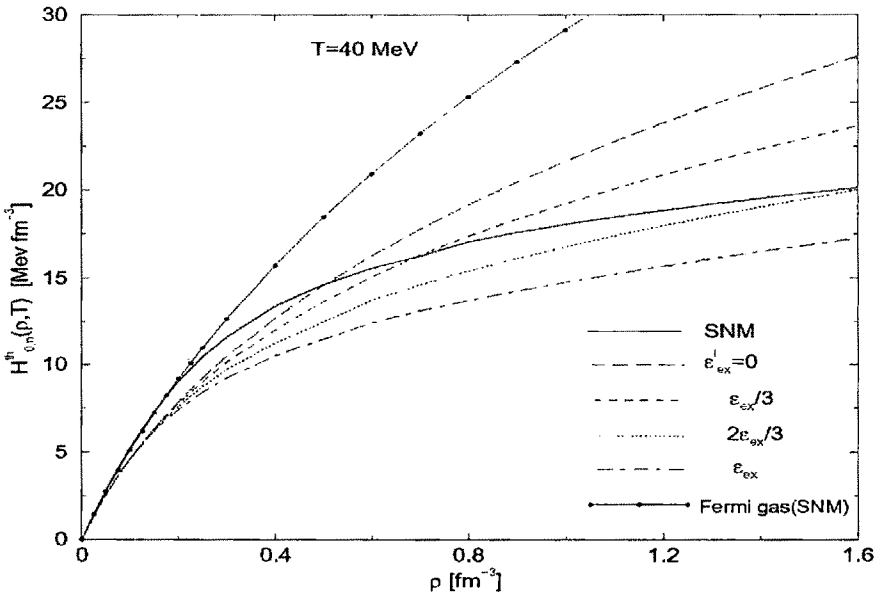

Figure 4.4. Thermal evolution of internal energy density, $H^{th}_{0,n}(\rho,T)$, in SNM and four cases of PNM corresponding to $\varepsilon'_{ex}=0$, $\varepsilon_{ex}/3$, $2\varepsilon_{ex}/3$ and ε_{ex} shown as a function of density ρ at temperature T= 40 MeV. Fermi-gas model results in SNM and PNM correspond to $\varepsilon_{ex}=0$ and $\varepsilon'_{ex}=0$, respectively.

4.2.2. Thermal evolution of free energy density

The thermal evolution of free energy density in SNM (PNM) can now be given in terms of entropy density, $TS_{0(n)}(\rho,T)$ and $H^{th}_{0(n)}(\rho,T)$ as

$$F^{th}_{0(n)}(\rho,T)=H^{th}_{0(n)}(\rho,T)-TS_{0(n)}(\rho,T). \tag{4.1.19}$$

$F^{th}_{0(n)}(\rho,T)$ in SNM (PNM) is calculated as a function of density at temperature $T=40$ MeV for the same cases as in Figure 4.4, and the results are shown in Figure 4.5. The thermal evolution of pressure can be given by,

$$P^{th}_{0(n)}(\rho,T)=\rho[\mu^{0(n)}(\rho,T)-\mu^{0(n)}(\rho,T=0)]-F^{th}_{0(n)}(\rho,T). \tag{4.1.20}$$

From the definition of effective chemical potentials, it is apparent that $[\mu^{0(n)}_{eff}(\rho,T)-\mu^{0(n)}_{eff}(\rho,T=0)] = [\mu^{0(n)}(\rho,T)-\mu^{0(n)}(\rho,T=0)]$. The effective chemical potential in case of SNM (PNM) at finite temperature is obtained in the process of self-

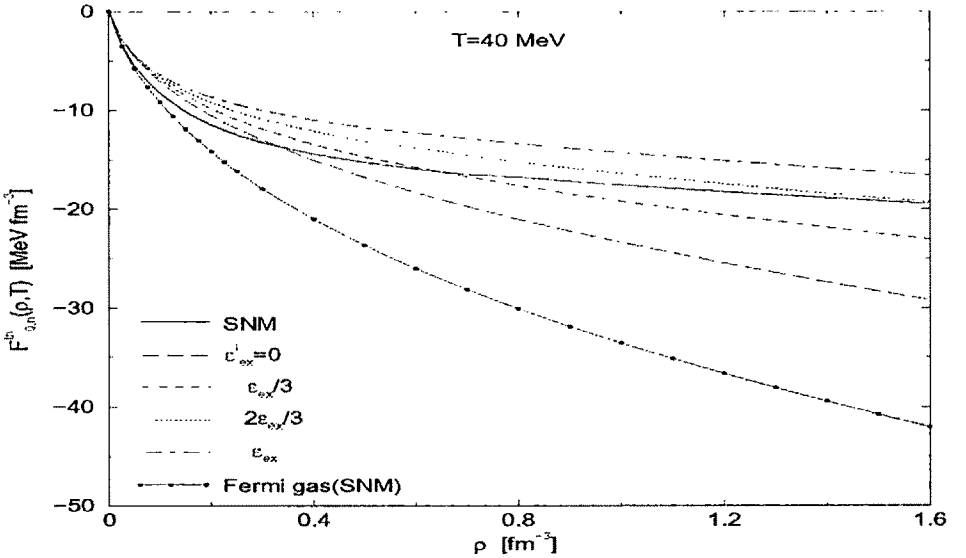

Figure 4.5. Thermal evolution of free energy density, $F^{th}_{0,n}(\rho,T)$, in SNM and four cases of PNM corresponding to $\varepsilon^{l}_{ex}=0$, $\varepsilon_{ex}/3$, $2\varepsilon_{ex}/3$ and ε_{ex} shown as a function of density ρ at temperature T= 40 MeV. Fermi-gas model results in SNM and PNM correspond to $\varepsilon_{ex}=0$ and $\varepsilon^{l}_{ex}=0$, respectively.

consistent evaluation of momentum distribution function $f_T^{SNM(PNM)}(\vec{k})$, whereas, its zero-temperature counterpart is obtained from eq.(3.2.2) (eq.(4.1.11)) by considering only the kinetic and finite range exchange terms evaluated at the Fermi momentum $k = k_{f(n)}$ corresponding to density ρ.

4.2.3. Thermal evolution of pressure

The thermal evolution of pressure, $P^{th}_{0(n)}(\rho,T)$, in SNM (PNM) as function of density at T = 40 MeV is given in Figure 4.6 for the same cases, as in Figure 4.5. The thermal evolutions of internal energy density and pressure have positive values both in SNM and PNM, whereas, it is negative in case of free energy density as can be seen from respective Figures 4.4, 4.5 and 4.6. It can also be seen from Figures 4.4 and 4.5 that thermal evolutions of internal energy density and free energy density for different cases of ε^{l}_{ex} in PNM show similar behaviour as in case of entropy density in Figure 4.3. For ε^{l}_{ex} in the range 0 to $2\varepsilon_{ex}/3$ the results of PNM crossover the respective SNM result at certain higher densities, whereas, there is no crossing over of PNM and SNM results at

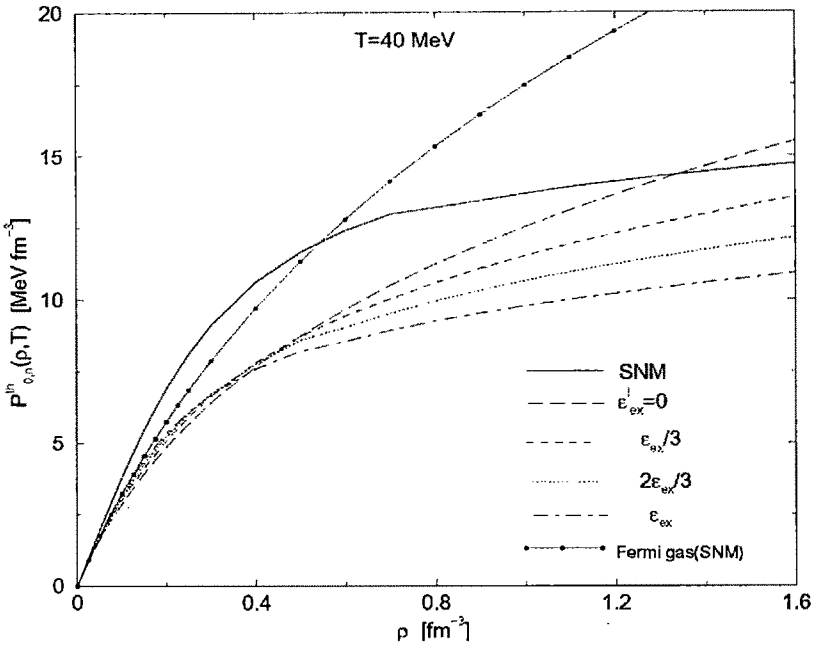

Figure 4.6. Thermal evolution of pressure, $P^{th}_{0,n}(\rho,T)$, in SNM and four cases of PNM corresponding to $\varepsilon^I_{ex}=0$, $\varepsilon_{ex}/3$, $2\varepsilon_{ex}/3$ and ε_{ex} shown as a function of density ρ at temperature T= 40 MeV. Fermi-gas model results in SNM and PNM correspond to $\varepsilon_{ex}=0$ and $\varepsilon^I_{ex}=0$, respectively.

any density in case ε^I_{ex} is in between $2\varepsilon_{ex}/3$ and ε_{ex}. For $\varepsilon^I_{ex}=2\varepsilon_{ex}/3$, the thermal evolution of internal energy density and free energy density in PNM approaches the SNM result asymptotically. Thus it is found that, like the case of entropy density, thermal evolutions of internal energy density and free energy density in PNM relative to SNM results have similar behaviour in the two different regions of ε^I_{ex}, specified by (a) and (b) in the foregoing discussion. However, in case of thermal evolution of pressure deviation from this common behaviour occurs as can be seen from Figure 4.6. The deviation from this common behaviour is due to the thermal evolution of chemical potential term, $[\mu^{0(n)}(\rho,T)-\mu^{0(n)}(\rho,T=0)]$. We shall now examine the thermal evolution of nuclear symmetry energy and free symmetry energy which are two important quantities in the studies of formation and cooling mechanism of neutron stars.

4.3. Thermal evolution of Nuclear Symmetry Energy

The nuclear symmetry energy at finite temperature, $E_S(\rho,T)$, can be obtained from the finite temperature expression of nuclear symmetry energy density defined in eq.(4.1.5) by dividing it with ρ,

$$E_S(\rho,T)=\frac{[H_n(\rho,T)-H_0(\rho,T)]}{\rho}=(e_n(\rho,T)-e_0(\rho,T)), \tag{4.2.1}$$

where, $e_n(\rho,T)$ and $e_0(\rho,T)$ are respectively the energy per particle in PNM and SNM at density ρ and temperature T. The thermal evolution of nuc lear symmetry energy $E_S(\rho,T)$ can be obtained by subtracting the zero-temperature result from it and we denote the quantity by the functional,

$$Q(\rho,T)=[E_S(\rho,T)-E_S(\rho,T=0)]. \tag{4.2.2}$$

The calculation of $Q(\rho,T)$ as a function of density at a given temperature T requires the knowledge of thermal evolution of the energy densities in SNM as well as in PNM. The thermal evolution in SNM is obtained by taking the difference of energy density expressions at finite T and zero-temperature given in eqs.(3.2.1) and (3.2.5) respectively. The resulting expression will contain only the kinetic energy terms and finite range exchange terms of finite T and zero-temperature expressions. Similarly, the thermal evolution of the energy densities of PNM can be calculated from eqs.(4.1.7) and (3.3.18). We have studied the thermal evolution of symmetry energy for the two representative values of ε_{ex}^{l}, namely, $\varepsilon_{ex}^{l}=(\varepsilon_{ex}^{l}+\varepsilon_{ex}^{ul})/6$ (Case A) and $\varepsilon_{ex}^{l}=(\varepsilon_{ex}^{l}+\varepsilon_{ex}^{ul})/2$ (Case B), those constitute the extreme cases obtained from the nature of effective mass splitting and analysis of Lane potential results as discussed in the Chapter-III. The results of the calculated density dependence of $Q(\rho,T)$ at different temperature T are given in Figure 4.7(a) and (b) for the two different splittings of the combination $(\varepsilon_{ex}^{l}+\varepsilon_{ex}^{ul})$ in cases A and B. It can be seen that $Q(\rho,T)$ is negative at low density and decreases with increase in density for both the cases A and B. With further increase in density ρ, the functional $Q(\rho,T)$ attains a minimum and then increases. However, in the higher density region the rate of increase of $Q(\rho,T)$ is faster in case A

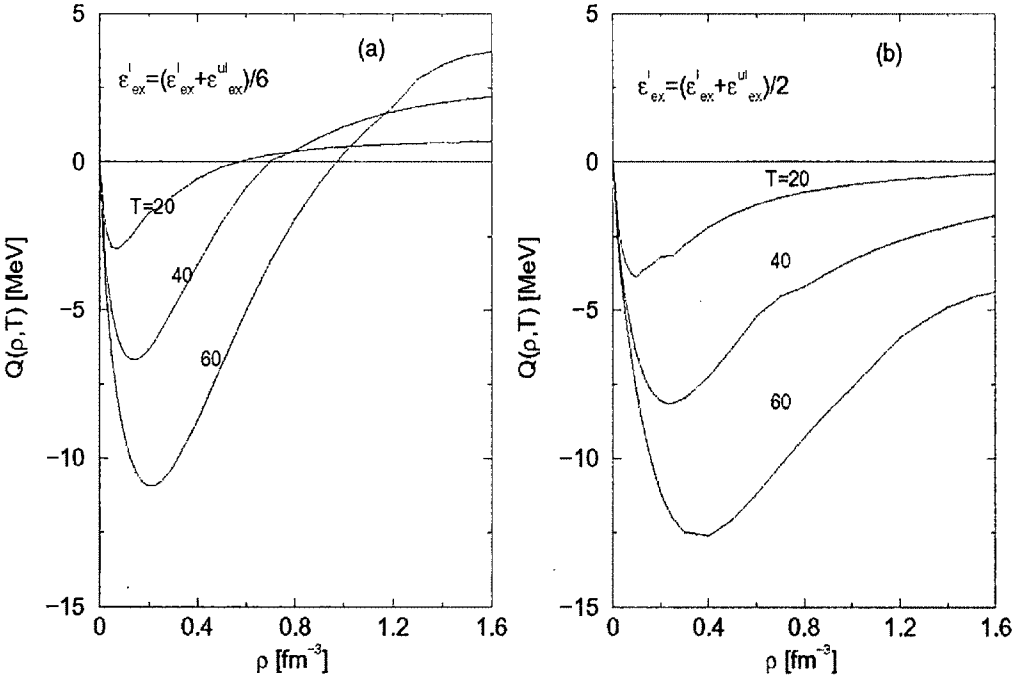

Figure 4.7. (a) Nuclear symmetry energy at temperature T relative to its zero temperature result (The functional $Q(\rho,T)$ in eq.(4.2.2)) shown as a function of density for case A at three different temperatures, T=20, 40 and 60 MeV. (b) Same as (a) for case B.

than in case B. As a result of this $Q(\rho,T)$ changes sign and becomes positive in the higher density region in case A as can be seen from Figure 4.7(a), whereas, it remains negative in case B for the entire range of density. As expected the effect of temperature on $Q(\rho,T)$ is found to increase with an increase in the magnitude of exchange strength parameter ε^{l}_{ex} in PNM as well as with temperature T.

4.3.1. Thermal evolution of Symmetry energy for EOSs corresponding to momentum independent mean field (Fermi gas model)

The results of $Q(\rho,T)$ for the ideal Fermi gas are shown in Figure 4.8 at three different temperatures. It can be seen from the Figure 4.8 that, $Q(\rho,T)$ assumes negative values at any temperature over the whole range of density. At a given density, $Q(\rho,T)$ takes larger negative value at higher temperature. With the increase in density, for a given

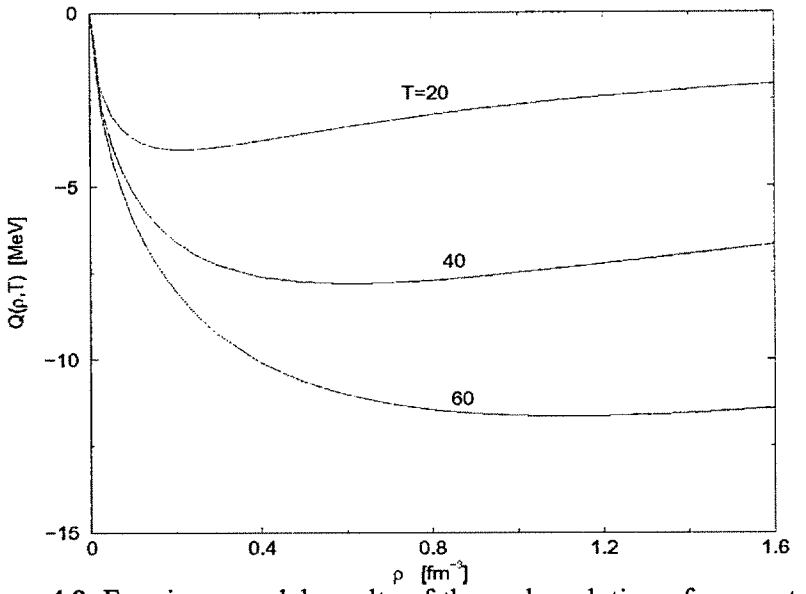

Figure 4.8. Fermi gas model results of thermal evolution of symmetry energy, $Q(\rho,T)$, shown as a function of density ρ at three different temperatures, T= 20, 40 and 60 MeV.

temperature, it decreases and then saturates after attaining a minimum in the high density region.

4.3.2. Thermal evolution of Symmetry energy for EOSs corresponding to momentum dependent mean field

In order to examine the effect of momentum dependence on the thermal evolution of symmetry energy, we have shown the results of the functional $Q(\rho,T)$ for the cases $\varepsilon_{ex}^{l}=0$, $\varepsilon_{ex}/3$, $2\varepsilon_{ex}/3$ and ε_{ex} in Figure 4.9 at temperature $T=40\ MeV$. For all the four cases, at a given temperature, $Q(\rho,T)$ decreases with the increase in density, attains a minimum and then increase with the increase in density. A changeover of sign in $Q(\rho,T)$ takes place if ε_{ex}^{l} lies in the range between 0 to $2\varepsilon_{ex}/3$ whereas $Q(\rho,T)$ remains negative all through the density region if ε_{ex}^{l} lies in the range between $2\varepsilon_{ex}/3$ to ε_{ex}. For $\varepsilon_{ex}^{l}=2\varepsilon_{ex}/3$, $Q(\rho,T)$ vanishes asymptotically at high density. The curves of $Q(\rho,T)$ are gradually pushed lower towards the ideal Fermi gas results as ε_{ex}^{l} increases from 0 to ε_{ex} implying that momentum dependent mean field plays a role to reduce the effect of temperature. The quenching effect in the high density region

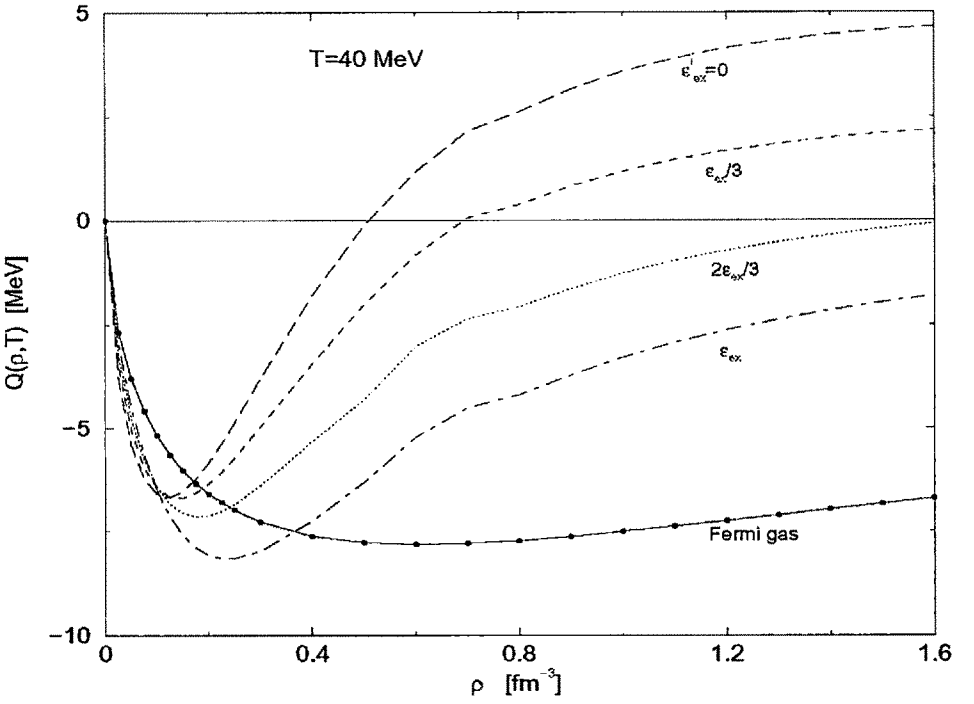

Figure 4.9. Thermal evolution of symmetry energy, $Q(\rho,T)$, shown as a function of density ρ at temperature T= 40 MeV for four cases of $\varepsilon'_{ex}=0,\ \varepsilon_{ex}/3,\ 2\varepsilon_{ex}/3$ and ε_{ex}. The Fermi gas model result is given as solid line with filled circles.

decreases with decrease in the attractive strength of the finite range exchange interaction between the unlike nucleons pair. It may be noted here that for given finite range exchange

interactions operating between two like and unlike nucleons, the temperature and density dependence of the functional $Q(\rho,T)$ does not depend on how the density dependence of zero-temperature symmetry energy $E_S(\rho,T=0)$ has been constrained.

4.4. Thermal evolution of Free Symmetry Energy

In the study of finite temperature nuclear matter properties the nuclear free symmetry energy plays a very important role. It has crucial importance in phenomena, such as, EOS of supernova matter, composition and cooling mechanism of newly born neutron stars, etc. The free energy density in case of SNM and PNM are defined as,

$$F_0(\rho,T)=H_0(\rho,T)-TS_0(\rho,T) \qquad (4.3.1)$$

and

$$F_n(\rho,T)=H_n(\rho,T)-TS_n(\rho,T)\,, \tag{4.3.2}$$

respectively, where $H_0(\rho,T)$ and $S_0(\rho,T)$; $H_n(\rho,T)$ and $S_n(\rho,T)$ are the respective energy densities and entropy densities.

Under the consideration that the quadratic expansion of the free energy to be valid we can express the free energy density in asymmetric nuclear matter as

$$F(\rho,T,Y_p)=F_0(\rho,T,Y_P=1/2)+(1-2Y_p)^2F_s(\rho,T), \tag{4.3.3}$$

where, $F_s(\rho,T)$ is the free symmetry energy density. Following the argument in expressing the nuclear symmetry energy in eq.(4.1.5) we can write the nuclear free symmetry energy density as,

$$F_s(\rho,T)=F_n(\rho,T,Y_P=0)-F_0(\rho,T,Y_P=1/2) \tag{4.3.4}$$

In view of the eqs. (4.3.1) and (4.3.2), the nuclear free symmetry energy density can now be expressed as

$$F_s(\rho,T)=\left[H_n(\rho,T)-H_0(\rho,T)\right]-T\left[S_n(\rho,T)-S_0(\rho,T)\right] \tag{4.3.5}$$

The thermal evolution of nuclear free symmetry energy relative to its zero temperature results is expressed through the functional

$$Q_F(\rho,T)=\frac{F_s(\rho,T)-F_s(\rho,T=0)}{\rho}, \tag{4.3.6}$$

where, $F_s(\rho,T=0)=\left[H_n(\rho,T=0)-H_0(\rho,T=0)\right]$. Thus $Q_F(\rho,T)$ can also be expressed in terms of thermal evolution of symmetry energy as,

$$Q_F(\rho,T)=Q(\rho,T)-T\left[S_n(\rho,T)-S_0(\rho,T)\right]. \tag{4.3.7}$$

Thermal evolution of free symmetry energy, $Q_F(\rho,T)$ can now be calculated as a function of density from the results of $Q(\rho,T)$ and entropy densities in SNM and PNM. The results of $Q_F(\rho,T)$ as a function of density for the same cases, as in Figure 4.9, are shown in Figures 4.10(a) and (b) at two different temperatures $T=40$ and 60 MeV, respectively. The corresponding ideal Fermi gas model results are also shown in the same figures. The results show that the thermal evolution of free symmetry energy $Q_F(\rho,T)$ is large positive at low values of the density for both momentum dependent and momentum independent cases, in contrast to the negative values of $Q(\rho,T)$, and it decreases with increase in density. The large positive values in the low density region is

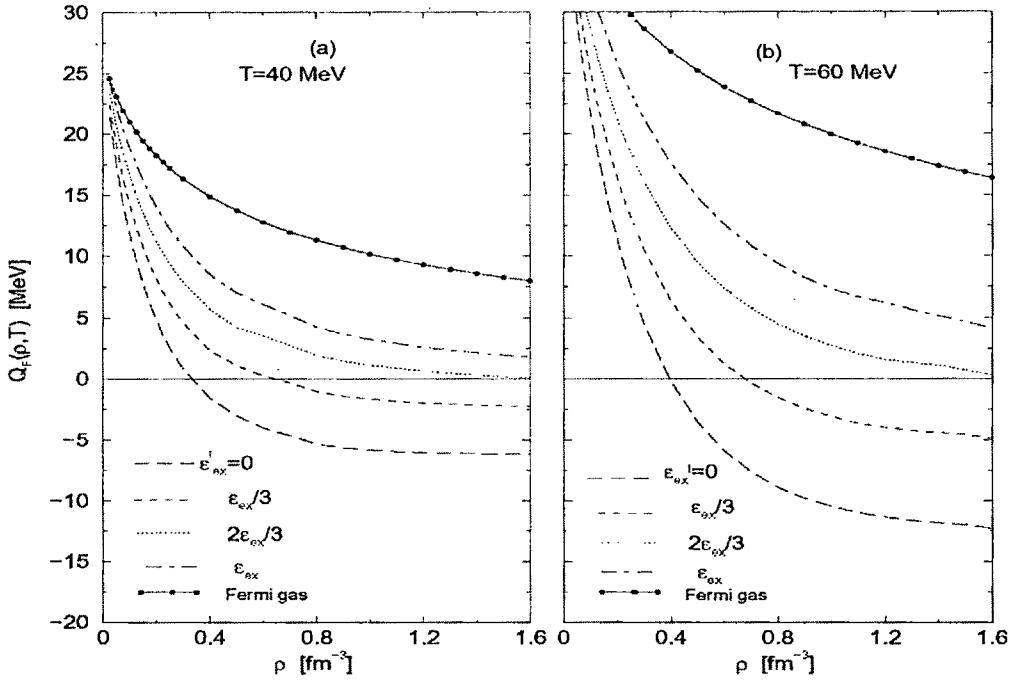

Figure 4.10. (a) Thermal evolution of free symmetry energy, $Q_F(\rho,T)$, as a function of density ρ for four cases of $\varepsilon_{ex}^{l}=0, \varepsilon_{ex}/3, 2\varepsilon_{ex}/3$ and ε_{ex} at temperature T= 40. (b) Same as (a) for T=60 MeV. The respective Fermi gas model results are given as solid lines with filled circles in the corresponding figures.

basically due to the fact that entropy in SNM is large compared to that in PNM in this density region and hence the factor $\frac{[S_n(\rho,T)-S_0(\rho,T)]}{\rho}$ in eq. (4.3.7) assumes large negative values in the low density region. The rate of decrease of $Q_F(\rho,T)$ slows down in the high density region for all the cases shown in the Figures 4.10(a) and (b). But the ideal Fermi gas model results of $Q_F(\rho,T)$ remain larger positive as compared to momentum dependent mean field cases over the whole range of density. The decrease in $Q_F(\rho,T)$ with increase in density in the momentum dependent mean field cases is relatively sharper compared to the ideal Fermi gas case and the rate of decrease also depends on the value of ε_{ex}^{l}. In case of $0 \le \varepsilon_{ex}^{l} < 2\varepsilon_{ex}/3$, $Q_F(\rho,T)$ becomes negative at certain density and approaches negative asymptotic value in the high density region. For $2\varepsilon_{ex}/3 < \varepsilon_{ex}^{l} \le \varepsilon_{ex}$, the result of $Q_F(\rho,T)$ remains positive at all densities

and approaches to a positive asymptotic value in the high density region showing similar behavior as that of the ideal Fermi model case. On the other hand, thermal evolution of $Q_F(\rho,T)$ for $\varepsilon_{ex}^{l}=2\varepsilon_{ex}/3$ does not become negative at any density and vanishes asymptotically. The behaviours of $Q_F(\rho,T)$ found for the different cases of ε_{ex}^{l} are true at any temperature. Thus, thermal evolutions of symmetry energy and free symmetry energy in the two ranges of ε_{ex}^{l}, specified by (a) and (b) in the foregoing discussions, have similar behaviour to what has been observed in cases of entropy density as well as thermal evolution of internal energy density and free energy density.

4.5. Neutron-proton effective mass splitting in ANM at $T=0$ for different choices of ε_{ex}^{l}

Two distinct behaviours in the thermal evolution of nuclear matter properties in PNM relative to their respective SNM results are found in the regions, ε_{ex}^{l} in between (a) 0 to $2\varepsilon_{ex}/3$ and (b) $2\varepsilon_{ex}/3$ to ε_{ex}. The results of thermal evolution of these properties in ANM will be in between the corresponding results in SNM and PNM and shall correspond to the same characteristic behaviour depending on the value of ε_{ex}^{l} in these two ranges. We shall now examine the n and p effective mass splitting in ANM at zero-temperature for different cases of ε_{ex}^{l} in the whole range between 0 and ε_{ex}. The calculation of n and p effective masses in ANM requires only the momentum dependent parts of the mean fields which are obtained from the finite range exchange interactions. The neutron and proton effective mass splitting at zero-temperature as functions of momentum k, asymmetry β and density ρ are shown in the Figures 4.11(a), (b) and (c) respectively for the three boundary cases $\varepsilon_{ex}^{l}=(\varepsilon_{ex}^{l}+\varepsilon_{ex}^{ul})/6$, $\varepsilon_{ex}^{l}=(\varepsilon_{ex}^{l}+\varepsilon_{ex}^{ul})/2$ and $\varepsilon_{ex}^{l}=2(\varepsilon_{ex}^{l}+\varepsilon_{ex}^{ul})/6$. The neutron and proton effective mass splitting is found to be increasing function of all the three variations, k, β and ρ, with increase in the difference between the exchange strength parameters, ε_{ex}^{l} and ε_{ex}^{ul}, acting between a pair of like and unlike nucleons, respectively. Thus the splitting is

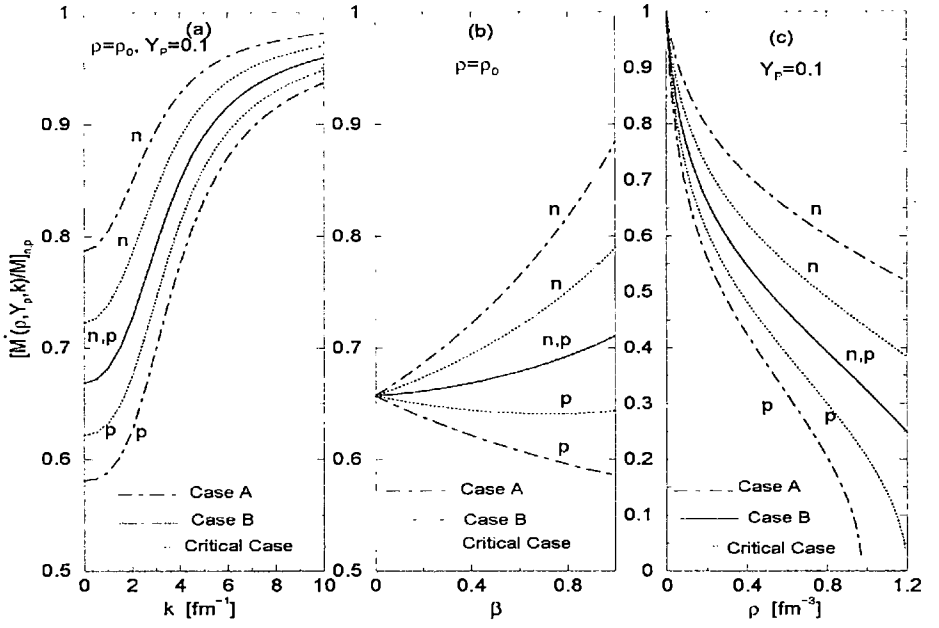

Figure 4.11. (a) Neutron and proton effective mass shown as function of momentum for the three different cases of splitting for a given proton fraction $Y_P = 0.1$ and at normal density ρ_0. (b) Same as (a) but shown as function of neutron-proton asymmetry at normal density. (c) Same as (a) but shown as function of density at a fixed proton fraction $Y_P = 0.1$.

maximum for case A. In case B, there is no splitting between the neutron and proton effective masses in ANM as the strength of exchange interaction between like pair and unlike pairs of nucleons are the same. Beyond this boundary value where the exchange strength between a pair of like nucleons becomes stronger than that of a unlike nucleons, the proton effective mass will be predicted to go over the neutron one that contradicts the largely accepted view of larger neutron effective mass than proton one in neutron rich matter. For the critical case that subdivides the whole range specified by case A and case B into two groups so far as the behaviour of entropy per particle in SNM and PNM is concerned, the results for neutron and proton effective mass splitting in ANM lies in between the two cases A and B. The results for neutron and proton effective mass splitting in ANM as a function of asymmetry $\beta = (1 - 2Y_p)$ obtained in our calculation for the three different cases is compared with the results of DBHF calculation [180] and is given in Figure 4.12. The results of our calculation for the

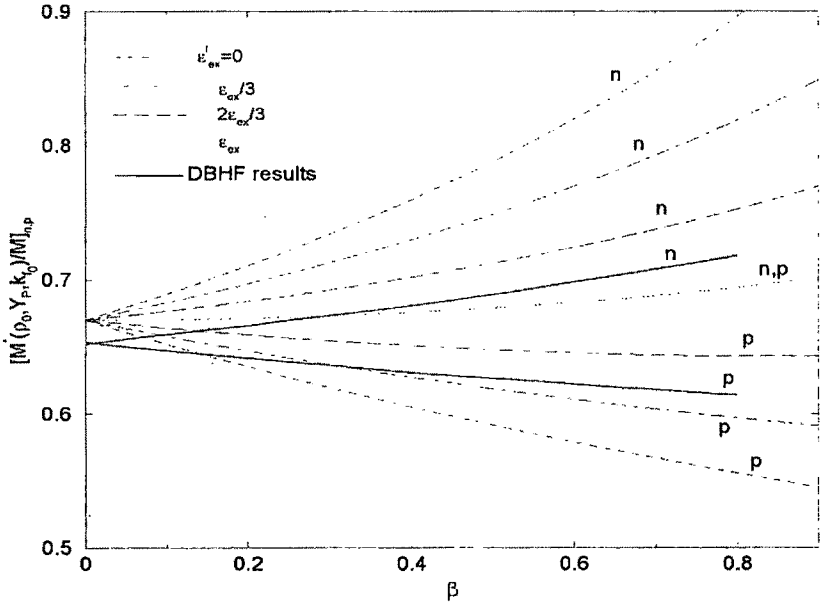

Figure 4.12. Neutron-proton effective mass plotted as function of neutron-proton asymmetry $\beta = (1-2Y_P)$ for different splitting strengths. The DBHF calculation of Sammarruca [180] (solid line) is also shown for comparison. The upper three curves are the neutron effective mass where as the lower curves are for proton effective mass.

critical value of ε^l_{ex} agree to a reasonable extent with the predictions of DBHF calculation. The difference between the curves of neutron effective mass (as well as proton effective mass) for $\varepsilon^l_{ex} = 2\varepsilon_{ex}/3$ and the DBHF results appearing in the figure is mainly due to the difference between the effective masses in SNM. It is to be noted here that for each of these three representative values of ε^l_{ex} we can determine the splitting of the rest two parameters, ε_0 and ε_γ, corresponding to the density dependent parts into like and unlike channels according to the procedure as discussed in the last chapter. The EOSs of ANM thus obtained for all these three cases give the same density dependence at zero-temperature, as may be seen from Figures 3.9 and 3.10, but vary widely in their momentum dependence as evident from Figure 4.11. Thus the EOSs corresponding to the three representative values of ε^l_{ex} exhibit widely varying thermal evolution of the nuclear matter properties as enumerated in the foregoing discussions. The calculation of the neutron and proton effective masses as well as the thermal evolution of nuclear matter properties discussed above in this section are possible only

with the knowledge of momentum dependent parts of the nucleonic mean fields. However the complete calculation of nuclear symmetry energy and nuclear free symmetry energy requires the complete knowledge of the EOS, both density as well as momentum dependent parts. Studies of these two properties at finite temperature has important relevance in isoscaling studies of multifragmentation phenomena and in supernovae matter as well as formation mechanism of neutron stars as will be discussed in the following chapter.

4.6. Conclusion

In this chapter we have made an attempt to constrain the momentum dependence of nuclear mean field by considering the thermal evolution of nuclear matter properties. The thermal evolution in nuclear matter has been calculated in terms of the thermal evolution in SNM and PNM. In absence of definite idea about the momentum dependence of PNM mean field, we have considered different representative cases within the allowed range of momentum dependence of PNM mean field. It has been found that the momentum dependence of the nuclear mean field has the important influence of reducing the effect of temperature. We have found a critical value $\varepsilon_{ex}^{l} = \frac{2}{3}\varepsilon_{ex}$ within the whole allowed range of ε_{ex}^{l}, i.e. $0 \le \varepsilon_{ex}^{l} \le \varepsilon_{ex}$. On both sides of this value, the thermal evolution in SNM and PNM show two contrasting behaviours. If $0 \le \varepsilon_{ex}^{l} \le \frac{2}{3}\varepsilon_{ex}$ then the thermal evolution in PNM crosses that of SNM at certain higher density. If $\frac{2}{3}\varepsilon_{ex} < \varepsilon_{ex}^{l} \le \varepsilon_{ex}$ then no such cross over phenomena takes place. Also entropy density in PNM also does not cross over that in SNM at any density. Since the PNM is a one component system, the entropy density in PNM should not cross that of SNM. Therefore it is less likely that the momentum dependence of PNM mean field should lie within the range $0 \le \varepsilon_{ex}^{l} \le \frac{2}{3}\varepsilon_{ex}$. For this critical value it has been found that, the magnitude of neutron-proton effective mass splitting in ANM agrees quite well with the results obtained in ab initio DBHF calculation.

CHAPTER-V

PROPERTIES OF NUCLEAR MATTER AT FINITE TEMPERATURE AND EQUATION OF STATE OF CHARGE NEUTRAL $n+p+e+\mu$ MATTER UNDER BETA EQUILIBRIUM

In the last chapter the thermal evolution of important nuclear matter properties like nuclear symmetry energy and free symmetry energy have been studied which requires only the knowledge of finite range exchange interactions acting between a pair of like nucleons and unlike nucleons. Within the framework of the formalism used in our work, it is the finite range exchange part of the interaction that determines the momentum dependence of the nuclear mean field and also simulates the temperature evolution of nuclear matter properties. From the studies on entropy per particle and thermal evolution of vario us nuclear matter properties in the last chapter it is clear that the momentum dependence of the nuclear mean field has the crucial role in making the system a more ordered one and also in counterbalancing the effect of temperature on the nuclear matter properties. In this context two contrasting behaviours have been noticed depending on the magnitude of splitting of the combined exchange strength parameter $(\varepsilon_{ex}^{l}+\varepsilon_{ex}^{ul})$ into like and unlike channels, ε_{ex}^{l} and ε_{ex}^{ul}, respectively. It is also found that there is a critical value of this splitting close to $\varepsilon_{ex}^{l}=2(\varepsilon_{ex}^{l}+\varepsilon_{ex}^{ul})/6$ (corresponding to $\varepsilon_{ex}^{ul}=4(\varepsilon_{ex}^{l}+\varepsilon_{ex}^{ul})/6$), that divides the admissible range of the splitting of the combined exchange strength parame ter $(\varepsilon_{ex}^{l}+\varepsilon_{ex}^{ul})$ into two distinct groups. In the case of splitting of the exchange strength parameter where ε_{ex}^{l} value lies below this critical value then the entropy in PNM can become more than that of SNM as the density increases and in this case the functional behaviour of properties like nuclear symmetry energy and free symmetry energy at finite temperature relative to zero temperature gets inverted in the high density region. On the other hand if the splitting is such that ε_{ex}^{l} value lies in the other half then entropy in PNM does not surpass the SNM result and the functional behaviors of properties like nuclear symmetry energy and free symmetry energy at finite temperature relative to zero temperature do not get inverted in the high density region. For the critical value of ε_{ex}^{l} the finite temperature results approach the zero-temperature ones asymptotically in the high density region. In the work of the present chapter we shall study the finite temperature nuclear matter properties as well as the EOS of beta equilibrated charge neutral $n+p+e+\mu$ matter for these three extreme cases of splitting of exchange strength parameter, namely, (i)

$\varepsilon_{ex}^{l} = (\varepsilon_{ex}^{l} + \varepsilon_{ex}^{ul})/6$ (case A) (ii) $\varepsilon_{ex}^{l} = (\varepsilon_{ex}^{l} + \varepsilon_{ex}^{ul})/2$ (case B) and (iii) the critical case $\varepsilon_{ex}^{l} = 2(\varepsilon_{ex}^{l} + \varepsilon_{ex}^{ul})/6$, in order to find out the differences in the prediction of the results.

5.1 Temperature dependence of Nuclear symmetry energy

The nuclear symmetry energy and free symmetry energy at finite temperature are defined in terms of the difference of energy density and free energy density in PNM and SNM at finite temperature respectively as,

$$E_S(\rho,T) = \frac{[H_n(\rho,T) - H_0(\rho,T)]}{\rho} = (e_n(\rho,T) - e_0(\rho,T))$$

$$F_{sym}(\rho,T) = \frac{[H_n(\rho,T) - H_0(\rho,T)] - T[S_n(\rho,T) - S(\rho,T)]}{\rho}.$$

The symmetry energy at finite temperature, $E_S(\rho,T)$, has crucial relevance in the isoscaling behaviour studies of multifragmentation phenomena in heavy-ion collision experiments at intermediate energies [133, 141, 181-183]. On the other hand, the free symmetry energy, $F_{sym}(\rho,T)$, at finite temperature plays important role in the formation and cooling mechanism of newly born neutron stars [136, 184-186].

The calculation of symmetry energy, $E_S(\rho,T)$, at non-zero temperature T requires the knowledge of energy densities in SNM and PNM as functions of ρ and T. The energy density of SNM for our interaction is given in eq.(3.2.1) and all the six parameters required for calculation are known fom saturation conditions and nuclear matter incompressibility and are given in table 2 of chapter-III. The results for energy density $H_0(\rho,T)$ in SNM as a function of density at different temperatures are shown in the Figure 5.1. The calculation in PNM for the three representative cases of splitting of the exchange strength parameter, $(\varepsilon_{ex}^{l} + \varepsilon_{ex}^{ul})$, as mentioned above now requires the additional splitting of the combined strength parameters of the density dependent parts, $(\varepsilon_0^{l} + \varepsilon_0^{ul})$ and $(\varepsilon_\gamma^{l} + \varepsilon_\gamma^{ul})$, into like and unlike channels. The parameter fixation in PNM has been discussed in chapter-III and the values of the parameters in case of these three representative cases are given in table 3 in the same chapter. The energy density in PNM, $H_n(\rho,T)$, as a function of density at different temperatures for the three cases, case A, case B and critical case, are shown in Figures 5.2(a), (b) and (c) respectively.

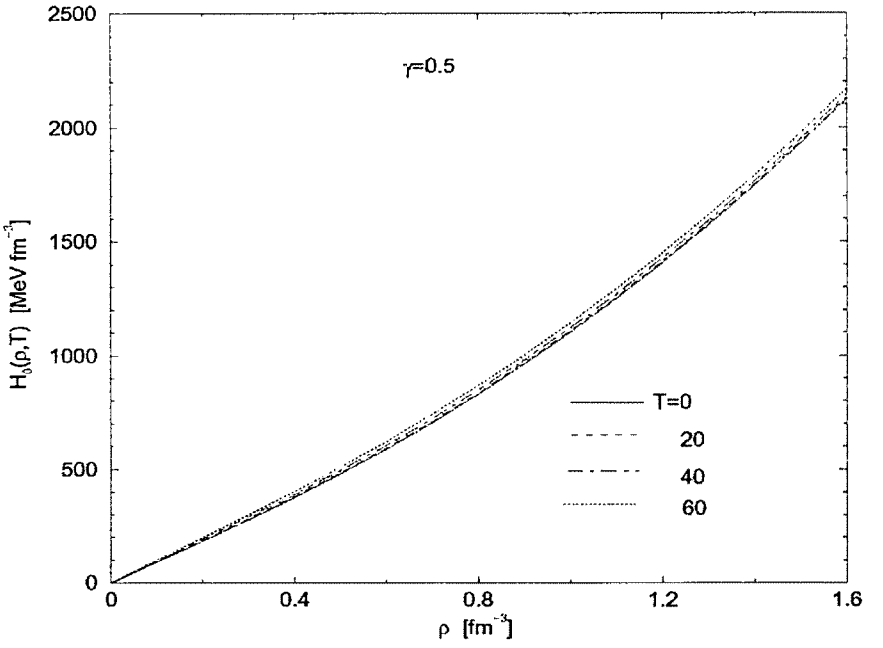

Figure 5.1. Energy density in SNM shown as a function of density at four different temperatures T=0, 20, 40 and 60 MeV.

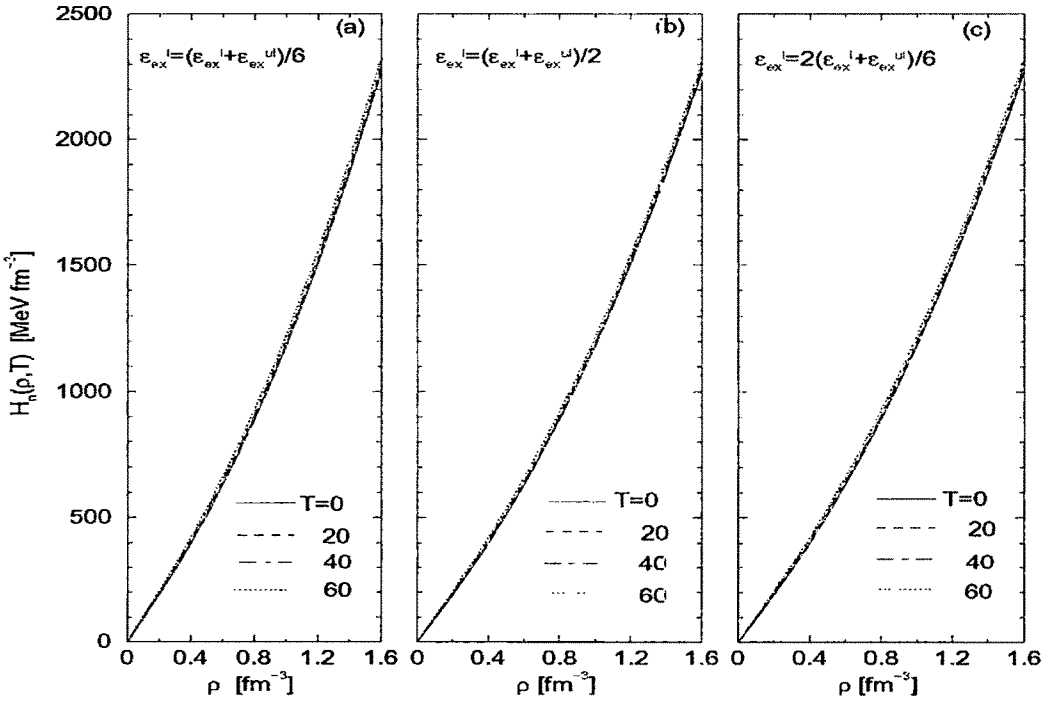

Figure 5.2. (a) Energy density in PNM shown as a function of density at four different temperatures T=0, 20, 40 and 60 MeV for case A. (b) Same as (a) for case B. (c) Same as (a) for the critical case.

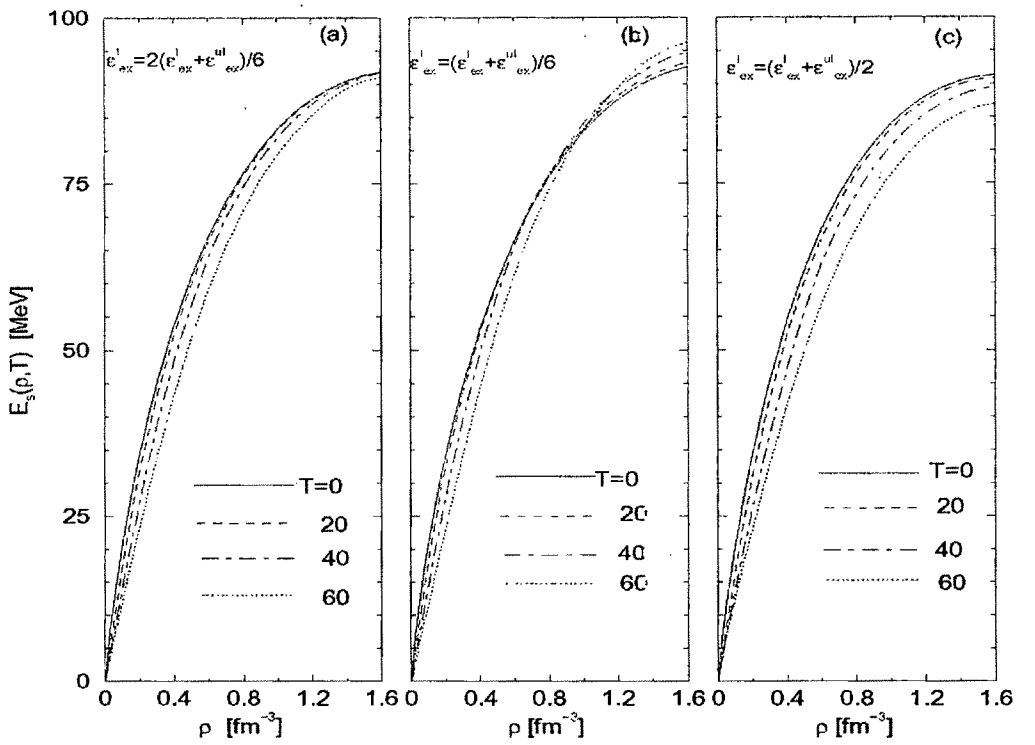

Figure 5.3. (a) Nuclear symmetry energy shown as a function of density for the critical case at temperatures T=0, 20, 40 and 60 MeV. (b) Same as (a) for case A. (c) Same as (a) for the case B.

The density dependence of nuclear symmetry energy $E_S(\rho,T)$ at different temperatures is shown in Figure 5.3(a) for the critical value of ε^{l}_{ex}. For this case, inversion in the functional relationship between the finite and zero-temperature results does not occur and the finite temperature result approaches the zero-temperature one asymptotically in the high density region as expected from earlier discussions in the previous chapter. In order to visualize the contrasting behaviour of density dependence of nuclear symmetry energy $E_S(\rho,T)$ in the cases of splitting of the exchange strength parameter on either sides of the critical value we have also calculated the results for the two other cases, $\varepsilon^{l}_{ex}=(\varepsilon^{l}_{ex}+\varepsilon^{ul}_{ex})/6$ and $\varepsilon^{l}_{ex}=(\varepsilon^{l}_{ex}+\varepsilon^{ul}_{ex})/2$, given as case A and case B, respectively. The results are shown in Figures 5.3(b) and (c) for the two cases A and B, respectively. The crossover phenomena resulting into an inversion of the functional relationship between the finite and zero-temperature results take place in the high density region in case A, whereas in case B, the finite temperature results remain below

the zero-temperature ones at all the densities considered. Under the formalism used in our work, the temperature dependence of the interaction part in nuclear matter properties is simulated through the momentum dependent part of the nuclear mean field which, in turn, arises from the exchange part of the interaction. Moreover, the temperature dependence of the symmetry energy has the behaviour that it decreases with increase in temperature, it is expected that in case of case B there will be a stronger temperature dependence in comparison to case A. The stronger temperature dependence in case B is a consequence of larger magnitude of the parameter ε_{ex}^{l} resulting into stronger momentum dependence in PNM as compared to case A. Thus for the case B, the curves of $E_S(\rho,T)$ are shifted more and more below the curve $E_S(\rho,T=0)$ with increase in temperature as can be seen in Figure 5.3(c) and the thermal evolution of the symmetry energy remains negative at all densities and all temperatures. Thus the functional $Q(\rho,T)$ remains negative in case B for the entire range of density shown in Figures 4.7(b). The relatively weaker momentum dependence in PNM in case A has the consequence of a weak temperature dependence in PNM that further decreases with increase in density resulting into a crossing over of the high temperature curves with the low temperature ones in the density region around $\rho \geq 0.8\, fm^{-3}$, as can be seen from Figure 5.3(b). Consequently the functional $Q(\rho,T)$ becomes positive at higher densities, as shown in Figures 4.7(a) for case A. On the other hand, for the critical case shown in Figure 5.3(a), the strength of momentum dependence in PNM is such that the effect of temperature gets washed out in the high density region and the curves of $E_S(\rho,T)$ approach to the $E_S(\rho,T=0)$ one asymptotically in the high density region. From the Figure 3.9 of chapter-III, it can be seen that the density dependence of $E_S(\rho,T=0)$ for the cases A and B are almost identical over the entire range of density. Thus a comparison of Figures 5.3(b) with 5.3(c) shows that different symmetry energies may have similar density dependence at zero temperature but they can differ significantly from each other at finite temperature. A comparison of the results obtained in our cases of different momentum dependence in PNM with the results in Ref.[176] shows that the temperature dependence of nuclear symmetry energy for case A shown in Figure 5.3(b) is similar to those obtained in Ref.[176] for their interaction with $x=0$.

5.1.1. Prediction of Symmetry energy from isoscaling analysis of Multifragmentation phenomena

The density dependence of symmetry energy at non-zero temperature is important in the studies of isoscaling analysis in multifragmentation phenomena [133, 141, 176, 181-183] as well as in the calculation of fractions of different particles in β-equilibrated $n+p+e+\mu$ matter [164, 177]. In the study of multifragmentation processes the ratio $R_{21}(N,Z)$ of the yields of a fragment with Z protons and N neutrons from two reactions reaching the same temperature T obeys an exponential relation $R_{21}(N,Z) \propto e^{\alpha N}$. The isoscaling coefficient α is related to the symmetry energy $E_S(\rho,T)$ as

$$\alpha = \frac{4E_s(\rho,T)}{T}\Delta\left[(Z/A)^2\right], \tag{5.1.1a}$$

where,

$$\Delta\left[(Z/A)^2\right] = (Z_1/A_1)^2 - (Z_2/A_2)^2 , \tag{5.1.1b}$$

is the difference between the $(Z_i/A_i)_{i=1,2}$ values of the two fragmenting sources created in the two reactions. The isoscaling coefficient α is extracted from the experimental data by plotting the number of isotopes formed for different Z, namely Z=2, 3, 4, etc., as function of neutron number, N. The slope of these different curves is same and given by α. The isoscaling coefficient α and the temperature T of the fragment emitting source are measured experimentally from which the value of $E_S(\rho,T)$ can be extracted from eqs. (5.1.1a & b). However, the freeze out density ρ_f of the fragmenting source at the site of formation of the particular nuclei has not yet been possible to extract from the experiments and therefore depends on the model used. This is the reason why different groups predict different values of the symmetry energy at same T extracted from the same experiments conducted at different laboratories. In order to see the model dependence of the value of freeze out density ρ_f of the fragmenting sources we calculate the symmetry energy $E_S(\rho,T)$ as a function of temperature for the two representative cases A and B in Figures 5.4(a) and (b) at different densities from $0.4\rho_0$ to ρ_0. In the same figures, the experimental data of the

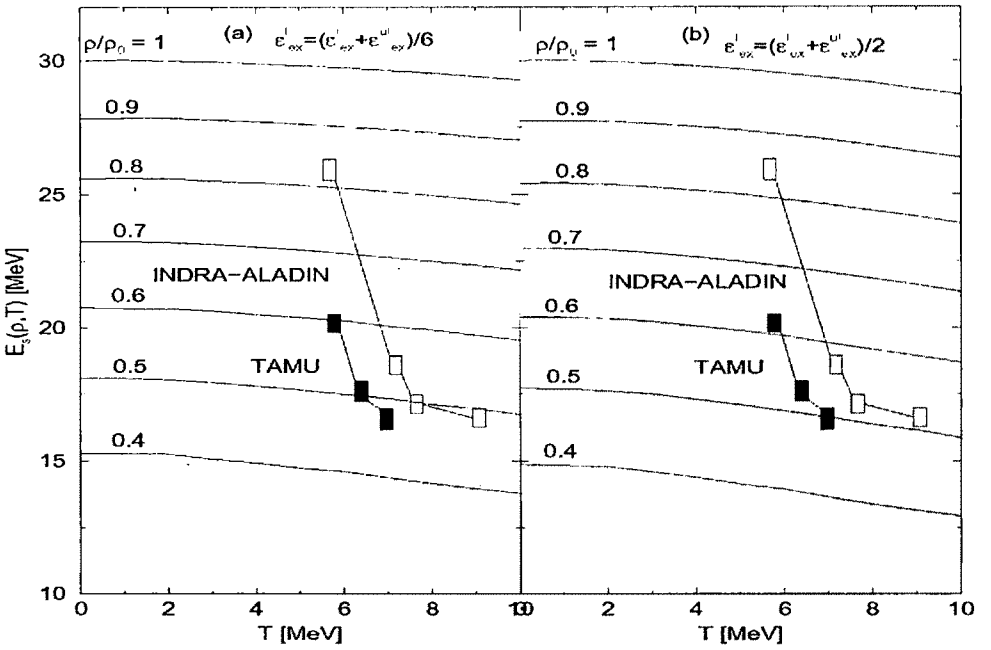

Figure 5.4. (a) Temperature dependence of symmetry energy for case A at different densities from $0.4\rho_0$ to ρ_0. The experimental data of the measured temperature dependent symmetry energy from Texas A&M university (TAMU) and INDRA-ALADIN collaboration at GSI are also included. (b) Same as (a) for case B.

measured temperature dependent symmetry energy from Texas A&M University (TAMU) [187] and the INDRA -ALADIN Collaboration at GSI [188, 189] are also included. The curves of $E_S(\rho,T)$ for same density ρ have similar temperature dependence for the two cases considered, except that the rate of decrease of symmetry energy with increase in temperature is relatively faster in case B compared to case A. From Figures 5.4(a) and (b) it is also clearly seen that the experimentally observed evolution of symmetry energy is mainly due to the change in density rather than temperature, as pointed out in Refs.[176, 190]. The average freeze-out density of the fragment emission source can be estimated from the measured temperature dependent symmetry energy based on isoscaling analysis in multifragmentation phenomena included in Figures 5.4(a) and (b). The average freeze-out density ρ_f for case A lies within $0.47\rho_0$ and $0.59\rho_0$ for TAMU data while it is within $0.49\rho_0$ and $0.83\rho_0$ for INDRA-ALADIN Collaboration data. On the other hand, for case B, ρ_f is found to be within $0.5\rho_0$ and $0.61\rho_0$ for TAMU data and between $0.52\rho_0$ and $0.84\rho_0$ for INDRA-

ALADIN Collaboration data. The shift in the freeze-out density ρ_f towards higher density in case B compared to case A is due to the fact that for a given density ρ below normal density ρ_0, the curve of $E_S(\rho,T)$ for case B is always below that of case A and the difference slowly increases with an increase in temperature and a decrease in density, as can be seen from Figures 4.5(a) and (b). It is interesting to compare the results of freeze-out density estimated in both the cases A and B with those obtained in Ref.[176]. For the interaction used in their study in Ref.[176] with $x=0$ the average freeze-out density ρ_f is within $0.41\rho_0$ and $0.52\rho_0$ for TAMU data while it is between $0.42\rho_0$ and $0.75\rho_0$ for INDRA-ALADIN Collaboration data. On the other hand, for the interaction with $x=-1$, ρ_f is within $0.57\rho_0$ and $0.68\rho_0$ for TAMU data and between $0.58\rho_0$ and $0.84\rho_0$ for INDRA-ALADIN Collaboration data. It may be mentioned here that in view of the recent work of Souza et. al. [191] the TAMU and INDRA-ALADIN Collaboration data need to be modified taking surface effect into account. But in any case the necessity to find out the freeze-out density in a particular reaction experiment in order to ascertain the value of $E_S(\rho,T)$ from isoscaling analysis remains unchanged. We have also repeated the calculation for the critical case and the results are shown in Figure 5.5. The average freeze-out density ρ_f in this case lies within $0.47\rho_0$ and $0.61\rho_0$ for TAMU data while it is within $0.49\rho_0$ and $0.84\rho_0$ for INDRA-ALADIN Collaboration data.

Since the temperature evolution of symmetry energy is built upon its zero-temperature result through the self-consistently evaluated Fermi-Dirac momentum distribution functions in SNM and PNM, the freeze out density ρ_f estimated in this way would also critically depend on the stiffness of the curve of $E_S(\rho,T=0)$ in the density region $\rho<\rho_0$. With an increase in the stiffness of $E_S(\rho,T=0)$ in this density region the freeze-out density ρ_f would gradually shift to lower and lower density. From an analysis of isoscaling data in multifragmentation phenomena it has been inferred in Ref.[133] that the density dependence of $E_S(\rho,T=0)$ should neither be

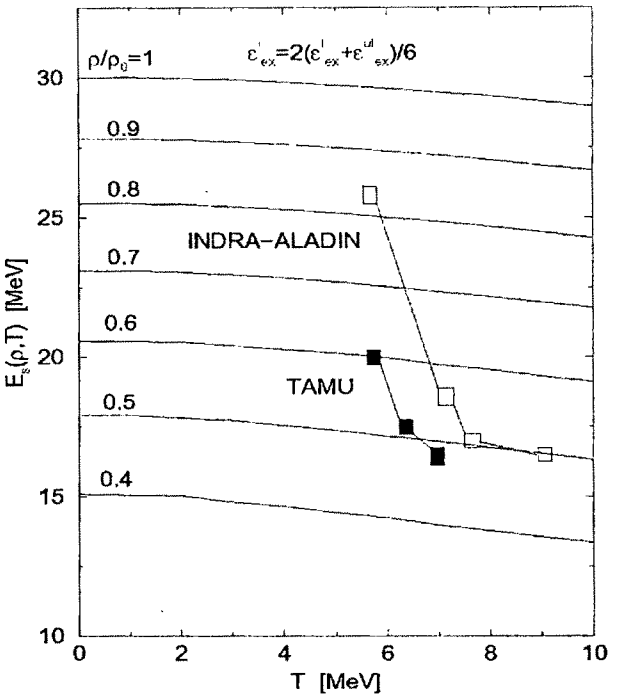

Figure 5.5. (a) Temperature dependence of symmetry energy for the critical case at different densities from $0.4\rho_0$ to ρ_0. The experimental data of the measured temperature dependent symmetry energy from Texas A&M university (TAMU) and INDRA-ALADIN collaboration at GSI are also included.

very stiff nor soft in the region $\rho < \rho_0$ and that the value of zero-temperature symmetry energy at half of the normal nuclear matter density, i.e., $\rho = \frac{\rho_0}{2}$, should have the order $18-20\,MeV$. In this context, we note that the value of $E_S(\rho = \frac{\rho_0}{2}, T = 0)$ is found to be $18.1\,MeV$ for case A , $17.7\,MeV$ for case B and $17.9\ MeV$ for the critical case.

The results of density dependence of nuclear symmetry energy density $H_s(\rho,T) = \rho E_S(\rho,T)$ defined in eq.(4.1.5) are given for the three cases, case A , case B and the critical case at different temperatures T = 0, 20, 40 and 60 MeV in Figures 5.6(a), (b) and (c) respectively. As expected the functional $H_s(\rho,T)$ has relatively a larger temperature dependence in case B compared to case A in so far as the decreasing trend of energy density with temperature is concerned, whereas, in critical case the temperature dependence is intermediate between these two cases which gets washed out in the high density region.

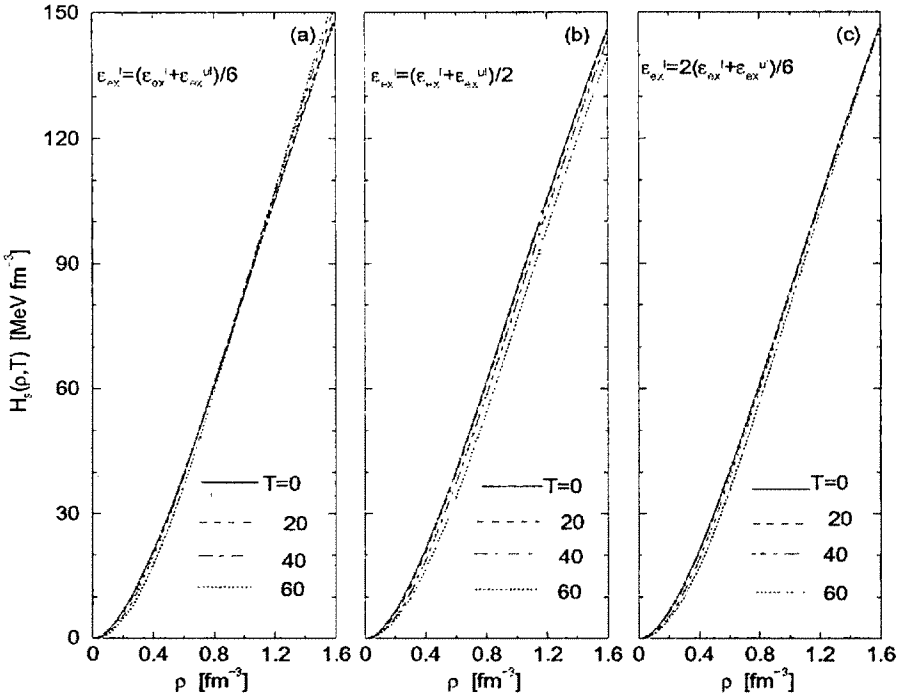

Figure 5.6. (a) Nuclear symmetry energy density shown as a function of density for case A at temperatures T=0, 20, 40 and 60 MeV. (b) Same as (a) for case B. (c) Same as (a) for the critical case.

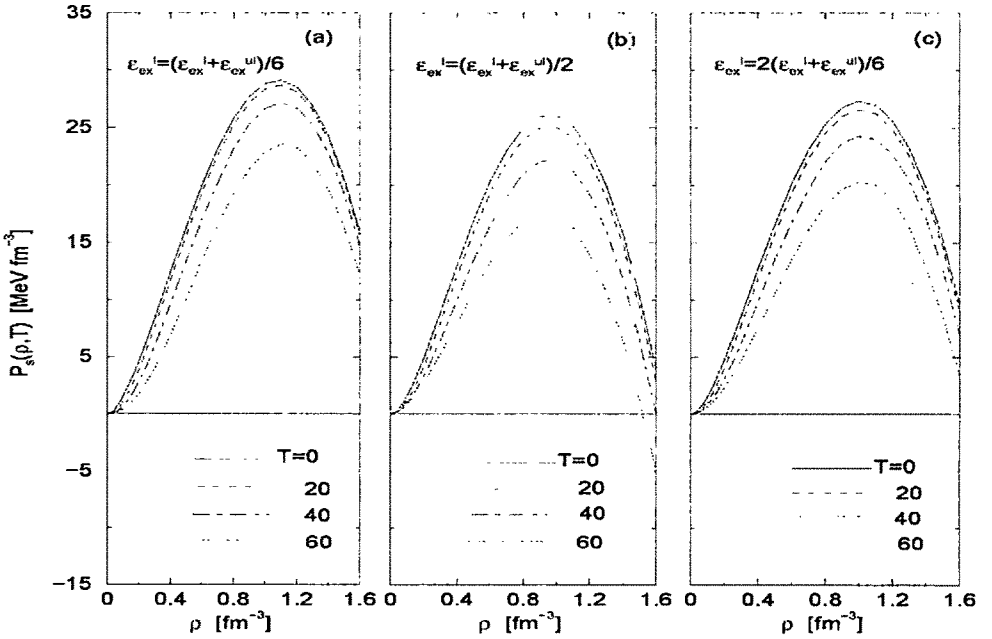

Figure 5.7. (a) Nuclear symmetry energy pressure shown as a function of density for case A at temperatures T=0, 20, 40 and 60 MeV. (b) Same as (a) for case B. (c) Same as (a) for the critical case.

5.1.2. Symmetry Energy Pressure at finite temperature

In Figures 5.7(a), (b) and (c) the density dependence of symmetry energy pressure $P_s(\rho,T)$ defined in eq.(4.1.6) are shown at different temperature T for the same three cases. It is seen that $P_s(\rho,T)$ is a decreasing function of T. However, the rate of decrease of $P_s(\rho,T)$ with temperature is faster in case B than in A, whereas, it is intermediate between these two for the critical case.

5.1.3. Free Symmetry Energy

The free energy per particle in SNM and PNM are given as $F_{snm}(\rho,T)=[H_0(\rho,T)-TS_0(\rho,T)]/\rho$ and $F_{pnm}(\rho,T)=[H_n(\rho,T)-TS_n(\rho,T)]/\rho$, respectively. The free energy per particle in SNM and the three cases in PNM are shown in Figures 5.8(a) and 5.9(a), (b) and (c), respectively, as function of density at different temperatures. In both the cases of SNM and PNM the free energy decreases with increase in temperature at a given density. The magnitude of decrease becomes smaller with increase in density. In PNM, for all the three cases considered, the curves corresponding to higher value of temperature lye below the curves for lower temperatures in the whole range of density unlike the case of symmetry energy that shows a crossing over phenomena for case A . The magnitude of decrease for the three cases of ε_{ex}^{l} at different values of density do not vary much giving nearly similar values for the three cases. However, there is a trend that the rate of decrease is relatively more in case of case A in comparison to case B, whereas, the behaviour for the critical case lies intermediate between these two cases. In Figure 5.8 (b), we have compared our results of the free energies in SNM at different temperatures with the results of Brueckener-Bethe- Goldstone calculations of Burgio et al.[192]. Our results agree quite well with the BBG results upto density $\rho \approx 0.3\ fm^{-3}$. Beyond this density, the curves of our calculations become stiffer than that of the BBG calculation.

We can now calculate the free symmetry energy,

$$F_{Sym}(\rho,T)=F_{pnm}(\rho,T)-F_{snm}(\rho,T), \tag{5.1.2}$$

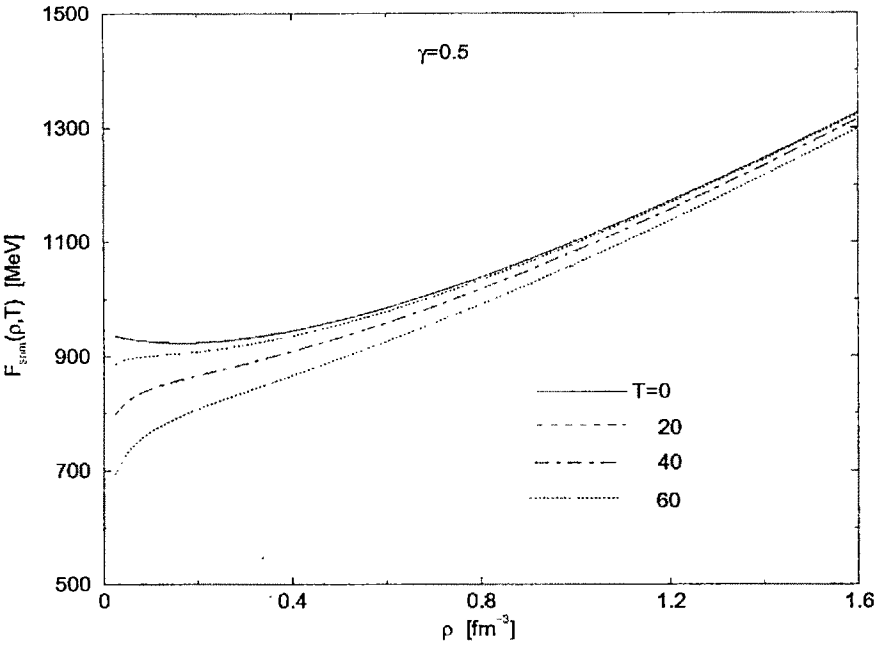

Figure 5.8. (a) Free energy in SNM shown as a function of density at four different temperatures T=0, 20, 40 and 60 MeV.

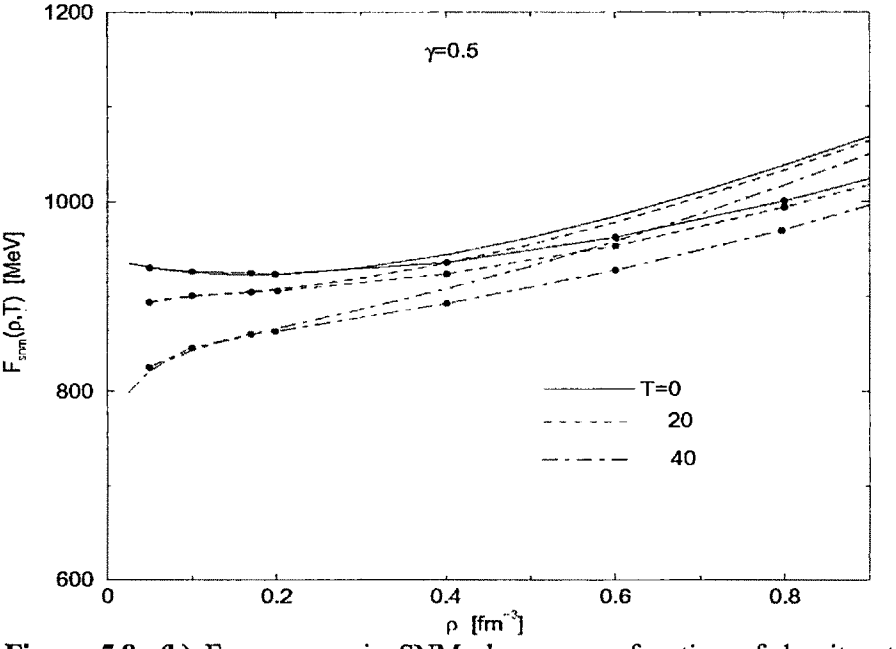

Figure 5.8. (b) Free energy in SNM shown as a function of density at three different temperatures T=0, 20 and 40 MeV and the results of the present formalism are compared with the BBG calculations of Burgio et al.[191]. In the figure the curves with solid circles represent the BBG calculations.

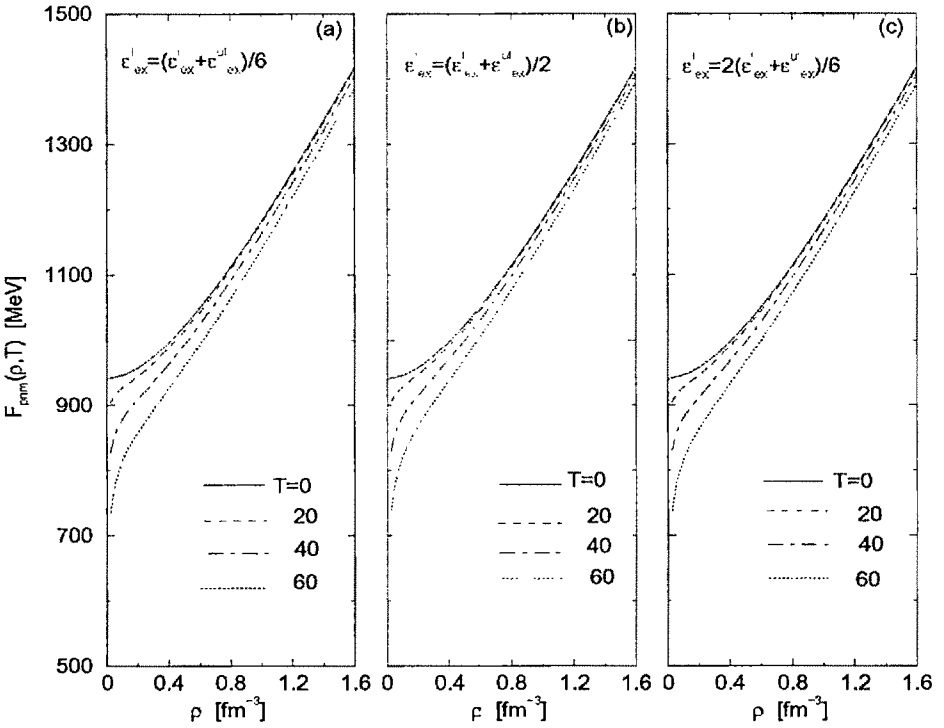

Figure 5.9. (a) Free energy in PNM shown as a function of density for case A at temperatures T=0, 20,40 and 60 MeV. (b) Same as (a) for case B (c) Same as (a) for the critical case.

as the difference between the free energy per particle in PNM and in SNM. The results of free symmetry energy, $F_{Sym}(\rho,T)$, for the three cases of ε_{ex}^{l} are shown as function of density at different temperatures in Figures 5.10(a), (b) and (c). The results, in general, show that the free symmetry energy increases with increase in temperature which iscontrary to the behaviour of nuclear symmetry energy that gives a decreasing trend. However, a similar crossing over phenomenon as noticed in the case of nuclear symmetry energy for case A is also found in the case of free symmetry energy. In case A for the free symmetry energy shown in Figure 5.10(a), at around density $\rho \approx 0.8 fm^{-3}$ the curves corresponding to higher temperatures which were lying above the zero temperature curve at lower densities, cross and lye below the zero temperature curve with further increase in density. This crossing over phenomena in case A is expected from the results of symmetry energy in Figure 5.3 and entropy in Figure 4.9 for the case. Similarly for case B in Figure 5.10 (b), expected result is also obtained that the finite temperature curves will not cross the zero temperature one and will lye above

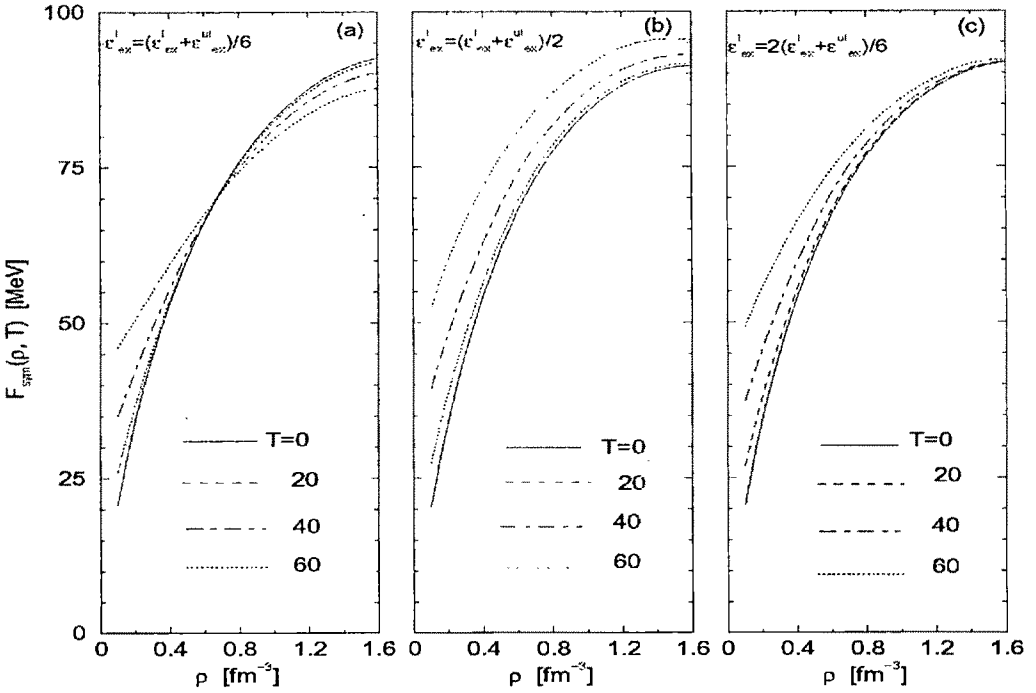

Figure 5.10. (a)Free symmetry energy shown as a function of density for the case A at temperatures T=0, 20, 40 and 60 MeV. (b) Same as (a) for case B. (c) Same as (a) for the critical case.

it at all densities considered. For the critical case in Figure 5.10(c) the result is as per expectation that the effect of temperature vanishes in the high density region and all curves approach the zero temperature result asymptotically.

5.2. Equilibrium proton fraction and EOS of charge neutral β -stable $n+p+e+\mu$ matter at finite temperature

In supernovae matter the inside temperature is as high as of the order $T \sim$10-40 MeV and asymmetry $Y_p(\rho,T) \approx 1/3$. The heavy element core of massive star inside the supernova matter undergoes a gravitational collapse resulting into either directly to a black hole or to a metastable proto neutron star. The newly formed neutron star under gravitational collapse mechanism of the supernovae-II has an initial temperature of the order 50 MeV and has a quite large proton fraction The large proton fraction initiates the so called URCA process and produces copious amount of neutrinos. The newly born neutron star cools rapidly via emission of neutrinos within few seconds and reaches a temperature less than 1 MeV. In situations which are governed by isothermal processes

the entropy changes, whereas, for isentropic processes the entropy is constant. Out of the limited numbers of works performed in this area of finite temperature neutron star calculation found in the literature, some have used the symmetry energy in their calculations [193, 194] and others have used the free symmetry energy [192]. In our earlier work [179] we have studied the EOS of NSM at finite temperature by taking the symmetry energy. Here we shall make the same study considering the free energy as the input in solving the beta stability condition. The important differences in the results of the two considerations will be discussed at appropriate places. The process of formation and cooling of the protoneutron stars can be basically considered as isentropic process where the free energy plays the crucial role. In view of this in the calculation of equilibrium proton fraction in charge neutral β-stable $n+p+e+\mu$ matter in supernovae matter and proto neutron stars, it is essential to consider the free symmetry energy instead of symmetry energy.

5.2.1 EOS of NSM at finite temperature

The β-stabiliy condition can now be expressed by using the quadratic approximation of the free energy density as given in eqs.(4.3.3 - 4.3.5). The difference between neutron and proton chemical potentials at a given density ρ and temperature T, in terms of free symmetry energy, can be expressed as

$$\mu_n(\rho,T)-\mu_p(\rho,T)=4(1-2Y_p(\rho,T))F_{sym}(\rho,T). \tag{5.2.1}$$

The β-stability condition becomes,

$$4(1-2Y_p(\rho,T))F_{sym}(\rho)=\left[C^2\hbar^2\left(3\pi^2\rho Y_e(\rho,T)\right)^{2/3}+M_e^2C^4\right]^{1/2}=\left[C^2\hbar^2\left(3\pi^2\rho Y_\mu(\rho,T)\right)^{2/3}+M_\mu^2C^4\right]^{1/2} \tag{5.2.2}$$

which is the same as given in eq.(3.3.13a) except that the symmetry energy, $E_s(\rho)$, is replaced by free symmetry energy, $F_{sym}(\rho,T)$. Here both the leptons e and μ are described as relativistic ideal Fermi gases. The charge neutrality condition is given by

$$Y_p(\rho,T)=Y_e(\rho,T)+Y_\mu(\rho,T). \tag{5.2.3}$$

Thus, the problem now reduces to solve the equation,

$$4\left[1-2Y_p(\rho,T)\right]F_{sym}(\rho,T)=\mu(\rho,T), \tag{5.2.4}$$

subject to the condition of charge neutrality in eq.(5.2.3). Here $\mu(\rho,T)$ is the β-equilibrium chemical potential corresponding to the equality in eq.(5.2.2). In this model the charge neutrality condition takes the form,

$$Y_P(\rho,T)=\frac{1}{\pi^2\rho}\sum_{i=e,\mu}\int_0^\infty \frac{k^2dk}{\exp\{[(C^2\hbar^2k^2+m_i^2C^4)^{1/2}-\mu(\rho,T)]/T\}+1}, \tag{5.2.5}$$

where, m_i with $i=e,\mu$ are the rest masses of electron and muon. If the density and temperature dependence of nuclear free symmetry energy $F_{sym}(\rho,T)$ is known, then eqs.(5.2.4) and (5.2.5) can be solved to obtain the β-equilibrium chemical potential $\mu(\rho,T)$, the leptonic fractions $Y_i(\rho,T)$, $i=e,\mu$, and the proton fraction $Y_P(\rho,T)$ at each density ρ and temperature T. Thus the composition of NSM at non-zero temperature in terms of fractions of neutron, proton, electron and muon at different nucleon density ρ and temperature T is essentially determined by the temperature and density dependence of nuclear free symmetry energy, $F_{sym}(\rho,T)$.

The EOS of β-equilibrated $n+p+e+\mu$ matter, i.e., NSM, is considered as an ideal mixture of a nucleonic and a leptonic part. The energy density and pressure in NSM can therefore be written as,

$$H^{NSM}(\rho,Y_p,T)=H^N(\rho,Y_p,T)+H^e(\rho,Y_e,T)+H^\mu(\rho,Y_\mu,T) \tag{5.2.6}$$

$$P^{NSM}(\rho,Y_p,T)=P^N(\rho,Y_p,T)+P^e(\rho,Y_e,T)+P^\mu(\rho,Y_\mu,T). \tag{5.2.7}$$

The nucleonic part of the energy density $H^N(\rho,Y_p,T)$ and pressure $P^N(\rho,Y_p,T)$ in NSM are calculated from the EOS of ANM described in eqs.(4.1.3)-(4.1.6) corresponding to the equilibrium proton fraction $Y_p(\rho,T)$ for given density ρ and temperature T. This requires the knowledge of energy densities $H_n(\rho,T)$ and $H_0(\rho,T)$ as well as pressures $P_n(\rho,T)$ and $P_0(\rho,T)$ in PNM and SNM as functions of density ρ and temperature T. On the other hand, the leptonic energy densities $H^e(\rho,Y_e,T)$ and $H^\mu(\rho,Y_\mu,T)$ as well as pressures $P^e(\rho,Y_e,T)$ and $P^\mu(\rho,Y_\mu,T)$ can be calculated in the relativistic ideal Fermi gas model by using the Fermi-Dirac momentum distribution functions of the leptons given in connection with eq.(5.2.5).

5.2.2. Composition of NSM at finite temperature for different choices of ε_{ex}^{l}

The temperature and density dependence of nuclear free symmetry energy $F_{sym}(\rho,T)$ obtained in our case shown in Figures 5.10(a), (b) and (c) are used now to solve eqs.(5.2.4) and (5.2.5) to calculate the $\beta-$equilibrium chemical potential $\mu(\rho,T)$, the leptonic fractions $Y_i(\rho,T)$, $i=e,\mu$, and the proton fraction $Y_P(\rho,T)$ at each density ρ and temperature T. The density dependence of $\mu(\rho,T)$ at different temperature T, thus obtained is shown in Figures 5.11(a), (b) and (c) for the three cases of our representative values of ε_{ex}^{l} corresponding to case A , case B and the critical case, respectively. The β-equilibrated chemical potential $\mu(\rho,T)$ is found to be a decreasing function of temperature relative to the zero temperature result in all the three cases. The magnitude of decrease of $\mu(\rho,T)$ with increase in temperature is relatively larger in case A compared to case B, whereas, in the critical case it lies intermediate between the two cases A and B. This means that the functional $[1-2Y_P(\rho,T)]F_{sym}(\rho,T)$ in β- equilibrated $n+p+e+\mu$ matter is a decreasing

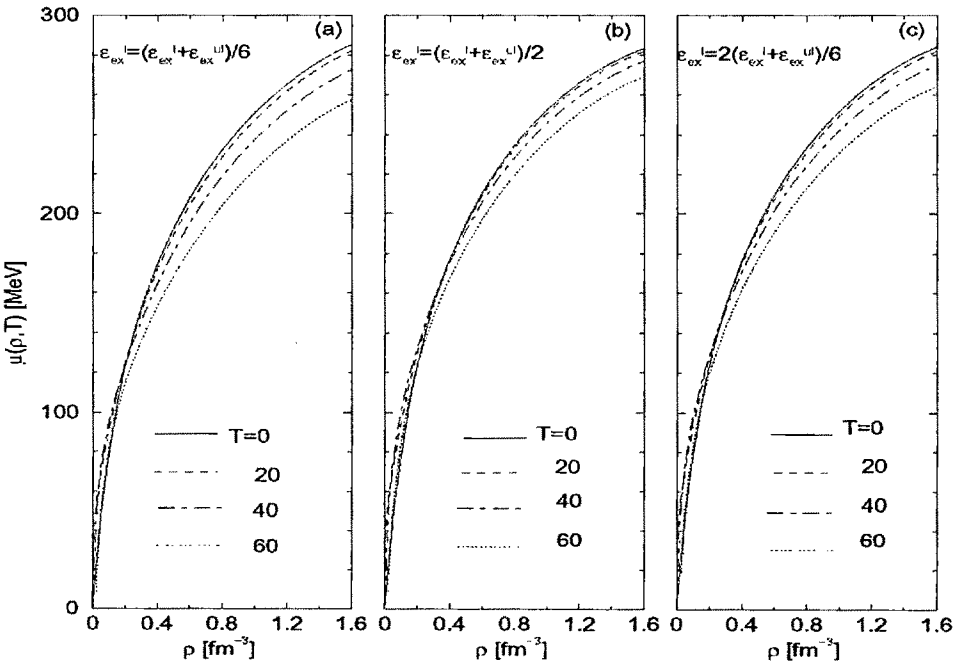

Figure 5.11. (a) Equilibrium chemical potential $\mu(\rho,T)$ in NSM shown as a function of density for case A at four different temperatures, T=0, 20, 40 and 60 MeV. (b) Same as (a) for case B. (c) Same as (a) for the critical case.

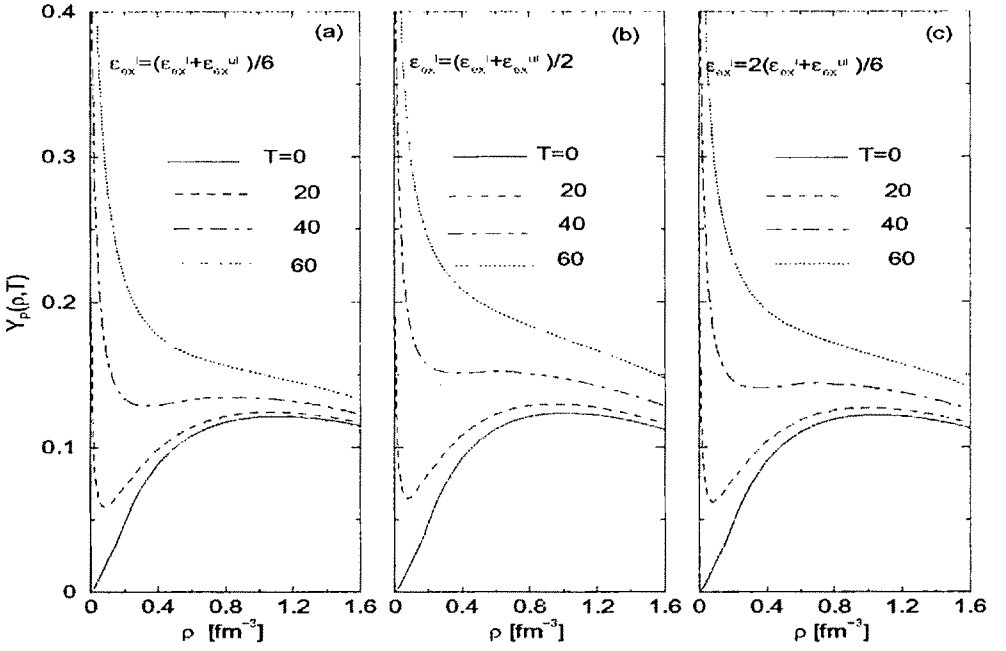

Figure 5.12. (a) Equilibrium proton fraction $Y_P(\rho,T)$ in NSM shown as a function of density for case A at four different temperatures, T=0, 20, 40 and 60 MeV. (b) Same as (a) for case B.(c) Same as (a) for the critical case.

function of temperature T at any given density ρ. In view of this the equilibrium proton fraction $Y_P(\rho,T)$ would increase in a region of density ρ where the free symmetry energy $F_{sym}(\rho,T)$ increases with temperature. The proton fraction $Y_P(\rho,T)$ also increases in a region of density ρ where $F_{sym}(\rho,T)$ decreases at a rate slower than $\mu(\rho,T)$ with increasing temperature. On the other hand $Y_P(\rho,T)$ decrease with increase in temperature T in a region of density ρ where $F_{sym}(\rho,T)$ decreases at a faster rate than $\mu(\rho,T)$ with increase in temperature. These points are illustrated in Figures 5.12(a), (b) and (c) where the density dependence of the calculated equilibrium proton fractions $Y_P(\rho,T)$ are given at different temperature T for the cases A, B and the critical case, respectively. The corresponding electron and muon fractions, and $Y_\mu(\rho,T)$, are shown as functions of density ρ in Figures 5.13(a), (b)and (c) and Figures 5.14(a), (b) and (c) respectively. So far as the variation in the density dependence of $Y_P(\rho,T)$ with increase in temperature is concerned, the complete domain of ρ in Figures 5.12 can be roughly divided into two parts: $\rho < \rho(T)$ and

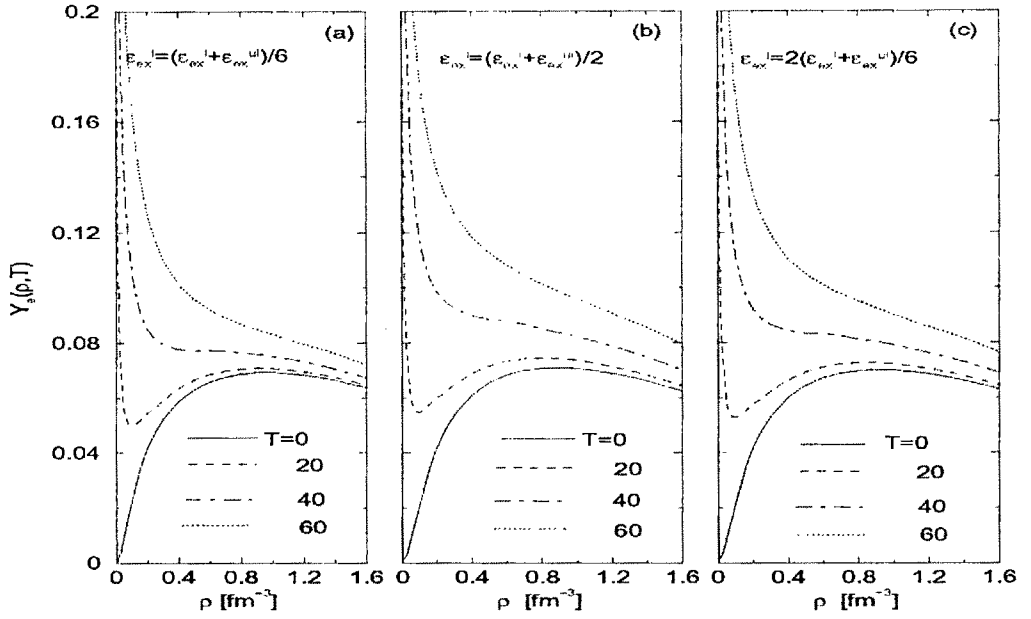

Figure 5.13.(a) Electron fractions, $Y_e(\rho,T)$corresponding to the equilibrium proton fraction $Y_P(\rho,T)$ in NSM shown as a function of density for case A at four different temperatures, T=0, 20, 40 and 60 MeV. (b) Same as (a) for case B. (c) Same as (a) for the critical case.

$\rho > \rho(T)$. Here $\rho(T)$ is a critical density corresponding to temperature T where $Y_P(\rho,T)$ has a minimum. It can be seen from Figures 5.12 that all the three cases exhibit similar density dependence of $Y_P(\rho,T)$ with increasing temperature in the region $\rho < \rho(T)$. The proton fraction $Y_P(\rho,T)$ increases sharply with decreasing density in this region when temperature increases. This is a consequence of the fact that the rate of decrease of $\mu(\rho,T)$ in this low density region is much faster than the decrease in $F_{sym}(\rho,T)$ with increasing temperature. On the other hand, the variation in the density dependence of $Y_P(\rho,T)$ in the region $\rho > \rho(T)$ with increasing temperature is found to be relatively larger for case B as compared to A. Comparing Figures 5.10, 5.11 and 5.12 in the region $\rho > \rho(T)$ it is seen that the effect of increasing temperature is manifested largely through an increase in the proton fraction $Y_P(\rho,T)$ in case B as compared to A. This is due to the fact that the rate of increase in free symmetry energy slows down in this region of density for case A as well as the chemical potential has a smaller value as compared to case B. This is a consequence of the fact that the nuclear

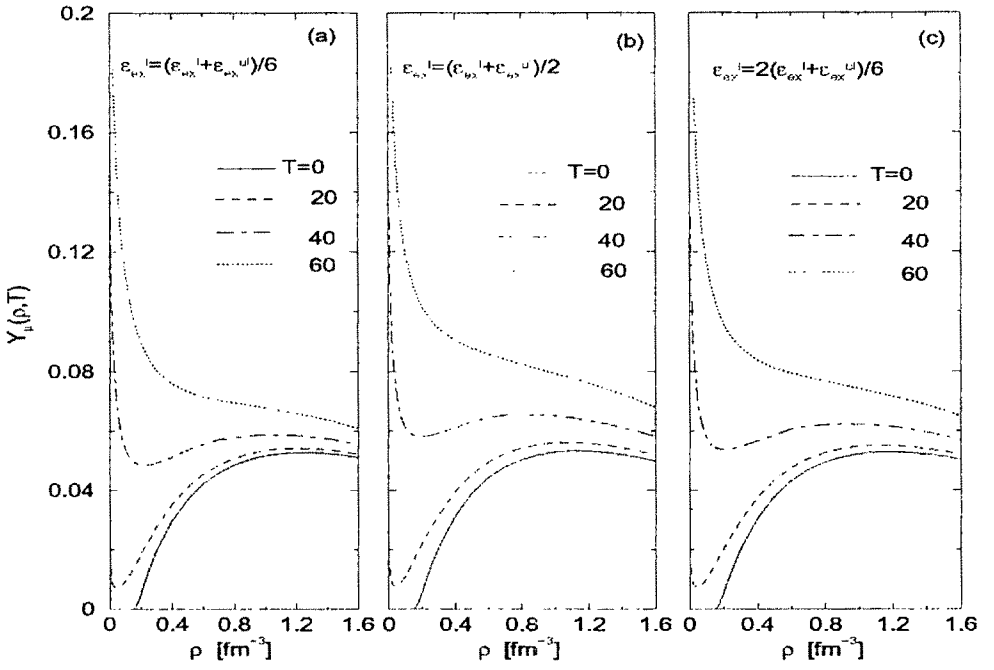

Figure 5.14. (a) Muon fractions $Y_\mu(\rho,T)$ corresponding to the equilibrium proton fraction $Y_P(\rho,T)$ in NSM shown as a function of density for case A at four different temperatures, T=0, 20, 40 and 60 MeV. (b) Same as (a) for case B.(c) Same as (a) for the critical case.

mean field in PNM has a stronger momentum dependence in case B than in case A due to the large difference in their values of exchange strength parameter ε_{ex}^{l}. The results for the critical case lie intermediate between these two cases. In order to have a better visualization of the above discussion we have shown the proton and lepton fractions as function of density at temperature $T = 40MeV$ for the three cases considered, in Figure 5.15. It may be noted here that the temperature dependence of the proton fraction calculated by taking the symmetry energy, $E_s(\rho,T)$, in the beta stability condition in eq. (5.2.1) instead of free symmetry energy, as has been done in our earlier work in Ref.[179], then we get an opposite behaviour in the results of proton fraction for case A and case B in comparison to the results obtained in the present calculation shown in Figure 5.12. In the case of our earlier work of Ref.[179] considering symmetry energy in beta stability condition, the effect of increase in temperature is manifested largely through an increase in the proton fraction $Y_P(\rho,T)$ in case A as compared to B. This can be seen from comparing the Figures 5.12(a) and (c) with the Figures 11(a) and (b)

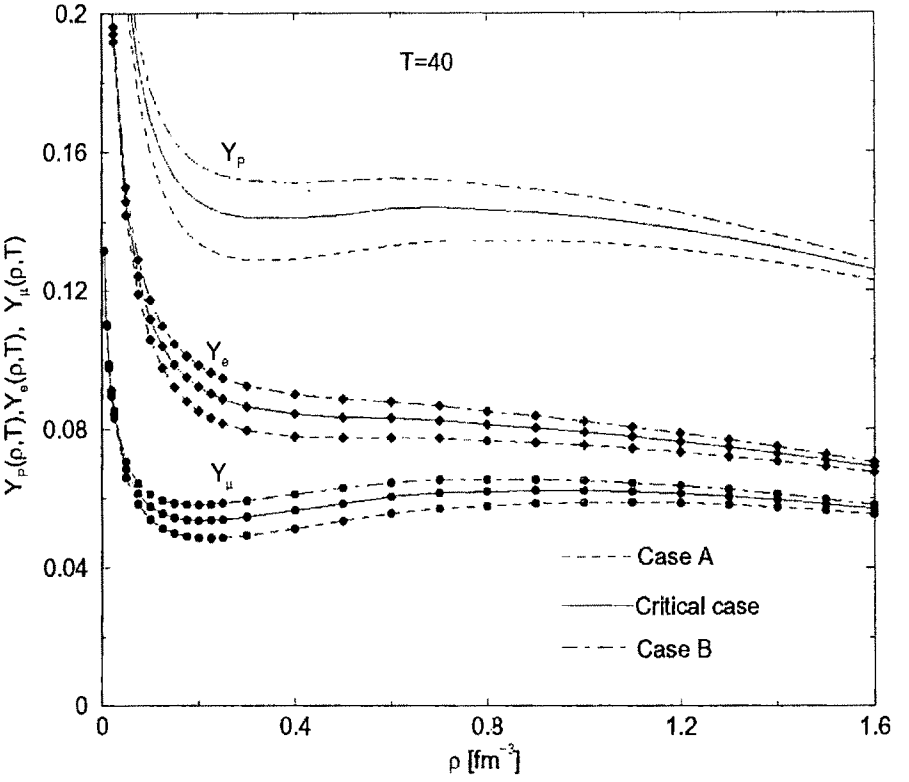

Figure 5.15. Equilibrium particle fractions of the neutron star matter as function of density for the three cases at temperature T=40 MeV. Curves with filled diamonds are for electron fractions. Curves with filled circles are for the muon fractions.

of Ref. [179]. Thus the composition of neutron star matter will have large differences under the two considerations for a given value of ε_{ex}^{l} and, therefore, also differ in cooling mechanism.

5.2.3. Cooling under direct URCA process for different choices of ε_{ex}^{l}

The fact that temperature dependence of the free symmetry energy $F_{sym}(\rho,T)$ and equilibrium proton fraction $Y_p(\rho,T)$ are sensitive to the choice of the splitting of the parameters ($\varepsilon_{ex}^{l}+\ \varepsilon_{ex}^{ul}$) into ε_{ex}^{l} and ε_{ex}^{ul}, it can have a crucial relevance in the study of thermal evolution of neutron stars. The neutron stars are born with an interior temperature of the order ~50 MeV, but rapidly cool via neutrino emission to temperature less than 1 MeV within seconds [177,195]. The conditions of direct URCA

processes in $n+p+e+\mu$ matter under β-equilibrium can be given by $Y_n^{1/3}(\rho,T) \leq Y_P^{1/3}(\rho,T) + Y_e^{1/3}(\rho,T)$ and/or $Y_n^{1/3}(\rho,T) \leq Y_P^{1/3}(\rho,T) + Y_\mu^{1/3}(\rho,T)$. The direct URCA process at $T = 60MeV$ is allowed over the whole range of density considered in case of case B, whereas, it continues starting from low density upto a density $1.3fm^{-3}$ and $1.5fm^{-3}$ in the case A and the critical case, respectively. Similarly at $T=40MeV$ the direct URCA process is allowed upto density $0.2fm^{-3}$, $1.0fm^{-3}$ and $1.3fm^{-3}$ in case of case A, the critical case and case B, respectively. At $T=20MeV$ direct URCA process is not allowed in all these thee cases. These results are, however, qualitative in nature in the sense that they are calculated on the basis of $n+p+e+\mu$ matter under $\beta-$equilibrium and presence of other hyperons, mesons or quarks have not been taken into consideration in this work. We further note that the occurrence/non-occurrence of direct URCA process with increase in temperature as discussed above would crucially depend on how the density dependence of symmetry energy $E_s(\rho,T=0)$ at zero temperature is fixed. In this context, it can be mentioned that the universal high density behaviour of the functional $S^{NSM}(\rho,Y_P,T=0) = \left[(1-2Y_p(\rho,T=0))^2 H_S(\rho,T=0)\right]_{NSM}$ is used to constrain the density dependence of $E_s(\rho,T=0)$ in our work. As a result of this, the density dependence of $E_s(\rho,T=0)$ for both the cases A and B given in Figure 3.10 of chapter-III differ little from each other over the entire region of density and also do not allow direct URCA processes.

5.2.4. Universal High density behavior of the functional $S^{NSM}(\rho,Y_P,T)$

The functional $S^{NSM}(\rho,Y_P,T)$ at finite temperature can be given by $S^{NSM}(\rho,Y_P,T) = \left[(1-2Y_p(\rho,T))^2 F_S(\rho,T)\right]_{NSM}$, where $F_s(\rho,T)$ is the free energy density, and the expression reduces to the zero-temperature expression at $T=0$. The asymmetric contribution to the nucleonic part of free energy density in NSM, i.e., $S^{NSM}(\rho,Y_P,T) = \left[(1-2Y_p(\rho,T))^2 F_S(\rho,T)\right]_{NSM}$ is shown in Figure 5.16 as a function of

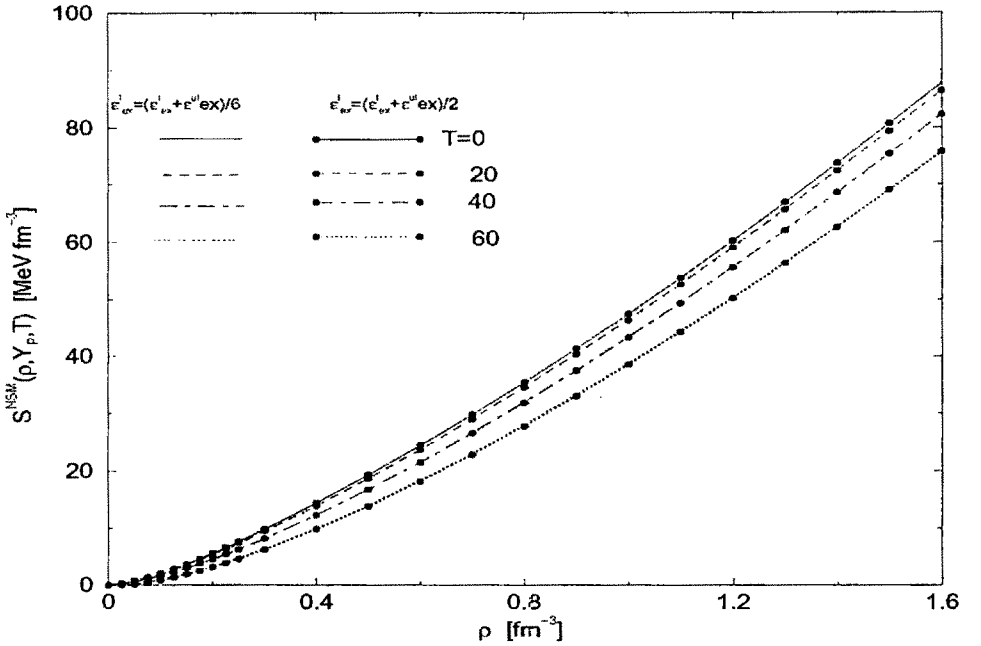

Figure 5.16. Asymmetric contribution to the nucleonic part of free energy density $S^{NSM}(\rho,Y_P,T)$ in NSM shown as a function of density at four different temperatures, T=0, 20, 40 and 60 MeV for the two cases A and B.

density ρ at different temperature T for the two extreme cases A and B. It is seen from Figure 5.16 that the curves of $S^{NSM}(\rho,Y_P,T)$ for these two different cases are the same over the entire range of density at any given temperature T. In this context we note that the universal high density behaviour of the functional $S^{NSM}(\rho,Y_P,T=0)$ at zero temperature was used to constrain the density dependence of nuclear symmetry energy $E_S(\rho,T=0)$ for both the cases A and B. Figure 5.16 shows that this universal high density behaviour is also valid at finite temperature. However, with increase in temperature the curves of $S^{NSM}(\rho,Y_P,T)$ are gradually pushed below.

5.3. EOS of NSM for the three choices of ε^l_{ex}

The density and temperature dependence of equilibrium proton fraction $Y_P(\rho,T)$ and chemical potential $\mu(\rho,T)$ obtained above can now be used to calculate the EOS of β-equilibrated $n+p+e+\mu$ matter (NSM) from eqs.(5.2.6) and (5.2.7).

5.3.1. Nucleonic contribution to energy density and pressure

The nucleonic part of the energy density and pressure, i.e., $H^N(\rho,Y_p,T)$ and $P^N(\rho,Y_p,T)$, comprise of contributions from symmetric part and asymmetric part of nuclear EOS as given in eqs.(4.1.3) and (4.1.4). The symmetric contributions, $H_0(\rho,T)$ and $P_0(\rho,T)$, are the same for the three cases A , B and the critical case. $H_0(\rho,T)$ as a function of density ρ and temperature T has been shown in Figure 5.1. The energy density $H_0(\rho,T)$ increases with the increase in temperature. The asymmetric contribution to the nucleonic part of energy density, $S^{NSM}(\rho,Y_p,T)$, is plotted in Figure 5.16 and has been discussed in section 5.2.4. In Figure 5.17, we have shown the density dependence of the symmetric contribution to the nucleonic part of pressure, $P_0(\rho,T)$ at different representative temperatures. $P_0(\rho,T)$ increases with increase in temperature. The asymmetric contribution to the nucleonic part of pressure in NSM, i.e., $P^N_{asy}(\rho,Y_p,T)=\left[(1-2Y_p(\rho,T))^2 P_S(\rho,T)\right]_{NSM}$ is shown as a function of density ρ at different values of temperature T in Figures 5.18(a), (b) and (c) for the three cases respectively. It is found that $P^N_{asy}(\rho,Y_p,T)$ decreases with increase in temperature for all the three cases considered.

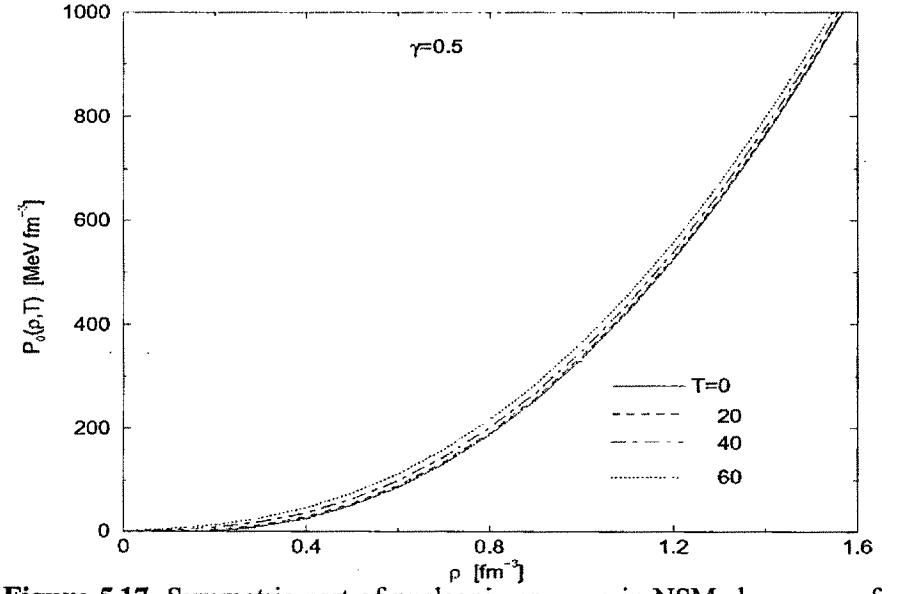

Figure 5.17. Symmetric part of nucleonic pressure in NSM shown as a function of density at four different temperatures, T=0, 20, 40 and 60 MeV.

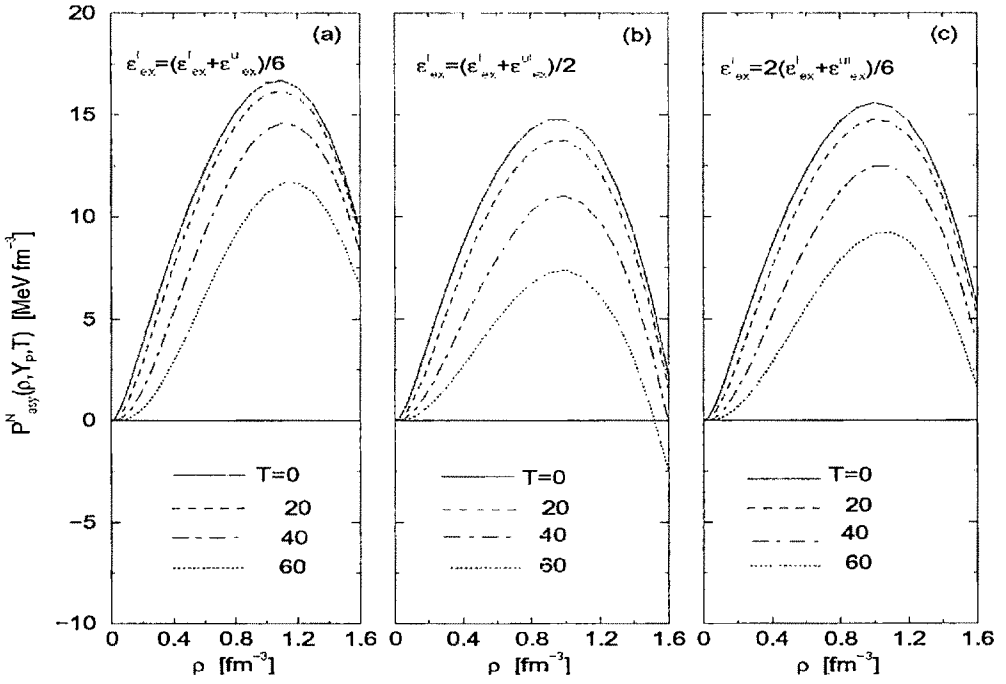

Figure 5.18. (a) Asymmetric contribution to the nucleonic part of pressure in NSM shown as a function of density for case A at four different temperatures, T=0, 20, 40 and 60 MeV . (b) Same as (a) for case B. (c) Same as (a) for the critical case.

5.3.2. Leptonic contribution to energy density

The total leptonic contribution to the energy density in NSM, $H^L(\rho,T)=H^e(\rho,Y_e,T)+H^\mu(\rho,Y_\mu,T)$, for the three cases A, B and the critical case are shown as functions of ρ at different temperatures in Figures 5.19 (a) , (b) and (c) respectively. The leptonic part of energy density is found to increase with increasing temperature. However, the rate of increase of $H^L(\rho,T)$ with temperature is relatively higher for case B as compared to A and the result for the critical case is intermediate between these two cases. The higher rate of increase in leptonic fraction in case B is due to the fact that the proton fraction $Y_P(\rho,T)$ increases at a faster rate with increasing temperature in case B than in A as can be seen from Figures 5.12(a) and (b). The temperature dependence of leptonic energy density found here for the different cases considered has shown an opposite trend to the results obtained in our earlier work [179], where the equilibrium proton fraction was calculated with the symmetry energy in the

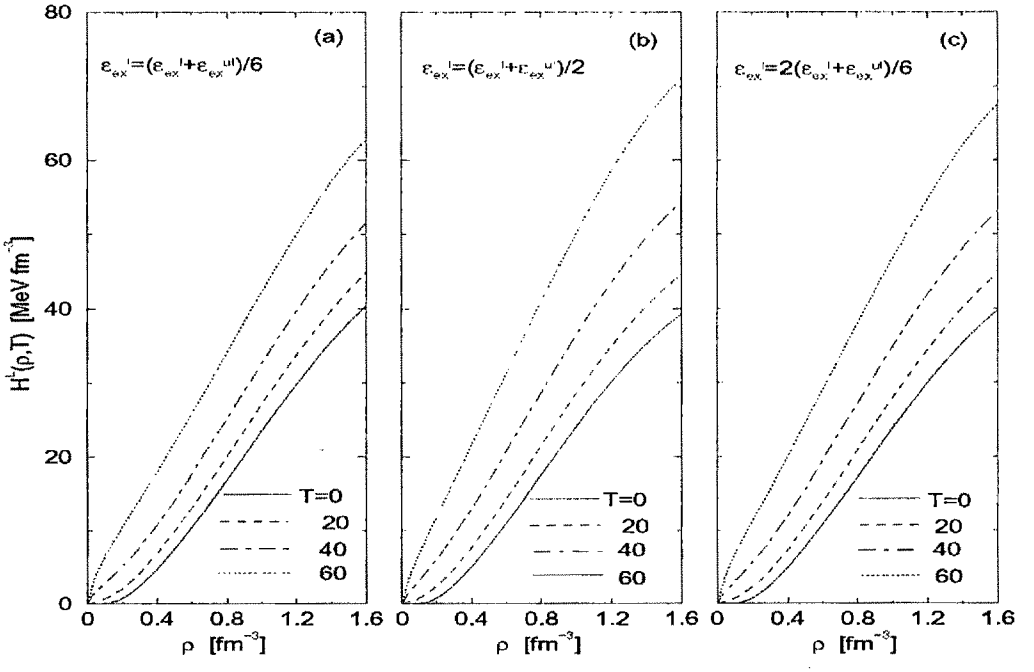

Figure 5.19. (a) Leptonic part of the energy density in NSM shown as a function of density for case A at four temperatures, T=0, 20, 40 and 60 MeV. (b) Same as (a) for case B. (c) Same as (a) for the critical case.

beta stability condition. This is obvious because in the calculation of Ref.[179] the temperature dependence of proton fraction in case A was obtained to be stronger than that of case B, a behaviour opposite to the present one.

5.3.3. Leptonic contribution to pressure

The total leptonic pressure $P^L(\rho,T)=P^e(\rho,Y_P,T)+P^\mu(\rho,Y_P,T)$ in NSM is given as a function of density ρ at different temperature T in Figures 5.20(a), (b) and (c) for cases A , B and the critical case. The leptonic part of the pressure $P^L(\rho,T)$ slowly decreases upto a temperature T=20 MeV and then it increases with further increase in temperature. This behaviour of the leptonic part of the pressure is similar to the trend obtained in our earlier calculation in Ref.[179] . But in the present case the rate of increase in leptonic part of the pressure with temperature in case B is more than that in case A, whereas, in the calculation of Ref.[194] the trend was opposite to the current one.

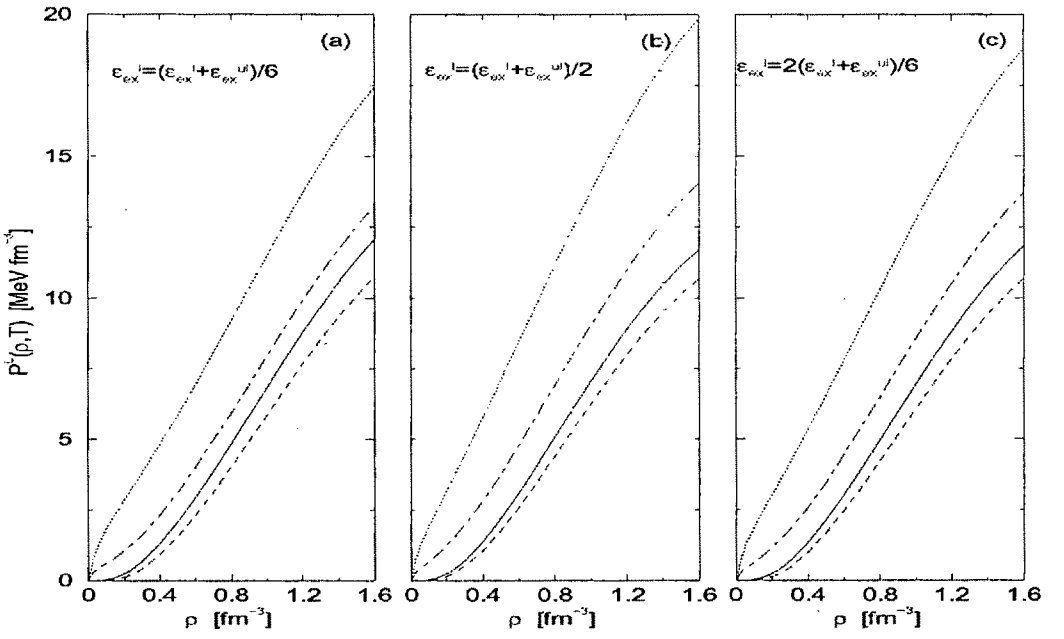

Figure 5.20. (a) Leptonic part of the pressure in NSM shown as a function of density for case A at four temperatures, T=0, 20, 40 and 60 MeV. (b) Same as (a) for case B. (c) Same as (a) for the critical case.

5.3.4. Total energy density and pressure

The total energy density $H^{NSM}(\rho, Y_P, T)$ and pressure $P^{NSM}(\rho, Y_P, T)$ in NSM, as given in eqs.(5.2.6) and (5.2.7), are calculated as functions of ρ at different temperatures for the three cases A, B and critical case and the results are shown in Figures 5.21(a), (b) and (c) and 5.22(a), (b) and (c), respectively. The energy density $H^{NSM}(\rho, Y_P, T)$ and pressure $P^{NSM}(\rho, Y_P, T)$ show a gradual slow increase with increase in temperature T for all the three cases A, B and the critical case. Mcreover, the results for the three different cases of splittings of $(\varepsilon_{ex}^{l} + \varepsilon_{ex}^{ul})$ considered here are similar and do not show any appreciable difference at finite temperature.

5.4. Neutron Star properties

The calculation of mass and radius of neutron star using TOV equation requires the energy density and pressure as input. It is therefore expected that for all the three cases A, B and critical case corresponding to different splitting of $(\varepsilon_{ex}^{l} + \varepsilon_{ex}^{ul})$ would

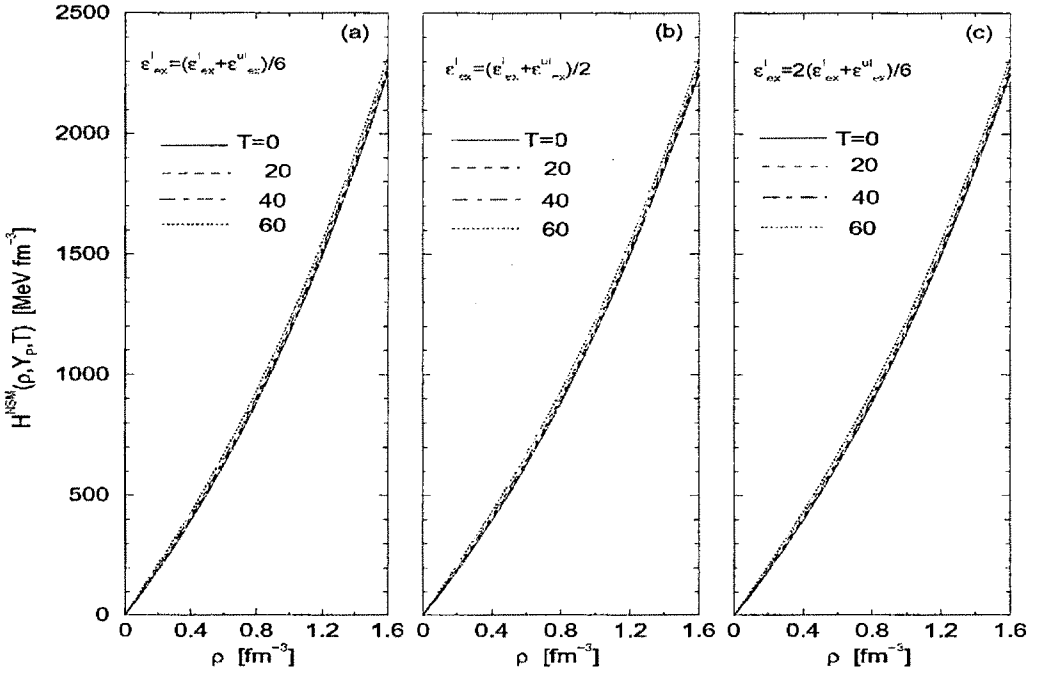

Figure 5.21. (a) Total energy density in NSM shown as a function of density for case A at four temperatures, T=0, 20, 40 and 60 MeV. (b) Same as (a) for case B. (c) Same as (a) for the critical case.

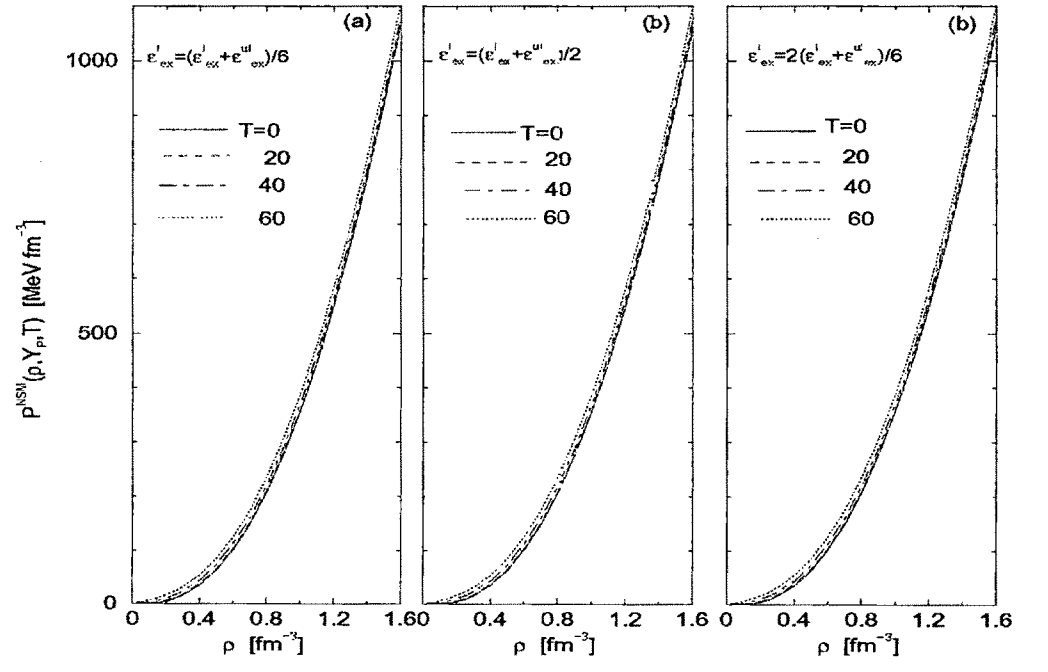

Figure 5.22. (a) Total pressure in NSM shown as a function of density for case A at four temperatures, T=0, 20, 40 and 60 MeV. (b) Same as (a) for case B. (c) Same as (a) for the critical case.

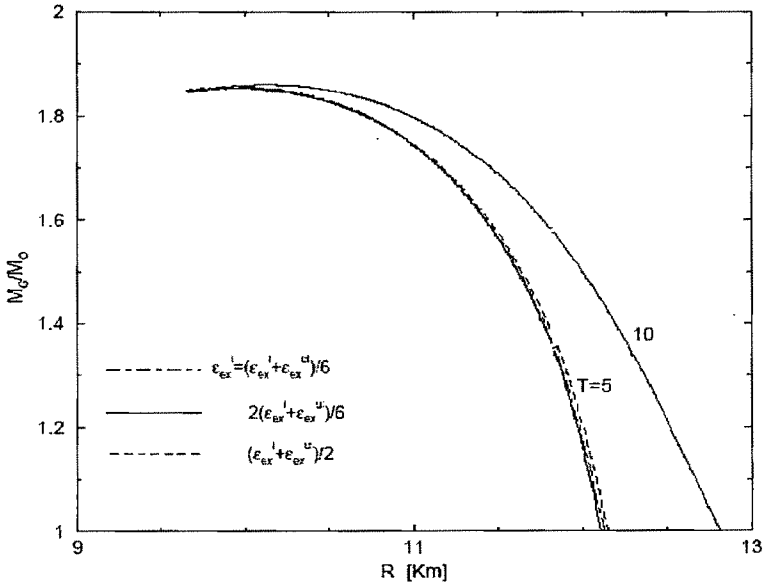

Figure 5.23. Mass Radius relation of Neutron star for the three cases at temperature T=5 MeV and for the critical case at temperature T=10 MeV.

predict similar results for the bulk properties, such as, mass and radius of neutron star at finite temperature. In order to verify this we have solved the TOV equation for EOS of NSM at temperatures $T = 5$ and 10 MeV. The mass versus radius $(M_G \sim R)$ relation is shown in the Figure 5.23 for the three cases of splitting of $(\varepsilon_{ex}^{l} + \varepsilon_{ex}^{ul})$ at temperature T=5 MeV. It is found that the results are similar for all the three cases considered and does not allow to draw any conclusion on the momentum dependence of mean field in PNM from the study of bulk properties of normal neutron stars at finite temperature.

The effect of temperature in neutron star can be seen by comparing the corresponding results of $(M_G \sim R)$ relation for the same EOSs at T=5 and 10 MeV in the same Figure 5.23. It can be seen that the radius of the neutron star increases with temperature. The maximum mass neutron star predicted at $T = 5MeV$ for the EOS of NSM corresponding to the critical case is 1.854 $M_\odot$ and radius 9.94 Kms in comparison to the corresponding values 1.86 $M_\odot$ and 10.13 Kms at T= 10 MeV. As we move from the maximum mass towards the lower mass region the radius shows a comparatively stiff increase in case of the neutron star at higher temperature. For the critical case the radius of 1.4 $M_\odot$ mass neutron star at T = 5 MeV increases form 11.2

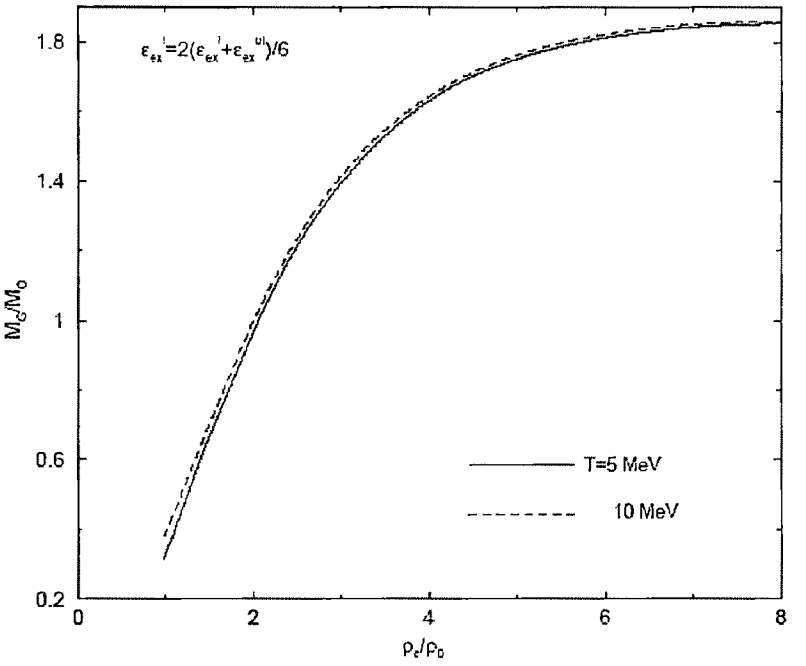

Figure 5.24. Neutron star Mass as a function of central density for the critical case at two different temperatures T=5 and 10 MeV.

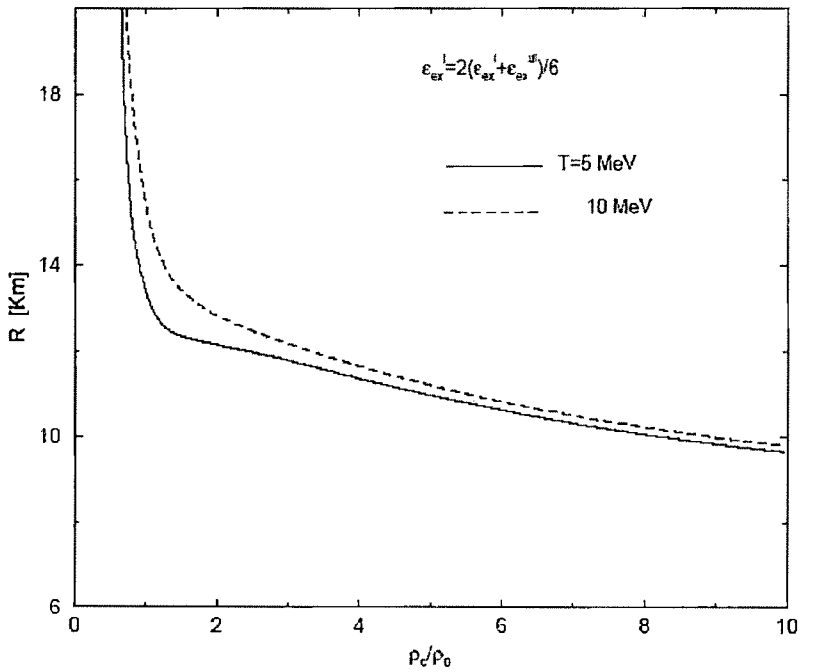

Figure 5.25. Neutron star radius as a function of central density for the critical case at two different temperatures T=5 and 10 MeV.

Kms to 12.2 Kms, as temperature rises to $T = 10$ MeV. The increase in radius with temperature is in qualitative agreement with the findings of the earlier works [186,194]. The central density of the neutron star also decreases with rise in temperature. The mass versus central density $(M_G \sim \rho_C)$ of the neutron star at $T = 5$ and 10 MeV are shown in the Figure 5.24 for the EOS of NSM corresponding to the critical case. The radius versus central density $(R \sim \rho_C)$ at these temperatures for the critical case are also shown in Figure 5.25. The radius decreases rapidly initially with increase in central density as it starts from low value and then approaches a constant value slowly which is in agreement with the findings in Refs.[186, 194].

5.5. Conclusion

Using the density dependent finite range Yukawa interaction we have studied the density and temperature dependence of Nuclear Symmetry energy and Free symmetry energy for the three choices of the parameter ε_{ex}^{l}, namely, $\varepsilon_{ex}^{l} = \varepsilon_{ex}/3, 2\varepsilon_{ex}/3$ and ε_{ex}. At low temperature we have compared our results of the Nuclear Symmetry energy with the experimentally extracted data from isoscaling analysis of the multifragmentation phenomena. It has been concluded from the discussion that the extracted evolution of symmetry energy from experiments are mainly due to the density rather than temperature. The composition of neutron star, i.e. β-stable $n + p + e + \mu$ matter, and equilibrium chemical potential have been calculated using Free symmetry energy. The chemical composition and hence the cooling via direct URCA process are found to be sensitive to temperature variation of the matter. From the total energy density and pressure, we have calculated the Neutron star properties. With the increase in temperature, it is found that the radius of neutron star increases which is in agreement with other works. We have found that the total energy density and pressure are almost the same irrespective of the choice of the parameter ε_{ex}^{l}. The neutron star properties also show marginal difference for the three different choices of ε_{ex}^{l}.

CHAPTER-VI

SUMMARY AND CONCLUSION

In this work we have studied the momentum and density dependence of nuclear mean fields and equation of state of nuclear matter. In this context, it is worth mentioning that the fundamental quantities are the neutron and proton mean fields as a function of momentum, total density, isospin asymmetry and temperature. The momentum dependence of the nucleonic mean fields is connected to the neutron and proton effective masses in nuclear matter, whereas, the study of equation of state is connected to the results of the mean fields at and around the Fermi momentum. The studies on these two important aspects (momentum and density dependence) of nuclear mean fields in isospin asymmetric nuclear matter at zero-temperature, $T = 0$, can be divided into two parts, (i) isoscalar part and (ii) isovector part. The isoscalar part pertains to the properties in SNM, whereas, the isovector part gives the contributions arising out of the asymmetry in neutron and proton in the nuclear matter medium. There are empirical/experimental constraints available for symmetric matter and hence the momentum and density dependence aspects of isoscalar part are understood to a reasonably satisfactory extent. On the otherhand, our understanding of momentum and density dependence of isovector part of the nuclear mean field is poor which may be attributd to the limited constraints; empirical or experimental, available in this case. The momentum dependence of isovector part of the nuclear mean field is connected to the neutron-proton effective mass splitting in isospin asymmetric nuclear matter, whereas, its behaviour at the Fermi surface is directly connected to the density dependence of symmetry energy. These two aspects, n-p effective mass splitting and density dependence of symmetry energy, are the two important areas of current nuclear research. In this thesis we have focused on these two important aspects within the framework of non-relativistic mean field formalism using finite range effective interactions.

In chapter-II, we have reviewed some of the earlier works and discussed a general framework as worked out by Behera et al.[64, 65, 153] by considering four interactions, direct and exchange, acting between pairs of like and unlike nucleons which are functions of separation distance between the pair of interacting nucleons and depends on the total nucleonic density of the medium. Under this formalism it has been shown that the density dependence of energy per particle in SNM is connected to the

isoscalar part of the mean field at Fermi surface. Similarly, the isovector part of the nuclear mean field at Fermi momentum is related to the density dependence of nuclear symmetry energy. These relations demonstrate that the nuclear mean fields are the crucial quantities in the studies of momentum dependence of isoscalar and isovector parts of the single particle potential and equation of states of nuclear matter. The uncertainty associated with the momentum dependence of isovector part of the nuclear mean field has been discussed in terms of not only diverging but also contradictory predictions on the results of neutron-proton effective mass splitting in isospin asymmetric nuclear matter by the different theoretical models. In the general framework, we have shown that the problem of n-p effective mass splitting centers around the splitting of the total finite range exchange interaction into interactions between like nucleon pairs (nn, pp-like channel) and unlike nucleon pairs (np-unlike channel) in ANM. The two types of contradicting behaviour of n-p effective mass splitting as predicted by different theoretical models could be reproduced by considering different splittings of the exchange interaction into like and unlike channels. It is shown that the isovector part of the nuclear mean field becomes a decreasing function of momentum in the case of stronger exchange interaction in the unlike channel than that of the like channel and consequently the neutron effective mass goes above the proton effective mass in ANM. On the contrary, if the splitting of the exchange interaction into the like channel is stronger compared to that in the unlike channel then the isovector part of the mean field becomes an increasing function of momentum and the proton effective mass lies over that of the neutron. This contradictory behavior has been shown explicitly by considering a single finite range interaction term having Yukawa form characterized by a strength and range parameters. The exchange strength and range parameters are determined by adopting a simultaneous minimization procedure using the constraint resulting from the optical model analysis of the nucleon-nucleus scattering data at intermediate energies that the attractive nuclear mean field should vanish at nucleonic kinetic energy around 300 MeV. The interaction thus obtained gives a good description of momentum dependence of isoscalar part of the mean field over a wide range of momentum and density consistent with the predictions of the microscopic calculations of Wiringa [66] using realistic hamiltonians.

By splitting this total exchange strength parameter into the like and unlike channels in different magnitudes, diverging as well as the contradicting behaviour of n-p effective mass splitting as found in cases of different models could be reproduced. The formalism has been extended to examine the effective mass splitting in the cases of Gogny and Skyrme-type interactions. The momentum dependent parts of isovector potential for the respective cases are worked out for the purpose. It is found that in the cases of Gogny interaction sets D1, D260, D280 and D300 the neutron effective mass lie above the proton one, where as, for D1S and D250 sets, the proton effective mass lies above that of the neutron. In case of Skyrme parameterization only the P- and D-state parameters, t_1, x_1, t_2, x_2 decide the nature of n-p effective mass splitting. The Skyrme sets having negative values of the resulting functional Q predict the neutron effective mass above the proton one and for positive values of Q, the proton effective mass goes above the neutron one. The Skyrme sets for which the functional Q vanishes, there is no n-p effective mass splitting in ANM. The values of the functional for several sets of Skyrme-interactions have been calculated and are given in table-1. Majority of the Skyrme-interaction sets correspond to the case where neutron effective mass is above the proton one and there are few Skyrme sets for which neutron and proton effective masses are equal in ANM. The SLy-sets, SKI-sets which are relatively recent and are constructed with the purpose for application to the isospin rich dense matter, particularly for neutron star calculations, predict the proton effective mass above the neutron one. Any attempt to analyze nuclear properties sensitive to the n-p effective mass splitting requires the variation of the magnitude of effective mass splitting without changing the nuclear matter properties. This was not possible with the available Skyrme interaction sets containing a single density dependent term. In such case the incompressibility is found to be strongly correlated with the effective mass and variation of the effective mass drastically changes the nuc lear matter incompressibility. The work of Cochet et al. [157] prescribed necessary modification by including an additional density dependent term that could enable to disentangle the correlation between the effective mass and incompressibility. By considering the exponent in one of the density dependent term of the Skyrme set to be $2/3$ one gains the freedom to vary the effective mass without changing the incompressibility. We have discussed the

work of Cochet et al. [157] in some detail. The advantage of the modification introduced by Cochet et. al. in Skyrme interaction is utilized by Leisinski et al. [131] to analyze the nuclear properties sensitive to n-p effective mass splitting by varying the magnitude of n-p effective mass splitting. The work of Leisinski et. al. has been discussed in this section. However, Leisinski et. al. have concluded that the existing Skyrme interaction needs to be improved in triplet-odd channel for further progress in this direction. The large uncertainty associated with the n-p effective mass splitting is a measure of our poor understanding of the momentum dependence of isovector part of the nuclear mean field. The situation is also similar with regards to the density dependence of isovector part of the nuclear mean field. The divergent results of the different theoretical models on the density dependence of nuclear symmetry energy are a measure of it. The density dependence of nuclear symmetry energy has crucial importance beyond standard nuclear physics, in astrophysical objects like supernovae and neutron stars. The growing experimental facilities for heavy ion collisions with radioactive ion beams raise hopes in the search for answers on these two important aspects of isovector part of the mean field. The technique used is to analyze the flow data by using transport model calculations. In these isospin dependent transport model calculations the inputs are the neutron and proton mean fields. Li et al. [81] in their attempt to constrain the density dependence of nuclear symmetry energy have analyzed the flow data by using neutron and proton mean fields resulting from their momentum dependent interaction (MDI). They have used different density dependence of nuclear symmetry energy keeping the momentum dependence of isovector part of the mean field unchanged. The work of Li et al. and the technique adopted in producing different density dependence of nuclear symmetry energy for the same n-p effective mass splitting has been discussed at length in this chapter. Their results on momentum dependence of isovector part of the mean field has been compared with our predictions considering different splittings of finite range exchange strength parameter. Both the results agree reasonably well for $\varepsilon_{ex}^{I} = 0.85\varepsilon_{ex}$. Rizzo et al. [84], considered a GBD type effective energy density and adjusted some parameters by hand in the momentum and density dependent terms to reproduce different n-p effective mass splitting for almost same density dependence of symmetry energy. Rizzo et al. have studied the

effect of two opposite types of n-p effective mass splitting on the flow data. Li [163] in an independent work has studied the energy dependence of the isovector part of mean field at normal nuclear matter density, i.e., Lane potential, using the effective energy density of Rizzo et al. for the two opposite cases of n-p effective mass splitting. With the success of constructing an effective energy density that can produce different momentum dependence of neutron and proton mean fields for the same density dependence of symmetry energy, Moustakidis and co-workers [164-166] examined the effect of temperature on various properties in ANM. In the formalism used by Moustakidis, the effect of temperature is simulated through the momentum distribution functions appearing in the momentum dependent parts of the mean fields and the EOS. Moustakidis has used similar functional form of effective energy density as used by Rizzo et al. but having two finite range terms having different ranges and strengths. The works of Rizzo et al. and Moustakidis and co-workers have been discussed in some detail in this chapter and the energy density from a finite range Yukawa interaction under the GBD-approximation has also been derived.

In Chapter-III, guided by the work of Behera et al. [64, 65, 153], we have constructed an effective interaction to study the mean field properties and EOS of ANM and to address the above mentioned problem of neutron – proton effective mass splitting. It is interesting to note that, with this effective interaction containing a single finite range term having Yukawa form, n-p effective mass splitting of desired magnitude can be reproduced by considering different splittings of finite range exchange strength parameter into like- and unlike-channels. The effective interaction contains a total of 11-number of adjustable parameters. Out of the 11-numbers of interaction parameters, only six in terms of their combination are required for complete description of SNM. The procedure for determination of these six parameters using the available constraints in SNM is discussed in this chapter. The parameter γ determines the stiffness of the EOS and the allowed range of it is found to be γ=1/12 to 1 subject to the condition that the pressure-density curve remains within the region extracted from the analysis of flow data in HI-collision experiments [68]. The study of ANM requires how the three strength parameters given in eq. (3.2.4) splits into like and unlike channels. In absence of adequate constraints available to decide the splitting of all three

strength parameters, we have first decided the allowed range of splitting for the finite range exchange strength parameter, $(\varepsilon_{ex}^{l}+\varepsilon_{ex}^{ul})$, keeping in view the result of Lane potential and the predictions of different microscopic methods which restricted ε_{ex}^{l} between 0 and $(\varepsilon_{ex}^{l}+\varepsilon_{ex}^{ul})/2$. It has been found that for the splitting $\varepsilon_{ex}^{l}=(\varepsilon_{ex}^{l}+\varepsilon_{ex}^{ul})/6$ the momentum dependence of Lane potential agrees reasonably well with the DBHF result while for $\varepsilon_{ex}^{l}=2(\varepsilon_{ex}^{l}+\varepsilon_{ex}^{ul})/6$ the agreement is well with the BHF results. For a given splitting of finite range exchange strength parameter the splitting of rest two strength parameters, namely, $(\varepsilon_{0}^{l}+\varepsilon_{0}^{ul})/2$ and $(\varepsilon_{\gamma}^{l}+\varepsilon_{\gamma}^{ul})/2$, are ascertained from assuming a standard value of symmetry energy at normal nuclear matter density and universal high density behaviour of asymmetric contribution of the nucleonic part to the EOS of charge neutral beta stable $n+p+e+\mu$ matter (NSM), $S^{NSM}(\rho,Y_p)$. In the process of ascertaining the universal high density behaviour, the slope of symmetry energy at normal density, $E_S'(\rho_0)$, which is related to the slope parameter, $L=3E_S'(\rho_0)$, is constrained. The value of the slope parameter of the EOSs corresponding to the variation of the exchange parameter splitting with in the range $\varepsilon_{ex}^{l}=(\varepsilon_{ex}^{l}+\varepsilon_{ex}^{ul})/6$ to $\varepsilon_{ex}^{l}=(\varepsilon_{ex}^{l}+\varepsilon_{ex}^{ul})/2$ thus predicted are lying with in the range 63-66 MeV. This is consistent with the range $60\le L\le 107$ MeV obtained from the analysis of both neutron thickness studies and isospin diffusion studies. Constraining the parameters in ANM in this way predicts the density dependence of symmetry energy of the EOS which is neither stiff nor very soft. The EOSs obtained corresponding to the different splittings of the finite range exchange parameter predict n-p effective mass splitting over a wide range, but give almost same density dependence of nuclear symmetry energy as can be seen from Figures 3.9 and 3.10. The results also compare well with the results of the microscopic calculation using realistic interaction as can be seen from the same figures. These EOSs are the example of the cases having same density dependence but differing widely in their momentum dependence.

The interaction used in the work has no explicit temperature dependence and the effect of temperature is simulated through the Fermi-Dirac distribution functions appearing in the exchange parts of the energy density and mean fields. The exchange

parts also decide the momentum dependence of the neutron and proton mean fields in nuclear matter. Hence the thermal evolution of nuclear matter properties has been examined in Chapter-IV to have more insight into the momentum dependence aspect of nuclear mean fields. In this Chapter-IV, the thermal evolution of nuclear matter properties in ANM, such as, energy density, pressure, entropy density, symmetry energy and free symmetry energy, have been studied using the parabolic approximation for energy in ANM. Under this parabolic approximation the study of ANM is equivalent to independent studies of SNM and PNM. Since the temperature effect is simulated through the Fermi-Dirac distribution functions appearing in the exchange parts of the energy density and mean fields we have, therefore, defined effective single particle energies in SNM and PNM only by taking the kinetic term and the finite range exchange term. The self-consistent evaluations of the distribution functions at non-zero temperature in SNM and PNM therefore determine the respective effective chemical potentials. Thus the thermal evolution of nuclear matter properties requires only the knowledge of range and exchange strength parameter in SNM and PNM. The exchange strength parameter in PNM can have values in between $\varepsilon_{ex}^{l}=0$ and $\varepsilon_{ex}^{l}=(\varepsilon_{ex}^{l}+\varepsilon_{ex}^{ul})/2$ as decided from the nature of n-p effective mass splitting in neutron rich asymmetric matter. We have studied the thermal evolution of nuclear matter properties for various representative values of ε_{ex}^{l} within this range. The results for the cases $\varepsilon_{ex}^{l}=0$ and $\varepsilon_{ex}=0$ in SNM and PNM correspond to their respective non-interacting Fermi gas model results. We have examined the occupation probability distribution functions in SNM and PNM as functions of momentum for given density at different temperatures. Apart from the well known fact that with temperature there will be spread of occupation probability distribution to the region of higher momentum, it is also noticed that the momentum dependence of the nucleonic mean field reduces the effect of temperature. The manifestation of this important aspect of momentum dependence of nuclear mean field has been examined in the cases of nuclear matter properties of SNM and PNM by calculating their respective thermal evolutions considering different representative values of ε_{ex}^{l} within its possible range 0 and $(\varepsilon_{ex}^{l}+\varepsilon_{ex}^{ul})/2$ in case of PNM. The results on entropy per particle in PNM show that it can exceed the SNM results at higher

density in the case $0 \le \varepsilon_{ex}^{l} < 2(\varepsilon_{ex}^{l} + \varepsilon_{ex}^{ul})/6$ and it does not exceeds that of SNM at any density for $2(\varepsilon_{ex}^{l} + \varepsilon_{ex}^{ul})/6 \le \varepsilon_{ex}^{l} \le (\varepsilon_{ex}^{l} + \varepsilon_{ex}^{ul})/2$. For $\varepsilon_{ex}^{l} = 2(\varepsilon_{ex}^{l} + \varepsilon_{ex}^{ul})/6$ the entropy in PNM approaches that of SNM in the asymptotic region of high density, which is true at any temperature. The behavior of entropy raises an obvious question that whether the entropy in PNM being a one component system, can exceed that of SNM which is a two component system!! Moreover, the Fermi gas model results on this aspect, which can be considered as pure quantum mechanical effect, show that the entropy in PNM is always less than that of SNM at any density and at any temperature. Even in absence of a concrete answer to the above raised question, the whole allowed region of ε_{ex}^{l} can be divided into two parts, $0 \le \varepsilon_{ex}^{l} < 2(\varepsilon_{ex}^{l} + \varepsilon_{ex}^{ul})/6$ and $2(\varepsilon_{ex}^{l} + \varepsilon_{ex}^{ul})/6 \le \varepsilon_{ex}^{l} \le (\varepsilon_{ex}^{l} + \varepsilon_{ex}^{ul})/2$ depending on either of the two possibilities. In case of thermal evolution of other properties, such as, energy density, free energy density similar behaviour has been observed. At a given temperature, these properties in case of PNM exceed that of SNM in the high density region for ε_{ex}^{l} value lying in the former range. The density at which the crossing over takes place has a higher value for larger magnitude of ε_{ex}^{l} in this range. On the other hand, no such crossing over phenomena occur when the value of ε_{ex}^{l} lies in the range specified latter and the behaviour is qualitatively similar to the corresponding Fermi gas model results. Hence the thermal evolutions in the cases of nuclear symmetry energy and nuclear free symmetry energy are found to change sign at the values of density where energy density and free energy density in PNM surpass that of SNM values in case of ε_{ex}^{l} in the range $0 \le \varepsilon_{ex}^{l} < 2(\varepsilon_{ex}^{l} + \varepsilon_{ex}^{ul})/6$, whereas, no such change of sign take place for the case where ε_{ex}^{l} lies in the range $2(\varepsilon_{ex}^{l} + \varepsilon_{ex}^{ul})/6 \le \varepsilon_{ex}^{l} \le (\varepsilon_{ex}^{l} + \varepsilon_{ex}^{ul})/2$. In the case of $\varepsilon_{ex}^{l} = 2(\varepsilon_{ex}^{l} + \varepsilon_{ex}^{ul})/6$ the thermal evolution in the cases of all of these nuclear matter properties in PNM approaches that of SNM results in the asymptotic region of high density. The n-p effective mass splitting in ANM at zero temperature as a function of asymmetry for these representative values of ε_{ex}^{l} has been calculated and shown in Figure 4.11(b). For relatively weaker momentum dependence in PNM the n-p effective

mass splitting is found to be wider. Thus as the strength ε_{ex}^{l} in PNM increases in magnitude starting from 0 the separation between the neutron and proton effective mass curves go on decreasing while, on the other hand, the density at which the thermal evolution of nuclear matter properties in PNM crosses the corresponding results of SNM go on increasing. At the critical value $\varepsilon_{ex}^{l} = 2(\varepsilon_{ex}^{l} + \varepsilon_{ex}^{ul})/6$ the thermal evolution in case of PNM approaches that of SNM asymptotically in the high density region. As ε_{ex}^{l} increases beyond this critical value no crossing over phenomena will occur at any density and the thermal evolution in PNM will remain smaller than that of SNM at all values of density. The n-p effective mass splitting in ANM for this critical value, $\varepsilon_{ex}^{l} = 2(\varepsilon_{ex}^{l} + \varepsilon_{ex}^{ul})/6$, is found to compare reasonably well with the results of the microscopic DBHF calculation, as has been shown in Figure 4.12. In absence of a concrete answer to the question raised in the above discussion we can not rule out the other possibilities of ε_{ex}^{l} in its allowed range. So in our subsequent study of nuclear matter properties and EOS of charge neutral beta stable matter at finite temperature in the next chapter-V, we have considered the three choices of ε_{ex}^{l}, namely, $\varepsilon_{ex}^{l} = (\varepsilon_{ex}^{l} + \varepsilon_{ex}^{ul})/6$ (case A), $2(\varepsilon_{ex}^{l} + \varepsilon_{ex}^{ul})/6$ (critical case) and $(\varepsilon_{ex}^{l} + \varepsilon_{ex}^{ul})/2$ (case B). The two choices about the critical value are equidistant from it and represent the cases of two distinct behaviours found in connection with the thermal evolution study.

The study of the thermal evolution of nuclear matter properties in chapter-IV required only the knowledge of the exchange part of the interaction. The complete study of each of these nuclear matter properties (instead of relative to their zero temperature results) requires the complete interaction. All the six parameters required in the study of SNM and their determination has been discussed in chapter-III. In the same chapter the procedure adopted to determine the splitting of the strength parameters ε_0, ε_γ into like and unlike channels, ε_0^{l}, ε_γ^{l} and ε_0^{ul}, ε_γ^{ul}, for given choice of splitting of exchange strength parameter has also been discussed. Thus for each of the three choices of ε_{ex}^{l} as given above as case A, B and critical value the EOS of PNM can be obtained. In this connection we have studied the symmetry energy, free symmetry energy at different temperatures by calculating the energy density as well as free energy density in SNM

and for the three cases of PNM. The energy densities in SNM and PNM are found to be increasing functions of temperature at a given density. The effect of temperature on energy density of SNM is found to be stronger than in PNM which can be understood in terms of the value of Fermi momentum corresponding to the same density. Since at given density the Fermi momentum in case of SNM is smaller than that of PNM, the effect of temperature will be more on SNM. Thus the symmetry energy which is the difference between the energy per particle in PNM and SNM is found to be a decreasing function of temperature, however in case A at a higher density about $\rho \approx 0.8\, fm^{-3}$ the finite temperature curves crosses the zero-temperature one implying that the temperature effect has become stronger in PNM as compared to SNM. In case B the finite temperature results do not show such crossing over phenomena and the finite temperature curves lies below the zero-temperature one at all values of density. In critical case the finite temperature curves approaches the zero-temperature result asymptotically in the region of high density implying the vanishing of the thermal effect at higher density. Hence it can be concluded that in case of relatively weaker momentum dependence in PNM mean field ($\varepsilon^{l}_{ex} < 2(\varepsilon^{l}_{ex} + \varepsilon^{ul}_{ex})/6$), the thermal effect on energy density of PNM becomes stronger than that of SNM at some higher density. However, for relatively stronger momentum dependence of PNM mean field ($\varepsilon^{l}_{ex} > 2(\varepsilon^{l}_{ex} + \varepsilon^{ul}_{ex})/6$) the temperature effect on energy density of PNM is less than that of SNM at all values of density. For $\varepsilon^{l}_{ex} = 2(\varepsilon^{l}_{ex} + \varepsilon^{ul}_{ex})/6$ the effect of temperature in SNM and PNM approaches the same value in the asymptotic region of high density. The results in these three cases are the expected ones as obtained from the thermal evolution study of the cases given in Figures. 4.5(a) and (b). The predictions of these three cases have been used to analyze the finite temperature results of symmetry energy extracted from the isoscaling analysis of multifragmentation phenomena in heavy-ion collision experiments. It has been found that the density range in the region $\rho < \rho_0$ within which the experimental data of nuclear symmetry energy at measured values of temperature lies in case A has relatively smaller values as compared to case B. This implies that the stiffness of the finite temperature symmetry energy curve for case A in this sub-nucleonic region of $\rho < \rho_0$ is more in comparison to case B. Thus, although the

three choices of momentum dependence of PNM mean field give same density dependence of symmetry energy at zero-temperature, their results at finite temperature vary quantitatively as well as qualitatively. The nuclear symmetry energy pressure which is related to the slope of the symmetry energy curve has been calculated as a function of density at different temperatures for the three cases of PNM. The qualitative features of the different curves for the three cases are similar where the symmetry energy pressure increases as density starts increasing from low value and the rate of increase slows down at higher density and ultimately starts decreasing after reaching a maximum. The rate of increase of the symmetry energy curve at low density region is comparatively more in case A compared to case B and the rate of decrease in high density region is comparatively less in case A compared to case B.

The free energies per particle in PNM and SNM have been found to be decreasing functions of temperature at a given density although the energy densities are increasing functions and this is due to the entropy factor. The free symmetry energy is calculated as the difference between the results of free energy per particle in PNM and SNM. The free symmetry for the three cases of PNM is found to be increasing function of temperature, but in case A it becomes a decreasing function relative to its zero-temperature result beyond certain higher density around $\rho \approx 0.8\, fm^{-3}$. In case B the free energy behaves as an increasing function at all values of density and in critical case the effect of temperature washes out in the asymptotic region of high density and the finite temperature result approaches the zero-temperature one. For relatively weaker momentum dependence in the mean field of PNM the increasing behaviour of free symmetry energy relative to its zero-temperature result becomes a decreasing one in the high density region where as for stronger momentum dependence the increasing trend does not reverse at any density. The free energy in SNM at different temperatures are also compared with the results obtained under Brueckner-Bethe-Goldstone (BBG) calculations. The agreement is quite good upto density $\rho \approx 0.3\, fm^{-3}$ beyond which our results become relatively stiffer than the BBG results.

Free symmetry energy at non-zero temperature has crucial role in the study of supernovae matter and formation mechanism of neutron stars. The isothermal processes those might be taking place in supernovae matter that has temperature in the range

10~40 MeV are crucially governed by the free energy. The nucleonic and leptonic fractions in the supernovae matter under isothermal condition are to be determined from the conditions as given in eqs. 5.2.3 and 5.2.4. By solving the two equations self-consistently the nucleonic and leptonic fractions as a function of density at different temperatures have been obtained. In the process of evaluation of the particle fractions in the beta equilibrated $n+p+e+\mu$ matter at non-zero temperature, one obtains the respective equilibrium chemical potential at the given density and temperature. The equilibrium chemical potential as a function of density at different temperatures show similar behaviour for the three cases of momentum dependence in PNM, given in Figures 5.11.(a), (b) and (c), where the chemical potential at a given density decreases with increase in temperature. However, the magnitude of decrease in case A is comparatively larger than that of case B. The stronger temperature dependence resulting into a smaller chemical potential in case A may be attributed to the relatively weaker momentum dependence in PNM in this case. Moreover, the rise of free symmetry energy slows down with increase in density in this case A. On the otherhand, the chemical potential in case B has relatively larger value as well as the free symmetry energy has a stiffer rise and hence the effect of temperature is largely manifested through an increase in proton fraction in case B as compared to case A. This is shown in Figures 5.12(a), (b) and (c) where one finds that the proton fraction in case B is more than case A at all values of temperature. This is also shown in Figure 5.15 where the results for the three cases are shown at a given temperature. The relatively higher value of proton fraction in case B allows the occurrence of direct URCA process over a wider density range compared to other two cases. However, in absence of any experimental/ empirical constraints on the URCA processes in neutron star matter it is not possible to decide on the momentum dependence of mean field in PNM and hence the n-p effective mass splitting in ANM.

The equilibrium proton fraction in the charge neutral beta equilibrated $n+p+e+\mu$ matter at finite temperature enables one to calculate the EOS of hot neutron star matter that is present in the protoneutron stars. The nucleonic parts of the energy density and pressure are calculated from the EOS of ANM corresponding to the asymmetry given by the value of the equilibrium proton fraction at given value of

density and temperature. In calculating the nucleonic contribution to the EOS of hot neutron star matter it has been found that the asymmetry contribution to the energy density at finite temperature, $S^{NSM}(\rho, Y_P, T)$, also obey the same universal high density behaviour that was used at zero-temperature to constrain the parameter in ANM. As a result of this the asymmetric contributions of the nucleonic part, $S^{NSM}(\rho, Y_P, T)$, in case A and B are found to be the same. This is because both free symmetry energy and equilibrium proton fraction in case A have relatively smaller values compared to case B and hence $(1-2Y_p(\rho,T))$ increases in the former case whereas it decreases in the latter case resulting into the same $S^{NSM}(\rho, Y_P, T)$ in the two cases. The asymmetric nucleonic contribution to pressure is found to be a decreasing function of temperature in both the cases A and B having the same characteristic behaviour that at a given temperature it increases with increase in density and attains a maximum value and then decreases with further increase in density. The rate of increase in case A is relatively more compared to case B. The symmetry parts of nucleonic contributions to energy density and pressure in neutron star matter are found to be increasing functions of temperature. The leptonic parts of energy density and pressure are calculated from the non interacting relativistic Fermi gas model consideration. Both the contributions are found to be increasing functions of temperature having relatively higher contributions in case B than case A. This is because the equilibrium proton fraction is more in case B than in case A. The leptonic and asymmetric nucleonic contributions to energy density and pressure in both the cases A and B are small compared to the symmetric contribution which is same in both the cases and hence the EOSs of neutron star matter at a given temperature are found to be almost same in both the cases A and B. The neutron star properties have been calculated for two different temperatures T=5 and 10 MeV for the critical case. It is found that the splitting of the exchange strength parameter does not have an appreciable affect on the bulk properties of neutron star matter except on its composition.

On the whole, a simple finite range effective interaction having Yukawa form has been used to study the two important aspects of ANM, namely, the density dependence of symmetry energy and n-p effective mass splitting in neutron rich dense matter. The procedure adopted in constraining the parameters in ANM using the

universal high density behaviour of the asymmetric contribution in neutron star matter predicts the density dependence of symmetry energy to be neither stiff nor very soft. This qualitative feature on the high density behaviour of nuclear symmetry energy is also in agreement with the extrapolation of the findings of the continuously going on experimental efforts to constrain the value of the symmetry energy in the density range at and below normal nuclear matter density. The neutron star can be considered as a suitable terrestrial laboratory for the study of high density behaviour of nuclear symmetry energy. However the existing available data on the composition and cooling mechanism of neutron star are not sufficient for the purpose. In this connection it may be mentioned that once an answer to the question that whether direct URCA process takes place in neutron stars or not can largely constrain the density dependence of symmetry energy. On the other important aspect of ANM, that is the momentum dependence of neutron and proton mean fields, we have made an effort to find a solution to it from the study of temperature effect on the nuclear matter properties. From the study it has been possible to sub-divide the whole allowed range for momentum dependence of neutron and proton mean fields into two parts. The actual behaviour will correspond to which of the two parts depends on the answer to the question raised whether the thermal evolution in PNM can exceed that of SNM at a higher density or not. The boundary line dividing the whole range into two parts corresponds to the critical momentum dependence of neutron and proton mean fields for which the thermal evolution in PNM can at best approach that of SNM in the asymptotic region of high density. In order to make further progress in these direction more experimental data on the observables sensitive to these two aspects of ANM from heavy-ion reaction studies involving radioactive ion beam as well as constraints from neutron star phenomenology are required. Further, it may be mentioned here that in the transport model analysis of heavy-ion collision data the neutron and proton mean fields are the basic inputs and the mean fields resulting from our simple interaction having the flexibility of predicting different momentum dependence of mean fields for same density dependence and vice-versa can be considered as an experimental advantage for the purpose.

REFERENCES

[1] H.A.Bethe, *Ann.Rev.Nucl. Sci.* **21**, 93-244 (1971).

[2] B. D. Day , *Rev.Mod.Phys*. **50**, 495 (1978).

[3] L. Satpathy in *Structure of Atomic Nuclei*, ed: L.Satpathy,(Narosa, New Delhi)(1999).

[4] A. Akmal, V. R.Pandharipande and D.G. Ravenhall, *Phys. Rev* **C 58** 1804 (1998).

[5] D.W.L. Sprung, *Adv.Nucl.Phys*. **5**, 225 (1972).

[6] B.Friedman and V.R.Pandharipande, *Nucl. Phys* **A361**, 502 (1981).

[7] V.R.Pandharipande and R.B.Wiringa, *Rev. Mod. Phys*.**51**, 821(1979).

[8] I.E.Lagaris and V.R.Pandharipande, *Nucl. Phys.* **A359**, 349 (1981).

[9] M.R.Anastasio, L.S.Celenza, W.S.Pong and C.M.Shakin, *Phys. Rep*.**100**, 327 (1983).

[10] C.J.Horowitz and B.D.Serot, *Phys. Lett.* **137B**, 287 (1984).

[11] C.J.Horowitz and B.D.Serot, *Nucl. Phys.* **464**, 613 (1987).

[12] R.Brockman and R.Machleidt , *Phys. Lett.* **149B**, 283 (1984).

[13] R.Brockman and R.Machleidt , *Phys. Rev*. **C42**, 1965 (1990).

[14] J.P.Blaizot, *Phys. Rep* **64**, 171 (1980).

[15] J.D.Walecka, *Annals of Physics(N.Y.)*. **83**, 413(1974).

[16] P.G. Reinhard, *Rep.Prog.Phys*. **52**, 439 (1989).

[17] J. Boguta and A.R.Bodmer, *Nucl. Phys.* **A 292,** 413 (1977).

[18] D.Vautherin and D.M.Brink, *Phys. Rev*. **C3**, 626(1972).

[19] T.H.R. Skyrme, *Phil.Mag*. **1** ,1043 (1959).

[20] T.H.R.Skyrme , *Nucl.Phys*. **9**, 615 (1959).

[21] M.Beiner, H.Flocard, Nguyen Van Giai and P.Quentin, *Nucl. Phys.* **A238**, 29 (1975).

[22] D.G.Ravenhall, C.D.Bennett and C.J.Pethick, *Phys. Rev.Lett* **28**, 978 (1972).

[23] J.M.Lattimer, *Ann. Rev.Nucl.Part.Sci* **31**, 337 (1981).

[24] P.Bonche, S.Levit, D.Vautherin, *Nucl.Phys.* **A427**, 278(1984).

[25] H.Jaqaman, A.Z.Mekjian, L.Zamick, *Phys. Rev.* **C27**, 2782(1983).

[26] R.K.Su, S.D.Yang, G.L.Li, T.T.S.Kuo, *Mod. Phys. Lett.* **A1**, 71(1986).

[27] H.S.Kohler: *Nucl. Phys.* **A258**, 301 (1976).

[28] H.Krivine, J.Treiner, O.Bohigas, *Nucl. Phys.* **A336**, 155 (1980).

[29] Nguyen Van Giai and N.Sagawa, *Nucl. Phys.* **A371**, 1 (1981).

[30] L.Zamick, *Phys.Lett* **B45**, 313 (1973).

[31] J.Rikovska Stone, J.C. Miller, R.Konewicz, P.D.Stevenson and M.R.Strayer, *Phys. Rev.* **C68**, 034324 (2003).

[32] W.D.Myers and W.J.Swiatecki, *Nucl. Phys.* **81**, 1 (1966).

[33] K.Pomorski and J.Dudek, *Phys. Rev.* **C 67**, 044316 (2003).

[34] J.Siemens and V.R.Pandharipande, *Nucl. Phys.* **A173**, 561 (1971).

[35] J.R.Buchler and L.Ingber, *Astrophys. J.* **170**, 1 (1971).

[36] O.Sjöberg, *Ann. Phys.* **A 78**, 39 (1974).

[37] J.R.Buchler and B.Datta, *Phys. Rev.* **C19**,494(1979).

[38] R.G.Seyler and C.H.Blanchard, *Phys. Rev.* **131**, 355 (1963).

[39] D.M.Brink and E.Boeker, *Nucl. Phys.* **91**, 1 (1967).

[40] D.Gogny in proceedings of the Int.Cof. on Nucl. Self consistent fields ed. G.Ripka, M. Porneuf , Amstermdam, North Hclland, pp 333 (1975).

[41] J.Decharge and D.Gogny, *Phys. Rev.* **C21**, 1568(1980).

[42] J.P.Blaizot, J.F.Berger, J.Decharge and M. Girod, *Nucl. Phys.* **A591**, 435 (1995).

[43] H.A. Gustfsson, H.H.Gutbrod, B.Kolb, H.Lohner, B.Ludewigt, A.M.Poskanzer, T.Reiner, H.Riedsel, H.G.Ritter, A.Warmark, F.Weik and H.Weiman, *Phys. Rev. Lett.* **52**, 1590 (1984).

[44] G.F.Berstch, H.Kruse and S.DasGupta, *Phys. Rev.* **C29,** 673 (1984).

[45] H.Kruse, B.V.Jacak and H.Stocker, *Phys. Rev . Lett* **54**, 289 (1985).

[46] E.Baron, J.Cooperstein and S. Kahana, *Nucl. Phys.* **A440**, 744 (1985).

[47] E.Baron, J.Cooperstein and S. Kahana, *Phys. Rev. Lett.* **55**, 126 (1985).

[48] E.Baron, H.A.Bethe, G.E.Brown, J.Cooperstein and S.Kahana, *Phys. Rev. Lett* **59**, 73(1987).

[49] T.L.Ainsworth, E.Baron, G.E.Brown, J.Coooperstein and M.Prakash, *Nucl. Phys.* **A464**, 740 (1987).

[50] C.Gale, G.F.Berstch and S.Das Gupta, *Phys. Rev.* **C35**, 1666(1987).

[51] J.Aichelin, A.Rosenbauer, G.Peilert, H.Stocker and W.Greiner, *Phys. Rev. Lett* **58**, 1926 (1987).

[52] G.F.Berstch, S.Dasgupta, *Phys. Rep.* **160**, 189(1988).

[53] W.A.Kuper, G.Wegman and E.R.Hilf, *Ann. Phys.*(N.Y.)**88**, 454 (1974).

[54] Q.Pan, P.Danielwicz, *Phys. Rev. Lett* **70**, 2062 (1993).

[55] V.de La Mota, F.Sebille, B.Remand, P.Shuck, *Phys. Rev.* **C46**, 667 (1992).

[56] J.Zhang, S.Dasgupta, C.Gale, *Phys. Rev.* **C50**, 1617 (1994).

[57] F.Haddad, F.Sebille M.Farine, V. de La Mota, P.Shuck, B.Johault, *Phys. Rev.* **C52**, 2013 (1995).

[58] P.Danielewicz et al., *Phys. Rev. Lett* **81**, 2438 (1998).

[59] P.Danielewicz, *Nucl. Phys.* **A 673** , 375 (2000).

[60] G.M.Welke, M.Praksh, T.T.S.Kuo, S.DasGupta, C.Gale, *Phys. Rev.* **C38**, 2101(1988).

[61] G.Q.Li, R.Machleidt, *Phys. Rev.***C45**, 2782 (1992).

[62] G.Q.Li, R.Machleidt, *Phys. Rev.***C48**, 2707 (1993).

[63] L.P.Csernai, G.Fai, C.Gale and E.Osnes, *Phys. Rev.* **C46**, 736(1992).

[64] B.Behera, T.R.Routray, R.K.Satpathy, *J.Phys.G: Nucl. Part. Phys.***24**, 2073(1998).

[65] B.Behera, T.R.Routray, B.Sahoo, R.K.Satpathy, *Nucl. Phys.***A609**, 770(2002).

[66] R.Wiringa, *Phys. Rev.* **C38**, 2967 (1988).

[67] T.R.Routray, B.Sahoo, R.K.Satpathy and B.Behera, *J.Phys.G: Nucl.Part.Phys*.**26**, 887 (2000).

[68] P. Danielewicz, R. Lacey, W.G. Lynch, *Science* **298,** 1592 (2002).

[69] P.Danielwicz, Proceedings of International Symposium on Nuclear Physics at Mumbai (India), **50B,** 66(2005).

[70] W.Zhan et al., *Int. J. Mod. Phys.* **E15,** 1941(2006) ; http://www.impcas.ac.cn/zhuye/en/htm/247.htm.

[71] Y.Yano, 'The RIKEN RI Beam Factory Project: A Status Report', *Nucl.Instr.Meth* **B261**, 1009(2007).

[72] http://www.gsi.de/fair/index_e.html

[73] http://www.ganil.fr/research/developments/spiral2/ n'existe plus.

[74] Whitepapers of the 2007 NSAC Long Range Plan Town Meeting, Jan., 2007, Chicago, http://dnp.aps.org.

[75] M.Colona, M.Di Toro, G.Fabri, S.Macccarone, *Phys. Rev.* **C57**, 1410 (1998).

[76] B.A.Li, C.M.Ko, W.Bauer, Topical Review, *Int. J. Mod. Phys.* **E7**, 147 (1998).

[77] P.Danielwicz, R.Lacey, W.G.Lynch, *Science* **298**, 1592 (2002).

[78] B.A.Li, *Phys. Rev. Lett* **88**, 192701 (2002).

[79] B.A.Li, *Nucl. Phys.* **A708**, 365(2003).

[80] C.B.Das, S.DasGupta, C.Gale, B.A.Li, *Phys. Rev.* **C67**, 034611 (2003).

[81] B.A.Li, C.B.Das, S.DasGupta, C.Gale, *Nucl. Phys.* **A735**, 563 (2004).

[82] B.A.Li, C.B.Das, S.DasGupta, C.Gale, *Phys. Rev.* **C69**, 011603(R) (2004).

[83] L.W.Chen, C.M.Ko, B.A.Li, *Phys. Rev.* **C69**, 054606 (2004).

[84] J.Rizzo, M.Colona, M.Di Toro, V.Grecco, *Nucl. Phys.* **A732**, 202(2004).

[85] L.W.Chen, C.M.Ko, B.A.Li, *Phys. Rev. Lett* **94**, 032701 (2005).

[86] B.A.Li, G.C.Yong, W.Zuo, *Phys. Rev.* **C71**, 044604 (2005).

[87] D.H. Youngblood, H.L. Clark, Y.W. Kui, *Phys. Rev. Lett.* **82**, 691(1999) .

[88] Y.W.Lui, D.H.Youngblood, Y.Tokimoto, H.L.Clark and B.John, *Phys. Rev.* **C 70,** 014307 (2004).

[89] Z.Y Ma *et al.*, *Nucl. Phys.* **A 703**, 222 (2002).

[90] D.Vretenar, T.Niksic and P.Ring, *Phys. Rev.* **C68**, 024310 (2003).

[91] G.Colo, N.Van Giai, J.Meyer, K.Bennaceur and P.Bonche, *Phys. Rev.* **C70**, 024307(2003).

[92] S.Shlomo, V.M.Kolomietz and G.Colo, *Eur. Phys. J.* **A30**, 23 (2006).

[93] T.Li *et al.*, *Phys. Rev. Lett.* **99**, 162503 (2007).

[94] U. Garg *et al.*, *Nucl. Phys.* **A788**, 36 (2007).

[95] B. ter Haar, R.Malfliet, *Phys. Rev. Lett.* **56**, 1237 (1986).

[96] B. ter Haar, R.Malfliet, *Phys. Rep.*,**149**, 207 (1987).

[97] R. Brockmann, R.Machleidt, *Phys. Lett.* **149B**, 283 (1984).

[98] R. Brockmann, R.Machleidt, *Phys. Rev.* **C42**, 1965 (1990).

[99] A.Bohnet, N.Ohtsuks, J.Aichelin, R.Linden and A.Faessler, *Nucl. Phys.* **A 494**, 349(1989).

[100] J.Jeanicke, J.Aichelin, N.Ohtsuka, R.Linden, A.Faessler, *Nucl. Phys.* **A 536**, 201(1992)

[101] G.Q.Li, Y.Lofty, S.W.Huang, A.Faessler, *J.Phys.G:Nucl.Part.Phys.* **18**, 291(1992).

[102] DaoT.Khoa, N.Ohtsuka, M.A.Matin, A.Faessler, S.W.Huang, E.Lehmann, R.K.Puri, *Nucl. Phys.* **A 548**, 102(1992).

[103] M.Baldo, I.Bo mbaci, G.Giansiracusa, U.Lombardo, *Phys. Rev.* **C40**, R491 (1989).

[104] A.Insolia, U.Lombardo, N.G.Sandulescu, A.Bonaser, *Phys. Lett.* **B 334**, 12 (1994).

[105] S.Kubis, and M.Kutschera, *Phys. Lett* **B399**, 191 (1997).

[106] B.Liu, V.Grecco, V.Baran, M.Colona and M.D.Toro, *Phys Rev.***C66**, 045201(2002).

[107] V.Greco, M. Matera , M.Colona, M.Di Toro, G.Fabri, *Phys Rev* **C63**, 035202(2001).

[108] V.Greco, M.Colona, M.Di Toro, G.Fabri and M. Matera, *Phys Rev* **C64**, 045203(2001).

[109] V.Greco, V.Baran, M.Colona, M.Di Toro, T.Gaitanos and H.H.Wolter, *Phys Lett* **B562**, 215 (2003).

[110] L.Scalone, M.Colona, M.Di Toro, *Phys. Lett.* **B461**, 9(1999).

[111] F.Matera, V.Yu.Denisov, *Phys. Rev.* **C.49**, 2816(1994).

[112] E.Chabanat, P.Bonche, P.Haensel, J.Meyer and R.Schaeffer, *Nucl. Phys.* **A627**, 710 (1997).

[113] K.Kolehmainen, M.Prakash, J.M.Lattimer, J.Treiner, *Nucl. Phys.* **A439**, 535(1985).

[114] H.M.M.Mansour, M.Hammad, M.Y.M.Hassan, *Phys. Rev.* **C56**, 1418(1997).

[115] D.Bandyopadhyaya, C.Samanta, S.K.Samaddar, J.N.De, *Nucl. Phys.* **A511**, 1(1990).

[116] S.J.Lee, A.Z.Mekjian, *Phys. Rev.* **C63**, 044605(2001).

[117] I. Bombaci and U.Lombardo, *Phys. Rev.* **C44**, 1892 (1991)

[118] W. Zuo, I. Bombaci and U. Lombardo, *Phys. Rev.* **C60**, 024605 (1999).

[119] I.Bombaci in *Isopspin Physics in Heavy-Ion Collisions at Intermediate Energies*, eds: B.A.Li and W.Udo Schroeder (Nova Science Publishers, Inc., New York)pp35(2001).

[120] F.Hoffman, C.M.Keil and H.Lenske, *Phys. Rev.* **C64**, 034314 (2001).

[121] P.E.Hodgson, *The Nucleon Optical Model* (Singapore: World Scientific) p.613 (1994).

[122] G.W.Hoffmann and W.R.Coker, *Phys. Rev. Lett.* **29,** 227 (1972).

[123] A.J.Koning and J.P.Delaroche, *Nucl. Phys.* **A 713**, 231 (2003).

[124] W. Zuo, L.G. Cao, B.A. Li, U. Lombardo, C.W. Shen, *Phys. Rev.* **C 72**,014005 (2005).

[125] E.Chabanat, P.Bonche, P.Haensel, J.Meyer and R.Schaeffer, *Nucl. Phys.* **A635,** 231 (1998).

[126] E.Chabanat, P.Bonche, P.Haensel, J.Meyer and R.Schaeffer, *Nucl. Phys.* **A643,** 441 (1998).

[127] Z.Y. Ma, J.Rong, B.-Q. Chen, Z-Y Zhu and H.Q. Song, *Phys. Lett.* **B604,** 170(2004).

[128] E.van Dalen, C Fuchs and A. Faessler, *Phys. Rev. Lett.* **95,** 022302 (2005).

[129] C.M.M.Jaminon, C.Mahaux, *Phys. Rev.* **C40**, 354(1989).

[130] F.Sammarruca, W.Barredo and P.Krastev , *Phys. Rev* **C 71,** 064306 (2005).

[131] T.Leisinki, K.Bennaceur, T.Duguet and J. Meyer, *Phys Rev* **C74,** 044315(2006).

[132] M.B.Tsang et al., *Phys. Rev Lett* **92,** 062701 (2004).

[133] D.V.Shetty, S.J.Yennello and G.A.Souliotis, *Phys. Rev.* **C 76,** 024606(2007).

[134] D.V.Shetty, S.J.Yennello, *Pramana J. Phys.***75,** 259 (2010).

[135] B.A.Li and L.W.Chen, *Phys. Rev* **C 72,** 064309 (2005).

[136] B.A.Li , L.W.Chen, C.M.Ko, *Phys. Rep.* **464,** 113 (2008).

[137] D.V.Shetty, S.J.Yennello and G.A.Souliotis: *Phys. Rev.* **C 75,** 034602(2007).

[138] M.B.Tsang et al., *Phys. Rev Lett* **102,** 122701 (2009).

[139] W. Reisdorf *et al., Nucl. Phys.* **A781**, 459 (2007).

[140] Y. Zhang, P.Danielewicz, M. Famiano, Z.L., W.G.Lynch and M.B.Tsang, *Phys. Lett.* **B664**, 145 (2008).

[141] A.Ono, P.Danielewicz , W.A.Friedman, W.G.Lynch and M.B.Tsang, *Phys. Rev.* **C 68,** 051601(R) (2003).

[142] W.D.Myers and W.J.Swiatecki, *Nucl. Phys.* **81**, 1 (1966).

[143] K.Pomorski and J.Dudek, *Phys. Rev.* **C 67**, 044316 (2003).

[144] B.A.Li, A.T.Sustich and B.Zhang, *Phys. Rev*.**C64**, 054604 (2001).

[145] B.A.Li, *Phys. Rev. Lett* **85**, 4221 (2000).

[146] Q.Li, Z.Li, E.Zhao and R.K.Gupta, *Phys. Rev.* **C71,** 054907 (2005).

[147] Q.Li, Z.Li, S.Soff, M.Bleicher and H.Stocker, *Phys. Rev.***C72**, 034613 (2005)

[148] B.A.Brown, *Phys. Rev. Lett.* **85**, 5296 (2000).

[149] G.C.Yong, B.A.Li, L.W.Chen, X.C.zhang, Phys. *Rev.* **C 80,** 044608 (2009).

[150] V.Greco, V.Baran, M.Colona, M.Di Toro, T.Gaitanos and H.H.Wolter, *Phys Lett* **B562**, 215 (2003).

[151] T.Klahn et al., *Phys. Rev.* **C74**, 035802 (2006).

[152] A.M.Lane: *Nucl Phys.***35**, 676(1962).

[153] B. Behera, T.R. Routray, A. Pradhan, S.K. Patra, P.K. Sahu, *Nucl. Phys.* **A753,** 367(2005).

[154] B.Behera, T.R.Routray and A.Pradhan, *Mod. Phys. Lett.* **A 20**, 2639(2005).

[155] C. Gale, G.M. Welke, M. Prakash, S.J.Lee, S.Das Gupta, *Phys. Rev.* **C 41**, 1545 (1990).

[156] J.Margueron, S.Goriely, M.Grasso, G.Colo and H. Sagawa, *J. Phys. G: Nucl. Part. Phys.* **36**, 125103 (2003).

[157] B.Cochet, K.Bennaceur, P.Bonche, T.Duguet and J.Meyer, *Nucl. Phys.* **A731**, 34 (2004).

[158] T.Duguet and P Bonche, *Phys. Rev.* **C67**, 054308 (2003).

[159] J.W.Negele and D.Vautherin, *Phys. Rev.* **C5**, 1472 (1972).

[160] J.W.Negele and D.Vautherin, *Phys. Rev.* **C11**, 1031 (1975).

[161] O.Bohigas, A.M.Lane and J.Martorell, *Phys. Rep.* **51**, 267 (1979).

[162] W.Zuo, A.Lejeune, U.Lombardo, J.F.Mathiot, *Eur. Phys. J.* **A14**, 469 (2002).

[163] B.A.Li, *Phys. Rev.* **C69**, 064602 (2004).

[164] C.Moustakidis, *Phys. Rev.* **C76**, 025805 (2007).

[165] C.Moustakidis, *Phys. Rev.* **C78**, 054323 (2008).

[166] C.Moustakidis and Panos, *Phys. Rev.* **C79**, 045806 (2009).

[167] C. Fuchs, *Prog. Part. Nucl. Phys.* **56** , 1(2006).

[168] C. Fuchs, A. Faessler, E. Zabrodin, Y.M. Zheng, *Phys. Rev. Lett.* **86**, 1974 (2001).

[169] C. Hartnack, H. Oeschler, J. Aichelin, *Phys. Rev. Lett.* **96**, 012302 (2006).

[170] D.H. Youngblood, C.M. Rozsa, J.M. Moss, D.R. Brown, J.D. Bronson, *Phys. Rev. Lett.* **39** ,1188 (1977).

[171] S. Shlomo, D.H. Youngblood, *Phys. Rev.* **C 47**, 529 (1993).

[172] B.K. Agrawal, S. Shlomo, *Phys. Rev.* **C 70** , 014308 (2004).

[173] B.K. Agrawal, S. Shlomo, V.K. Au, *Phys. Rev.* **C 72** , 014310 (2005).

[174] B.K. Agrawal, S.K. Dhiman, R. Kumar, *Phys. Rev.* **C 73** , 034319 (2006).

[175] M M Sharma, *Nucl. Phys.* **A 816**, 65 (2009).

[176] J.Xu, L.W.Chen, B.A.Li and H.R.Ma , *Phys. Rev.* **C75,** 014607 (2007).

[177] L.W.Chen, F.S.Zhang, Z.H.Lu, W.F.Fi, Z.Y.Zhu and H.R.Ma, *J. Phys. G: Nucl. Part. Phys.* **27,** 1799(2001).

[178] L.G.Cao, U. Lombardo, C.W. Shen and N.V.Giai , *Phys. Rev* **C 73,** 014313 (2006).

[179] B.Behera, T.R.Routray and S.K.Tripathy, *J. Phys. G: Nucl. Part. Phys.***36,** 125105 (2009).

[180] F.Sammarruca: arxiv:1002.1046v1[nucl-th] (2010).

[181] A.Ono, P.Danielewicz , W.A.Friedman, W.G.Lynch and M.B.Tsang, *Phys. Rev.* **C 70,** 041604(R) (2004).

[182] G.A.Souliotis, D.V. Shetty, A. Keksis, E.Bell, M.Jandel, M.Veselsky and S.J.Yennello, *Phys. Rev.* **C 73,** 024606(2006).

[183] J.Iglio, D.V.Shetty, S.J.Yennello, G.A.Souliotis, M.Jandel, A.L.Keksis, S.N.Soisson, B.C.Stein, S.Wuenschel and A.S.Botvina, *Phys. Rev.* **C 74,** 024605(2006).

[184] M.Prakash, I.Bombaci, M.Prakash, P.J.Ellis, J.M.Lattimer, R.knorren, *Phys. Rep.* **280**, 1(1997).

[185] T.Takatsuka, S.Nishizaki and J.Hiura, *Prog. Theor. Phys.* **92**, 779 (1994).

[186] T.Takatsuka, *Prog. Theor. Phys.* **95**, 901 (1996).

[187] D.V.Shetty *et al., arXiv:nucl*-ex0606032(2006).

[188] A.Le Fèvre *et al.*, for the ALADIN and INDRA Collaboration, *Phys. Rev. Lett.* **94,** 162701(2005).

[189] W.Trautmann *et al.* for the ALADIN and INDRA Collaboration, *arXiv: nucl*-ex 0603027v1(2006).

[190] B.A.Li and L.W.Chen, *Phys. Rev* **C 74,** 034610(2006).

[191] S.R. Souza, M.B.Tsang, R.Donangelo, W.G.Lynch and A.W.Steiner, *Phys. Rev.* **C78,** 014605 (2008).

[192] G.F.Burgio, M.Baldo, O.E.Nicotra, H.J.Schulze, *Astrophys. Space Sci.* **308,** 387(2007).

[193] G.H.Bordbar and N.Riazi, *Int. J. Theor. Phys.* **40,** 1671(2001).

[194] G.H.Bordbar, S.M.Zebajad and R.Zahedinia, *Int. J. Theor. Phys.* **48,** 61(2009).

[195] J.M.Lattimer and M.Prakash, *Science* **304,** 536 (2004).